HIGHWAY RESEARCH RECORD

Number 460

Traffic Safety Barriers and Lighting Supports

14 reports
prepared for the
52nd Annual Meeting

Subject Areas

22 Highway Design
27 Bridge Design
51 Highway Safety

HIGHWAY RESEARCH BOARD
DIVISION OF ENGINEERING NATIONAL RESEARCH COUNCIL
NATIONAL ACADEMY OF SCIENCES—NATIONAL ACADEMY OF ENGINEERING
Washington, D.C. 1973

NOTICE

These papers report research work of the authors that was done at institutions named by the authors. The papers were offered to the Highway Research Board of the National Research Council for publication and are published here in the interest of the dissemination of information from research, one of the major functions of the Highway Research Board.

Before publication, each paper was reviewed by members of the HRB committee named as its sponsor and accepted as objective, useful, and suitable for publication by the National Research Council. The members of the review committee were chosen for recognized scholarly competence and with due consideration for the balance of disciplines appropriate to the subject concerned.

Responsibility for the publication of these reports rests with the sponsoring committee. However, the opinions and conclusions expressed in the reports are those of the individual authors and not necessarily those of the sponsoring committee, the Highway Research Board, or the National Research Council.

Each report is reviewed and processed according to the procedures established and monitored by the Report Review Committee of the National Academy of Sciences. Distribution of the report is approved by the President of the Academy upon satisfactory completion of the review process.

ISBN 0-309-02193-6
Library of Congress Catalog Card No. 73-17671
Price: $4.60

CONTENTS

FOREWORD

The 14 papers in this RECORD deal with the design, testing, analysis, and suggested warrants for the use of roadside safety devices such as barrier curbs, guardrails, median barriers, crash cushions, and breakaway sign supports and light poles. Of particular interest is the extensive use many of the authors have made of scale-model testing, mathematical models, computer analysis programs, and computer-generated drawings to simulate and more thoroughly study the many variables associated with the dynamic action of moving and impacting vehicles.

Dunlap analytically develops a method to define and determine the redirective effectiveness of barrier curbs of limited height (12 in. or less). In a second paper, he employs computer program simulation techniques to evaluate the vehicle impact-vaulting potential of several in-service curb-guardrail combinations. He concludes that a properly designed curb-guardrail combination can be an efficient redirective system in which the curb acts as a low-damage deflector for many impacts and the guardrail acts as a backup barrier.

Fay and Kaplan describe the scale-modeling techniques they employed to develop and test an energy-absorbing barrier or crash cushion composed of a family of parabolic corrugated-metal arches oriented parallel to the roadway surface to form a guardrail for glancing side impacts and to deform plastically to absorb the energy of a vehicle impacting into the nose.

Marquis, Hirsch, and Nixon report on research that included a full-scale vehicle-impact test and was performed to expand the use of the steel-drum crash cushion to a portable or mobile trailer system to protect slowly moving or stopped maintenance vehicles working on the highways.

Paar reports on research performed in the Netherlands to develop a suitable highway safety barrier for use on soft shoulders and bridges. The resulting system is composed of 2 parallel and opposite W-shaped metal rails that are separated by metal spacers and diagonal stiffeners as necessary and mounted on lightweight or breakaway posts.

Giavotto describes a computer program developed in Italy to simulate the impacts of various vehicles with guardrail systems. He reports that this digital simulation system has been used to predict the performance of various barrier systems, including the system reported by Paar. The results agree with those of actual full-scale vehicle tests.

Young, Post, and Ross employ computer program techniques to simulate a 4,000-lb vehicle impacting the Texas concrete median barrier at various speeds and impact angles. They use computer-generated drawings to compare the simulated results with corresponding frames from high-speed films of actual full-scale vehicle-impact tests.

Post, Hirsch, and Nixon report on the results of full-scale impact tests conducted with a large loaded tractor-trailer truck on the Texas concrete median barrier. The longitudinally reinforced but unanchored barrier was undamaged and successfully redirected the truck in tests performed at 35 mph and 19 deg, 34 mph and 16 deg, and 45 mph and 15 deg.

Brewer studies the effect of the barrier beam on the energy-absorbing capability of a guardrail system as a whole and uses a synthetic system model as a tool for optimizing the size of beam and supports to produce the most cost-effective total system.

Ross et al. employ computer simulation techniques to study the dynamic response of a passenger vehicle traversing embankment side slopes at various speeds and departure angles. This information is used to develop a severity index, which is compared to the severity index for a vehicle impacting a W-section guardrail. An equal-severity curve is developed as a criterion for guardrail installations on embankments.

Post, Hirsch, Hayes, and Nixon report on full-scale vehicle-impact tests to evaluate and compare the performance of 3 median barrier designs of different configurations and lateral stiffnesses. Factors considered were vehicle decelerations, vehicle damage, occupant injury, construction and maintenance costs, median widths, and traffic volumes.

McCollom describes a study to develop a more economical, lightweight slip base for breakaway roadside sign supports. Instrumented physical tests were conducted by using experimental stress analysis techniques to develop a more accurate plate design method.

Walton, Hirsch, and Rowan conducted full-scale vehicle-impact tests to determine the impact behavior of 50-ft high median-mounted luminaire supports with frangible transformer bases and of secondary collisions of vehicles striking downed poles in traffic lanes. An index was developed to describe the relative hazard created by the proximity and frequency of luminaire supports.

Zobel describes the results of 16 full-scale vehicle-impact tests performed to evaluate 3 kinds of metal posts for relatively small roadside signs. He concludes that these designs do not constitute a hazard to seat-belted vehicle occupants and, thus, do not require breakaway action.

—Eric F. Nordlin

BARRIER-CURB REDIRECTION EFFECTIVENESS

Duane F. Dunlap, Highway Safety Research Institute,
University of Michigan

Barrier curbs are used extensively along some urban freeways and in front of bridge rails. Heretofore, the redirective effectiveness of such curbs has never been quantified. A method developed for this purpose makes it possible to define the redirective effectiveness of a given curb at any particular installation site. Research has shown that barrier-curb redirection performance can be described in terms of a limiting characteristic velocity that is the component of vehicle velocity normal to the curb face. This boundary and representative on-site distributions of vehicle speed and ran-off-the-road angle can be used to compute a measure of curb redirection effectiveness. This is accomplished by integrating over the 2 distributions with integration limits supplied by the redirection boundary. Two barrier curb cross sections are evaluated by using speed and angle data. The Belgian Trief curb is shown to be effective in redirecting 27.4 percent of the expected population of impacting vehicles. A more efficient barrier curb, developed in West Germany, is shown to redirect 70.4 percent of the same population. In light of these results and because curb impacts produce little vehicle damage, it is recommended that more optimum barrier curbs be developed. Their use, where appropriate, would be in place of or in combination with guardrails.

•IN CURRENT highway design practice, curbs control rainfall drainage; deter vehicles from leaving the roadway; delineate the road edge; present a finished appearance; and aid in orderly roadside development (1). The discussion that follows is directed to the effect that curbs have on safely redirecting vehicles that leave the roadway. The curbs under consideration are of the type commonly called barrier curbs.

DEFINITIONS

In general, curbs are classified as barrier or mountable. Mountable curbs are designed so that vehicles can cross them if necessary. They are low, have flat or round sloping faces, are usually no more than 6 in. high, and are generally used in areas where use of the road edge for emergency stops is permitted.

Barrier curbs, on the other hand, are relatively high and steep-faced, are designed to inhibit vehicles from leaving the pavement, and are between 6 and 12 in. high. If the face slopes, the slope does not exceed 1 in. per 3 in. of height. The upper corner is often rounded or chamfered to discourage the wheel rim from biting into the curb face.

PERSPECTIVE

Use of the curb as a device for redirecting errant vehicles has probably been considered by highway designers since the earliest days of paved road construction. However, this use has never been universal and in recent years has fallen into disfavor, particularly in front of guardrails (2). In current practice, therefore, low barrier curbs (12 in. in height or less) are usually not used for redirection; they are sometimes used for drainage control and roadway delineation but are designed to be mountable,

particularly true along high-speed urban highways to allow disabled vehicles easy access to the shoulder (1).

One of the main objections to using barrier curbs along roadways is that such curbs tend to limit the drivers' use of the adjacent roadway and, thus, to reduce the effective road width. Some evidence suggests that drivers tend to veer away from structures having a formidable appearance, but conflicting evidence indicates that drivers soon become accustomed to such structures and, after a reasonable period, drivers use the full road width (3). In any case, experience has generally shown that curbs placed 4 to 6 ft beyond the traffic pavement edge cause little reduction in effective lane width (1).

In terms of redirection effectiveness, it is obvious that a curb whose height is below the center of mass of a vehicle will cause an overturning moment upon impact. Therefore, a barrier curb of limited height can never be expected to redirect vehicles over the full range of operational impact conditions. On the other hand, in the range of conditions under which a curb can be effective in redirection, vehicle damage resulting from striking the curb will be far less than that which would result from striking a guardrail. Therefore, the development of efficient barrier curbs and the assessment of their effectiveness seem well worth the effort.

HISTORICAL BARRIER CURB DEVELOPMENT

The first published research on curb mounting and redirection was carried out in 1953 by the California Division of Highways (4). The research consisted of 149 full-scale impact tests on 11 curb cross sections (Fig. 1). All curbs were considered to be barrier curbs except curb X, which was mountable. Of the 11 curbs, 8 were 9 in. high, 1 was 6 in. high (the mountable curb), and 2 were 12 in. high. The two 9-in. curbs, V and VI-M, were found to be most efficient in redirection. Both curbs were rounded at the top and undercut. Curb VI-M was fitted with a metal facing to reduce tire-curb friction forces and, thus, reduce the tendency for mounting. All curbs in the test series were standard cross sections then in use on California highways.

As the result of these tests, a second series of barrier curb tests was undertaken in 1955 so that specific recommendations could be made for the design of more efficient barrier curbs (5). Four basic cross sections were tested; shims were used to achieve a desired height as shown in Figure 2. The designs were essentially modifications of the V and VI-M designs shown in Figure 1.

Conclusions from the 2 test series indicated that an efficient barrier curb should be at least 10 in. high, be undercut, and have a moderately smooth surface texture. A very smooth surface tends to redirect a vehicle back into traffic at a relatively high angle, whereas an overly rough surface enhances mounting. The upper corner should be rounded so as to reduce the tendency of the wheel rim to grab onto the curb top. The curb design that incorporates all these features is shown in Figure 3a. Unfortunately, that design was never evaluated, but somewhat similar ones were tested in Canada and West Germany.

The Canadian test (6) was conducted as part of a larger study to determine the efficiency of the curb in combination with various guardrails as a redirection system. Only a single test was made at a velocity of 64 mph and an angle of 20 deg. Redirection did not occur. The cross section is shown in Figure 3b.

Five tests were made on the West German cross section (Fig. 3c) with various vehicles at speeds ranging between 29 and 48 mph and at angles of 10 and 15 deg (7). All tests resulted in a redirection except one involving a Volkswagen at 48 mph and 15 deg. Mounting in this test was attributed in some degree to the vehicle's rear engine configuration and low total mass. Test results are shown in Figure 4.

The Belgium Trief curb (Fig. 5) is another example of a barrier curb having specific design features to enhance redirection. In an interesting series of tests conducted in England (8), the redirective character of the Trief curb was found to conform to the equation

$$V \sin \alpha = \text{constant} = K \qquad (1)$$

Figure 1. California test curbs in 1953.

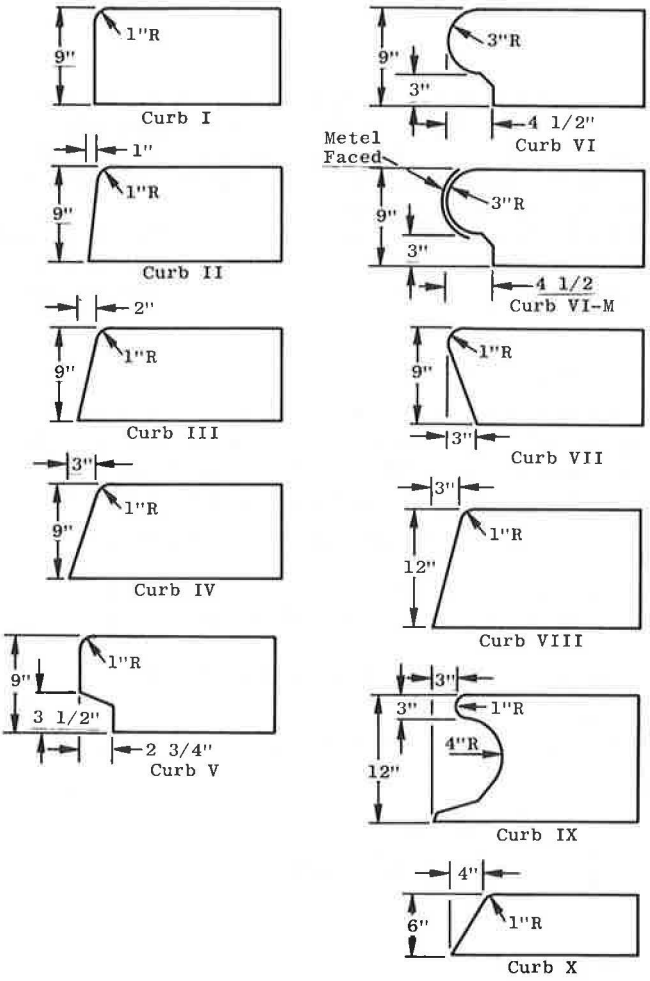

Figure 2. California test curbs in 1955.

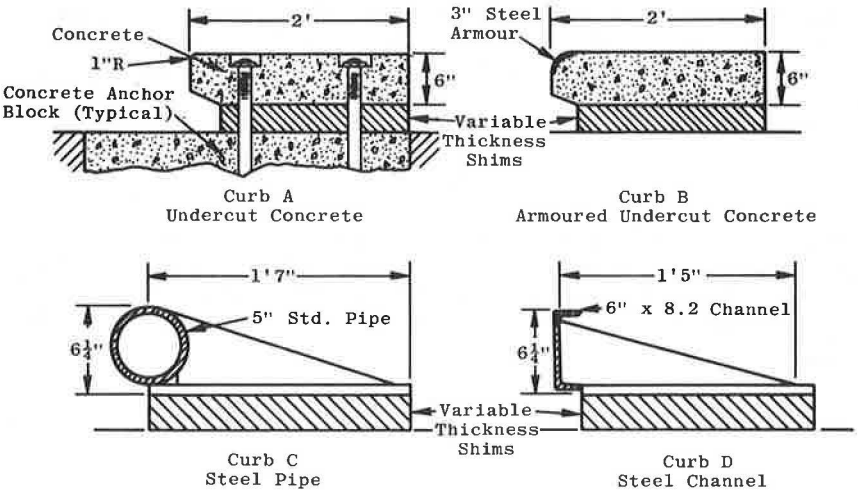

where

V = impact velocity, and
α = impact incidence angle.

In effect, whenever the component of vehicle velocity normal to the curb was larger than a fixed value, the vehicle would mount. Below that value, redirection would occur. The test results are shown in Figure 5. The influence of tire-curb friction on mounting was confirmed in those tests in that the mounting velocity at a 15-deg impact angle increased from 12 to 20 mph when the tire and curb were wet.

Another class of higher curbs, which could more properly be called concrete guardrails (e.g., the GM barrier), has also received considerable research attention in the last decade. These are reviewed elsewhere (9), however, and are not directly associated with the present discussion.

ANALYSIS

To determine the efficiency of a barrier curb as a redirective device requires a measure of effectiveness. For this analysis, the measure was chosen to be the percentage of the total errant vehicle population that could be expected to be redirected by a given barrier curb. Four kinds of data are required to determine this percentage:

1. The redirective performance of particular barrier curbs in terms of speed and angle;
2. The distribution of vehicle speeds in the operational traffic environment;
3. The distribution of ran-off-the-road angles in the operational traffic environment; and
4. The statistical correlation between the data obtained for items 2 and 3.

Fortunately, all 4 kinds of data are available.

In generalized mathematical terms, the desired percentage measure can be written in the following form:

$$P[V < V_p(\alpha)] = \int_0^{\pi/2} \int_0^{V_p(\alpha)} f(V, \alpha) dV \, d\alpha \qquad (2)$$

where V and α are the same as for Eq. 1 and

$V_p(\alpha)$ = specific curb redirective performance limit expressed in terms of α, and
$f(V, \alpha)$ = joint frequency function of velocity and angle for ran-off-the-road vehicles.

Equation 2 expresses the probability that a vehicle leaving the roadway will be within the redirective performance limits of a specific barrier curb.

With the redirective performance of a specific curb expressed in the form of Eq. 1, $V_p(\alpha)$ can be expressed as

$$V_p(\alpha) = \frac{K}{\sin \alpha} \qquad (3)$$

The value of K for the Trief curb is about 3.1 mph, and the corresponding value for the Elsholz curb is about 9.1 mph. The two performance boundaries are shown in Figure 6.

Figure 6 also shows a curve that indicates the boundary below which vehicle speed and impact angle can be expected to be uncorrelated. The equation for this curve is given as follows (10):

$$\alpha = \cos^{-1}\left(1 - \frac{gy\mu}{V^2}\right) \qquad (4)$$

Figure 3. California optimized, Canadian undercut, and West German Elsholz undercut curbs.

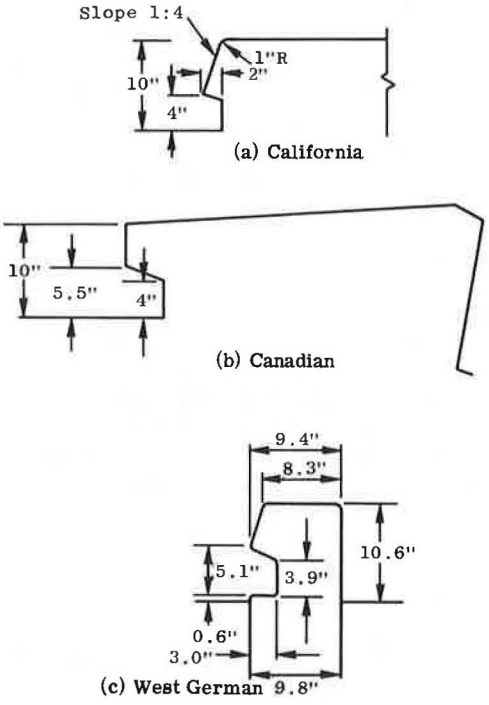

Figure 4. Results of Elsholz curb test.

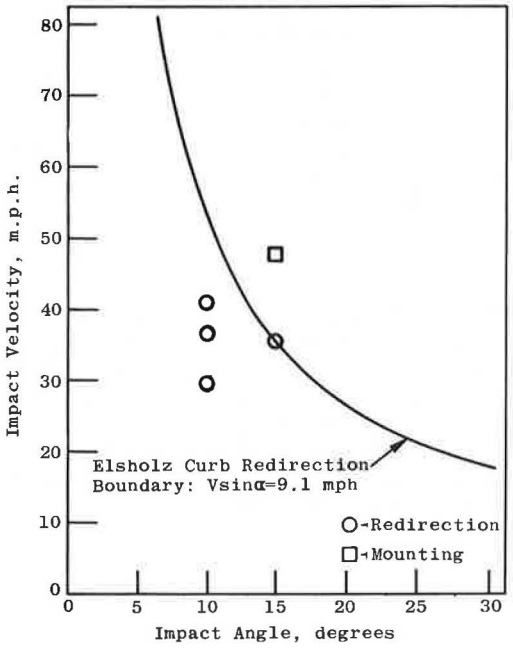

Figure 5. Results of Trief curb test.

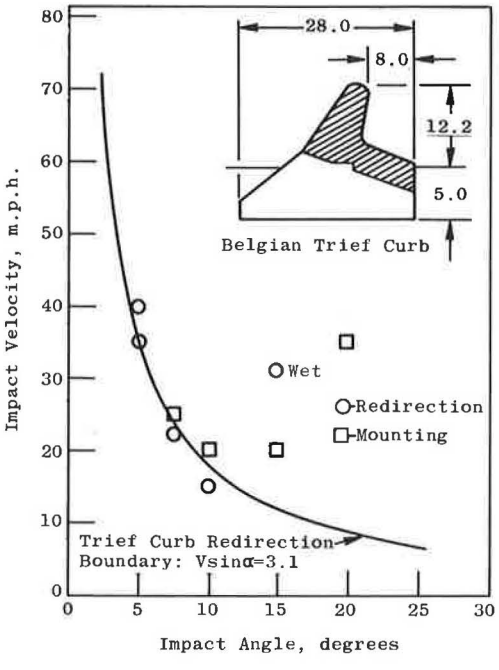

Figure 6. Redirection and correlation boundaries.

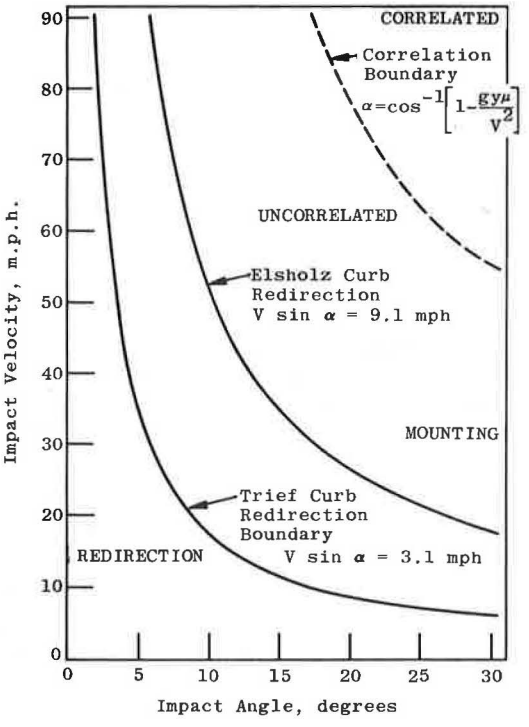

where

g = gravitational constant,
y = distance from initial vehicle c.g. straight-ahead path to curb, and
μ = tire-road friction coefficient.

Equation 4 yields the maximum vehicle path angle (impact angle in this case) that can be achieved for a given road width and friction characteristics as a function of velocity. Figure 6 shows values of y and μ of 19 ft and 0.6 respectively. All combinations of velocity and angle under this curve are achievable and, hence, can be expected to be uncorrelated. That being the case, the joint velocity-angle frequency function can now be written as

$$f(V, \alpha) = g(V)h(\alpha) \tag{5}$$

Thus, distributions of angle and velocity can be considered separately.

Velocity distribution data were chosen to represent urban traffic conditions. Urban traffic conditions are most meaningful in evaluating barrier curbs because they are primarily used in urban areas. The specific data were taken from Michigan Department of State Highways survey station 010, which is located in Ingham County on Mich-43 where the posted speed limit is 40 mph (11). Ran-off-the-road angle data were taken from the Hutchinson study (12) and are shown in Figures 7 and 8.

With the changes discussed above, Eq. 2 can now be written as follows:

$$P\left(V < \frac{K}{\sin \alpha}\right) = \int_0^{\pi/2} \int_0^{\frac{K}{\sin \alpha}} h(\alpha)g(V)dVd\alpha \tag{6}$$

The indicated integration volume is shown in Figure 9. The Elsholz curb performance boundary and the correlation boundary are shown. Carrying out the integration indicated by Eq. 6 leads to

$$P\left(V < \frac{K}{\sin \alpha}\right) = \int_0^{\pi/2} \left[G\left(\frac{K}{\sin \alpha}\right) - G(0)\right] h(\alpha)d\alpha$$

$$= \int_0^{\pi/2} G\left(\frac{K}{\sin \alpha}\right) h(\alpha)d\alpha \tag{7}$$

where G(V) is the distribution function corresponding to g(V) and G(0) = 0.

Equation 7 in its present form requires that G (K/sin α) and h(α) be described analytically. Because both the speed and angle data are in tabular form, it was found that a discrete summation process worked more readily than the indicated integration. In mathematical terms, the discrete process can be written as follows:

$$P\left(V < \frac{K}{\sin \alpha}\right) = \sum_{i=1}^{h} G\left(\frac{K}{\sin \alpha_i}\right) h(\alpha_i)\, \Delta\alpha_i$$

$$= \sum_{i=1}^{h} G\left(\frac{K}{\sin \alpha_i}\right) h(\alpha_i, \Delta\alpha_i) \tag{8}$$

Figure 7. Urban speed distribution and frequency.

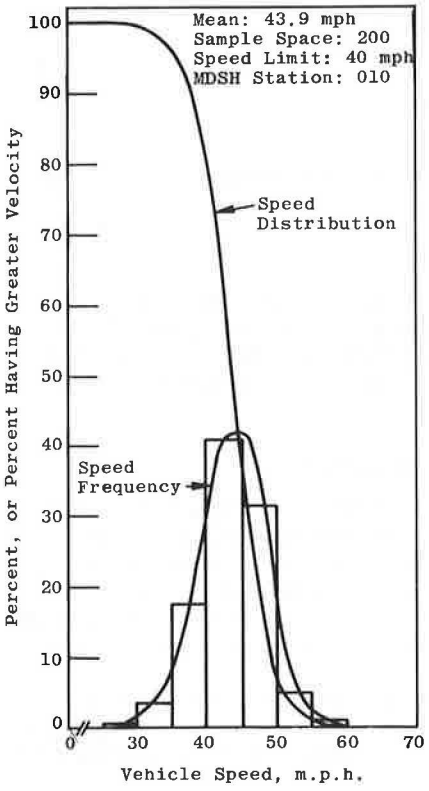

Figure 8. Encroachment angle distribution and frequency.

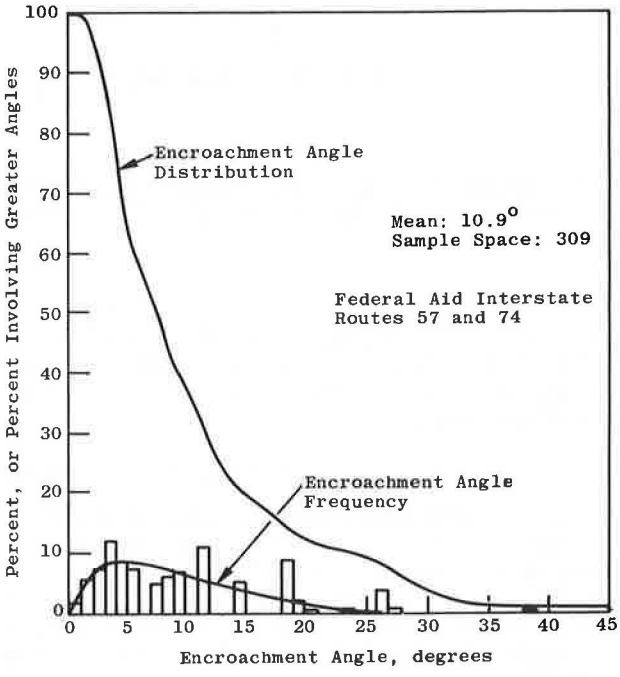

Figure 9. Angle-velocity integration volume.

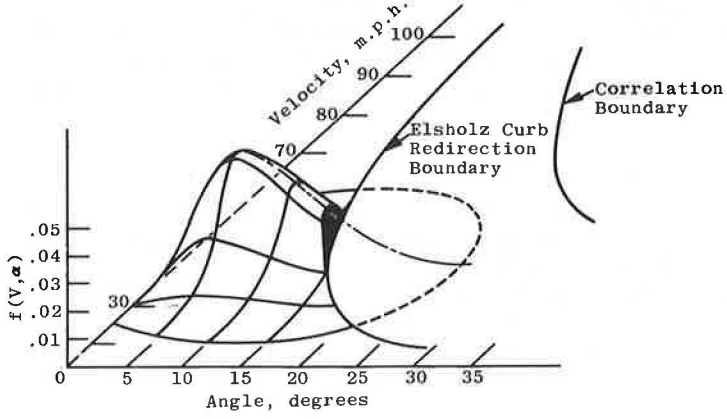

where

$$h(\alpha_1, \Delta\alpha_1) = h(\alpha_1)\Delta\alpha_1 \cong \int_{\alpha_1 - \frac{\Delta\alpha_1}{2}}^{\alpha_1 + \frac{\Delta\alpha_1}{2}} h(\alpha)d\alpha \qquad (9)$$

The quantity $h(\alpha_1, \Delta\alpha_1)$ turns out to be the percentage of the total sample space of ran-off-the-road angles that occur within the interval $\Delta\alpha_1$.

RESULTS

When a K value of 9.1 mph is used for the Elsholz curb, the summation process defined by Eq. 8 yields a value of 0.704 for $P(V < K/\sin \alpha)$. In other words, 70.4 percent of all vehicles striking the Elsholz curb would be redirected under urban traffic conditions. The corresponding value for the Trief curb under the same circumstances is 27.4 percent.

CONCLUSION AND RECOMMENDATIONS

It is evident that a carefully designed barrier curb can be an effective redirection device. In addition, vehicle damage can be expected to be substantially less when a vehicle impacts with a curb than when it runs into a guardrail. Curb installation costs are also somewhat less, and the curb can be made to serve a greater number of functions. A barrier curb of limited height (12 in. or less) can never be so effective in redirection as a guardrail, however. Use warrants must, therefore, be carefully defined.

On balance, it would seem appropriate to reexamine the use policy for barrier curbs as well as to initiate the development of more nearly optimal redirective cross sections. The potential for eventual gain in redirective effectiveness versus vehicle damage cost is well worth pursuing.

ACKNOWLEDGMENT

The research reported here was financed under the Highway Planning and Research Program and was sponsored by the Michigan Department of State Highways. The contents of this paper reflect the views of the author who is responsible for the facts and accuracy of the data presented. The contents do not necessarily reflect the official views or policies of the sponsor. This report does not constitute a standard, specification, or regulation.

REFERENCES

1. A Policy on Geometric Design on Rural Highways. AASHO, Washington, D.C., 1965.
2. Michie, J. D., and Calcote, L. R. Location, Selection, and Maintenance of Highway Guardrails and Median Barriers. NCHRP Rept. 54, 1968.
3. Edholm, S. Examples of Vehicle Speed and Distance to Edge Marking. Svenska Vagfor Tidskr, Sweden, Vol. 52, Nov. 1965, pp. 366-370.
4. Beaton, J. L., and Peterson, H. A Report on Dynamic Testing of Various Designs of Highway Bridge Curbing—Roadway Barrier Curb Investigation. Calif. Div. of Highways, Dec. 1953.
5. Field, R. N., and Beaton, J. L. Final Report of Full-Scale Dynamic Tests of Bridge Curbs and Rails. Calif. Div. of Highways, Aug. 1957.
6. Hénault, G. G., and Perron, H. Research and Development of a Guide Rail System for a High-Speed Elevated Expressway. Highway Research Record 152, 1966, pp. 36-65.
7. Elsholz, J. Tests Concerning the Turn-Away Effect of Curb Stones. Strasse und Autobahn, Vol. 19, No. 4, April 1968.

8. Jehu, V. J. Safety Fences and Kerbs. Traffic Engineering and Control, Vol. 5, No. 9, Jan. 1964.
9. Dunlap, D. F., Grote, P., Fram, D. M., and Mashinter, W. Investigation of the Dynamic Impact Characteristics of Roadside Structures. Highway Safety Res. Inst., Univ. of Michigan, Ann Arbor, May 1972.
10. Shoemaker, N. E., and Radt, H. Summary Report of Highway Barrier Analysis and Test Program. Cornell Aeronaut. Lab., Rept. VJ-1472-V3, July 1961.
11. Speed Report. Mich. Dept. of State Highways, Rept. 66, Oct. 1971.
12. Hutchinson, J. W. The Significance and Nature of Vehicle Encroachment on Medians of Divided Highways. Univ. of Illinois, Urbana, Highway Eng. Series 8, Dec. 1962.

CURB-GUARDRAIL VAULTING EVALUATION

D. F. Dunlap, Highway Safety Research Institute, University of Michigan

Impact evaluations are presented for several curb-guardrail combinations. The evaluations are carried out by conservatively assessing the possibility that a vehicle will vault a guardrail after it impacts a curb. Three parameters are examined: approach velocity, approach angle, and guardrail setback from the curb face. Vaulting analyses are carried out by using curb-impact simulation data as input to an analytically derived vaulting equation. All curb-guardrail combinations subjected to evaluation were found to be free of potential vaulting problems. A review of all known curb-guardrail tests shows no identifiable cases of vaulting by standard passenger-car test vehicles. A review of curb-guardrail use and the development of optimized curb-guardrail configurations are recommended.

•CURB-GUARDRAIL combinations represent a marriage of roadside redirection devices. The utility of such combinations seems obvious. Low-energy vehicles striking the curb at small angles are redirected with little damage. For vehicles climbing the curb, the guardrail acts as a positive secondary retainer. The use of curb-guardrail combinations is currently in disfavor, however, because of the tendency of the curb to cause a vehicle to vault the guardrail (1, 2). Recommended practice, therefore, is to locate the curb behind the guardrail if a curb is needed for reasons other than vehicle redirection.

In Michigan, a number of different curb-guardrail combinations are installed at numerous locations along the state highway system. The variety of systems is the result of design changes and improvements in both curb and guardrail standards. Because of the lack of uniformity and the nonconformity to current recommended design practices, the Michigan Department of State Highways (MDSH) contracted with Wayne State University and the Highway Safety Research Institute to evaluate several in-service curb-guardrail combinations that were considered to have uncertain impact performance characteristics. Impact evaluations are discussed for the 6 combinations that were evaluated. Evaluations were made on the basis of assessing the possibility of a vehicle vaulting the backup guardrail after an impact with the curb. The work of other organizations is reviewed to place the state of the art of curb-guardrail performance and development in proper perspective.

STATE-OF-THE-ART REVIEW

An extensive review of the published curb-guardrail test data can be found elsewhere (3). The data are for a large variety of curb-guardrail combinations, none of which is exactly like any of the 6 configurations under evaluation (4, 5, 6, 7, 8, 9). In addition, most configurations were tested just once, and a wide variety of test conditions was used. Generalizing on the accumulated data is therefore rather difficult, but the following discussions detail areas where, despite the difficulties, specific generalizations can be made.

The primary question relative to using a combined curb-guardrail system is whether the curb contributes adversely to the redirective performance of the guardrail. The existing test results were, therefore, categorized in terms of curb height, rail height, and rail setback to examine whether a vehicle would likely vault over or tunnel under a guardrail when the guardrail is fronted by a curb. However, in all tests examined, no case of tunneling was found and only one questionable case of vaulting was discovered. Several examples of structural failure on the part of the guardrail were

noted, but these were considered to be independent of curb-guardrail dynamics. In the single case of possible vaulting, a 17,500-lb city bus struck a concrete bridge rail, broke through the rail, and came to rest straddling the rail (8). It is uncertain, therefore, whether the structural failure of the rail contributed to the final position of the bus or whether no vaulting would have occurred if the rail had remained intact. Because of the questionable result of that test and the unusually large test vehicle that was employed, it is safe to say that vaulting, as a result of curb-guardrail dynamic interaction, has not been identified as a serious problem in any known test program.

Engineering intuition suggests that vaulting is a problem, however, and attempts have been made to use vehicle-curb dynamic jump data as a basis for specifying guardrail height and setback as a function of curb height. The dynamic jump phenomenon is associated with the jumping motion of the vehicle as it mounts the curb and is bounced into the air. The term dynamic jump was first coined by researchers at the California Division of Highways during the first impact investigations of curb-guardrail combinations in 1955 (7). An example of one of the dynamic jump curves published at that time is shown in Figure 1.

Based on those jump curves, it was concluded that guardrails (in this case bridge rails) used in combination with a curb and set back farther than 5 in. from the curb face must be higher than guardrails used without a curb. The formula arrived at for barrier curbs between 9 and 12 in. high required that the guardrail height be increased 5 in. for each 1 ft of setback up to a maximum height of 48 in.

CURB-GUARDRAIL VAULTING ANALYSIS

Dynamic jump data derived from curb-impact simulation exercises were used to predict the vaulting characteristics of the various MDSH curb-guardrail combinations. The curb impact simulation exercises were carried out with the HVOSM program (10) and are fully described elsewhere (3). Except for the curb dynamic jump data, the vaulting prediction technique is mainly analytical.

The conditions that will result in a vehicle vaulting a guardrail through dynamic interaction with a curb can come about in 2 ways. In one case the vehicle can receive enough impulse from the curb to vault completely over the guardrail without making contact. In the second case the vehicle does not clear the guardrail, makes contact, and rolls over the rail, whose top acts as a fulcrum. Cases of complete vaulting can be readily determined from vehicle geometry and dynamic jump data from curb simulation exercises. Roll-over vaulting, however, requires some additional analysis.

The limiting conditions that will result in roll-over vaulting can be determined by energy and momentum considerations. Suppose, as shown in Figure 2, that the vehicle has been redirected parallel to the guardrail and has just made initial contact. As indicated, the vehicle has a roll rate of $\dot{\phi}_o$ and a velocity $\overline{V}_G$ in a plane normal to the rail line. It is assumed that the line of contact is the axis 0, the axis about which the vehicle would roll if roll-over vaulting occurs, and that this axis remains fixed. $\overline{V}_G$ can then be divided into velocity components along and normal to the line between the vehicle c.g. and the axis of rotation, $\overline{V}_a$ and $\overline{V}_n$, respectively.

It will be assumed now that the velocity component $\overline{V}_a$ is lost through energy dissipated in the collision process. (That is, the impulsive forces acting along the line between the c.g. and axis of rotation are dissipated in a perfectly inelastic collision process. This velocity component contributes nothing to the resulting roll-over phenomenon and merely allows the vehicle to remain in contact with the rail without rebound.) The resulting vehicle motion will be a pure rotation about the point 0.

The only torque applied to the vehicle during the collision process is the result of forces applied at the point 0. Therefore, if moments are summed about this point, the sum of moments will be zero. Similarly, the moment of momentum about the point will be constant during the collision because no moments act to change it. Thus, the moment of momentum about 0 is conserved, and the following equation can be written (11):

$$I_{c.g.}\,\dot{\phi}_o + \frac{W_v}{g}\,DV_n = \left(I_{c.g.} + \frac{W_v}{g}\,D^2\right)\dot{\phi}_f \qquad (1)$$

where the initial moment of momentum about 0 is given on the left, and the final moment of momentum about 0 is given on the right. Therefore, just after impact, the vehicle angular rate about 0, as the result of the collision, will be

$$\dot{\phi}_f = \frac{I_{o.g.}\dot{\phi}_o + \frac{W_v}{g} DV_n}{I_{o.g.} + \frac{W_v}{g} D^2} \tag{2}$$

where

$I_{o.g.}$ = vehicle roll moment of inertia about a longitudinal axis through the c.g.,
$\dot{\phi}_o$ = vehicle roll rate about a longitudinal axis through the c.g., and
W_v = total vehicle weight.

The remaining terms shown in Figure 2 are defined as follows:

$F = F_o + K + (C - L)S$
$G = -(z' + F)$
$h = \frac{G - d \sin \phi_o}{\cos \phi_o}$
$D = \sqrt{h^2 + d^2} = \tan^{-1} \frac{h}{d}$

The limiting conditions that will result in roll-over vaulting can now be determined by energy considerations. Suppose that at the time of initial guardrail contact the vehicle is in such a position and has just the necessary angular and linear velocities to roll over the guardrail and no more. Under those conditions, as the vehicle rolls it will come to rest with its c.g. directly over the rail top, as shown in Figure 2, when $\phi + \beta = 90$ deg. The vehicle's potential energy at this roll position will just equal the kinetic energy associated with the angular velocity at the time of initial impact.

The kinetic energy just after impact is given by the expression

$$KE = \tfrac{1}{2}\left(I_{o.g.} + \frac{W_v}{g} D^2 \dot{\phi}_f^2\right) \tag{3}$$

The potential energy relative to a horizontal reference line through the pivot point is

$$PE = W_v D \sin(\phi + \beta) \tag{4}$$

The potential energy at initial impact is

$$PE = W_v D \sin(\phi_o + \beta) \tag{5}$$

and at the neutral point, where $\phi + \beta = 90$ deg, is

$$PE = W_v D \tag{6}$$

The difference in the 2 quantities is the kinetic energy that is converted to potential energy as the vehicle rolls over.

Thus, if the roll motion results in the vehicle coming to rest at $\phi + \beta = 90$ deg, then

$$\tfrac{1}{2}\left(I_{o.g.} + \frac{W_v}{g} D^2\right)\dot{\phi}_{fr}^2 = W_v D[1 - \sin(\phi_o + \beta)]$$

or

$$\dot{\phi}_{fr} = \sqrt{\frac{2W_v D[1 - \sin(\phi_o + \beta)]}{I_{o.g.} + \frac{W_v}{g} D^2}} = \Lambda \tag{7}$$

$\dot{\phi}_{fr}$ (= Λ) is the roll rate just necessary to cause the vehicle to come to rest at $\phi + \beta$ = 90 deg. If the vehicle does not come to rest and $\dot{\phi}_f$ exceeds $\dot{\phi}_{fr}$, roll-over vaulting will occur, and vice versa.

In using Eq. 7, one must make several assumptions regarding the choice of the time point for values of ϕ_o, $\dot{\phi}_o$, and $\overline{V}_n$. As the vehicle crosses the curb, it does not strike the guardrail such that the vehicle is parallel to the rail as shown in Figure 2. Rather, as shown in Figure 3, the left front of the vehicle first strikes the rail, and the vehicle rotates parallel to the rail as it is redirected. During the process the distance P varies from H $\sin(\alpha + \epsilon)$ to d. Therefore, whether roll-over vaulting will occur was determined by evaluating Eq. 7 for the most adverse values of ϕ_o, $\dot{\phi}_o$, and $\overline{V}_n$ occurring during the interval of redirection. In addition, values of F_o representing both the top and bottom of the W-beam guardrail were chosen as pivot points so as to bound the effects of barrier torsional deflection. Predictions of satisfactory curb-guardrail performance with respect to roll-over vaulting are, therefore, expected to be conservative.

RESULTS

Each of six curb-guardrail combinations was evaluated by the use of Eq. 7. Initial values for ϕ_o, $\dot{\phi}_o$, Z′, and $\overline{V}_n$ were obtained from simulated curb-impact runs, which are described elsewhere (3). A plan view of a typical curb impact run from which these data were obtained is shown in Figure 4. Curb and gutter cross sections used in combination with the various guardrail and median barrier designs are shown in Figure 5.

Curbs A, B, and D and Dual Blocked-Out Median Barrier

A typical cross section of the dual blocked-out median barrier with curbs A, B, or D is shown in Figure 6. The dimension C (Fig. 2) has a maximum value of 167 in., or 13 ft 11 in. The minimum value was taken to be 3 ft or 35 in. (i.e., the minimum distance between the barrier face and the back of the curb and gutter section is 4 in.).

Results from the application of Eq. 7 and the assumptions described thereafter are given in Table 1. The ratio of max $\dot{\phi}_f/\Lambda$ is never greater than one for any of the impact conditions. Therefore, neither vaulting (jumping the rail completely without contact) nor roll-over vaulting occurs. For curb A, the closest approach to incipient roll-over vaulting occurs for the 60-mph and 25-deg case with the rail set back 12 ft and with the pivot point assumed to be at the rail bottom. The ratio for these conditions is 0.79. Some of the data for the 60-mph and 10-deg case are missing because the vehicle was entrapped by the curb before reaching those setback distances. The highest value for curb B is 0.47 and occurs at 60 mph and 25 deg for a 12-ft setback. The largest value for curb C is 0.31 and also occurs in the 60-mph and 25-deg case near maximum setback.

On the basis of the analysis presented here, it can be concluded that curbs A, B, and D each will perform satisfactorily in combination with all standard setback configurations of the dual blocked-out median barrier.

Curbs B and D and Type B Guardrail

A typical installation for a type B guardrail in combination with either curb B or D is shown in Figure 7. The setback dimension C is 25 in. for curb B and 23 in. for curb D. Data are given in Table 2. Maximum values occur for 60-mph and 25-deg impact conditions. In neither situation is there a likelihood of vaulting, however. It can be concluded, therefore, that curbs B and D can be expected to perform satisfactorily in combination with the type B guardrail.

Curb C and Type B Guardrail

A typical installation combination for curb C and type B guardrail is also shown in Figure 7, and data are given in Table 3. The setback is 30.5 in. The highest value is 0.40 for V = 50 mph and α = 25 deg. Therefore, roll-over vaulting is not expected to occur, and this curb-guardrail combination can be expected to perform satisfactorily.

Figure 1. Dynamic jump curves.

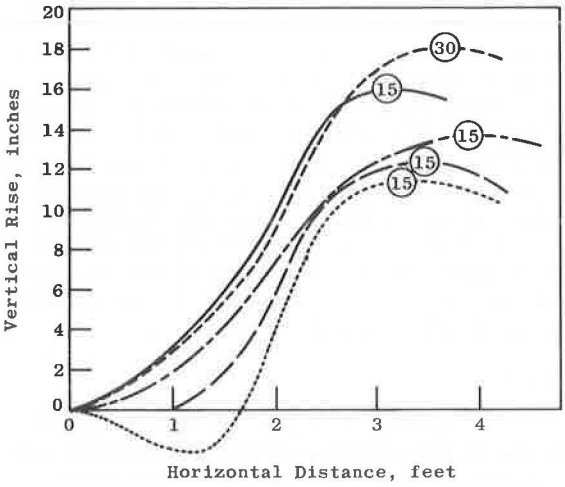

Curb	Angle	Speed	Curve
A9	7.5	60	– – – –
A9	15.0	30	———
A10	15.0	45	—·—·—
A10	20.0	30	·····
A11	20.0	30	———

NOTE: Circled numbers indicate distance in feet along vehicle path from point of impact to crest of jump.
Vertical rise is referenced to right front of car frame.

Figure 2. Roll-over vaulting analysis geometry.

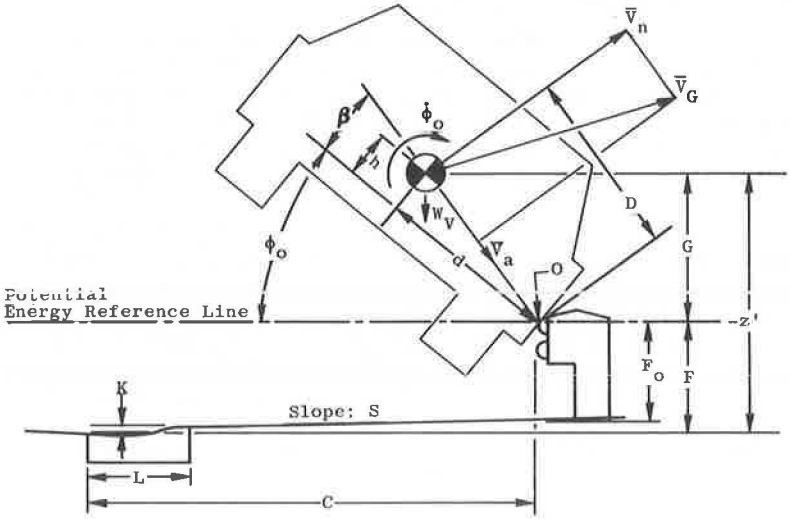

Figure 3. Redirection geometry.

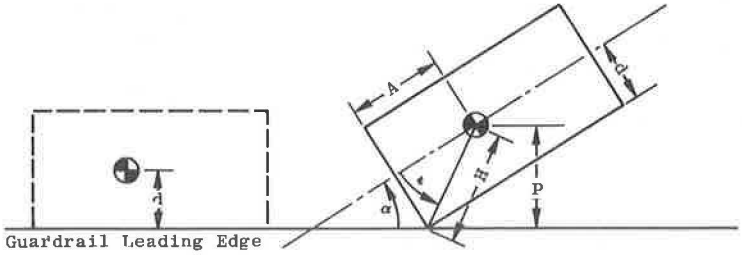

Figure 4. Typical impact simulation at 40 mph, 25 deg, and sloped median.

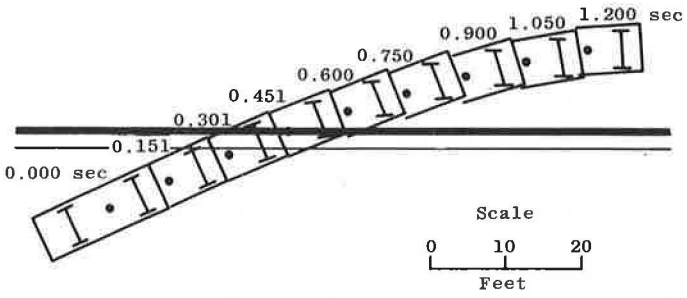

Figure 5. Michigan standard curb sections.

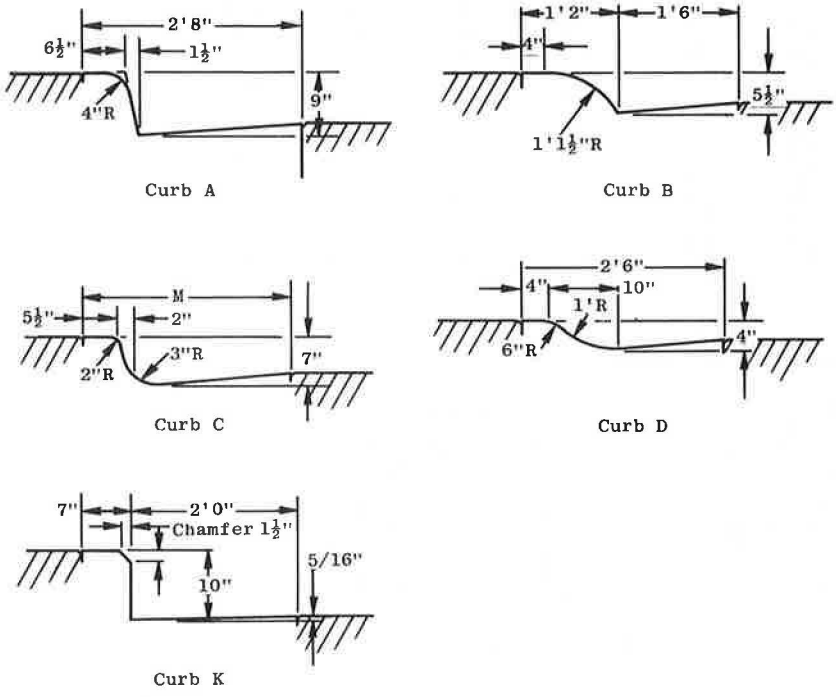

Figure 6. Typical median with curbs A, B, or D and dual blocked-out median barrier.

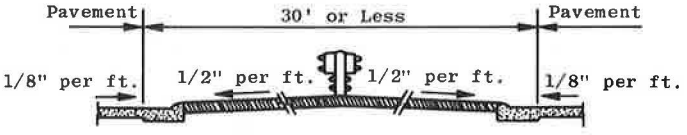

Table 1. Ratio of max $\dot{\phi}_f/\Lambda$ for curbs A, B, and D and dual blocked-out median barrier.

Initial Conditions			Curb A		Curb B		Curb D	
V (mph)	α (deg)	C (ft)	Rail Top, 32.125 In.	Rail Bottom, 20.125 In.	Rail Top, 32.125 In.	Rail Bottom, 20.125 In.	Rail Top, 32.125 In.	Rail Bottom, 20.125 In.
40	25	14	-0.03	0.16	-0.12	0.30	-0.14	0.27
		12	-0.05	0.25	-0.10	0.30	-0.18	0.24
		10	-0.06	0.28	-0.15	0.24	-0.21	0.21
		8	-0.03	0.32	-0.16	0.25	-0.21	0.16
		6	-0.03	0.27	-0.24	0.12	-0.26	0.11
		4	-0.15	0.14	-0.27	0.13	-0.25	0.13
		3	-0.20	0.16	-0.26	0.13	-0.26	0.14
60	10	14	—	—	-0.06	0.17	-0.06	0.17
		12	—	—	-0.05	0.20	-0.04	0.20
		10	—	—	-0.05	0.19	-0.08	0.16
		8	0.24	0.32	-0.11	0.12	-0.13	0.09
		6	0.25	0.33	-0.13	0.08	-0.14	0.07
		4	0.25	0.34	-0.14	0.07	-0.16	0.08
		3	-0.05	0.14	-0.15	0.08	-0.17	0.08
60	25	14	0.15	0.74	-0.18	0.46	-0.26	0.31
		12	0.19	0.79	-0.18	0.47	-0.28	0.30
		10	0.09	0.67	-0.27	0.35	-0.32	0.22
		8	-0.01	0.57	-0.30	0.31	-0.35	0.23
		6	-0.28	0.29	-0.41	0.11	-0.40	0.14
		4	-0.37	0.17	-0.38	0.16	-0.36	0.21
		3	-0.42	0.14	-0.45	0.13	-0.39	0.21
80	10	14	0.18	0.22	-0.06	0.25	-0.10	0.25
		12	0.18	0.23	-0.05	0.25	-0.10	0.25
		10	0.18	0.24	-0.07	0.28	-0.11	0.18
		8	0.13	0.36	-0.15	0.19	-0.17	0.12
		6	0.14	0.38	-0.17	0.13	-0.17	0.10
		4	0.16	0.39	-0.20	0.11	-0.21	0.12
		3	-0.10	0.17	-0.21	0.11	-0.22	0.11

Figure 7. Type B guardrail with curbs B, D, and C.

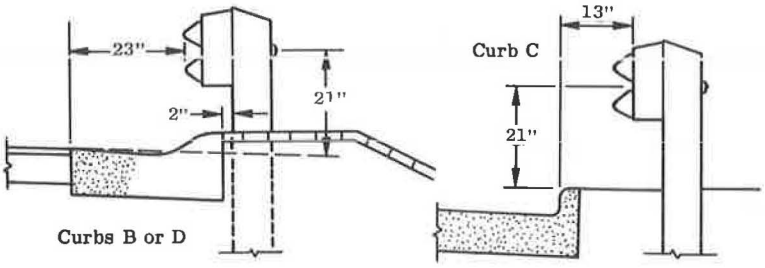

Table 2. Ratio of max $\dot{\phi}_f/\Lambda$ for curbs B and D and type B guardrail.

Initial Conditions		Curb B[a]		Curb D[b]	
V (mph)	α (deg)	Rail Top, 27 In.	Rail Bottom, 15 In.	Rail Top, 27 In.	Rail Bottom, 15 In.
40	25	-0.15	0.31	-0.11	0.35
60	10	-0.09	0.19	-0.07	0.23
60	25	-0.19	0.44	-0.15	0.52
80	10	-0.12	0.27	-0.09	0.32

[a]C = 25 in. [b]C = 23 in.

Table 3. Ratio of max $\dot{\phi}_f/\Lambda$ for curb C and type B guardrail.

Initial Conditions			
V (mph)	α (deg)	Rail Top, 27 In.	Rail Bottom, 15 In.
30	25	-0.07	0.25
50	10	-0.03	0.17
50	25	-0.14	0.40

Note: C = 30.5 in.

Curb K and Types B and C Guardrail

Typical cross sections showing curb K in combination with type B and type C guardrails are shown in Figure 8. Tabulated data for predicting vaulting are given in Table 4. Because there is only a $1\frac{1}{2}$-in. difference in elevation in the 2 rails, the data are somewhat similar. The type B rail is the lower of the two, however, and the values for it are slightly higher.

The maximum value of $\dot{\phi}_t/\Lambda$ is 0.70, and that occurs for a maximum setback of 42 in., an impact speed of 80 mph, and an angle of 10 deg. This value indicates no vaulting will occur. An indicated trend, however, suggests vaulting might occur if the setback were on the order of 5 ft. Therefore, it should be emphasized that a prediction of no vaulting is solely based on an assessment of the indicated design (Fig. 8) with the specified setback limits. With these ground rules, curb K in combination with guardrail types B and C can be expected to perform satisfactorily.

VALIDATION OF RESULTS

The results presented in this section hinge on the validity of the HVOSM model in simulating vehicle-curb impacts. The simulation validity was checked by a comparison between the simulation results and the dynamic jump data obtained from the California curb-impact studies made in 1963 (12). Unfortunately, the only vehicles used in those tests were small sports cars and a 1960 Ford 4-door sedan. This latter vehicle weighed 4,318 lb, whereas the 1966 Ford Custom used in the simulation weighed 3,510 lb. The comparison is, therefore, not an exact one but should be representative.

The test and simulation comparison is shown in Figure 9. The curves represent the trajectory of a point on the vehicle fender closest to the curb as it crosses a 6-in. mountable curb at 60 mph and 25 deg. The maximum difference between the 2 trajectories is about 4 in.; the lighter 1966 vehicle jumps higher than the 1960 model. The simulation results are within a reasonable tolerance of actual test data. Furthermore, because the simulated vehicle jumps higher, it seems probable that, if an error exists in predicting curb-guardrail vaulting performance, it lies in predicting vaulting when none occurs rather than vice versa. Thus, additional evidence suggests that the vaulting performance evaluations are conservative.

CONCLUSIONS AND RECOMMENDATIONS

Curb-guardrail combinations of various varieties have been tested by several organizations. Dynamic jump data have shown the tendency for vehicles to bound into the air after a curb impact. The possibility, therefore, exists for a vehicle to receive a jump impulse from the curb and vault over the adjacent guardrail. No conclusive evidence of a vaulting problem has been identified as the result of any known test program, however. Furthermore, the conservative analysis of vaulting potential carried out for each of the 6 curb-guardrail combinations predicts no vaulting. Therefore, although intuition suggests that vaulting is a potential problem, this has not proved to be the case. Care should be taken, however, to ensure that height and setback of guardrails installed behind curbs satisfy prescribed minimums (3).

Current practice is oriented toward not using curbs in front of guardrails. It would seem worthwhile to examine this policy in light of the current findings. A recently developed barrier curb appears to be an efficient redirective device (13). Seventy percent of the vehicles striking this curb in urban traffic conditions can be expected to be redirected (3). Vehicle damage in these encounters can be expected to be modest—far less than can be expected if the vehicle were to strike a guardrail. For those vehicles climbing the curb, a secondary retainer is obviously required. Thus, the utility of the curb-guardrail combination is evident. It is recommended that further research be initiated to better define the cross section for a barrier curb optimized for redirection. Furthermore, it is recommended that the total redirective performance of this curb be optimized in combination with standard guardrail configurations.

Figure 8. Types B and C guardrail with curb K.

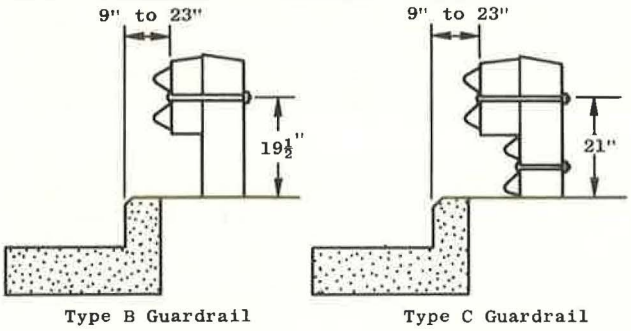

Table 4. Ratio of max $\dot{\phi}_f/\Lambda$ for curb K and types B and C guardrail.

Initial Conditions			Type B		Type C	
V (mph)	α (deg)	C (in.)	Rail Top, 25.5 In.	Rail Bottom, 13.5 In.	Rail Top, 27 In.	Rail Bottom, 15 In.
40	25	42	0.01	0.40	-0.03	0.34
		36	-0.03	0.35	-0.07	0.30
		30	-0.03	0.35	-0.07	0.30
60	10	42	0.32	0.46	0.30	0.45
		36	0.12	0.30	0.10	0.28
		30	0.06	0.26	0.04	0.23
60	25	42	-0.11	0.53	-0.18	0.45
		36	-0.13	0.48	-0.19	0.40
		30	-0.17	0.42	-0.24	0.34
80	10	42	0.43	0.70	0.40	0.67
		36	0.08	0.37	0.04	0.33
		30	0.01	0.29	-0.02	0.25

Figure 9. Comparison of test and simulation dynamic jump data.

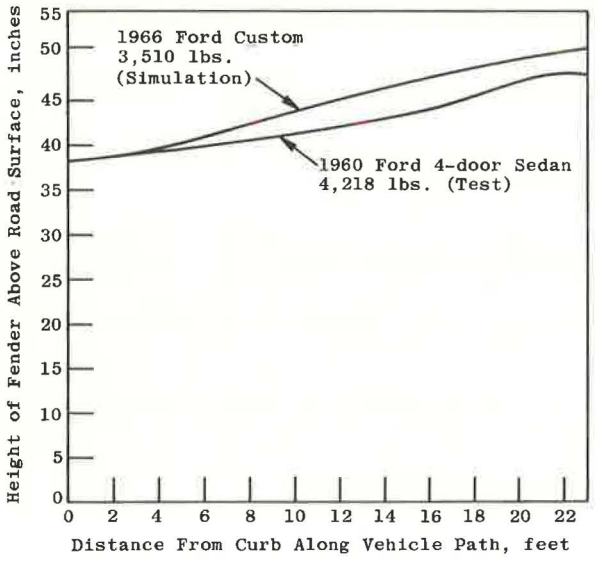

ACKNOWLEDGMENT

The research reported here was financed under the Highway Planning and Research Program and was sponsored by the Michigan Department of State Highways and the Federal Highway Administration. The contents of this paper reflect the views of the author, who is responsible for the facts and the accuracy of the data presented. The contents do not necessarily reflect the official views or policies of the sponsors. This report does not constitute a standard, specification, or regulation.

REFERENCES

1. Michie, J. D., and Calcote, L. R. Location, Selection, and Maintenance of Highway Guardrails and Median Barriers. NCHRP Rept. 54, 1968.
2. Michie, J. D., and Bronstad, M. E. Location, Selection, and Maintenance of Highway Traffic Barriers. NCHRP Rept. 118, 1971.
3. Dunlap, D. F., Grote, P., Fram, D. M., and Mashinter, W. Investigation of the Dynamic Impact Characteristics of Roadside Structures. Highway Safety Res. Inst., Univ. of Michigan, Ann Arbor, May 1972.
4. Böhringer, A., Roschmann, R., and Domhan, M. Collision Tests on Guardrails. Federal Ministry of Transp. and Road Res. Soc., West Germany, Rept. 98, 1970.
5. Graham, M. D., Burnett, W. C., Gibson, J. L., and Freer, R. H. New Highway Barriers: The Practical Application of Theoretical Design. Highway Research Record 174, 1967, pp. 88-183.
6. Beaton, J. L., and Field, R. N. Dynamic Full-Scale Tests of Median Barriers. HRB Bull. 266, 1960, pp. 78-125.
7. Field, R. N., and Beaton, J. L. Final Report of Full-Scale Dynamic Tests of Bridge Curbs and Rails. California Div. of Highways, Aug. 1957.
8. Beaton, J. L., and Field, R. N. Dynamic Full-Scale Tests of Bridge-Rails. California Div. of Highways, Dec. 1960.
9. Hénault, G. G., and Perron, H. Research and Development of a Guide Rail System for a High-Speed Elevated Expressway. Highway Research Record 152, 1966, pp. 36-65.
10. McHenry, R. R., and Deleys, N. J. Vehicle Dynamics in Single Vehicle Accidents—Validation and Extension of a Computer Simulation. Cornell Aeronaut. Lab., Rept. VJ-2251-V-3, Dec. 1968.
11. Goldstein, H. Classical Mechanics. Addison-Wesley, Reading, Mass., 1959.
12. Field, R. N., and Johnson, M. H. Dynamic Full-Scale Impact Tests of Cable Type Median Barriers—Test Series IX. California Div. of Highways, June 1965.
13. Elsholz, J. Tests Concerning the Turn-Away Effect of Curb Stones. Strasse und Autobahn, Vol. 19, No. 4, April 1968.

ENERGY-ABSORBING CORRUGATED METAL HIGHWAY BUFFER

Richard J. Fay and Michael A. Kaplan, Denver Research Institute, University of Denver

A new concept in energy-absorbing highway buffers was developed and tested with scale models. The buffer is made of corrugated-metal elements that deform plastically on impact and absorb the energy of the impacting vehicle. The buffer has a parabolic shape to form a gradual transition between an energy-absorbing buffer for frontal impacts and an energy-absorbing guardrail for glancing, side impacts. The model buffer was found to perform well in a variety of situations including head-on, angled, and glancing impacts. Scale-model testing was found to be a valuable tool; tests were conducted for a small fraction of the cost and time of full-scale tests. Additional scale-model tests and some full-scale tests will need to be conducted before the design is completed.

•ENERGY-ABSORBING highway buffers should be designed according to certain performance criteria (1):

1. The buffer mass activated at impact should be small compared to the weight of the impacting vehicle;
2. The impacting vehicle should be assumed to be rigid;
3. The force-displacement curve should be such that a range of vehicles can be stopped without excessive loads being imposed on the lighter vehicles or excessive stopping distances being required for the larger vehicles;
4. Buffer deformation and motion should be localized to the immediate area of the impacting vehicle;
5. The buffer should not eject material onto the traveled roadway;
6. The buffer should not store mechanical energy;
7. The center of gravity of each portion of the barrier should be above the center of vehicle load application;
8. The buffer should not produce significant angular accelerations until the vehicle has been entrapped; and
9. The lateral stiffness of the buffer should be increased greatly toward the base.

The objective of our program was to develop a simple, inexpensive buffer satisfying those criteria and capable of performing well in a broad spectrum of impact situations including head-on, head-on off-center, angled-nose, angled-side, and glancing impacts. Further, it was desired that the barrier meet specific requirements of potential locations in the Colorado highway system. In general, those included (a) the capability to stop 60-mph vehicles weighing from 2,000 to 6,000 lb and having an average deceleration not exceeding 12.5 g in head-on impacts, (b) the capability to stop vehicles impacting the nose at speeds as high as 60 mph and angles as great as 20 deg to the longitudinal axis with lateral barrier displacement not exceeding 7 ft, and (c) the capability to stop vehicles impacting the side at speeds as high as 60 mph and angles as great as 10 deg with lateral barrier displacement not exceeding 7 ft and the vehicle not impacting the rigid support structure.

The authors initially conceived the idea of using a family of parabolic corrugated-metal arches oriented parallel to the surface of the roadway so that they would form a guardrail for glancing side impacts and would deform plastically to absorb the energy of a vehicle impacting the nose. This buffer was subjected to a variety of scale-model

tests; modified buffers were also tested. Scale-model testing was used throughout the program to minimize costs. The validity of this approach has been demonstrated (2).

TESTING

Buffer testing was done with 1:25 scale models and a facility developed earlier (2). In the model tests, only the features known to affect the performance were simulated. The vehicle was a rigid wooden block equipped with wheels; it had no doors, fenders, lights, or other trim and did not deform on impact with the barrier. However, it had the proper mass and mass distribution (it was hollowed out on the underside), size, and coefficient of friction between the tires and the operating surface. Therefore, it was similar to the full-sized vehicle dynamically, except for minor differences that might occur from suspension-system deformation on the full-sized vehicle. The rigid model vehicle had the advantages of being reusable, being standardized, and giving conservative results (vehicle deformation reduces the amount of energy that the buffer must dissipate). The scale-model vehicle was equipped with brakes to simulate the resistance to rebound of a vehicle with the transmission in gear.

Scale Factors

It was shown in the earlier report (2) that the 1:25 scale model should have a fifth of full-scale velocity to produce impact accelerations of the same magnitude in the model and the prototype. For ease of interpretation, the results of the tests were appropriately factored to full scale.

Facilities

The scale-model barrier (buffer) testing facility is shown in Figure 1. It consists of a table equipped with a pneumatic launcher for the scale-model vehicle, an adjustable mounting for the barrier, a backstop to prevent the vehicle from leaving the table, and instrumentation for controlling the speed and taking data from the barrier crash. The speed of the vehicle was controlled by a pressure regulator in the pneumatic system. A timing station equipped with photo transistors and an electronic chronograph was used to take vehicle velocity data prior to impact with the buffers. A 16-mm high-speed movie camera mounted above the table was used to photograph the interaction of the vehicle and the barrier. A Vanguard motion analyzer was used to analyze the movies to determine the approximate displacement, velocity, and acceleration of the vehicle as functions of time. A 35-mm camera was used to take before-and-after photographs of the buffers.

Buffer Construction

The buffers were made of 0.003-in.-thick 1100-0 aluminum sheet cut into strips and corrugated by a pair of specially designed rollers. The corrugated strips were formed by hand, on curved dies, to the desired shape. Contact cement was used to fasten these together to form the buffers.

BUFFER DEVELOPMENT

Three well-defined types of metal arch buffers were studied in the course of the project: Type 1 consists entirely of 2 or more parabolic corrugated-metal arches, type 2 consists of metal arches and barrels, and type 3 consists of corrugated-metal arches and corrugated-metal stiffening elements.

Type 1

The original buffer, shown in Figure 2, performed well in head-on impacts (Fig. 3) and satisfied many of the buffer performance criteria. We learned that the force-displacement curve could be modified considerably by adjusting the corrugation depth and metal thicknesses in the 2 arches and by varying the number of arches in the buffer.

Figure 1. Scale-model barrier testing facility.

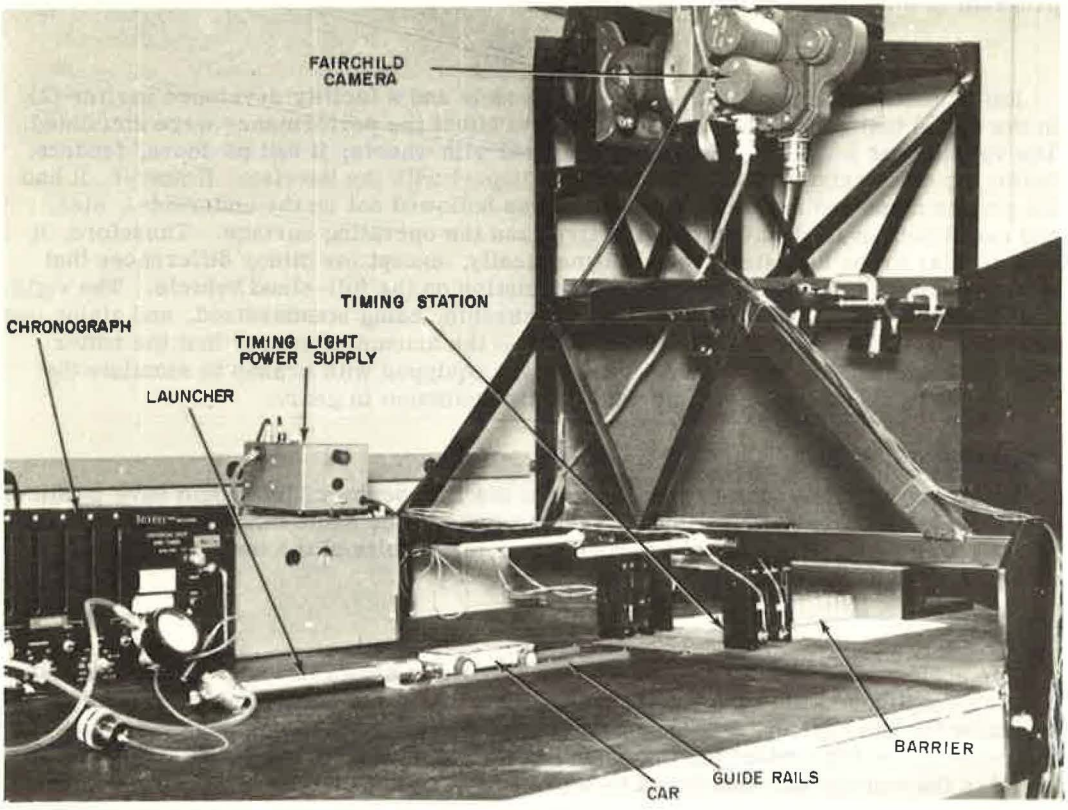

Figure 2. Type 1 buffer.

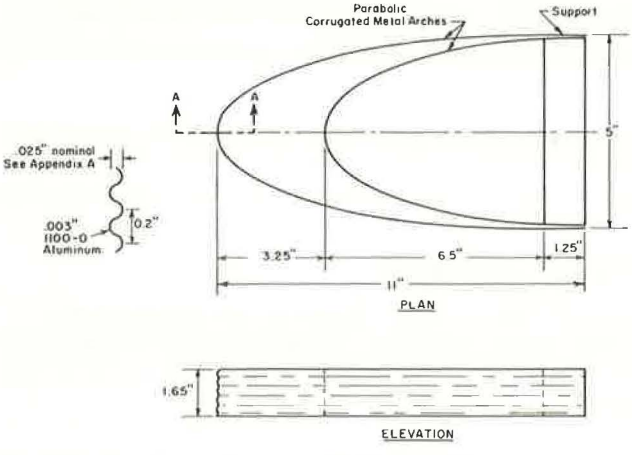

Note: Barrier elements are fastened together by contact cement at overlap points or as indicated.

Figure 3. Performance of type 1 buffer and Texas barrel barriers in head-on impact.

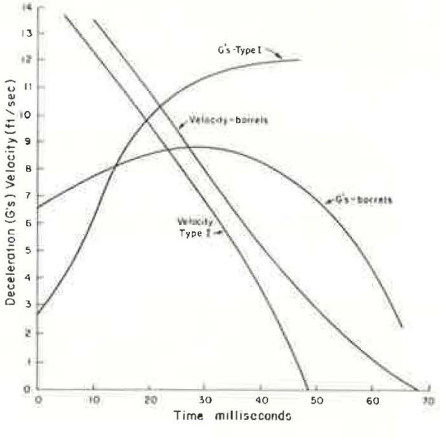

In glancing impacts the buffer acted as an energy-absorbing guardrail, redirecting the vehicle. Although holding considerable promise, this buffer had 2 serious limitations: (a) It provided no protection from the supporting structure for a hard glancing or an angled-side impact because the buffer arches terminated flush with the side of the support, and (b) it exhibited excessive lateral displacement in impacts at angles greater than approximately 10 deg.

In an attempt to maintain the simplicity of the buffer while providing protection from the support and minimizing the lateral displacement, we added stiffening leaves to the sides in the hope that this would increase lateral stiffness near the support so that a glancing vehicle would be redirected around the support. These were relatively ineffective in protecting the vehicle from the support, but the lateral displacement in angled impacts was reduced and the head-on performance was not adversely affected.

Type 2

From the results with the type 1 buffer, we concluded that it was necessary to increase lateral rigidity and to space the outside arch away from the side of the support to prevent vehicle contact with the rigid structure. This led to the development of the type 2 buffer (Fig. 4), which was wider, at its base, than the support. The stand-off between the outer arch and the side of the support was filled with scaled 55-gal drums like those used in the barrel buffer test reported earlier (2). The barrels were attached to the 2 arches, stiffening the buffer laterally.

Type 2 buffer performed very well in head-on, glancing, and angled-side impacts, but the lateral deflection in angled impacts was excessive. Also, the portion involving the barrels was too rigid. In some off-center head-on impacts and in some angle impacts on the nose, the barrel sections tended to act as columns, causing high g forces on the vehicle.

Type 3

The barrels were eliminated to minimize the column effect, internal stiffeners were added to provide lateral stiffening, and the spacers between the 2 arches were retained. The resulting type 3 buffer (Fig. 5) performed well in a variety of impact situations including head-on and nose impacts at angles as great as 20 deg to the longitudinal axis as well as angled and glancing impacts. Figure 6 shows a scale-model buffer before and after a head-on impact with a scale-model 4,000-lb vehicle at approximately 60 mph. (In all subsequent tests discussed in this report, a scale-model 4,000-lb vehicle was used.)

High-speed movies were taken of several impacts with the type 3 buffer and analyzed to determine the approximate displacement, velocity, and deceleration of the vehicle as a function of time. Figure 7 shows the results of the head-on test shown in Figure 6. The average deceleration of 7 to 8 g was well within the established limits of 12.5 g average.

A nose impact at 20 deg with the longitudinal axis is shown in Figure 8; the performance curves are shown in Figure 9. The deceleration peak is higher than the head-on impact because stopping distance is limited by the need to hold the lateral deflection of the buffer within the 7-ft limit. Other buffers that use cables for longitudinal stability have still higher decelerations in angle impacts.

The results of 3 tests with 4.0- and 4.5-ft off-center head-on impacts are shown in Figures 10, 11, and 12. The performance is a considerable improvement over that of the type 2 buffer. Performance curves for a 4.5-ft off-center impact are shown in Figure 13. Since significant lateral vehicle movement resulted, both the longitudinal x and transverse y displacements, velocities, and decelerations are plotted; the resultant deceleration is also plotted. In this case, the deceleration is higher than desired although, for this vehicle, it comes close to averaging 12.5 g. A reduction in the overlap of the interior brace would probably bring the deceleration for the off-center impacts down to a more desirable level. In the test shown in Figure 14, a 6.0-ft offset was used and the vehicle was redirected as desired.

The results of 5- and 10-deg nose impacts are shown in Figures 15 through 18. Buffer performance in these tests was excellent.

Figure 4. Type 2 buffer.

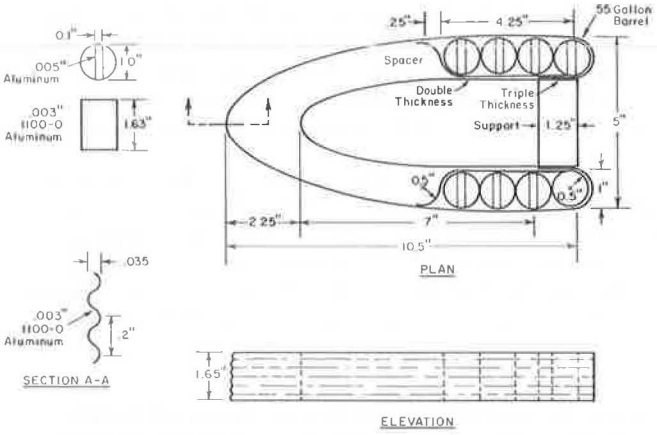

Note: Barrier elements are fastened together by contact cement at overlap points or as indicated.

Figure 5. Type 3 buffer.

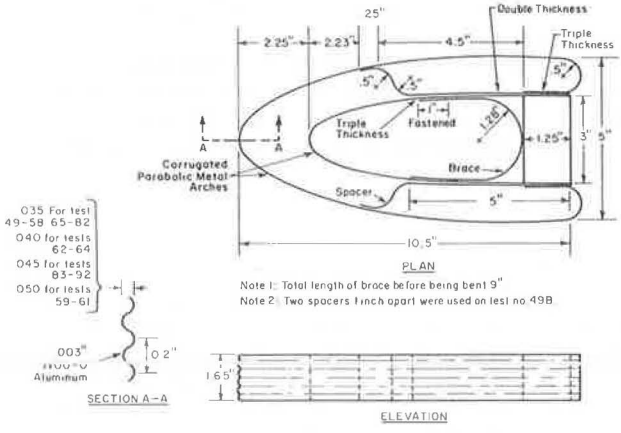

Note 1: Total length of brace before being bent 9"
Note 2: Two spacers 1 inch apart were used on test no. 49B.

Note: Barrier elements are fastened together by contact cement at overlap points or as indicated.

Figure 6. Type 3 buffer test 83, head-on impact at 59.24 mph.

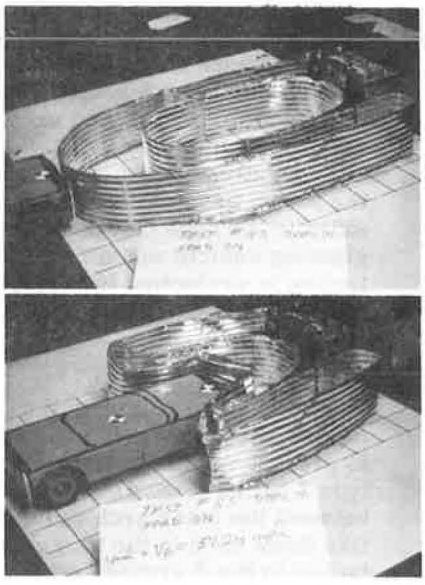

Figure 7. Performance curves for type 3 buffer test 83.

Dependent variables and time are given for full scale barrier
Type of Impact: Head on
Velocity of Impact: 59.24 MPH
Weight of Vehicle: 4000 lbs.

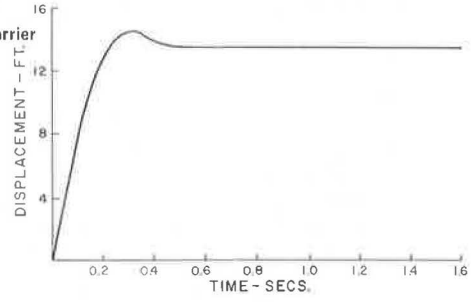

A. Displacement

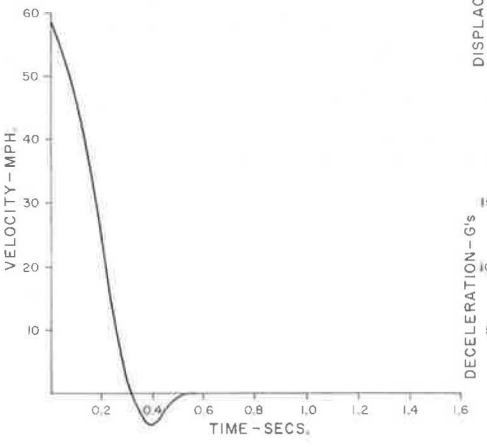

B. Velocity

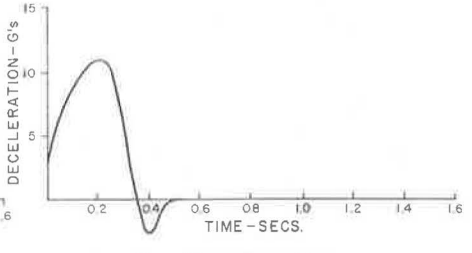

C. Deceleration

Figure 8. Type 3 buffer test 84, 20-deg angle nose impact at 53 mph.

Figure 9. Performance curves for type 3 buffer test 84.

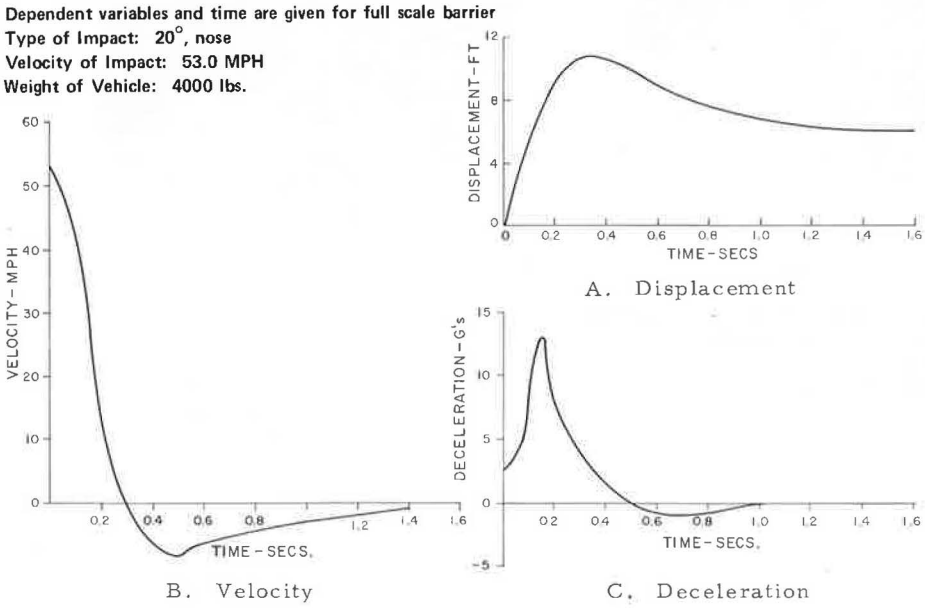

Figure 10. Type 3 buffer test 85, 4-ft off-center head-on impact at 53 mph.

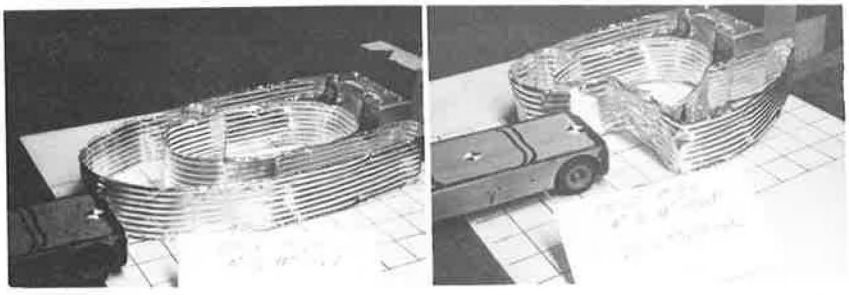

Figure 11. Type 3 buffer test 86, 4-ft off-center head-on impact at 53 mph.

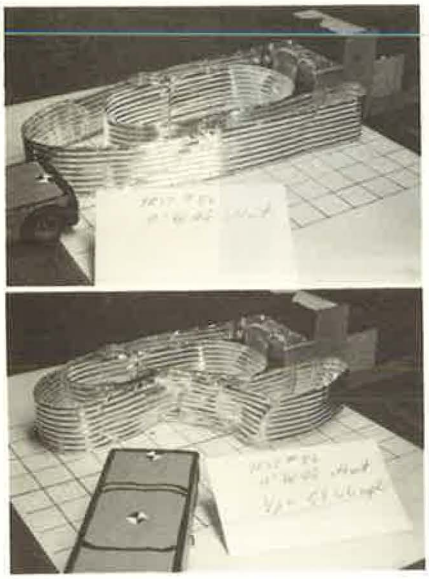

Figure 12. Type 3 buffer test 87, 4.5-ft off-center head-on impact at 54.84 mph.

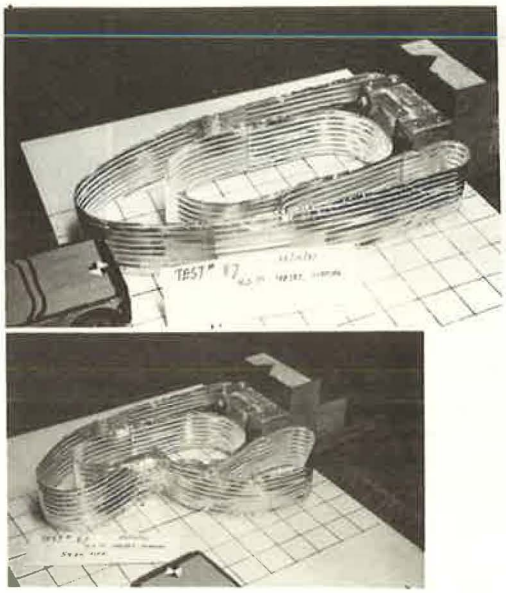

Figure 13. Performance curves for type 3 buffer test 87.

Dependent variables and time are given for full scale barrier
Type of Impact: 4.5 ft. offset, head on
Velocity of Impact: 54.84 MPH
Weight of Vehicle: 4000 lbs.

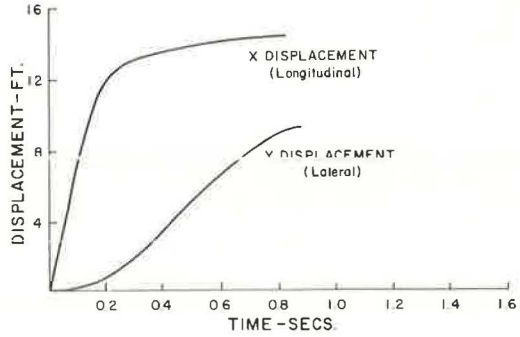

A. Displacement

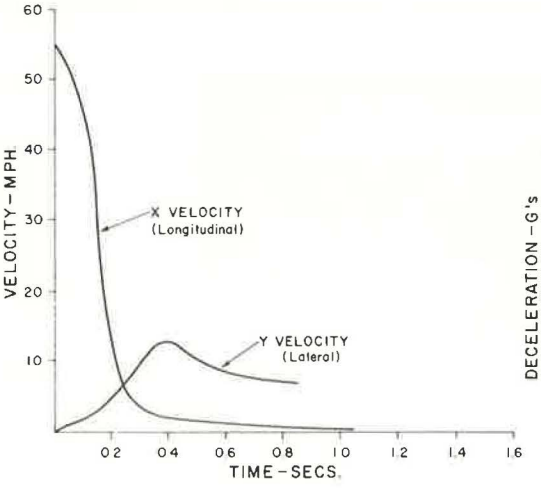

B. Velocity

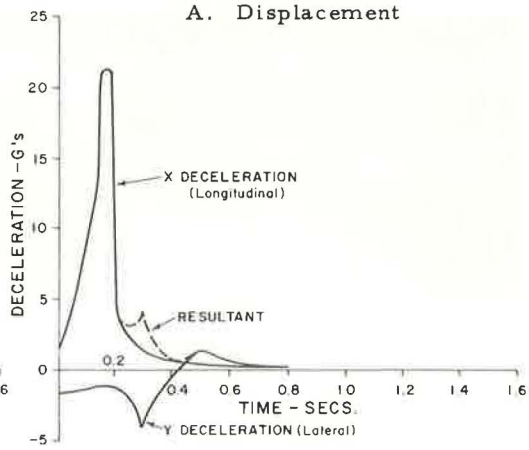

C. Deceleration

Figure 14. Type 3 buffer test 90, 6.0-ft off-center head-on impact at 62.99 mph.

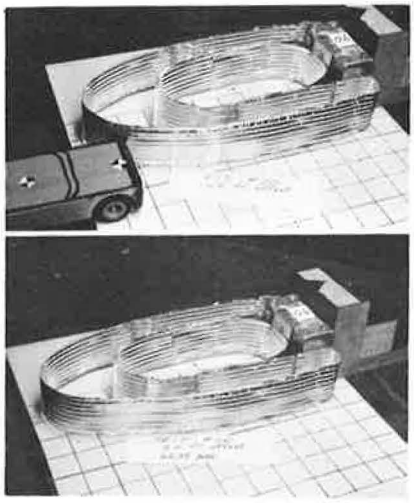

Figure 15. Type 3 buffer test 91, 5-deg angle nose impact at 62.5 mph.

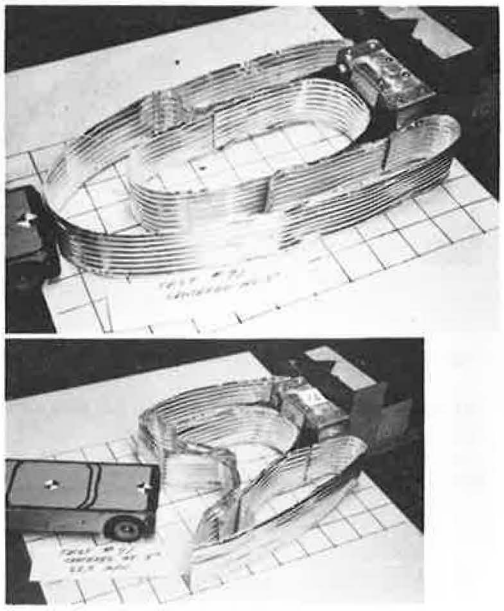

Figure 16. Performance curves for type 3 buffer test 91.

Dependent variables and times are given for full scale barrier
Type of Impact: 5.0°, nose
Velocity of Impact: 62.5 MPH
Weight of Vehicle: 4000 lbs.

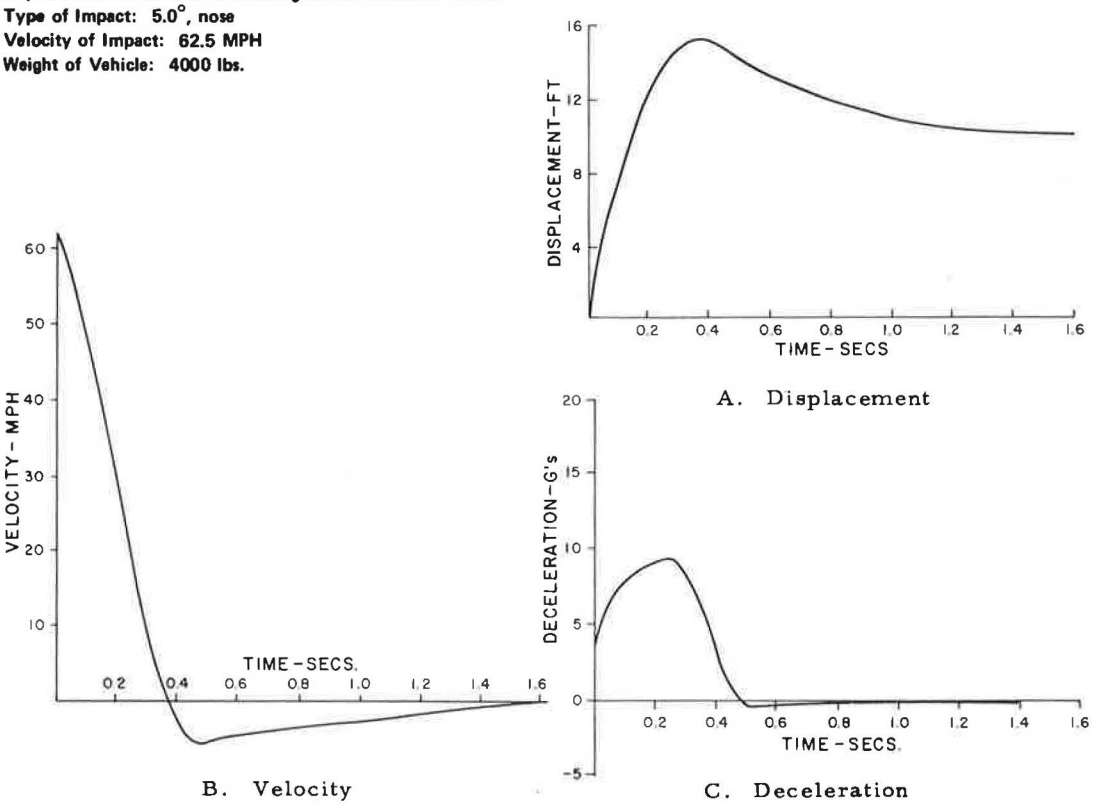

Figure 17. Type 3 buffer test 92, 10-deg angle nose impact at 61.96 mph.

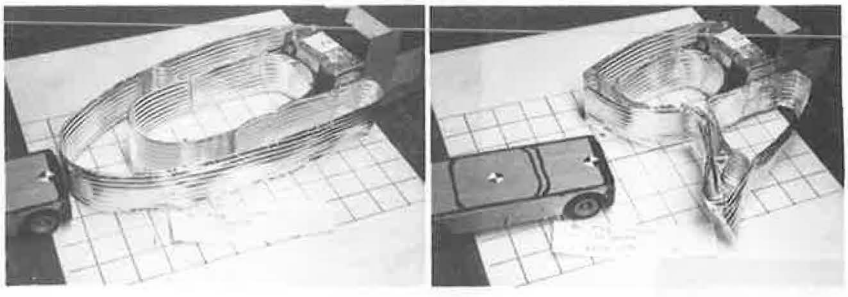

Figure 18. Performance curves for type 3 buffer test 92.

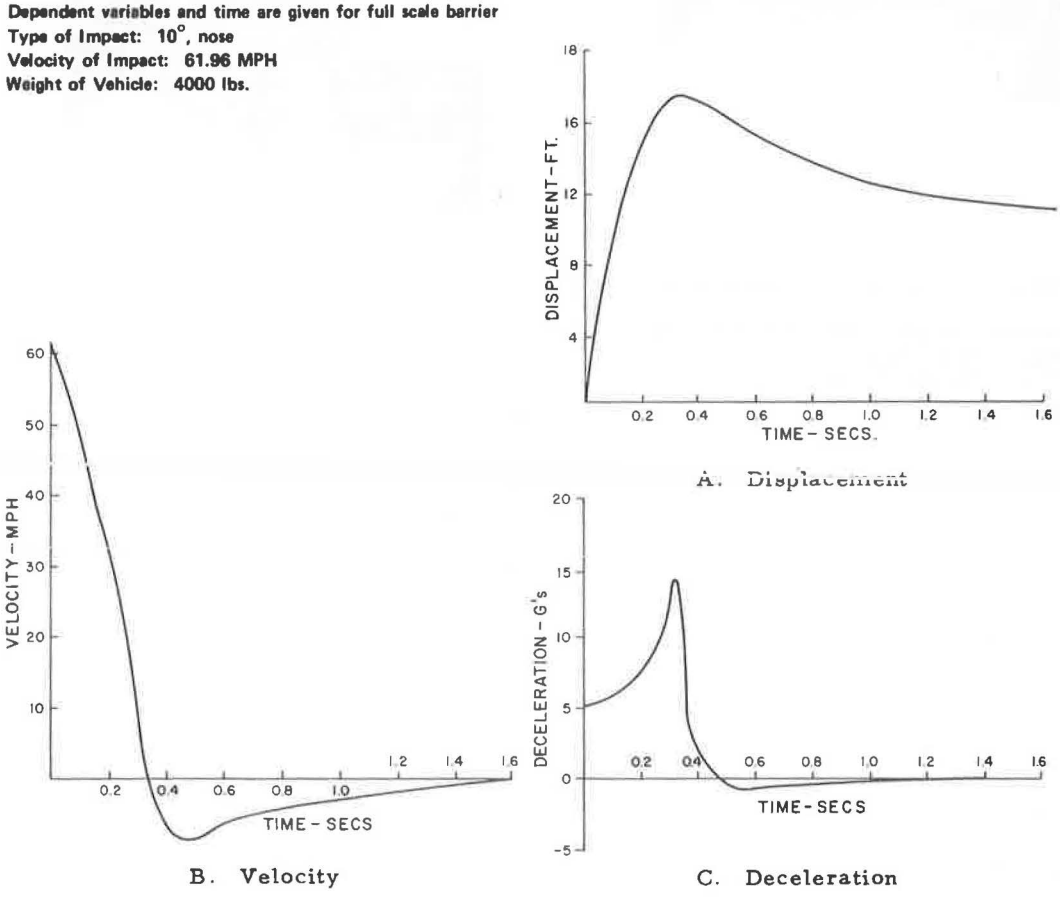

CONCLUSIONS

The corrugated-metal arch buffer, although simple in design, performed very well in a wide variety of scale-model impact situations. The type 3 buffer has demonstrated an overall performance that merits additional studies and, eventually, full-scale tests. In addition, another version of this barrier should be developed for locations where lateral space is limited. This would require the addition of lateral stiffening such as cables, breakaway posts, or shoes in guides to limit the lateral deflection of the buffer in angled impacts so that the buffer cannot encroach on the traveled roadway.

This study has demonstrated the usefulness of scale modeling in the development of a new buffer. The entire program, costing little more than one full-scale buffer crash test, included several different impacts on variations of 3 types of buffers. The results of these tests in the form of before-and-after measurements, photographs, and high-speed films provided valuable insights that can be gained only through testing. The tests were done at a fraction of the cost of full-scale tests. Therefore, the program had a great deal of flexibility within a limited budget.

ACKNOWLEDGMENT

This work was made possible by a contract with the Colorado Department of Highways.

REFERENCES

1. Kaplan, M. A., Hensen, R. J., and Fay, R. J. Space Technology for Auto-Highway Safety. Highway Research Record 306, 1970, pp. 25-38.
2. Fay, R. J., and Wittrock, E. P. Scale-Model Test of an Energy-Absorbing Barrier. Highway Research Record 343, 1971, pp. 75-82.

TEXAS CRASH-CUSHION TRAILER TO PROTECT HIGHWAY MAINTENANCE VEHICLES

E. L. Marquis and T. J. Hirsch, Texas Transportation Institute; and
J. F. Nixon, Texas Highway Department

The Texas crash-cushion trailer, which now has wheels, is a workable and easily used implement for the protection of personnel and equipment, especially during maintenance operations on highways and streets. One crash test to verify the design theory showed that the equations of mechanics predicted results that were very close to the test results. The Texas crash-cushion trailer differs from other crash cushions in that the object supporting the crash cushion is itself movable. This means that fewer steel drums are required but also that the trailer and backup maintenance truck will travel some distance if impacted by an errant vehicle. The distance traveled after impact and the number of steel drums required are determined by equations of momentum and friction.

•THE EFFECTIVENESS of the Texas crash cushion in contributing to highway safety is well documented (5, 7, 8). Previous research and field experience with this device have focused on protecting an errant motorist from a high-speed collision with a rigid obstacle. Common examples are elevated gores and bridge piers in median areas.

The purpose of this research was to use this energy-absorbing device on a trailer to protect slowly moving or stopped maintenance vehicles working on highways. The Texas crash-cushion trailer (TCCT) is to be used to protect highway maintenance equipment and personnel as well as motorists. An important requirement of the TCCT is that it be portable or mobile, easily constructed by highway maintenance personnel, and adaptable to dump trucks and other highway department vehicles.

DESIGN OF TEXAS CRASH-CUSHION TRAILER

The design of the TCCT is based on the law of conservation of momentum and on the dissipation of kinetic energy by plastic deformation of steel drums and through friction. This is somewhat different than the design of fixed crash cushions, which absorb energy by plastic deformation of steel drums only. The critical energy-absorbing condition for the design of the crash-cushion trailer will occur for an impact in which the automobile, crash cushion, and restraining mechanism (usually a truck) are in line at the time of impact (Fig. 1).

For this condition the momentum of the automobile (or striking vehicle) before impact will be equal to the total momentum of the system immediately after impact. Based on plastic impact,

$$\frac{W_c}{g} V_c = \frac{W_c + W_b + W_t}{g} V \qquad (1)$$

where

W_c = total weight of automobile, lb;
W_b = total weight of portable crash cushion, lb;
W_t = total weight of truck, lb;
V_c = velocity of automobile at impact, ft/sec;
V = velocity of entire system immediately after impact, ft/sec; and
g = acceleration due to gravity, ft/sec^2.

Solving for the velocity of the entire system after impact yields

$$V = \frac{W_c}{W_c + W_b + W_t} V_c \tag{2}$$

For a truck weighing 9,500 lb, a portable crash cushion weighing 2,000 lb, an automobile weighing 4,500 lb, and an impact speed of 60 mph (88 ft/sec), we have

$$V = \frac{4,500}{4,500 + 2,000 + 9,500} 88 = 24.75 \text{ ft/sec or } 16.88 \text{ mph}$$

The kinetic energy (KE) of the automobile before impact is computed by the formula

$$KE = \frac{MV^2}{2}$$

$$KE = \frac{4,500 \times (88)^2}{2 \times 32.2} = 541,000 \text{ ft-lb} \tag{3}$$

The kinetic energy of the automobile, crash cushion, and truck after impact is

$$KE = \frac{(4,500 + 2,000 + 9,500)(24.75)^2}{2 \times 32.2} = 152,000 \text{ ft-lb}$$

Consequently, 389,000 ft-lb of energy would be absorbed in the impact by plastic deformation of the steel drums in the crash-cushion trailer.

According to White and Hirsch (1), a single 20-gauge tight-head steel drum with 8-in. diameter holes in the top and bottom will absorb 9,000 ft-lb of energy under slowly applied loads. The dynamic factor has been shown to be 1.5 (7). Therefore, each barrel will absorb 1.5 × 9,000 or 13,500 ft-lb of dynamic energy. This would mean that the portable crash cushion would require 28.8 steel drums, but would have 30 barrels to achieve a rectangular configuration.

Figure 2 was developed as a design aid from the foregoing theory. The number of barrels required is plotted against the weight of the resisting truck for impacting vehicles of 2,000, 4,000, and 45,000 lb. The design impact speed is 60 mph in each case. A crash-cushion trailer generally weighs within 15 percent of the values shown. The design vehicle weight range is that recommended by the Federal Highway Administration (2). Figure 2 can serve as a tool for designing portable crash cushions and for comparing the limiting conditions.

After the barrels have deformed plastically and absorbed 389,000 ft-lb of energy, there still remain 152,000 ft-lb of energy because of the entire system moving at 24.75 ft/sec. If all of the wheels of the truck are locked, then the distance required to stop the vehicle is

$$d = \frac{KE \text{ (after impact)}}{W_t \mu} \tag{4}$$

where μ is the coefficient of friction, say, 0.7 for tires to concrete. Then,

$$d = \frac{152,000}{9,500 \times 0.7} = 22.9 \text{ ft}$$

Portable Crash Cushion in Motion

Although the critical design for the energy absorption of the crash cushion itself is for the stationary condition, the critical condition for the distance traveled after impact occurs when the crash cushion and towing vehicle are in motion. Such a condition, for example, occurs during the protection of a paint-stripping machine. In that instance,

both the impacting vehicle and the impacted assembly have initial momentum and kinetic energy. Based on plastic impact and conservation of momentum,

$$\frac{W_c}{g} V_c + \frac{W_b + W_t}{g} V_t = \frac{W_c + W_b + W_t}{g} V \tag{5}$$

or

$$V = \frac{W_c V_c + (W_b + W_t) V_t}{W_c + W_b + W_t} \tag{6}$$

If V_c = 60 mph and V_t = 10 mph for a 4,500-lb vehicle and 9,500-lb truck,

$$V = \frac{4,500 \times 60 + (2,000 + 9,500)\ 10}{4,500 + 2,000 + 9,500} = 24.06 \text{ mph or } 35.29 \text{ ft/sec}$$

The kinetic energy before impact is

$$KE = \frac{4,500 \times 88^2}{2 \times 32.2} + \frac{11,500 \times 14.667^2}{2 \times 32.2} = 580,000 \text{ ft-lb}$$

The kinetic energy remaining after impact is

$$KE = \frac{(4,500 + 2,000 + 9,500)\ 35.29^2}{2 \times 32.2} = 309,000 \text{ ft-lb}$$

The change in kinetic energy is 271,000 ft-lb.

Because 271,000 is less than 389,000, the stationary condition governs for plastic energy absorption. However, the stopping distance with all truck wheels locked is

$$d = \frac{KE \text{ (after impact)}}{W_t \mu} = \frac{271,000}{9,500 \times 0.7} = 40.75 \text{ ft}$$

Figure 3 was developed by using the above theory and a series of initial speeds of the truck and portable crash-cushion unit.

Angle Impact

The above calculations consider only the effects of a head-on impact. Angle impacts are possible and, in fact, probable and should be considered. The most probable use for a crash-cusion trailer is to protect maintenance crews on Interstate highways where the usual maneuver is a 1-lane crossover. The impact angle can be determined from the formula (9)

$$\theta = \cos^{-1}\left(1 - \frac{\mu g d}{V^2}\right) \tag{7}$$

The maximum angle from this formula would be about 8 deg for a vehicle speed of 60 mph, a 12-ft lane width, and a coefficient of friction, μ, of 0.7.

Techniques developed by Emori (11) can be used to divide the velocity into longitudinal and tangential components, and energy assumed absorbed along these lines by adding to the analysis the factor

$$KE = \frac{I_o W^2}{2} \tag{8}$$

Figure 1. Crash-cushion trailer before test.

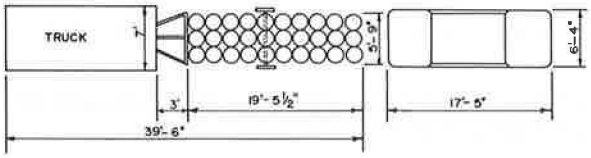

Figure 2. Number of barrels in crash-cushion trailer versus truck weight for several automobile weights.

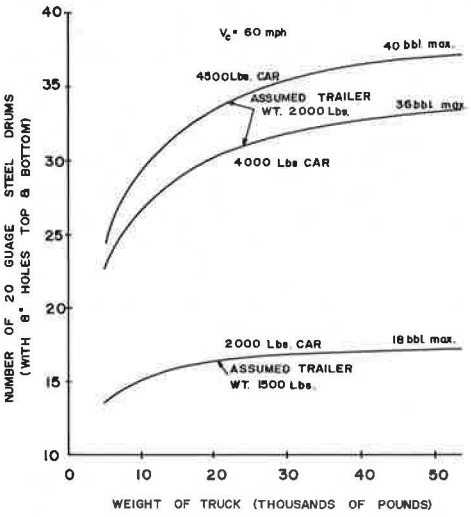

Figure 3. Stopping distance versus truck weight for various initial truck speeds.

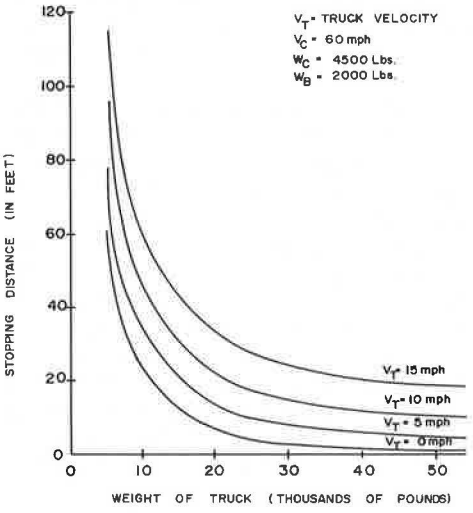

where

W = the angular velocity, and
I_o = mass movement of inertia of the truck and crash-cushion combination about the combined mass center.

This energy is then being absorbed by friction of the tires. The maximum angular displacement of the truck is less than 20 deg for these conditions.

Test Crash-Cushion Trailer Design

The test design was based on an impacting vehicle weighing 4,500 lb, a portable crash cushion weighing 2,000 lb, and a truck weighing 9,500 lb. This design is the same as that of the sample calculated above and required 30 steel drums. The crash-cushion trailer was designed to be attached to a standard maintenance dump truck of 5 yd^3 capacity. The truck used was a Dodge D-600 dump truck manufactured in 1963, weighing 9,315 lb. The estimated weight of the crash-cushion trailer was 2,010 lb.

The design of the test portable crash cushion is shown in Figure 4. The drawbar on the truck required some minor modifications to accommodate the 5-point hookup, and the attachments were hand-fitted to the truck. Five points were considered necessary to stabilize the trailer and make it act more nearly as a unit with the towing truck when towing at low speeds or stationary. These additional points were located to produce horizontal and vertical stability of the portable crash cushion. That is, they would prevent the trailer from jackknifing during impact and the impacting vehicle from submarining. Pictures of the completed crash-cushion trailer are shown in Figure 5.

With the exception of the removable arms, all connections were welded. The 4 removable arms were bolted to the face of the portable crash cushion and to the truck. Two technicians pulled the portable crash cushion to the test site and made the complete hookup in less than 5 minutes.

VEHICLE CRASH TEST

The crash-cushion trailer was hooked to the truck (only the trailer hitch was used) and towed around the TTI safety proving grounds at speeds as high as 50 mph for qualitative observation. After this exercise, the steel drums connected to the trailer axle and the row directly behind the axle had slightly deformed tops. This indicated the desirability of moving the axle farther to the rear of the trailer to reduce the cantilever effect of the rear steel drums. The auxilliary connections were made, and the trailer was towed at speeds as high as 25 mph around curves as great as 20 deg. The trailer tracked the truck to a remarkable degree in view of the rigid attachment. There was, however, an abnormal amount of wear to the tires because of side slippage. At lower speeds this wear was insignificant, especially when compared to the life-saving potential.

The primary test was the dynamic or crash test on the stationary truck and crash-cushion unit. For this test, the unit was placed near the north end of the apron of the TTI safety proving grounds. Ample distance to the end of the pavement was allowed for the unit to slide after impact. The arms were bolted in place, the truck was placed in gear (ignition turned off), and the parking brake was set.

The impacting vehicle was a 1964 Chevrolet weighing 4,060 lb. Lateral and longitudinal accelerometers were located on the right and left frame members of the vehicle chassis. The vehicle was towed toward the target by a reverse tow-guidance system (3). The initial impact speed was 63.3 mph and the impact angle was 0 deg (head on) in the center of the rear end of the crash-cushion trailer. Figure 6, a series of pictures from the moving-picture cameras, shows the sequence of events of the test starting at impact. The truck is virtually stationary until the barrels have been crushed to nearly the maximum that occurred during the test. This is important to the use of the system in the field because it shows that most of the energy is absorbed by the crash cushion before the energy wave reaches the truck. In turn, this shows that the instantaneous peak or jolt is at a minimum to anyone seated in the truck. It follows then that there would be little or no damage to the truck. In fact, personnel of TTI and the highway department examined the truck and could find no damage.

Figure 4. Truck crash-cushion trailer assembly.

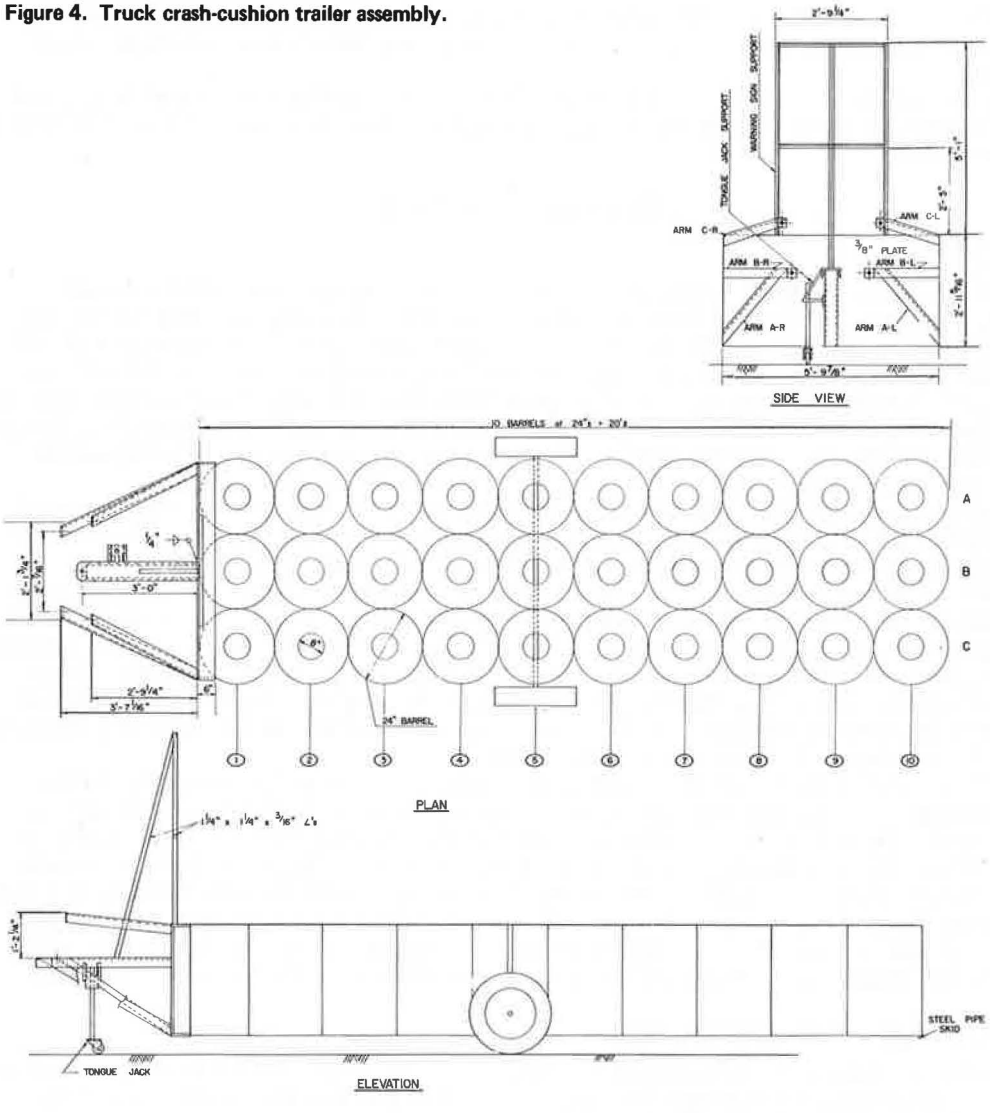

Figure 5. Test crash-cushion trailer before test.

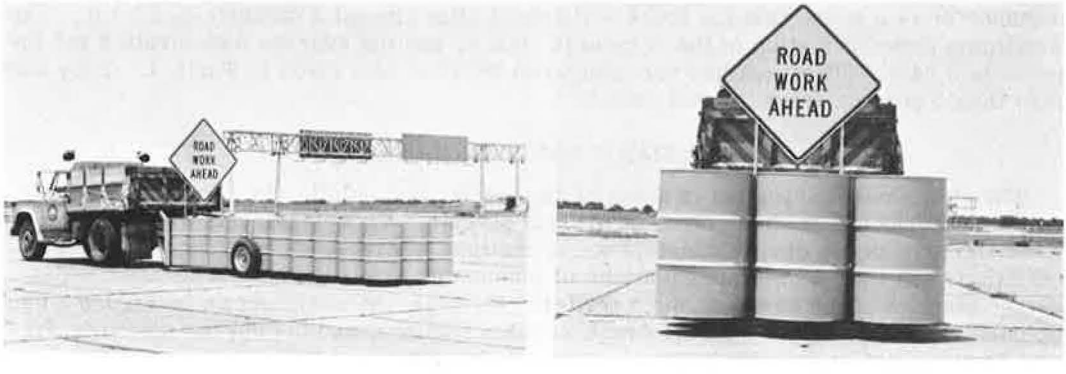

Figure 7 shows the impacting automobile before and after the impact. A minimum amount of damage occurred to the vehicle. In fact, only the 2 inside headlights were broken.

Figure 8 shows the crash cushion after the test and after the vehicle had been pried loose and driven away. Quite obviously, most of the available energy of the steel drums had been used.

DISCUSSION OF RESULTS

Test Data

The data from the tests were collected from 3 different sources: field measurements, electronic instrumentation, and photographic instrumentation. The electronic instrumentation included an Inter-Range Instrumentation Group (IRIG) with 8 available channels (3). Two channels each were used for longitudinal acceleration, lateral acceleration, speed, and spares. The data were transmitted to a central receiver, put on a magnetic tape, and stored. The acceleration data were then filtered through an 80-Hz filter and transferred with the speeds to paper tape in the visicorder. An Impact-O-Graph was used for backup data in the event of a malfunction of the IRIG.

Three high-speed data cameras and 2 documentary cameras were used to record the test and to obtain additional data. A complete description of data reduction techniques using the Vanguard motion analyzer is given in another report (3).

Table 1 gives a summary of the more important test data. There are several comparisons to the theory shown and described in detail below. There is a 1.7-ft difference between the maximum forward motion of the vehicle and the final position of the vehicle. Of this, the truck rebounded approximately 1 ft, which was probably due to the movement of the truck acting against the compression of the engine. Also, the barrier and vehicle rebounded an additional 0.7 ft, indicating that there was some elasticity remaining in the barrier and the front end of the vehicle.

Figure 9 shows the longitudinal and acceleration trace from the visicorder of the IRIG system. The peak g occurs during the period when the first row of steel drums is crushed. The entire crash-cushion trailer started moving forward at 211 msec, the point where the vehicle, cushion, and truck move as a unit. The vehicle deceleration zeros out the first time at 366 msec, about the time the truck achieves maximum speed. After that time, the acceleration trace (not shown) ranges from less than 1 to 0 negative g. Hence, we see that most of the energy is absorbed in plastic deformation of the barrels and elastic and plastic deformation of the vehicle, as the analysis predicted.

Correlation of Theory and Test Data

The theory based on conservation of momentum and kinetic energy described earlier produced results that are in excellent agreement with the test data when the test values are used. That is, from the conservation of momentum and substituting values given in Table 1 into Eq. 1, we compute V at the end of the crash = 24.5 ft/sec and the change in kinetic energy = 399,640 ft-lb.

The calculations indicated that the number of barrels used is 29.60 with a cushion distance of 14.8 ft and that the truck will travel after impact a distance of 22.0 ft. The maximum forward motion of the vehicle is 36.8 ft, and the average deceleration for the event is 3.64 g. (These values are compared with the data given in Table 1. They vary less than 5 percent from the test data.)

SUMMARY AND CONCLUSIONS

The crash-cushion trailer is a workable, easily used solution for protection against certain classes of accidents on highways and streets. Those accidents are the ones most likely to occur during maintenance operations where head-on or near head-on collisions are likely. Simple equations of mechanics are extremely accurate for the design and use of the crash-cushion trailer. Further, the curve shown in Figure 2 can be used for the design of specific crash-cushion trailers, and the curves shown in Figure 3 will assist in the safe location of the crash cushion.

Figure 6. Crash-cushion trailer during test.

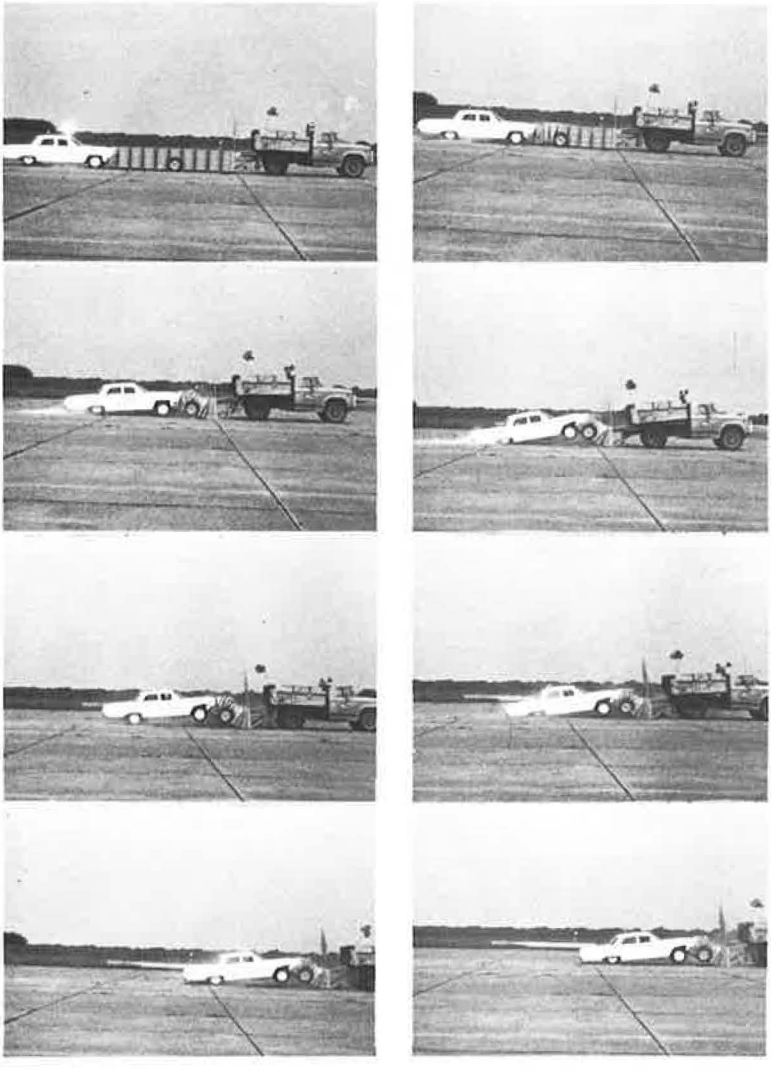

Figure 7. Test vehicle before and after test.

Figure 8. Crash-cushion trailer after test.

Table 1. Test data.

Item	Test Data	Computation
Initial speed		
ft/sec	92.8	
mph	63.3	
Maximum forward motion of vehicle, ft	36.4	36.8
Time to end of forward motion, sec	1.856	
Maximum forward motion of truck, ft	21.0	22.0
Final vehicle forward motion, ft	34.7	
Final truck forward motion, ft	20.0	
Final vehicle deformation, ft	0.2	
Final cushion deformation, ft	14.5	14.8
Average deceleration ($V^2/2gS$), g	3.67	3.64
Maximum longitudinal acceleration, g	-15.2	
Average longitudinal acceleration to end of significant peak, g	-6.6	
$\Delta V/\Delta t$ (to 0.366 sec), g		

Figure 9. Longitudinal accelerometer test data.

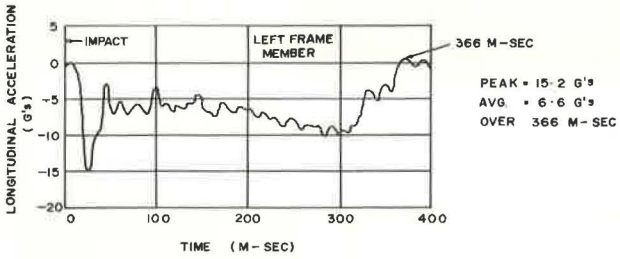

The structural connections between the crash-cushion trailer and the truck or other stabilizing vehicle should be adequate or even over-designed. The backup plate, also, should be stiff enough so that as uniform a restraining force as possible will be applied to the barrels during an accident.

The crash-cushion trailer can be used in 3 basic maintenance or construction operations. The first is in detour situations where a missed detour might result in injury to the vehicle occupants or to workers. In this situation, the crash-cushion trailer with its towing vehicle could be anchored on a temporary basis for the duration of the hazard and then moved to a new location as maintenance or construction progressed.

Another possible use is as a temporary stationary crash cushion to protect workers on travel lanes or on shoulders as they performed routine maintenance such as mowing, guardrail repair, chug-hole repair, trash collection. A driver could stay in the truck and move along with the task.

A third type of operation is a moving operation in which the progress of the operation proceeds at a much slower speed then that of the traffic. Such operations include striping of traffic lanes and placing traffic buttons.

A crash-cushion trailer for municipal streets could be much smaller than one used on high-speed expressways. The distance a crash-cushion trailer is placed from or follows an obstacle or worker to be protected should be governed by calculations for a safe distance or from curves shown in Figure 3. An adequate margin of safety should be used for the final distance.

REFERENCES

1. White, M. C., and Hirsch, T. J. Highway Crash Cushions. Texas Transp. Inst., Spec. Rept., Nov. 1971.
2. Tamanini, F. J., and Viner, J. G. Energy Absorbing Roadside Crash Barriers. Civil Eng., Jan. 1970, pp. 63-67.
3. Test and Evaluation of Vehicle Arresting, Energy Absorbing, and Impact Attenuation Systems. Texas Transp. Inst., Nov. 1971.
4. Nordlin, E. F., Woodstrom, J. H., and Doty, R. N. Dynamic Tests of an Energy Absorbing Barrier Employing Steel Drums. Calif. Div. of Highways, Jan. 1971.
5. Hirsch, T. J., and Ivey, D. L. Vehicle Impact Attenuation by Modular Crash Cushion. Texas Transp. Inst., June 1969.
6. White, M. C., Ivey, D. L., and Hirsch, T. J. In-Service Experience on Installations of Modular Crash Cushions. Texas Transp. Inst., Dec. 1969.
7. Hays, G. G., Ivey, D. L., and Hirsch, T. J. Flexbeam Redirectional System for the Modular Crash Cushion. Texas Transp. Inst., Oct. 1970.
8. Olson, R. M., Post, E. R., and McFarland, W. F. Tentative Service Requirements for Bridge Rail Systems. NCHRP Rept. 86, 1970.
9. Weaver, G. D., Hankins, K. D., and Ivey, D. L. Factors Affecting Vehicle Skids: A Basis for Wet Weather Zoning. Texas Transp. Inst., Rept. 135-2F, Feb. 1973.
10. Emori, R. I., and Tani, M. Vehicle Trajectories After Intersection Collision Impact. Paper presented at SAE Annual Meeting, Jan. 1970.

CRASH-BARRIER RESEARCH AND APPLICATION IN THE NETHERLANDS

H. G. Paar, Institute for Road Safety Research, Voorburg, The Netherlands

In the Netherlands the Institute for Road Safety Research carried out research into the most suitable crash barriers for soft soil and for bridges. Based on a number of requirements, the research resulted in a series of structures that provide optimum protection in soft soil and on bridges under various conditions. The barriers comprise in principle a horizontal beam consisting of 2 W-shaped rails and spacers every 1.33 m, provided if necessary with diagonal bars, and of posts with various structural characteristics. On this basis, the Netherlands authorities issued provisional guidelines for crash barriers in soft soil and on bridges on and over expressways. These are now being used generally on national highways.

•IN 1963, the Netherlands Minister of Transport decided that all expressways carrying 20,000 vehicles or more a day should be provided with median crash barriers because of the great increase in the number of vehicles crossing medians with fatal results. The barriers then built were similar to those in use in other countries (especially the United States and Germany).

Although accident statistics showed that the use of those barriers reduced the number of median crossings, there was often an increase in the number of recorded accidents involving casualties. The Institute for Road Safety Research was, therefore, asked to develop a crash barrier that would not have the apparent disadvantages of the customary ones. This research was commenced in 1964 and was provisionally completed in 1970 (1). The research was not limited to median barriers, but included shoulder barriers, the essential difference of which is that they can be hit from one side only. Meanwhile, Rijkswaterstaat, the agency that has authority over all national highways, has issued provisional guidelines, based on the results, for building crash barriers on expressways. Most local road authorities also follow those guidelines.

Even before the conclusion of the research into crash barriers in soft soil, a need arose to seek a solution for the specific problems of crash barriers on bridges. This led to separate research, which was commenced right after completion of the previous research and which, because of the experience already gained, was completed in 2 years. A report on these investigations is being prepared (2).

As there had already been very close contact with Rijkswaterstaat during the research, provisional guidelines for building crash barriers on bridges in and over expressways were completed almost parallel with the investigations. A summary of these guidelines and those for soft soil barriers is given in another report (3).

FUNCTIONAL REQUIREMENTS

Both investigations were based on a number of functional requirements. Each type of barrier was put to the test against these.

The first requirement is that the vehicle must not be able to enter the barrier-protected hazard area, such as an adjoining roadway, a steep embankment, or the edge of a bridge. Therefore, the vehicle must not break through the barrier, run under or over it, or topple over it. Although that requirement is very important, especially at the edges of bridges where the hazard risks are generally very great, it may nevertheless be varied somewhat, where risks are not so great, such as where there are wide medians or fairly flat obstacle-free shoulders.

Compliance with this first requirement, however, is not enough. Not only must a barrier stop vehicles that may go off the road, it must also really provide protection. Thus, the second requirement is that injury must be prevented to occupants of colliding cars and that damage to these cars must be as slight as possible. The decisive factors are the forces exerted by the barrier and the vehicle's consequent longitudinal and lateral decelerations. The extent of the permissible decelerations is still debatable. The provisional norms are those for cars whose occupants are not wearing seat belts. These originate in the United States and are lateral max 3 g, longitudinal max 5 g, and total max 5 g (4). Those figures, however, are definitely not final but depend on factors such as whether seat belts are worn and the internal construction of the vehicle. As changes occur in the years ahead, those norms may also change.

Besides protection of the car itself, the traffic the car leaves must not be exposed to any additional danger. Hence, a third requirement is that the car must not rebound into traffic flow and, if at all possible, should stop off the roadway.

In the case of heavy traffic densities, a barrier damaged by one impact may be hit again in the same place before repairs are made. The fourth requirement, therefore, is that the barrier should continue to be reasonably operational after being hit. The fifth and last requirement is that it must be possible to repair the barrier quickly after a collision with minimum inconvenience or danger to traffic.

STRUCTURAL REQUIREMENTS

To translate the functional requirements into the structural requirements that crash barriers must satisfy requires a consideration of the types of vehicles. In the Netherlands, road traffic consists mostly of private cars weighing 500 to 1,500 kgf, but there are also a considerable number of buses and lorries weighing as much as 50 tf. To prevent a vehicle that has run off the road from running into traffic, the barrier must have enough longitudinal strength to resist the forces that occur. During the investigations it was found that, if the barrier and the anchorings at the beginning and end can absorb 40 tf without breaking, even the heaviest impacts will not break the barrier in the normal course of events.

The requirement that no vehicles should push under the barrier or topple over it is difficult to meet in view of the big variety of vehicles. To eliminate the risk of vehicles toppling over requires that the forces between the barrier and the vehicle be applied above the center of gravity or close to it. That is impossible, however, for all vehicles. The barrier, therefore, has to be exactly high enough for normal private cars not to push under it, i.e., no more than about 45 cm above the road surface. A measure, which is then required to ensure that lorries do not topple over, is the flexibility of the barrier, which is also necessary for limiting vehicle decelerations. This flexibility limits the barrier's reactive forces on the vehicle and thereby reduces the danger of its toppling over. This means that the height of the barrier must remain about the same during deflection and that the wheels must not hit any upright edges, such as gutters or curbs, that could cause the vehicle to topple.

As stated, lateral decelerations can be kept low by the deflection of the barrier. In the case of extreme impacts on the 2-lane roads most common in the Netherlands (speed 100 km/h, impact angle 20 deg), at least 1-m deflection is necessary to obtain acceptable decelerations if the deflection is gradual. In view of Dutch traffic patterns, that applies to private cars, and deflection for lorries under the same conditions will be greater. If the deflection is kept within reasonable limits, the forces must increase progressively as the deflections proceed further.

Longitudinal decelerations can be kept low by ensuring that the impacting vehicle encounters no discontinuities in the barrier. The start of the barrier must be built so that there can be no head-on collisions with it or else that decelerations during any such impact remain within reasonable limits. Posts in the crash barrier must be impossible to hit or be constructed so that they give easily when hit.

To ensure that the vehicle does not rebound into the traffic flow requires that the exit angle be small and that the vehicle continue to travel almost parallel to the barrier. This can be achieved with very gradual barrier deflection. Research has shown that a

ratio of 1:40 between the extent of the deflection and the length of the deflection wave gives very good results. In addition, the deflection must be due primarily to plastic deformation, for elastic deformation may cause severe rebounds.

So that a vehicle diverted and brought to a stop in this way is not a dangerous obstacle to other traffic, there should be a large enough recover area between the roadway and the crash barrier. Impacts are also fewer when barriers are not so close to the roadway. The recover area moreover makes it possible to repair the barrier with little inconvenience to traffic.

For easy maintenance and economy of installation, the various crash barriers, whether for soft soil or for bridges, should have as many standardized parts as possible.

STRUCTURAL DESIGN

The research was mainly experimental. For barriers in soft soil, more than 100 impact tests were made. They were carried out with private cars weighing between 500 and 2,000 kgf (impact angles 12, 15, and mostly 20 deg; speeds between 70 and 110 km/h) and with lorries and buses weighing between 3,500 and 10,000 kgf (impact angles 15 and mostly 20 deg; speeds between 50 and 80 km/h). For the bridge barriers, about 50 impact tests were made with the same vehicles under similar conditions. In addition, a mathematical model was devised for simulating impacts with the developed and similar structures.

The research related to a very wide variety of barriers. On the whole, the concrete barriers that then existed failed to meet all the requirements. Although most concrete barriers were practically impenetrable and suffered little damage, lorries still tended to overturn and decelerations and vehicle damage were too great to be acceptable. No effort was, therefore, made to develop a more suitable concrete barrier. Situations do occur, however, where no other barrier is possible, especially where there is very little space. Based on U.S. research (5), a concrete barrier, having the New Jersey barrier cross section, is still recommended under such conditions.

Cable barriers also failed to satisfy all the requirements. Decelerations were indeed slight, but the outcome of impacts was not always predictable, and there is thus no guarantee that cars will not break through them. In addition, such barriers were very badly damaged and ceased to operate. They have, therefore, been abandoned entirely.

The research ultimately showed that steel structures having normal W-shaped guide rails were the most satisfactory. Structures were made that had standardized parts and provided a solution in the most common circumstances. Figure 1 shows a number of possible structures in soft soil; Figure 2 shows a number of structures for bridges.

Of those structures, the flexible offset 2-rail barrier is most recommended. It has a 0.8-m-wide beam consisting of 2 normal W-shaped guide rails connected every 1.33 m by spacers, resting on posts every 4 m, the design of which depends on the barrier's location (soft soil or bridge surface). In both cases the post is made so that it allows the barrier to deflect fairly easily.

When collided with, this barrier functions as follows: The colliding vehicle first hits the top corrugation of the rail because it is slightly inclined (at an angle of 6 deg), initiating the desired movement of the barrier, i.e., rotation around an imaginary pivot below or just at ground level. The barrier located in soft soil has a flattened post that cuts easily through the soil; a post on a bridge surface tears easily because it has a comparatively weak weld at the base. As the barrier bends, resistance to deflection gradually increases, among other things, because torsional forces build in the beam and longitudinal forces build in the 2 W-rails. This continues until the rail touches the ground at the side away from the impact. Measured horizontally at the front rail, the deflection is now about 1 m. This is approximately what happens when a private car weighing about 1,000 kgf hits the barrier at 100 km/h at an angle of 20 deg (Fig. 3).

With more severe impacts the play of forces on the barrier changes because the rear rail is forced against the ground. This greatly increases the resistance to deflection and causes the required 2-stage effect, whereby the deflection, which human tolerance does not require to be greater, is kept within limits. When hit by heavy

trucks, however, the barrier may deflect as much as 2 m. During deflection the front (top) rail always stays at a height of at least 75 cm, preventing the colliding vehicle from overturning.

Extensive research was undertaken in connection with designing both soft-soil and bridge barriers (the post is the only part that is materially different). For soft-soil barriers a post was sought that cuts easily through the soil when the barrier deflects and that greatly resists lateral bending. The ultimate solution was a 76-mm-diameter tube having a wall-thickness of 5 mm and the underground part of about 1m flattened to 33 mm thick. Inasmuch as the soil structure very common in the Netherlands is rather loose, this post has little ground resistance when the barrier is deflected and the pivot is low. This is a major factor in achieving the required 1:40 deflection; even with greater deflections, the posts remain almost completely under the barrier so that there is little danger of vehicles colliding with them. This eliminates the artificial pivot, in the form of a concrete sphere (4, p. 7) used earlier.

In addition, rupture bolts in the post-spacer joint ensure that the impact has no serious consequences in the way of extreme decelerations by the vehicle. Those bolts also ensure that the necessary flexibility, although it may not be ideal, continues to exist when the ground is frozen.

The bridge barrier post has the IPE 100 cross section. For the flexible barrier, only the body of the post is welded to the baseplate with a 3-mm rupture weld. This barrier, therefore, also gives easily and has the desired 1:40 deflection. The risk is greater of hitting the post of a bridge barrier than of a soft-soil barrier because the pivot is practically at road-surface level. Because of the weak rupture weld, however, the deceleration of a vehicle colliding with the post is slight. The spacer was based on German research that found it to be the most satisfactory (6). It is very rigid and has as a special feature an easily bending lip in the bottom corrugation of the rail. This ensures that the load on the bottom corrugation does not become excessive with great deflection. That is particularly effective when a lorry's wheel bolts cut into the rail.

Although it may seem illogical at first sight, the offset 2-rail barrier is also used where it can only be hit from one side, for instance on shoulders. As the foregoing has shown, the rear corrugated rail has a definite function in securing the necessary beam rigidity and in supporting the 2-stage effect.

The great deflection of the flexible barrier makes it impossible to use it where there is insufficient space. In such cases, a less flexible structure will have to be used. In the flexible barrier, the rigidity of the beam, the resistance of the posts, and the number of posts form a balanced unit that gives the required form of deflection. The barrier must, therefore, be stiffened very carefully.

For a bridge barrier, a diagonal bar is first placed in the beam in every third field formed by the rails and the spacer. That stiffens the beam so that more posts will deflect. If the post-to-post distance remains the same, the length of the deflection wave will then be greater than 40 times the deflection. More posts can now be used, reducing the length of the deflection and stiffening the structure as a whole. Possible post-to-post distances are 2.67 and 1.33 m. For crash barriers in soft soil, a post-to-post distance of 2.67 m is first applied, after which diagonal bars are fixed; otherwise, the principle is the same.

If a barrier that has 1.33 m between posts still deflects too much for local conditions, various types of stabilizing plates can be used for soft-soil barriers to impede the post's movement. For crash barriers on bridges, the welding method can be adapted by welding not only the body but also the front flange (in barriers that can only be hit from one side) or all around (in barriers that can be hit from both sides). The welds can also be made thicker. The effect on deflection of the various stages of stiffening crash barriers in soft soil is shown in Figure 4. The curves are similar for crash barriers on bridges. In Figure 4, D = dynamic deflection of rear rail, and $I = Gv/3.6\ g \sin i$, where G = vehicle weight in kgf, v = vehicle speed in km/h, g = acceleration of gravity in m/sec^2, and i = impact angle (20 deg in tests). Because there is no 2-stage effect with very stiff barriers, the spacing at the back can be omitted. This gives a saving of about 20 cm, but part of this is lost again because the beam is narrower and hence not so stiff.

Figure 1. Offset 2-rail barrier in soft soil.

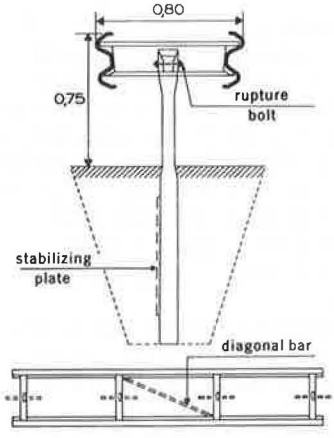

Figure 2. Offset 2-rail barrier on bridge.

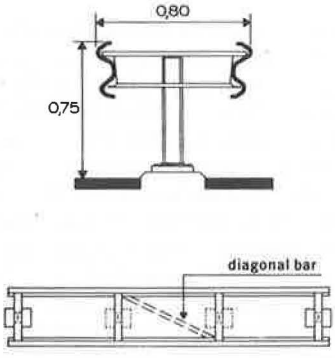

Figure 3. Collision of 1,150-kgf vehicle with soft-soil barrier at 100-km/h speed and 20-deg impact angle.

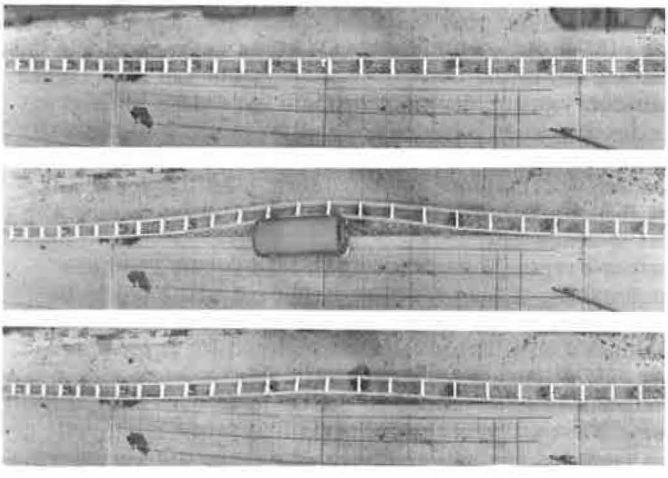

Figure 4. Deflection curves of offset 2-rail barriers in soft soil.

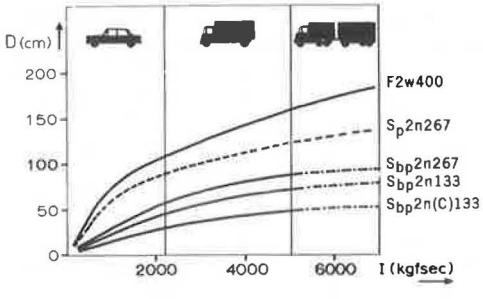

The flexible barriers obtained met all functional requirements best. The soft-soil barrier will suffer less damage from minor collisions than the bridge barrier because one or more posts of the latter will always have to be replaced. The stiffened barriers also satisfied most of the requirements, except that in comparable collisions the lateral decelerations especially will be greater because the barrier is stiffer. These decelerations are still so slight, however, that the occupants of a light private car can even survive a severe collision with a very stiff barrier (certainly if they are wearing safety belts; the maximum lateral deceleration will then be no more than about 7 g for some tenths of a second).

Proper operation of the barriers demands that there be no internal or external discontinuities. Transitions from flexible to stiffer barriers must be very gradual and nothing must prevent the barrier deflecting, for instance, rigid obstacles immediately behind it. Some discontinuities, however, are unavoidable. For instance, some play has to be allowed at joints in bridges, and that adversely affects barrier operation. At the moment a solution appears to be fitting a hydraulic shock absorber parallel to the joint. A similar problem occurs on bridges with moving sections. A solution is being sought and is likely to be found.

Emergency vehicles, such as police cars and ambulances, should be able to cross the median easily at some points. That was solved by building a movable part in the barrier. Under normal conditions this guarantees a continuous barrier with practically the same characteristics as the normal barrier, but in emergencies it can easily be opened leaving a passage of about 4.70 m.

INSTALLING BARRIERS

Crash barriers are only justified if colliding with them is less dangerous than entering the protected hazard area. The decision process applied for expressways is shown in Figure 5. Medians (without obstacles) wider than 12 m are not usually provided with barriers, nor are shoulders where there are no hazards within 10 m of the roadside. These figures are based on data gathered in the United States (7).

Based on the research results, provisional guidelines for expressways have been issued in the Netherlands, as stated above. On the one hand they give cross sections for new roads, allowing for the construction of crash barriers; on the other, they give solutions for (existing) situations where there is too little space for flexible barriers. It is in these particular cases that the standardization is such a great advantage. The recommended barriers and their location in the cross section, in soft soil and on bridges in new roads, are shown in Figures 6 to 12. All dimensions in the figures are in meters. The meaning of the codes is as follows:

Description	Code
Flexible, no diagonal bars in beam, 2 offset rails, rupture device, post-to-post distance 4 m	$F2_W400$
Flexible, no diagonal bars in beam, 2 offset rails, posts only welded at body to baseplates, post-to-post distance 4 m	F2B400
Stiff, diagonal bars added in beam and post-to-post distance reduced, 1 offset rail (2 W-rails), posts only welded at body to baseplates, post-to-post distance 1.33 m	$S_{bp}1B133$
Stiff, diagonal bars added in beam and post-to-post distance reduced, 1 offset rail (1 rail, 1 strip with same cross section), posts only welded at body to baseplates, post-to-post distance 1.33 m	$S_{bp}1_sB133$

There must be no curbs or gutters in front of the posts with a difference in height greater than 0.05 to 0.07 m, either in soft soil or on bridges. In soft soil, the normal deflection of the posts must not be prevented by surface metal, gutters, or similar obstructions immediately behind the posts.

Figure 5. Decision model for use of crash barriers on expressways.

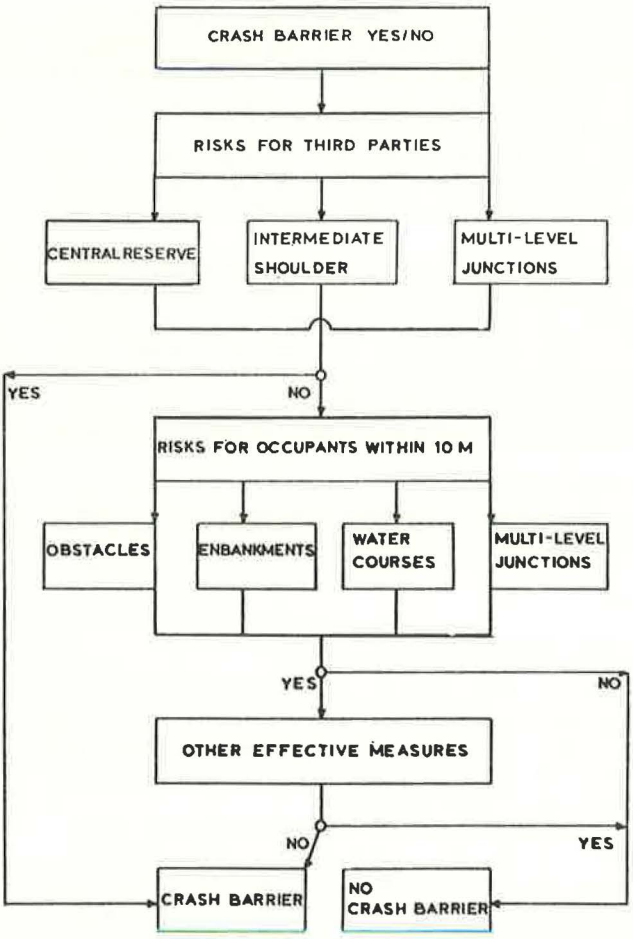

Figure 6. Barrier F2w400, without obstacles, in soft soil in median.

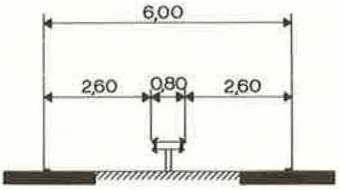

Figure 7. Barrier F2w400, with obstacles, in soft soil in median.

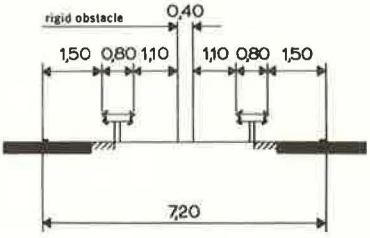

Figure 8. Barrier F2w400, without obstacles, in soft soil on shoulder.

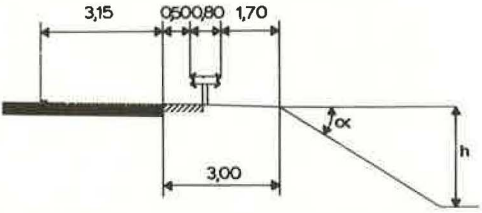

Figure 9. Barrier F2w400, with obstacles, in soft soil on shoulder.

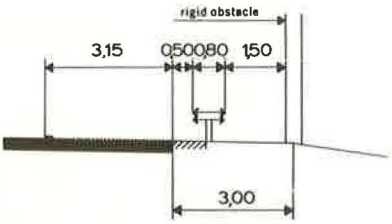

Figure 10. Barrier $S_{bp}1B33$, without obstacles, on bridge in median.

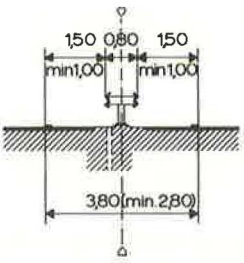

Figure 11. Barrier $S_{bp}1B133$, with obstacles, on bridge in median.

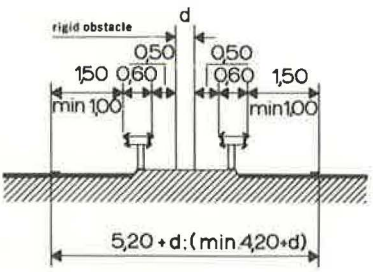

Figure 12. Barrier $S_{bp}1_sB133$, with inspection path, on bridge on shoulder.

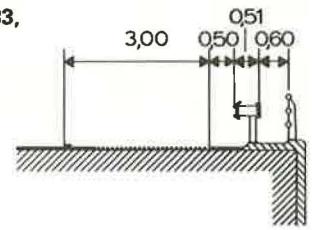

PRACTICAL EXPERIENCE

Unfortunately, accident statistics in the Netherlands are not differentiated to such an extent that the effect of crash barriers on the number and outcome of accidents can be ascertained. Although they are regrettably rather old, some general figures of fatal accidents are as follows:

Year	Fatal Median Accidents
1962	20
1963	31
1964	40
1965	40
1966	16
1967	8

The impression is that there has been a further decrease since 1967. Since 1965, better structures have been built based on the provisional research results. From 1962 to 1966, the annual median accidents involving casualties were about 40 percent of all such expressway accidents. The decrease was fairly quick after that, however, to about 20 percent in 1968. The impression is that it has meanwhile fallen further.

All these figures relate to median barriers in soft soil. No data whatsoever are available for bridge barriers, one reason being that barriers based on the new guidelines are only of very recent date.

At the end of 1966 an interesting comparison was made of the overall construction and maintenance costs of various crash barriers for soft soil. Although there has since been a substantial increase in cost levels, the relation remains the same, and the figures are still valuable.

Barrier	Installation Cost (Fl./m)	Avg Repair Cost (Fl./case)
Cable	26	550
Offset, 2-rail with wooden posts and spacers (California)	75	550
Offset, 2-rail with INP 14 posts and spacers less stiff than now recommended	40	440
Flexible offset, 2-rail, built on same principles as flexible barrier	40	85

The following can be added. The low repair costs of the flexible offset barrier are due mainly to the fact that most cases of damage (caused by private cars) are so slight that the barrier can be pushed upright again with a jack and requires no replacement, a process that may take about half an hour. Besides, the cases in the above comparison are those of damage in which the road authority had to take action to restore the barrier to its former state. With the recommended barriers, however, it regularly happens that damage through minor impacts is so slight that it disappears again in the course of time because of the self-righting effect. Hence, average repair costs for this barrier would be lower still if all collisions were taken into account.

Finally, the car concerned in most of the collisions is not known because it was apparently able to continue its journey after the accident, indicating that the damage was slight.

REFERENCES

1. Slop, M. Roadside Safety Structures: A Description of the Crash Barriers Developed in the Netherlands. Inst. for Road Safety Res., Voorburg, Netherlands, Rept. 1970-6, 1970.

2. Crash Barriers for Bridges. Inst. for Road Safety Res., Voorburg, Netherlands, in press.
3. Beukers, B., and Asmussen, E. Roadside Safety Structures: Research and Applications. Assn. Internat. Permanente des Congrès de la Route, Paris, Rept. Quest. 4, The Road in Relation to Traffic Requirements, 14th World Congress, 1972.
4. Michie, J. D., Calcote, L. R., and Bronstad, M. E. Guardrail Performance and Design. NCHRP Rept. 115, 1972.
5. Michie, J. D., and Calcote, L. R. Location, Selection, and Maintenance of Highway Guardrails and Median Barriers. NCHRP Rept. 54, 1968.
6. Böhringer, A., Rosehmann, R., and Domhan, M. Anfahrversuche an Leitplanken. Innenministerium Baden-Württemberg, Stuttgart, 1969.
7. Stonex, K. A., and Skeels, P. C. Development of Crash Research Techniques at the General Motors Proving Ground. Highway Research Record 4, 1963, pp. 32-49.

MATHEMATICAL MODEL FOR IMPACT TESTS ON CRASH BARRIERS

V. Giavotto, Technological University, Milan, Italy

A computer program has been developed that simulates impacts of various vehicles with guardrail barriers. This program is a digital simulation system, making use of several mathematical models. The vehicle simulation is composed of 3 major segments: the vehicle as a rigid body, the steering gear, and the deformation of the body due to the impact. The barrier is essentially a structured beam on many flexible supports; the beam is divided into a certain number of elements connected to each other at the nodes. The vehicle and the barrier work in the following combinations: dynamics of the vehicle alone before impact when the barrier is motionless and undeformed; dynamics of the vehicle and the barrier exerting forces on each other after impact; dynamics of the vehicle and the barrier not exerting forces on each other when they have no contact and the barrier oscillates because of inertia; and dynamics of the vehicle alone when there is no contact with the barrier, which is motionless and deformed. A certain number of full-scale tests have been computed, and a fair agreement with experimental results has been obtained. The use of such a program will substantially reduce the number of full-scale tests.

•AT THE END of 1968 the Institute for Road Safety Research in the Netherlands realized the importance of having a mathematical model to simulate the impact of a vehicle against a guardrail barrier. Such a mathematical model was mainly intended to correlate results of simulations and full-scale tests and then to predict results so that the number of actual tests needed to evaluate the behavior of the barrier could be reduced. The advantages of such a mathematical device are quite obvious; the cost of a computation, though not negligible, is always considerably lower than the cost of a full-scale test. We expected that the model could reduce the total cost of the work of developing and evaluating the barriers mentioned or enable more extensive work to be done at the same price.

The work started with the development of a relatively simple model in which the barrier was considered as a continuous beam supported by posts. For the reaction of the posts, the model used experimental data, in terms of force versus displacement and rate displacement, obtained by means of dynamic tests. The vehicle model was already pretty well defined, including complete dynamics and the body deformation due to the impact.

A far more complicated model was then desired that would take into account the stiffening of the beam brought about by diagonal bars between the rails, the effect of large deflections, the second-stage effect (i.e., the increase in stiffness occurring when one rail hits the ground), and other aspects not included in the first model.

That new model required a much larger memory space and computing time and hence a greater computer cost. But at that time it was possible to limit the cost to about that of the former model by using improved programming techniques that were developed at the Aerospace Department of Politecnico of Milan for structural analysis. Without those new techniques, total computing time would have been more than 20 times greater.

At present the mathematical model has reached a rather high level of development and has been tested with the experimental results of full-scale tests conducted by the

Institute for Road Safety Research. It is really more than a mathematical model; it is a digital simulation system, which in part makes use of several mathematical models.

DIGITAL SIMULATION SYSTEM

The simulation system is essentially a program consisting of different parts or segments. The program itself chooses which part it has to use and how it has to combine the various segments during the simulation. For example, the main parts, the vehicle and the barrier, can work in the following combinations:

1. Dynamics of the vehicle alone before impact when the barrier is motionless and undeformed;
2. Dynamics of the vehicle and the barrier exerting forces on each other after the impact;
3. Dynamics of the vehicle and the barrier not exerting forces on each other when they have no contact and the barrier oscillates because of its inertia; and
4. Dynamics of the vehicle alone when there is no contact with the barrier, which is no longer oscillating.

In configurations 1 and 4 the positions of the vehicle and the barrier are compared; and when an interference occurs between the side of the vehicle and the barrier (vehicle and barrier undeformed in configuration 1, deformed in configuration 4), the computation is turned into configuration 2. In configuration 2 the vehicle and the barrier are considered connected at a certain number of points at which a certain number of mutual forces are exerted. Each mutual force cannot be a pull, and when one force begins to be a pull the corresponding point is no longer a point of contact. When there is no longer a point of contact, the computation is turned into configuration 3.

Figure 1 shows a general flow chart of the simulation system. In configuration 1, phase 2 is bypassed by test 3. In configuration 2, phase 2 is executed. In configuration 3, phase 2 is still executed, but there is no connection (and force) between the vehicle and the barrier. In configuration 4, phase 2 is again bypassed by test 3, which, obviously, is a rather complex test. Test 4 decides when the computation has to be terminated: That may happen when the computation has actually reached the end point, which has to be specified among input data, or when the roll angle of the vehicle becomes greater than 1 radian. At that point the vehicle will certainly overturn, but the program cannot simulate the subsequent motion.

VEHICLE

The vehicle simulation is composed of 3 major segments:

1. The vehicle as a rigid body,
2. The steering gear, and
3. The deformation of the body due to the impact.

Segment 1 computes the motion of the vehicle considered as a rigid body with 6 degrees of freedom (Fig. 2). The forces acting are only forces of gravitation and ground reactions (one for each wheel). No consideration is given to aerodynamic forces. The vertical component of each ground reaction is computed as a function of the corresponding vertical deflection of the suspension and tire; the horizontal component, or cornering force (Fig. 3), equals the vertical component multiplied by a cornering force coefficient, which is a function of the angle of sideslip (Fig. 4). The maximum value, DFCM, of that coefficient may have different values, depending on the nature and the condition of the road surface.

The movement of the steering gear may be a priori known as input data, when someone is operating the steering wheel, or during the specified time intervals may be computed from the dynamics of the steering mechanism. That is done in a rather complete scheme that considers also gyroscopic couples on the wheels, the effect of caster, inclination, and pneumatic trail (Fig. 3). (Pneumatic trail is the backward displacement of the centroid of the contact area between the tire and the road surface. It increases with the vertical reaction and with the angle of sideslip and produces a torque that tends

Figure 1.

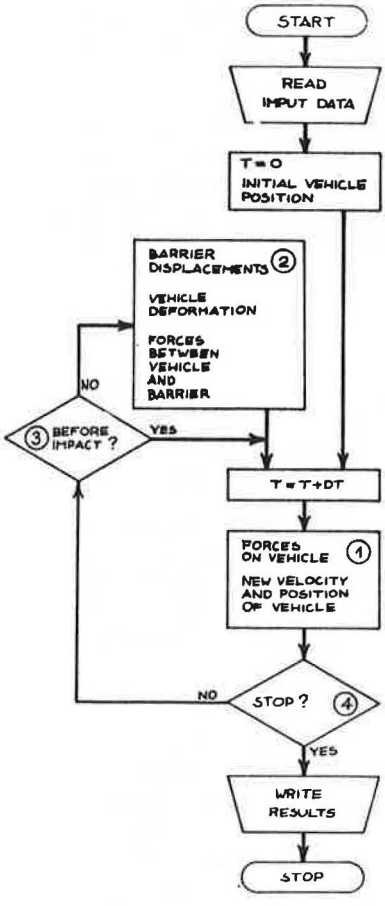

Figure 2.

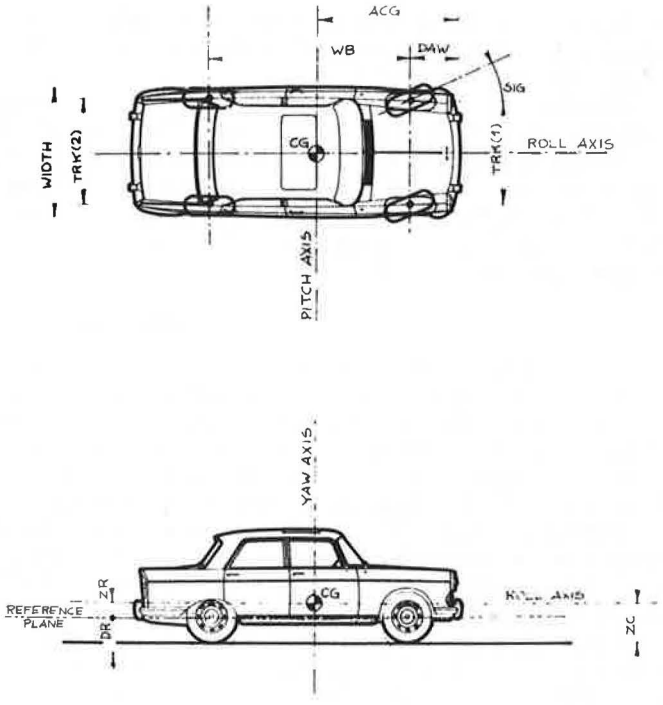

Figure 3.

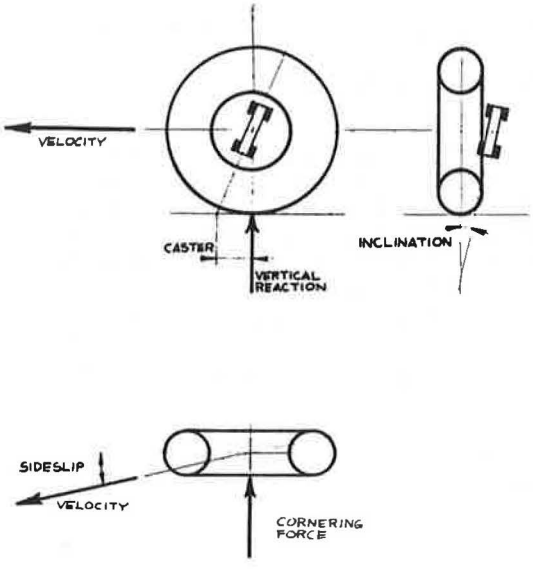

Figure 4.

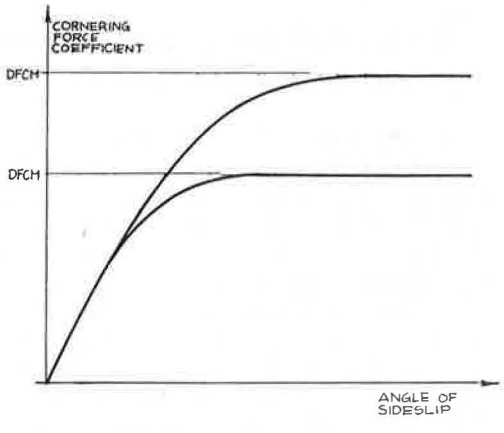

to move the steering gear in the sense of reducing the sideslip.) In this way the simulation will cover any movement of the vehicle that can be obtained by operating or abandoning the steering wheel.

The third segment, which works when the vehicle is in contact with the barrier, simulates the deformation of the body. The contact may take place at a certain number of points, to be assigned, up to a maximum of eight (Fig. 5). The force-deflection diagram at each point consists of a softer part, followed, after deflection reaches the value SBER(I), by a stiffer part. For decreasing deflection, the force decreases even more steeply, and after the force has reached zero a certain amount of plastic deformation remains present.

BARRIER

The barrier is essentially a continuous beam on flexible supports. The beam is divided into a certain number of elements connected with each other at the nodes (Fig. 6). An element is that part of the beam between 2 spacers and may have a diagonal bar (Fig. 7). Some of the nodes are connected to the flexible supports. If no external force acts on an element between the nodes, the element deformation is completely represented by the superimposition of the 6 modes shown in Figure 8.

The diagonal bar, if present, exerts a force T depending on the relative displacement δ of its terminal points. The model for the force T is shown in Figure 9. To increase δ, beginning from $\delta = 0$, T increases elastically up to the value TA of the friction force; then T = TA. T in turn increases elastically after δ has reached the value allowed by the play, GPOS, between the bolts and the holes to the value TS of the limit bearing force. After that point, the bolt starts bearing the sheet of the rail, increasing the actual play. To decrease δ, T decreases elastically. For negative values of T the model is the same, but a different value, GNEG, of the play may be specified.

The model for the motion of the sections of the beam is shown in Figure 10. It is a rigid rotation around point 0, mainly due to constraints of the posts, followed by a rigid rotation around point 0_1, when the rear rail collides with the ground. When the values of CRO, CRV, and CRC are properly chosen, that model will represent a good approximation of the motion observed in full-scale tests. For the reactions of the posts, experimental values are used, which were recorded in dynamic tests (1), and plotted versus displacements (Fig. 11). Displacement is decreased by the assumption that the force linearly decreases; the slope starts down beyond point A, where the reaction reaches its maximum value. As long as the rear rail is in contact with the ground, contact reactions are also present and are assumed to be perfectly elastoplastic (Fig. 12).

The main effects of large displacements are as follows:

1. A certain amount of tension builds up in the beam and produces a stiffening effect; and
2. Because of the constraint of the posts (Fig. 13), a certain amount of secondary bending takes place and causes the deflection.

That bending, although not very great, may have a rather strong stiffening effect because it takes place around the axis of maximum bending stiffness of the rail (axis bb, Fig. 7). The tension on the beam depends on the elongation as shown in Figure 14. Varying the values of the limit friction force, ENNA, and the play makes it possible to simulate different expansion joints. In the bending of the beam, some plastic deformations are also possible; this occurs when the yield stresses are exceeded.

After the vehicle has moved into its new position, a new equilibrium configuration is found that corresponds to a small time increment dt (Fig. 15). Typical figures for that time increment, which have been extensively used in computations with practically the same results, are 5 and 2.5 ms.

At every step all the nonlinear forces, such as diagonal and post reactions, are linearized in the small interval between 2 consecutive steps so that the new equilibrium configuration is the solution of the matrix equation

$$\{P\} = [K]\ \{v\}$$

Figure 5.

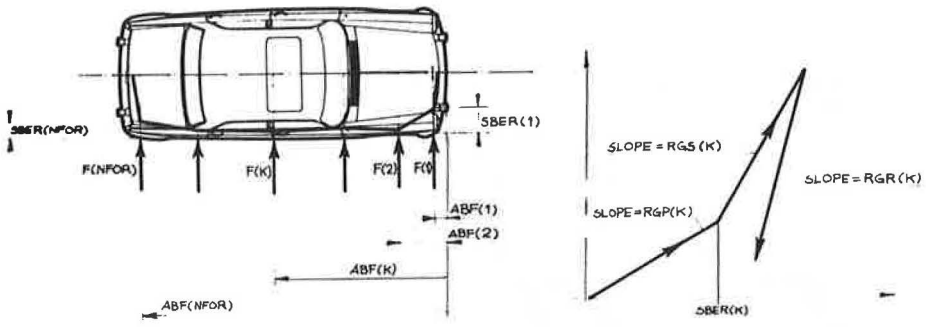

Figure 6.

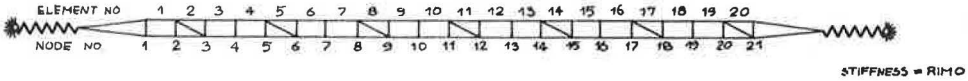

EXAMPLE :

MCAMP = 20 NPAL = 2 INDIAG = 2 NDIAG = 3

Figure 7.

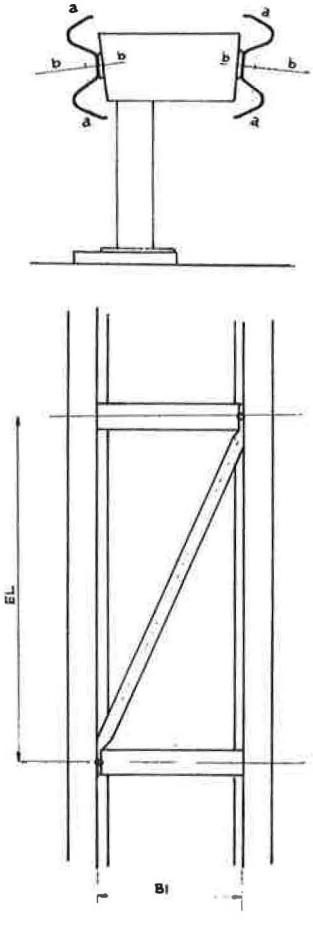

Figure 8.

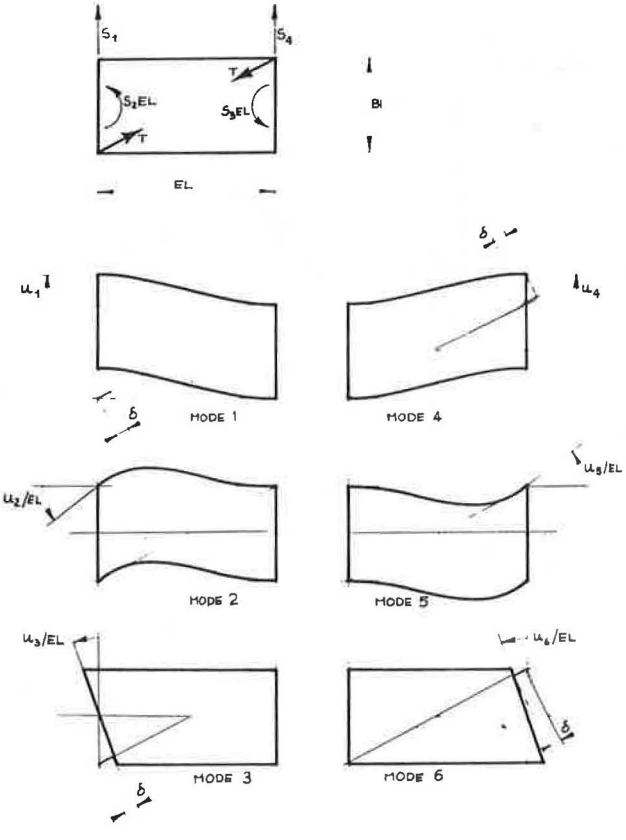

Figure 9.

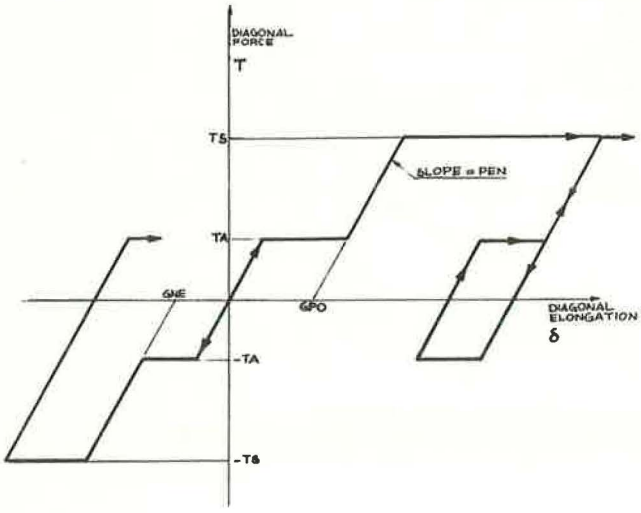

Figure 10.

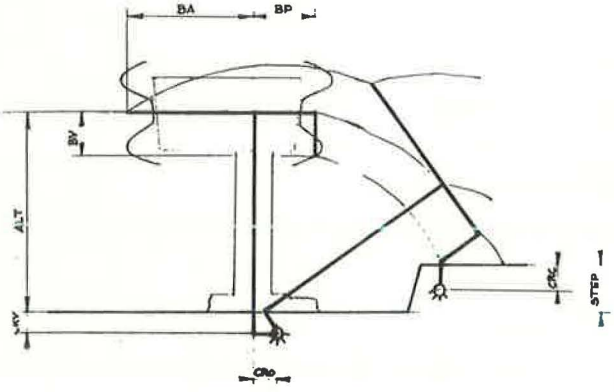

Figure 11.

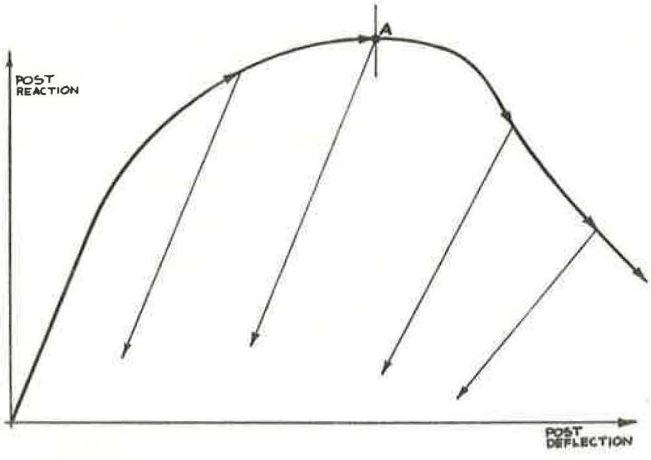

Figure 12.

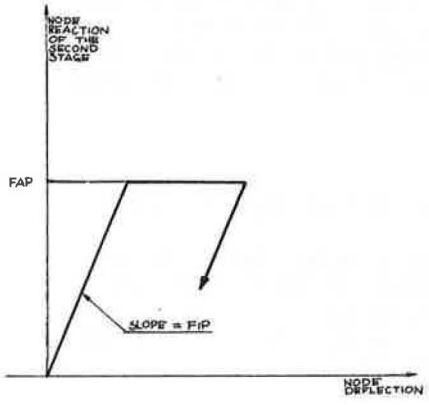

Figure 13.

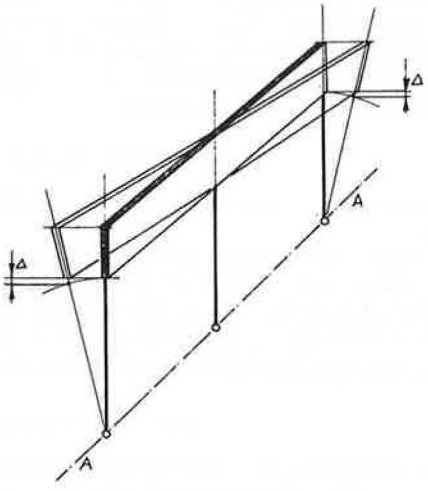

Figure 14.

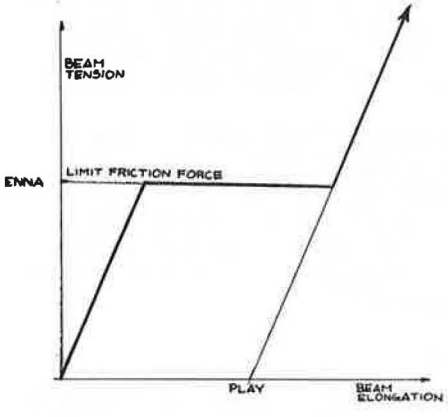

Figure 15.

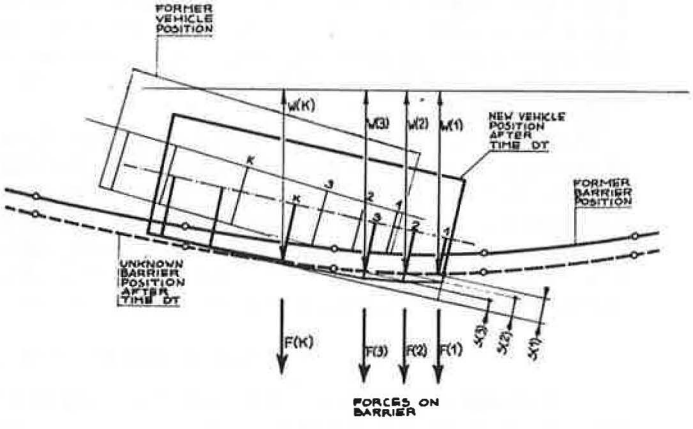

Figure 16.

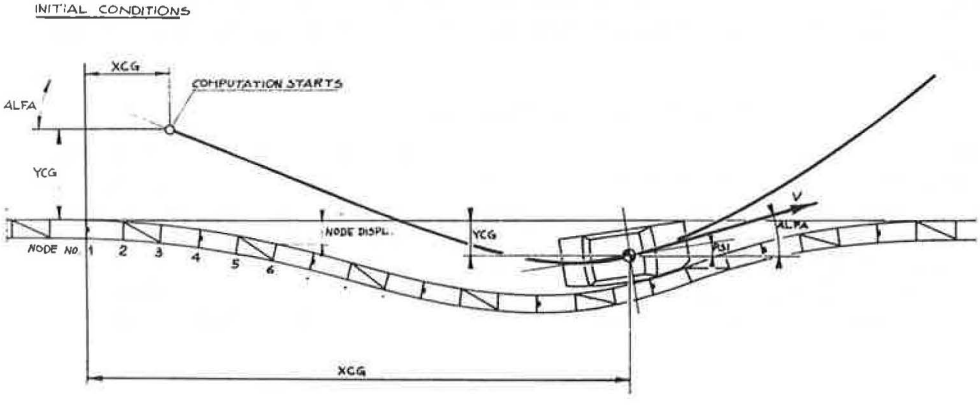

where {v} is the column matrix of the unknowns, which are the normalized displacement at every node (3 per node, Fig. 8) and the displacements of the points of contact between vehicle and barrier. The stiffness matrices [K] and {P} are computed at each step by superimposition of the contribution of the elements, posts, diagonals, vehicle contact forces, and barrier inertial forces (see Appendix). Some velocity-dependent forces (damping) may also be considered.

INPUT DATA

Input data are divided in 3 main groups: vehicle data, barrier data, and computation parameters.

So far vehicle data have been prepared for 5 vehicles: a private car, 2 buses, a light lorry (3 t), and a heavy lorry (24 t at maximum loads). These vehicles will be used as test models for simulating impacts against different types of barriers. Computation parameters are mainly the position and the velocity of the vehicle at the start of computation (Fig. 16) and the maneuvers of the steering gear.

OUTPUT DATA

The output is, for every time increment, the motion of the vehicle and the deformation of the barrier. The vehicle output data are position, attitude, deformation of the body, velocity, steer angle, and accelerations of several points of the vehicle. The barrier output data are the deflections of all the nodes.

Several computations have been prepared with input data corresponding to the full-scale tests conducted by the Institute for Road Safety Research. They compare the output of the simulation with experimental records. The comparison each time shows a fair agreement; in some instances the agreement was not so good because the experimental figure for the velocity of the vehicle could not be more accurately deduced from high-speed films.

Figures 17, 18, 19, and 20 show the comparison of the simulated final deformation of the barrier and the full-scale tests. The results were also visually presented by simulation films for comparison with the high-speed films of the actual tests. The simulation films were made with consecutive still pictures of a model, at $\frac{1}{20}$ scale, which was fixed for every picture in the configuration specified by the simulation system for every time increment. The simulation films showed an extremely good general agreement with the actual films taken from the same angle of view.

CONCLUDING REMARKS

The digital simulation system that has been developed for impact tests against guardrail barriers has proved to be a valuable tool. It may reduce the cost of a test program or, better still, greatly enlarge the extent of a program without increasing the cost. In fact, it may permit a considerable reduction of the number of full-scale tests, which require a relatively long time for preparation, execution, and interpretation and are rather costly. For example, the first simulation program, which is now under development, comprises more than 200 simulations with different vehicles on different types of bridge parapets.

ACKNOWLEDGMENTS

The author expresses his great obligation to the Institute for Road Safety Research for giving him an opportunity to undertake this work. He feels indebted to all those friends who helped him in this extensive and complex task. In particular, he wishes to thank H. G. Paar, W. H. M. van de Pol, and E. Thoënes of the Institute for Road Safety Research for their close collaboration and generous practical help. He also wishes to remember C. Cardani, P. Mantegazza, L. Puccinelli, and L. Savioni of Aerospace Department, Politecnico of Milan, for their very valuable cooperation.

Figure 17.

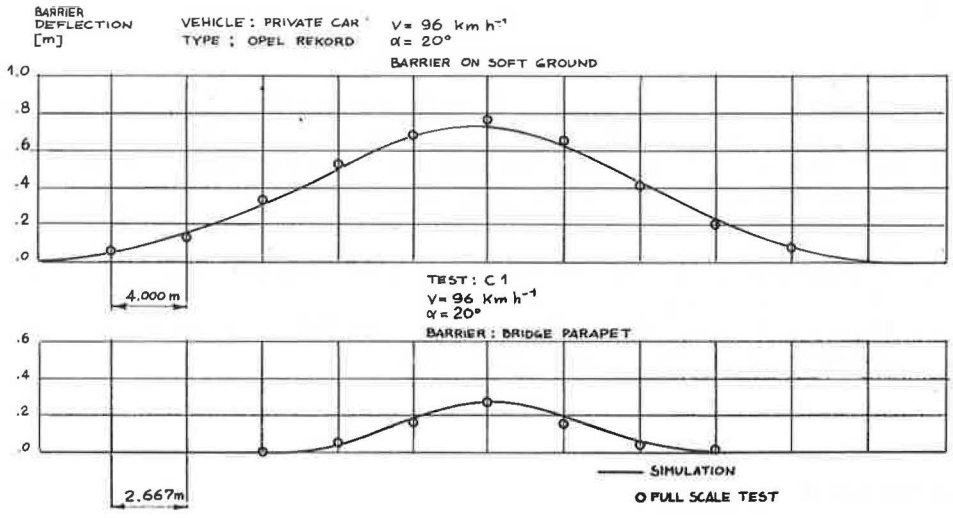

Figure 18.

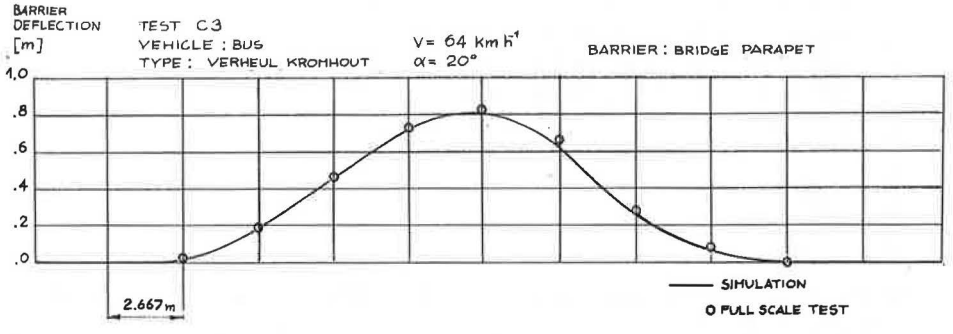

Figure 19.

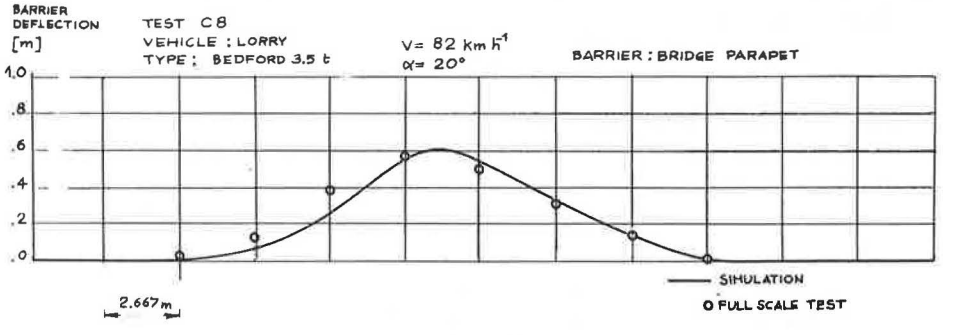

Figure 20.

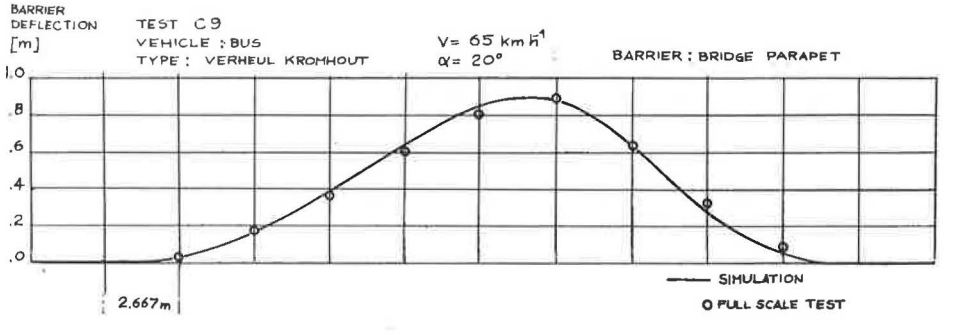

REFERENCES

1. Schulze, R. A. P. J. Dynamic Tests With Guide-Rail Barrier Posts. IWECO-TNO, Delft, Rept. 5064, Vols. 1, 2, and 3, 1970. (In Dutch.)
2. McLean, A. The Use of Flight Simulation in the Development of the SAAB AJ 37 Viggen System. 7th ICAS Congress, Rome, 1970.
3. Przemieniechi, J. S. Theory of Matrix Structural Analysis. McGraw-Hill, New York, 1969.
4. Zienkiewicz, O. C. The Finite Element Method in Engineering Science. McGraw-Hill, London, 1971.
5. Giavotto, V., and Caprile, O. Barriere di sicurezza stradali. Fondamenti teorici ed applicazioni. Milan, SINA Rept., 1967.

APPENDIX

MATRIX EQUATIONS

The nomenclature used in the equations below is defined as follows:

u = normalized beam displacements,
w = displacements of the contact points,
v = displacements comprising u and w,
dt = time interval,
P = known terms,
K = stiffness,
T = diagonal force,
S = generalized element forces, and
F = contact forces.

The following brackets are used for matrix notation: { } for a column matrix and [ ] for every other matrix.

The 6 generalized forces $\{S'\}$ of 1 element, without a diagonal bar and without contact forces between the nodes, are related to the corresponding displacements $\{u\}$ by the matrix equation

$$\{S'\} = [k'] \{u\} \tag{1}$$

where $[k']$ is the element stiffness matrix.

If the diagonal bar exerts a force T, the generalized element forces undergo an increment by the quantities

$$\{S''\} = \{M\} T \tag{2}$$

which are proportional to T through the column matrix $\{M\}$.

If δ is the relative displacement of the end points of the diagonal bar, force T may have the following linearized expression:

$$T = T_0 + T_1\delta \tag{3}$$

which is valid for a small variation of δ.

From Eq. 2 and the Principle of Virtual Works,

$$\delta = \{M\}^T \{u\} \tag{4}$$

where $\{M\}^T$ is the row matrix transpose of $\{M\}$.

Then from Eqs. 2 and 4,

$$\{S''\} = \{M\}\, T_1\, \{M\}^T \{u\} + \{M\}\, T_0 \tag{5}$$

If a certain number of contact points is present in the element between the nodes, the corresponding forces $\{F\}$ may have the following linearized expression, derived from the stiffness of the vehicle body:

$$\{F\} = \{F_0\} - [F_1]\, \{w\} \tag{6}$$

where $\{w\}$ is the absolute displacement of the contact points. From the barrier side, the displacements $\{w\}$ are the sum of the part:

$$\{w'\} = [L]\, \{u\} \tag{7}$$

due to elements and the part

$$\{w''\} = [H]\, \{F\} \tag{8}$$

due to the direct action of the forces. Then,

$$\{w\} = [L]\, \{u\} + [H]\, \{F\} \tag{9}$$

The contact forces $\{F\}$ must be equilibrated by increments of the generalized forces of the elements.

$$\{S'''\} = -[L]^T \{F\} \tag{10}$$

Solving Eq. 9 for $\{F\}$ by substituting in Eq. 6, we have the following additional equation for the unknowns $\{w\}$:

$$\{F_0\} = [H]^{-1} \{w\} + [F_1]\, \{w\} - [H]^{-1} [L]\, \{u\} \tag{11}$$

Superimposing the effects of the diagonal bar and the contact forces, we have finally

$$\left\{\begin{matrix} S \\ \hline F_0 \end{matrix}\right\} = \left[\begin{matrix} k_{uu} & k_{uw} \\ \hline k_{wu} & k_{ww} \end{matrix}\right] \left\{\begin{matrix} u \\ \hline w \end{matrix}\right\} \tag{12}$$

where

$$\{S\} = \{S'\} + \{S''\} + \{S'''\} - \{M\}\, T_0 \tag{13}$$

$$[k_{uu}] = [k'] + \{M\}\, D_1\, \{M\}^T + [L]^T [H]^{-1} [L] \tag{14}$$

$$[k_{wu}] = [k_{uw}]^T = -[H]^{-1} [L] \tag{15}$$

$$[k_{ww}] = [H]^{-1} + [F_1] \tag{16}$$

Equation 12 may also be written, in a shorter notation, as

$$\{S_e\} = [k_e]\, \{v_e\} \tag{17}$$

where $[k_e]$ is a symmetrical matrix.

It is now possible to assemble the stiffness matrix of the complete structure by simply summing the contribution of the elements, posts, diagonals, vehicle contact forces, and barrier inertial forces to obtain the final matrix equation:

$$\{P\} = [K]\, \{v\} \tag{18}$$

Equation 18 must be solved for unknowns {v}, which are the node displacements {u} and the absolute displacements {w} of the contact points.

It is worth noting that matrix [K] is a symmetrical band matrix if the unknowns are so ordered (at each step) that each of the unknowns {w} is placed between the displacements {u} of the 2 nodes of the element having the corresponding contact point. Therefore, the best time and memory occupation techniques are applicable to solve Eq. 18.

SIMULATION OF VEHICLE IMPACT WITH TEXAS CONCRETE MEDIAN BARRIER: TEST COMPARISONS AND PARAMETER STUDY

Ronald D. Young, Edward R. Post, and Hayes E. Ross, Jr.,
Texas Transportation Institute, Texas A&M University

The highway-vehicle-object simulation model, a computer program developed at Cornell Aeronautical Laboratory, has been modified to simulate a vehicle impacting the Texas concrete median barrier at speeds from 50 to 80 mph and angles from 5 to 25 deg. The barrier was impacted by a 4,000-lb sedan for angles of 7, 15, and 25 deg at 60 mph. The results of those full-scale tests were closely approximated by the modified simulation model. Comparisons of simulation and test results are presented in computer-generated drawings of the vehicle during impact, frames from the high-speed film, and plots relating predicted and measured accelerometer readings. After the simulation of the full-scale tests, a parameter study on impact conditions was conducted. The model simulated a 4,780-lb vehicle impacting the barrier at speeds of 50, 70, and 80 mph at angles of 5, 10, and 15 deg for each of those speeds. For speeds less than 70 mph, the results were in line with findings of other researchers. For speeds of 70 mph and greater and impact angles of 15 deg and greater, automobile roll-over can be expected. The results of all simulated impacts with the barrier are presented graphically with regard to a severity index, which quantifies the severity of each crash based on vehicle accelerations.

•EVALUATION of barrier systems usually includes full-scale vehicle crash tests. Those tests are often quite expensive, and many man-hours are required for all phases of the test program. A more ideal method of studying the performance of barriers is by computer simulation.

The original version of the highway-vehicle-object simulation model (HVOSM), which was formerly known as CALSVA (1, 2), was capable of predicting automobile behavior for impact with certain types of barriers, provided the automobile crash was moderate (12 to 18 in.). The types of barrier systems that can be studied with the HVOSM are those whose lateral resistance to vehicle penetration is independent of the longitudinal position of the vehicle contact. The Texas concrete median barrier (CMB) is a rigid barrier and falls within this category. The HVOSM was modified by the Texas Transportation Institute (TTI) to include hard points within the automobile structure. Hard points simulate the effects caused when very stiff automobile members are encountered, such as the engine, a frame member, or a wheel assembly. Basic details of HVOSM (1, 2, 3) and the description of the hard-point modifications (4) are not included in this report.

Comparisons are made between experimental data from full-scale crash tests of the CMB and simulated results from the modified HVOSM (including hard points). The crash test data were obtained from another research program (5) sponsored by the Texas Highway Department. In general, good correlation exists between simulated and experimental results.

A parametric study of the CMB was conducted by using the HVOSM, and the results are described. The parametric study was used to determine the barrier's performance

characteristics for a range of vehicle encroachment conditions. Factors used in measuring the performance were the vehicle's exit angle, maximum pitch and roll angle, and a severity index that quantified the impact severity.

COMPARISON OF EXPERIMENTAL DATA WITH PREDICTIONS BY HVOSM

Sponsors and researchers felt that a good correlation between simulation and testing was a prerequisite to conducting parametric studies of the CMB with the HVOSM.

The 3 tests used in the comparisons (5) consisted of passenger cars (roughly 4,000-lb in weight) being towed into a full-scale model of the CMB, model I-70 (designated CMBI-70), at approximately 60 mph for impact angles of 7, 15, and 25 deg. The CMBI-70 designation is used when illumination poles are placed atop the barrier. The exterior dimensions of the barrier are the same, however, whether illumination is used or not. Accelerometers were mounted to the structural framework of the vehicles and were oriented to measure the lateral and the longitudinal components of vehicle acceleration. Vehicle motion was recorded on high-speed film from rear, side, and overhead views. These films were used to determine the automobile's speed and angle at impact and to provide a comparison of the vehicle's simulated and actual motion.

As explained earlier, the computer simulation used was a modified version of the HVOSM (4). Certain limitations dictated the description of the CMB by a combination (or superposition) of the program's "curb impact" and "barrier impact" capabilities. As shown in Figure 1, the sloping face of the barrier was simulated as a curb (line 1-2), and the upright face was simulated as a vertical rigid barrier (line 2-3). In the simulation, tire-curb interaction is accounted for, but tire-rigid barrier interaction is not. However, since good comparisons between simulations and tests were obtained (for both kinematics and accelerometers), it would appear that tire contact with the upright face is of secondary importance. For the same reason, the omission of slope 4-5 (Fig. 1) was apparently not detrimental to the simulation. This is not surprising in view of the relative dimensions of the tires to the length of line 4-5 and the high impact speeds. Likewise, idealizing the upright face as vertical rather than sloped a few degrees proved to be adequate representation. For the shallow angle impact of 7 deg, the whole barrier could have been defined as one high curb (1), but for the sake of uniformity all cases were defined as described above.

Data corresponding to the CMB and the test vehicles, such as vehicle weight, barrier and vehicle dimensions, and impact speed and angle, were read into the HVOSM program. All computer input data are documented elsewhere (6).

Plots of the predicted and measured acceleration components at points corresponding to the locations of accelerometers in the actual vehicle were made. Drawings of the simulated impacts were generated by a computer program (7). The program produces a perspective drawing of the vehicle and barrier at selected times, using vehicle position as determined from the HVOSM. These line drawings were then compared with corresponding photographs taken from the high-speed photography of the test.

The results of the comparisons are shown in Figures 2 through 7. The test results are for a vehicle impacting on the left (driver) side of the vehicle, while the simulation is on the opposite (passenger) side. For this reason, the accelerometer results are expressed in terms of impact side of the vehicle. Time of initial impact was taken as zero, and the times shown on the figures are with respect to impact time. Comparisons were stopped when the vehicle lost contact with the barrier.

The comparison of test photographs and computer drawings shown in Figures 2, 3, and 4 is very good for all 3 tests. Comparing the wheel positions, height of climb, and relative position of vehicle body to the ground shows that the simulation accurately computed the motions of the test vehicle. The small differences observable between the positions of simulated and actual vehicles is largely attributable to a standard automobile that was used for all the computer drawings and that was not necessarily of the same dimensions as the actual test vehicles. A second noticeable discrepancy is the appearance of the simulated vehicle to penetrate the barrier in a few instances. The program that produces the computer drawing cannot show sheet metal crushing, although it is accounted for in the HVOSM.

Figure 1. Idealization of CMBI-70 for computer simulation.

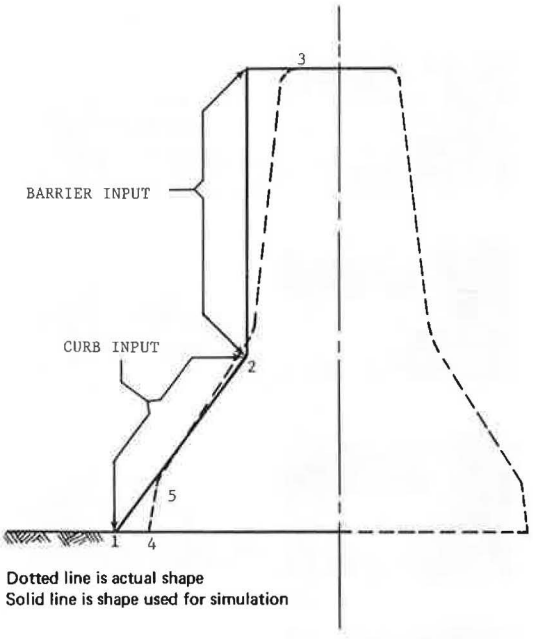

Dotted line is actual shape
Solid line is shape used for simulation

Figure 2. Simulation and test results for 4,000-lb vehicle impacting CMB at 63 mph and 25 deg.

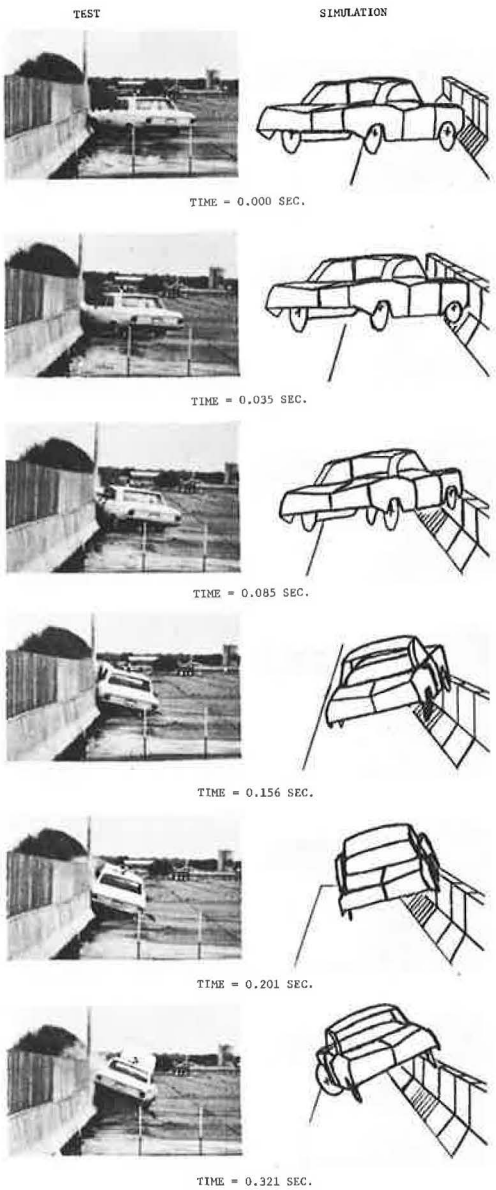

Figure 3. Simulation and test results for 4,210-lb vehicle impacting CMB at 59.6 mph and 15 deg.

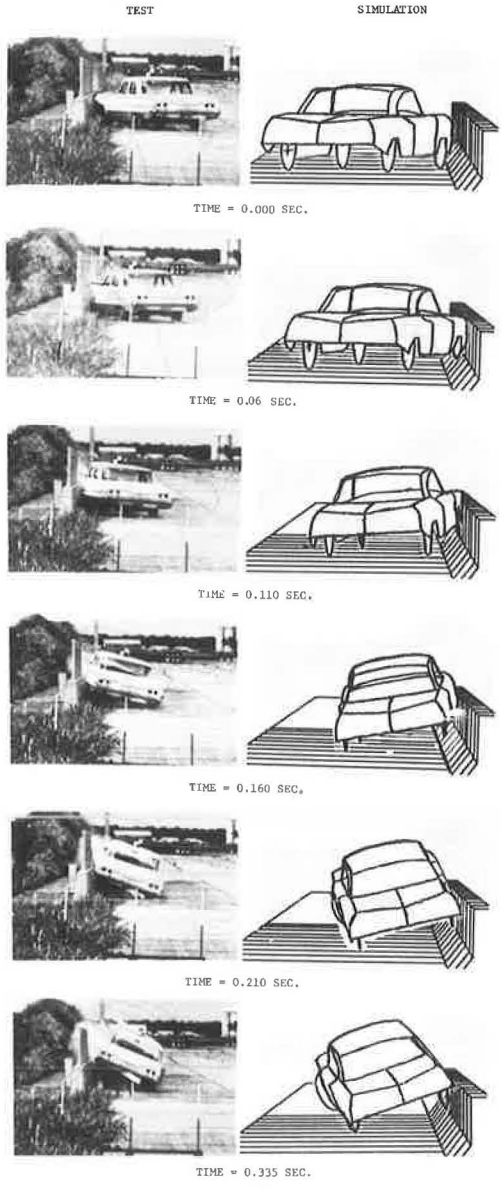

Figure 4. Simulation and test results for 4,210-lb vehicle impacting CMB at 61.9 mph and 7 deg.

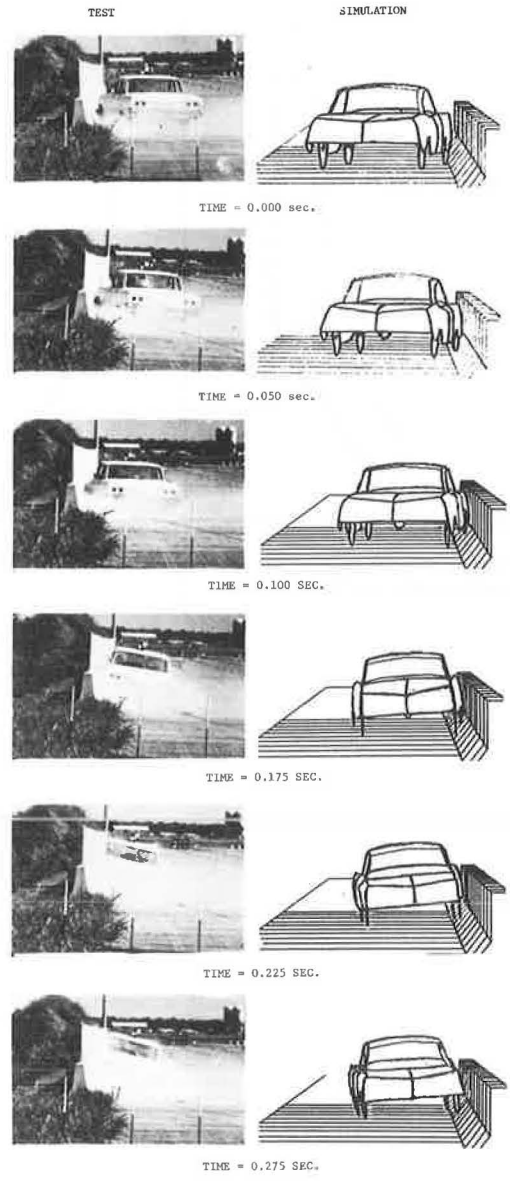

Figure 5. Acceleration on impact side of 4,000-lb vehicle at 63 mph and 25 deg.

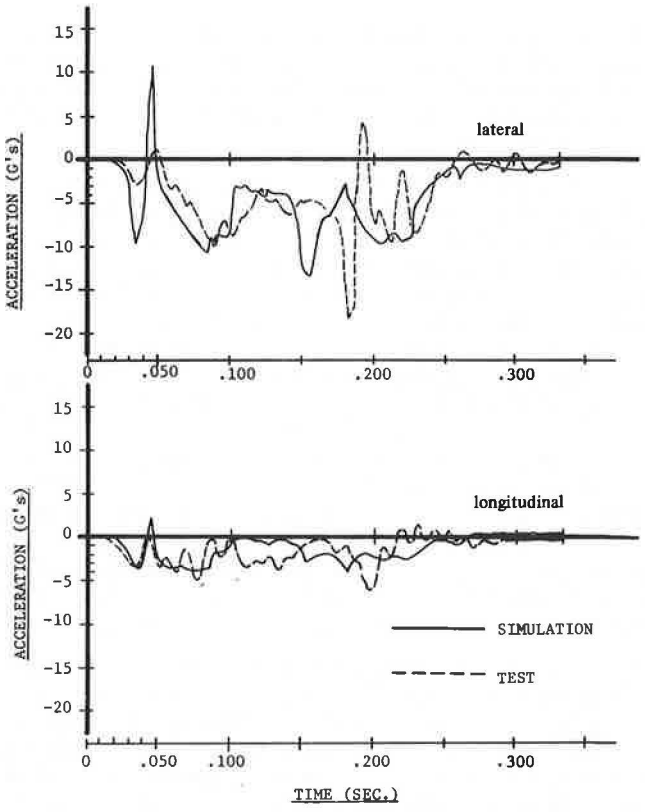

Figure 6. Acceleration on impact side of 4,210-lb vehicle at 59.6 mph and 15 deg.

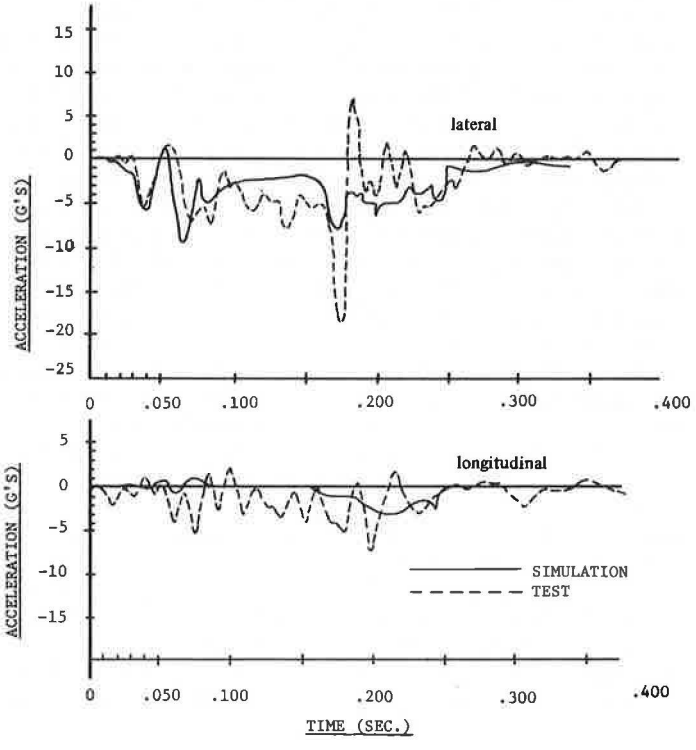

The comparisons of simulated and measured acceleration components shown in Figures 5 and 6 can be considered good, whereas the comparison shown in Figure 7 can only be considered poor. Fortunately, the discrepancies occurring in all 3 cases, whether slight or major, can be explained in terms of 2 basic differences between the actual and simulated vehicles.

1. The actual vehicle structure comprises structural subassemblies, each possessing its own vibrational characteristics (natural frequencies and damping). However, the simulated vehicle structure (wheels and suspension systems excluded) is a rigid mass that is undamped and free of natural frequencies of vibration. Therefore, the actual accelerometers will respond to those structural vibrations that do not contribute to vehicle redirection and, accordingly, will not be felt by an occupant. Correspondingly, the simulated accelerometers respond only to those actions that cause vehicle redirection or rigid body motion because the simulation is devoid of structural vibrations except those stemming from the wheels and suspension systems.
2. In the actual case, the effect of a force applied to the vehicle structure is diminished or damped before reaching an accelerometer located some distance away from the point of application. In some cases, if the distance is large enough and the force is of short duration, the effect may be damped out completely and, hence, undetected by the accelerometer. However, in the simulated case, all forces applied to the vehicle structure are transferred to the center of gravity of the rigid body as an equivalent force-couple system such that all simulated accelerometers respond instantaneously regardless of their location on the structure.

The simulated lateral accelerometer traces shown in Figure 5 exhibit an oscillation of ±11 g between 30 and 50 msec, which was not recorded by the test accelerometers. That is caused by the front wheel violently engaging the suspension bumper stops as it first hits the barrier at the large impact angle of 25 deg. The same probably occurred in the test, but, because the accelerometers were located about 6.5 ft behind the front wheel (just ahead of the rear wheel mounted to the frame member), the effects of those short-duration forces were largely damped out before reaching the accelerometers.

The test lateral accelerometer traces shown in Figures 5 and 6 reveal oscillations between 175 and 200 msec, which were not predicted by the simulation. Those represent structural vibrations of the frame member, to which the accelerometers were mounted, and were induced by oscillations of the rear axle assembly when the rear wheel encountered the barrier. All of the differences in accelerations explained thus far were vibrational in nature and produced negligible net changes in velocity and, hence, did not contribute to vehicle redirection. This is upheld by the fact that the comparisons of vehicle position are excellent (Figs. 2, 3, and 4).

The huge spike appearing in Figure 7 has 2 possible explanations. First, it is highly probably that this spike is also the result of a structural vibration caused by the rear wheel impacting the barrier. The vibration could have been critically damped, explaining the existence of only 1 spike. Furthermore, the reason that higher levels were recorded for this test, although it was less severe (only slight sheet metal damage), could be a result of the accelerometers being more directly aligned with the blow because of the small pitch and roll motions of the vehicle. If this explanation is accepted, the spike can be disregarded as not contributing to redirection of the vehicle, and the accelerometer comparison can be considered good.

However, as a second explanation, it is conceivable that initial tire contact caused the vehicle to rotate (yaw) parallel to the barrier without appreciably changing the vehicle's velocity vector (magnitude or direction). The vehicle would then have impacted the barrier in this position, causing an abrupt change in lateral velocity. In fact, for 60 mph at 7 deg, the component of velocity normal to the barrier is 10.7 ft/sec, which corresponds to the area under the spike in question. This comparison is justifiable in this case because the car was parallel to the barrier when the spike occurred. If this explanation is accepted, the question remains as to whether this is a reproducible phenomenon or an abnormality. Until this question is answered, the HVOSM accelerometer results cannot be discounted, especially because good acceler-

ometer comparisons were achieved for the 2 higher angles of impact, and good vehicle position comparisons were attained for all 3 tests.

Considering all facets of the comparison, it can be concluded that the HVOSM (with added structural hard points) provides a good simulation of an automobile impacting a rigid barrier of the CMB type. Hence, it follows that the results of the parameter study can be treated with added confidence.

PARAMETER STUDY

The modified version of the HVOSM computer program (4) was used to study the dynamic behavior of an automobile impacting the CMB. The objective of the parametric study was to determine the performance characteristics of the CMB for a range of vehicle encroachment conditions. Factors used to measure barrier performance consisted of the vehicle's exit angle, maximum pitch and roll angle, and an index to quantify the severity.

Severity Index

The automobile acceleration severity index (SI) was used to quantify the relative severity of an automobile impacting a traffic barrier. The severity index takes into consideration the combined effects of the longitudinal, lateral, and vertical accelerations of the automobile at its center of mass. The SI is computed as follows:

$$SI = \sqrt{\left(\frac{G_{LONG}}{G_{XL}}\right)^2 + \left(\frac{G_{LAT}}{G_{YL}}\right)^2 + \left(\frac{G_{VERT}}{G_{ZL}}\right)^2} \qquad (1)$$

The terms in the numerator are the computed or measured accelerations of the automobile, and the terms in the denominator are the limit or tolerable accelerations of the automobile.

An in-depth discussion of the background and development of Eq. 1 is given in another report (9). Information relating tolerable accelerations to degree of occupant restraint, rate of onset or rise time, and time duration of accelerations is included in that discussion. In the study presented here, the tolerable accelerations were for an unrestrained occupant, rise times greater than 0.03 sec, and a time duration of 0.050 sec. The limit or tolerable accelerations for these conditions (9) are assumed to be

$$G_{XL} = 7 \text{ g}$$
$$G_{YL} = 5 \text{ g}$$
$$G_{ZL} = 6 \text{ g} \qquad (2)$$

There has been much discussion of the relation of the severity index to the probable level of occupant injury. The authors have interpreted an SI of unity to imply that occupants will sustain injuries that border on the serious type. Until more data are available on limit accelerations and the interaction relation itself, there appears to be no other logical way to interpret the index.

In addition, vehicle accelerations have never been translated into expected g levels on the occupant, and until such a correlation becomes available the possible applications of the severity index must be qualified. The index in its present form is intended for comparing the severity of one event to another and can also serve as an aid in making decisions concerning highway modifications that should effect a reduction in occupant injury and loss of life. However, it must be emphasized that the index, as defined by TTI researchers (here or elsewhere), has never been intended for direct assessment of human injury and, therefore, should not be used in that regard.

Simulations

Nine different automobile impacts with the CMB were simulated. The impact speeds were 50, 70, and 80 mph, and for each speed there were 3 impact angles: 5, 10, and 15

deg. The simulated automobile had the properties of a 1963 Ford Galaxie weighing 4,780 lb. Also included in this phase of the study were the 3 impacts simulated in the validation study at angles of 7, 15, and 25 deg and an impact speed of approximately 60 mph. These 12 different impact conditions are representative of the majority of accidents involving traffic barriers. The results of the 12 runs are given in Table 1.

All impact data for the computer runs, including vehicle and barrier information, are reported elsewhere (6). Some of the significant parameters are as follows: hard-point stiffness, 2,500 lb/in.; sheet metal crushing coefficient, 2 lb/in^3; automobile-barrier coefficient of friction, 0.3; and tire-curb coefficient of friction, 0.50.

In some instances, the roll angle of the vehicle was still increasing at the termination of the computer run. Rather than rerun those cases (which would have been uneconomical), a formula was developed to estimate the roll angle beyond the termination point. This relation was used to determine the maximum roll angle and thereby determine whether roll-over would have occurred. Its derivation is shown in Figure 8.

Barrier Performance

Model simulation indicates that the vehicle will roll over during a collision with a CMB at impact speeds of 70 and 80 mph and an impact angle of 15 deg. Also, at 63 mph and 25 deg the vehicle is very near roll-over. The roll angle given in Table 1 is the maximum roll angle of the automobile and may or may not occur when the automobile is in contact with the barrier.

The maximum pitch angle of the automobile appears more sensitive to impact angle than to impact speed (Table 1). In any event, the pitch angle remains small for any angle of impact and appears to be insignificant when the motion of the automobile is considered.

Height of the front tire climb on the face of the CMB is given in Table 1. During a 5-deg collision, the front tire of the automobile climbs roughly 5 to 7 in. on the lower inclined CMB surface; and, during a 10-deg collision, the tire climbs roughly 9 to 12 in. on the lower surface. As indicated, the climb height was not available in some cases because tire-rigid barrier interaction is not accounted for in the HVOSM. However, based on an analysis of the output, it is doubtful that the tire climb would have exceeded the height of the barrier in those cases.

A desirable characteristic of a traffic barrier is that a colliding automobile be redirected at a shallow exit angle in order to minimize the danger to traffic. The exit angles given in Table 1 were determined at the time the vehicle lost contact with the barrier. The exit angle appears to be more sensitive to impact angle than to impact speed. In all cases, however, the exit angles were shallow.

Another criterion used to determine barrier performance was the relative severity of the impact as measured by automobile accelerations. A severity index is given in Table 1 for each of the 12 runs studied. Figure 9 shows the severity index versus impact angle for 4 impact speeds. The apparent inconsistency of the 60-mph case is attributable to the differences in vehicle weight and dimensions. For speeds of 50, 70, and 80 mph the vehicle weighed 4,780 lb; in the 60-mph case, the vehicle weighed 4,210 lb. The hard-point stiffness, sheet metal crushing coefficient, automobile-barrier coefficient of friction, and tire-curb coefficient of friction were the same for all 4 speeds. The results, therefore, suggest that the severity of a lighter vehicle impacting the barrier may be more than that of a heavier vehicle, all other factors being the same.

Figure 10 shows impact speed versus impact angle for a severity index of 1.0. The 4 points on the curve were obtained from the intersection of the SI = 1.0 line with the 4 respective speed curves shown in Figure 9. The data may be useful in selecting roadway locations where the CMB can be safely used. For a given roadway, an upper limit on impact angle can be estimated (8) as a function of the roadway's design speed and surface conditions and the distance from the roadway to the barrier. If the combination of design (or impact) speed and impact angle falls above the curve, it may be advisable to select a more flexible barrier.

Figure 7. Acceleration on impact side of 4,210-lb vehicle at 61.9 mph and 7 deg.

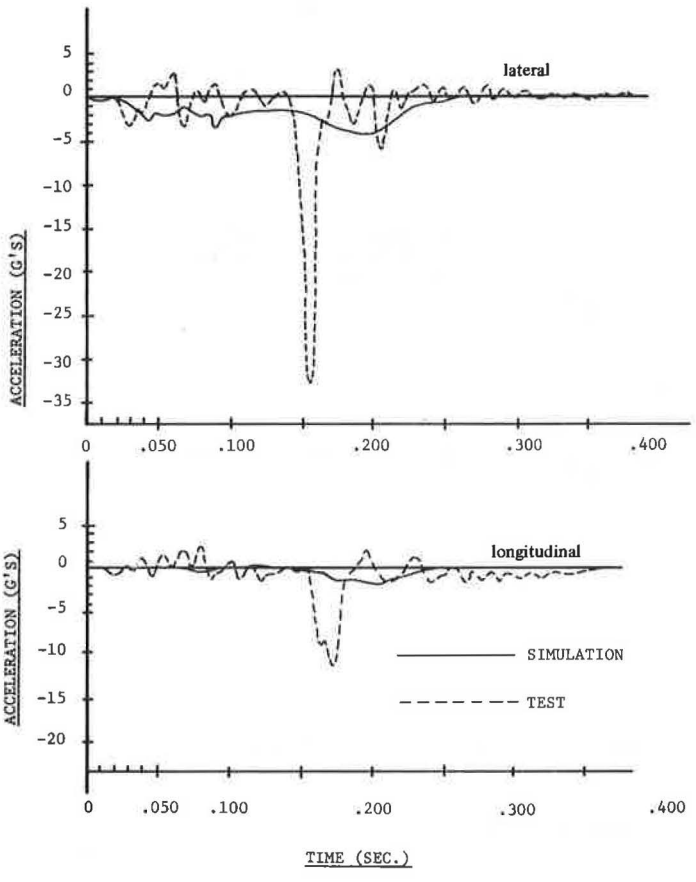

Figure 8. Estimation of maximum roll angle.

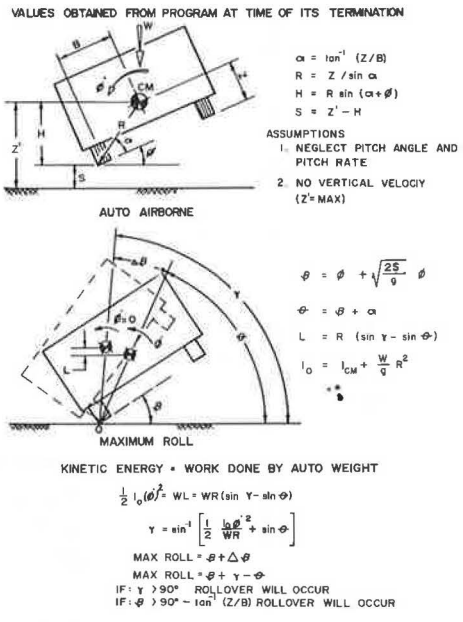

Table 1. Results of CMB simulations.

Run	Auto Weight (lb)	Impact Conditions: Speed (mph)	Impact Conditions: Angle (deg)	Automobile Kinematics: Max Roll (deg)	Max Pitch (deg)	Front Tire Climb (in.)	Exit Angle[a] (deg)	Avg Accelerations During Primary Impact: G_{long}	G_{lat}	G_{vert}	Severity Index
1	4,780	50.0	5.0	1.3	0.9	4.6	1.1	0.49	1.61	0.12	0.33
2	4,780	70.0	5.0	2.2	1.5	6.5	0.3	0.72	2.53	0.43	0.52
3	4,780	80.0	5.0	3.3	1.8	7.1	0.1	0.21	2.90	0.54	0.58
4	4,780	50.0	10.0	4.2	3.2	8.6	2.5	1.13	2.99	0.94	0.64
5	4,780	70.0	10.0	19.5[b]	5.0	11.2	1.2	0.16	5.06	2.03	1.07
6	4,780	80.0	10.0	34.6[b]	5.8	12.6	1.2	1.92	6.42	2.61	1.38
7	4,780	50.0	15.0	15.0[b]	6.5	11.9	3.6	0.47	4.29	1.38	0.91
8	4,780	70.0	15.0	RO[c]	6.6	NA[d]	2.7	2.81	6.44	3.16	1.45
9	4,780	80.0	15.0	RO[c]	6.1	NA[d]	2.9	3.24	7.49	3.29	1.66
10	4,210	61.9	7.0	4.7	2.3	7.4	2.2	1.07	3.21	0.64	0.67
11	4,210	59.6	15.0	21.0[b]	8.2	13.2	5.5	2.78	6.86	2.92	1.48
12	4,000	63.0	25.0	37.0	8.6	NA[d]	5.1	6.47	11.23	4.38	2.54

[a]When vehicle loses contact with barrier.
[b]Estimated roll obtained by energy expression using initial conditions from computer simulation at the time it was terminated.
[c]Roll-over.
[d]Not available.

Figure 9. Severity index of CMB as related to vehicle encroachment conditions.

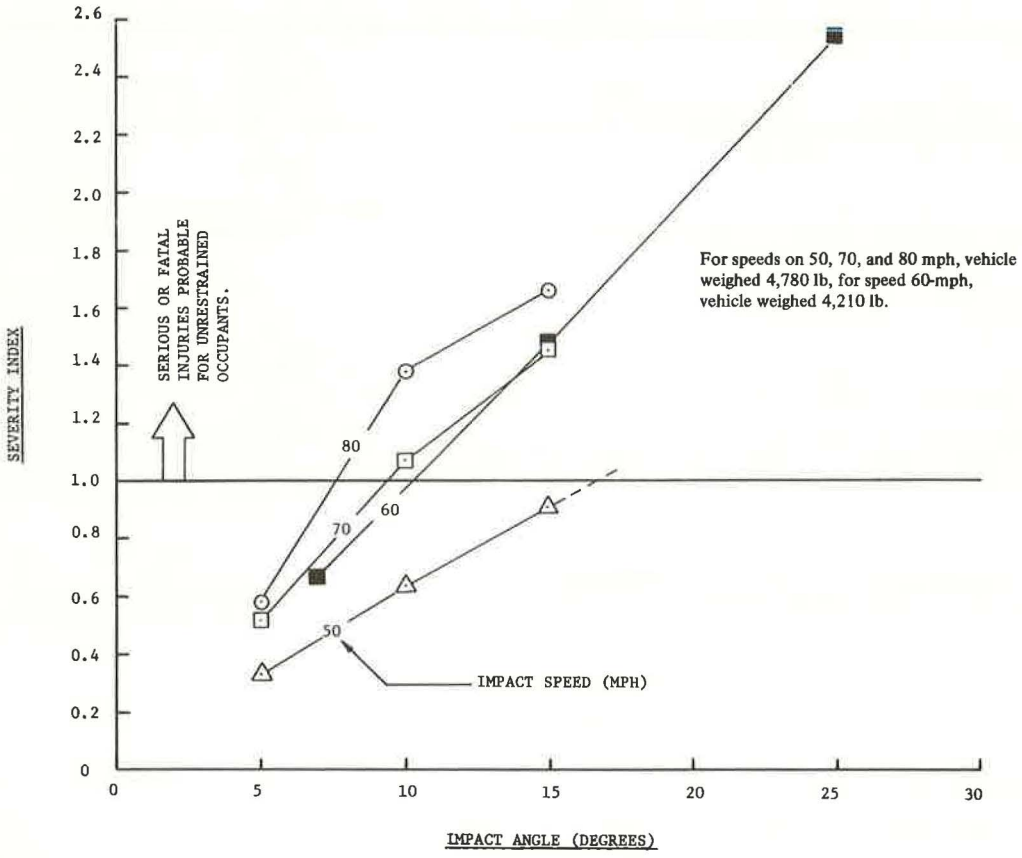

Figure 10. Relation of encroachment conditions at severity index near unity for CMB.

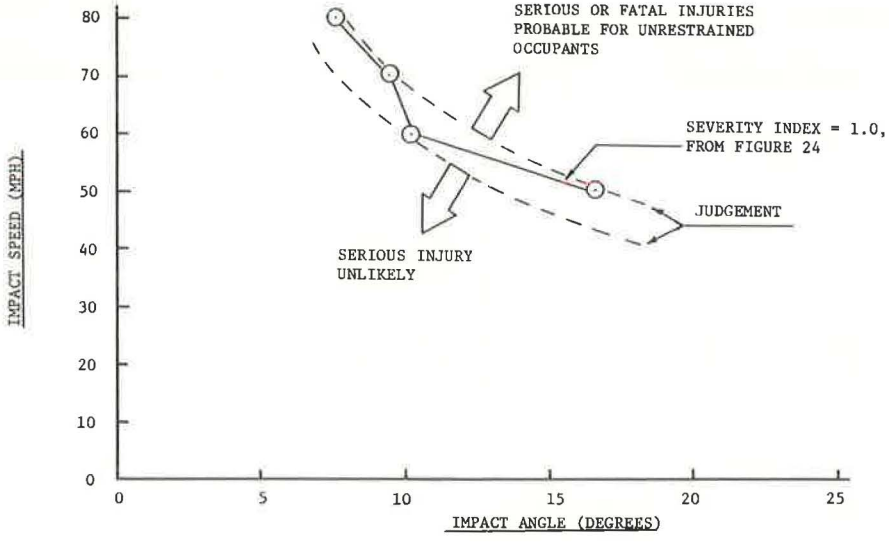

SUMMARY OF RESULTS

1. The impact subroutines of HVOSM were modified by TTI to account for the effects of hard-point contacts (frame members, motor block) that occur when large vehicle deformations occur.
2. The modified HVOSM computer program (with hard points) can accurately predict automobile accelerations, motions, and external forces due to an impact with the CMB. This conclusion is based on a good correlation that was obtained between full-scale test results and simulations by HVOSM.
3. As a result of a parametric study with HVOSM, the following conclusions are made with regard to the CMB performance:

a. For impact speeds of 70 mph and greater and impact angles of 15 deg and greater, automobile roll-over can be expected;

b. For impact speeds of 80 mph and less and impact angles of 15 deg and less, there was no tendency for the automobile to vault or climb over the barrier;

c. In each of the 12 impact conditions studied, the automobile's exit angle was shallow after impact with the barrier; and

d. A graphical presentation was made of the impact angles and speeds for which the barrier can presumably redirect an automobile without serious injuries to the occupants.

ACKNOWLEDGMENTS

This research was sponsored by the Texas Highway Department in cooperation with the Federal Highway Administration. The authors sincerely thank Norman J. Deleys and Raymond R. McHenry of Cornell Aeronautical Laboratory for providing generous professional assistance in the form of copies of their previous work on modifying their model to include the effect of vehicle structural hard points in simulating automobile-barrier crashes. Thanks are also extended to John F. Nixon and David Hustance of the Texas Highway Department and Edward V. Kristaponis of the Federal Highway Administration for their cooperation in meeting the uncertainties of this particular research effort and their patience in awaiting the reported results.

REFERENCES

1. McHenry, R. R., and Segal, D. J. Determination of Physical Criteria for Roadside Energy Conversion Systems. Cornell Aeronaut. Lab., Inc., Buffalo, VJ-2251-V-1, July 1967.
2. McHenry, R. R., and Deleys, N. H. Vehicle Dynamics in Single Vehicle Accidents: Validation and Extensions of a Computer Simulation. Cornell Aeronaut. Lab., Inc., Buffalo, VJ-2251-V-3, Dec. 1968.
3. Young, R. D., Edwards, T. C., Bridwell, R. J., and Ross, H. E., Jr. Documentation of Input for the Single Vehicle Accident Computer Program. Texas Transp. Inst., College Station, Res. Rept. 140-1, July 1969.
4. Young, R. D., Post, E. R., Ross, H. E., Jr., and Holcomb, R. M. Simulation of Vehicle Impact With the Texas Concrete Median Barrier—Vol. 1: Test Comparisons and Parameter Study. Texas Transp. Inst., College Station, Res. Rept. 140-5, June 1972.
5. Hirsch, T. J., Hayes, G. G., and Post, E. R. Vehicle Crash Test and Evaluation of Median Barriers for Texas Highways. Texas Transp. Inst., College Station, Res. Rept. 146-4, June 1972.
6. Young, R. D., Post, E. R., and Ross, H. E., Jr. Simulation of Vehicle Impact With the Texas Concrete Median Barrier—Vol. 2: Computer Input Data. Texas Transp. Inst., College Station, Res. Rept. 140-5, Sept. 1972.
7. Theiss, C. M. Perspective Picture Output for Automobile Dynamics Simulation. Cornell Aeronaut. Lab., Inc., Buffalo, VJ-2251-V-2R, Jan. 1969.

8. Graham, M. D., Burnett, W. C., Gibson, J. L., and Freer, R. H. New Highway Barriers: The Practical Application of Theoretical Design. Highway Research Record 174, 1967, pp. 88-183.
9. Ross, H. E., Jr., and Post, E. R. Criteria for Guardrail Need and Location on Embankment—Vol. 1: Development of Criteria. Texas Transp. Inst., College Station, Res. Rept. 140-4, April 1972.

TRUCK TESTS ON TEXAS CONCRETE MEDIAN BARRIER

Edward R. Post and Teddy J. Hirsch, Texas Transportation Institute,
Texas A&M University; and
John F. Nixon, Texas Highway Department

The Texas concrete median barrier, with inclined surfaces, satisfactorily restrained and redirected a large 48,800-lb tractor-trailer truck with load under the full-scale impact test conditions of 35 mph at a 19-deg angle, 34 mph at a 16-deg angle, and 45 mph at a 15-deg angle. The truck was remotely controlled from a chase pickup vehicle. There was damage to the sheet metal of the front fender and running board of the tractor. Estimated repair cost was less than $200. Maintenance of the barrier would require, at most, a light sandblasting job to remove the unsightly tire scrub markings. The small amount of concrete spalling that occurred in the immediate area of impact would require no maintenance. The fence and light pole on top of the barrier were not damaged.

•RECENT accident information compiled by the Texas Highway Department and reported by Olson (1) shows that the number of trucks involved in traffic barrier fatal accidents has increased from 16 to 21 percent over a period of approximately 2 years. These accident figures include single-unit trucks, combination tractor-trailer trucks, and pickup trucks. Highway engineers are, therefore, very much concerned over the inadequate height and strength of many current types of traffic barriers.

The massive concrete traffic barrier, with a lower inclined surface of about 55 deg, has proved to be under test and field conditions an effective design in restraining and redirecting automobiles. Tests conducted by Lundstrom (2) have further demonstrated that the concrete barrier performed satisfactorily in restraining and redirecting a single-unit 16,000-lb truck, with load, under the impact conditions of 37 mph and 13 deg.

The promising medium-sized truck test results of Lundstrom (2) on the concrete barrier were instrumental in the development of additional research. The objective of this research project was to tentatively determine, based on a limited number of full-scale tests, the capability of the Texas concrete median barrier to restrain and redirect a large-sized tractor-trailer truck under typical highway encroachment conditions.

DESCRIPTIONS AND PROCEDURES FOR TESTS

Median Barrier

The median barrier used in the full-scale truck tests was the rigid Texas concrete median barrier, designated as CMB-70. Earlier tests conducted by Hirsch (3) demonstrated that the Texas CMB remained intact in restraining and redirecting a standard-sized 4,000-lb passenger vehicle under the severe impact conditions of 60 mph and 25 deg.

The CMB, shown in Figure 1, has a weight of 507 lb/lin ft, a height of 32 in. above the roadway, a lower 10-in. high inclined surface of 55 deg, a base width of 27 in., and a top width of 8 in.

The CMB was constructed in two continuous length sections of 50 and 150 ft as shown in Figure 1. The construction joint between the two sections offers no lateral restraint. The light pole was mounted on top of the shorter 50-ft section. Three 18-in. diameter drilled concrete shafts were used to support the shorter 50-ft section against possible overturning due to wind and vibratory forces on the light pole. The longer 150-ft section, on which the truck tests were conducted, contains no mechanical anchors

to the roadway. The 1-in. layer of hot-mix asphalt at the base of the CMB was used to provide some restraint to sliding during a vehicle collision. Details of the chain-link fence and light pole were discussed by Hirsch (3).

Test Vehicle

The test vehicle used in the full-scale tests was a large-sized tractor-trailer truck weighing 48,800 lb with load. The truck in a loaded condition prior to the tests is shown in Figure 2. Pertinent data of the truck are shown in Figure 3.

The truck trailer was loaded with concrete blocks weighing 22,800 lb. The arrangement of the concrete blocks is shown in Figure 2c and Figure 3. The blocks were stacked to an average height of about 24 in. over a distance of about two-thirds the length of the trailer.

The wheel loads and height measurements of the truck before and after loading are shown in Figure 3. The lumped center-of-mass of the loaded trailer body (excluding the rear tandem wheel assemblies) is located at a height slightly above the top of the concrete blocks and at a height of 6.0 ft above the level roadway, and the location of the lumped center-of-mass of the tractor is approximately 2.6 ft above the roadway.

Truck Control Apparatus

A 5-channel radio remote system was used to control the truck from a chase pickup vehicle. The truck control apparatus consisted of on-off steer control (hydraulic), on-off clutch control (pneumatic), on-off trailer brake control (pneumatic), and on-off accelerator pedal control (pneumatic).

The on-off steer control apparatus consisted of a 4-way hydraulic solenoid valve and a double-acting hydraulic cylinder coupled between the front axle and the tie rod of the truck. A pump, driven by the truck engine, was used as the hydraulic power source. The 4-way hydraulic solenoid valve unit, mounted in the toolbox of the truck, is shown in Figure 4a.

The on-off clutch and accelerator pedal truck controls both had a 3-way pneumatic valve and a single-acting pneumatic cylinder. The truck air compressor was used as the pneumatic power source. The single-acting pneumatic cylinders, mounted on the clutch and accelerator pedal, are shown in Figure 4.

The on-off brake control consisted of a 3-way pneumatic valve spliced into the brake air lines of the truck trailer. The brakes on the truck tractor were not used to minimize the possibilities of jackknifing.

The test truck was started from a rest position by a pushing second vehicle. In the rest position, the truck was in gear with its engine running and its clutch disengaged by the pneumatic control cylinder. After reaching a sufficient speed, the pushing vehicle reduced its speed and turned away. The clutch of the test truck was then engaged, and the truck proceeded on toward the barrier under power and under the control of the chase pickup vehicle.

The angle of steer and the accelerator pedal truck controls were held fixed in position subsequent to the instant of barrier contact. The brakes of the truck trailer were applied after the truck was clear of the 200-ft long barrier test section.

Truck Instrumentation

An Impact-O-Graph was used to record the longitudinal, lateral, and vertical acceleration components of the truck tractor compartment at a location on the floor and directly under the passenger seat. The Impact-O-Graph was remotely turned on from the chase pickup vehicle just prior to impact with the CMB.

DISCUSSION AND EVALUATION OF TESTS

Barrier Performance

Three full-scale angle collision truck tests, designated as CMB-5, CMB-6, and CMB-7, were conducted on the Texas CMB. The CMB, subjected to the impact conditions measured below, performed satisfactorily in restraining and redirecting the loaded 48,800-lb

Figure 1. Texas concrete median barrier (CMB-70).

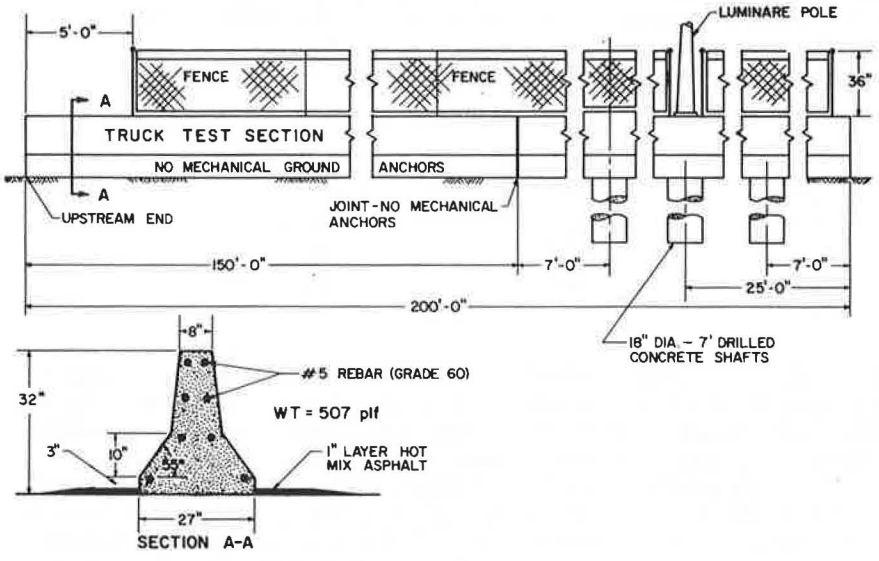

Figure 2. Test truck in loaded condition prior to tests.

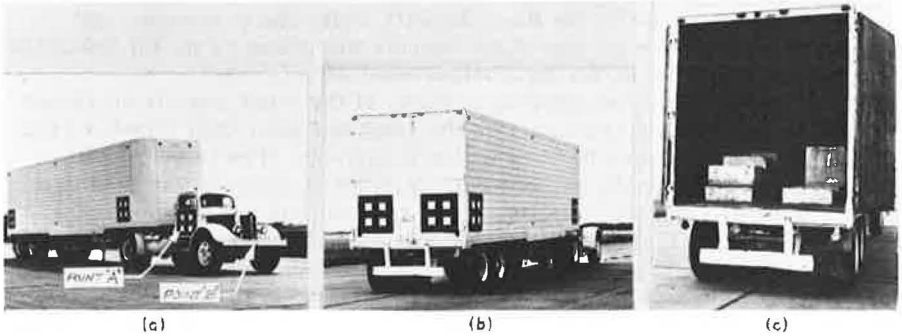

Figure 3. Pertinent truck data.

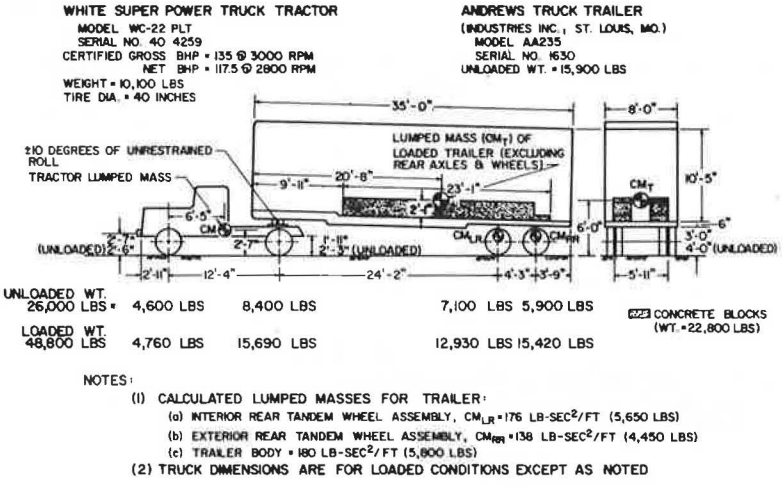

NOTES:

(1) CALCULATED LUMPED MASSES FOR TRAILER:
- (a) INTERIOR REAR TANDEM WHEEL ASSEMBLY, CM_{LR} = 176 LB-SEC^2/FT (5,650 LBS)
- (b) EXTERIOR REAR TANDEM WHEEL ASSEMBLY, CM_{RR} = 138 LB-SEC^2/FT (4,450 LBS)
- (c) TRAILER BODY = 180 LB-SEC^2/FT (5,800 LBS)

(2) TRUCK DIMENSIONS ARE FOR LOADED CONDITIONS EXCEPT AS NOTED

tractor-trailer truck. No permanent rotational and lateral displacements of the unanchored and continuously reinforced 150-ft barrier test section were visible. Test conditions were as follows:

Test	Measured Impact Speed (mph)	Measured Impact Angle (deg)
CMB-5	34.9	19.1
CMB-6	33.8	15.5
CMB-7	44.7	15.0

Truck Motion

Sequence panning photographs of the truck motion during redirection are shown in Figures 5 and 6 for the CMB-5 test, Figure 7 for the CMB-6 test, and Figure 8 for the CMB-7 test. End-view sequence photographs of the truck motion were not available for the CMB-6 and CMB-7 tests because of a camera malfunction.

The vertical motion of a point on the tractor bumper relative to the top of the CMB is shown in Figure 9 for the 3 tests. The bumper point selected was located, as shown in Figure 2a, at the midheight of the bumper and at the longitudinal centerline of the tractor. The highest bumper rise above the top of the barrier was about 7 in. for the CMB-5 and CMB-6 tests; the highest rise was about 11 in. for the CMB-7 test.

The vertical motion of a point on the tractor door relative to the top of the barrier is also shown in Figure 9. This point, designated as point "A" in Figure 2a, was normal to the Impact-O-Graph mounted on the floor directly under the passenger seat. The highest rise of point "A" above the top of the barrier was about 14 in. for the CMB-5 test; the highest rise was about 18 in. for the CMB-6 and CMB-7 tests.

Figure 9 shows that the vertical and pitching motions of the truck tractor continued throughout the entire length of barrier contact as the front and rear dual wheels of the tractor rode up and down on the lower barrier inclined surface. The truck remained in contact with the barrier because the remote-control steering system was held in a straight ahead position before and after impact. The vertical and pitching motions were much more pronounced in the 45-mph CMB-7 test than in the two 10-mph CMB-5 and CMB-6 tests.

Comparisons of the rolling motion of the truck trailer during the 3 tests are shown in Figure 10. The rolling motion plots were obtained from an analysis of the high-speed film using the Vanguard Motion Analyzer and the IBM 360/65 computer. Measurements of the tractor-trailer truck swivel connection showed that the rolling motion of the trailer was independent of the tractor for angles of about 10 deg and less. As shown in Figure 10, the trailer rolling motion in the CMB-5 and CMB-6 tests was less than 8 deg and, hence, independent of the tractor rolling motion. In the CMB-7 test, however, the trailer rolling motion was not independent of the tractor rolling motion. The trailer in the CMB-7 test reached a maximum roll angle of 17 deg at a time of 1.2 sec after impact. It can be seen in the sequence photographs of Figure 9 that, at a time of 1.2 sec, the tractor rear dual wheels on the passenger side were lifted off the ground for a height of about 7 in. as a result of the trailer roll angle exceeding the unrestrained swivel roll angle of 10 deg. This observation may be significant for the selected truck under a higher impact speed of, for example, 50 to 55 mph, in that the inertia of the tractor would greatly assist in minimizing the possibility of roll-over (provided that the swivel roll pin does not fracture) and, if the swivel roll pin does fracture, there may be a possibility that the trailer would roll over the CMB.

Truck Damage

The damage to the truck was relatively minor. The sheet metal damage of the tractor after the CMB-5 test is shown in Figure 11a. The sheet metal and bumper damage of the tractor after the CMB-5, CMB-6, and CMB-7 tests is shown in Figure 11b. Dam-

Figure 4. Remotely operated on-off truck controls.

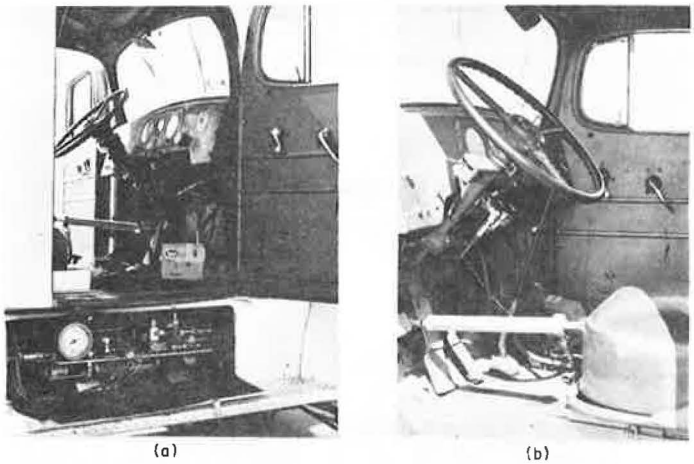

Figure 5. Sequence photographs of CMB-5 test (side view).

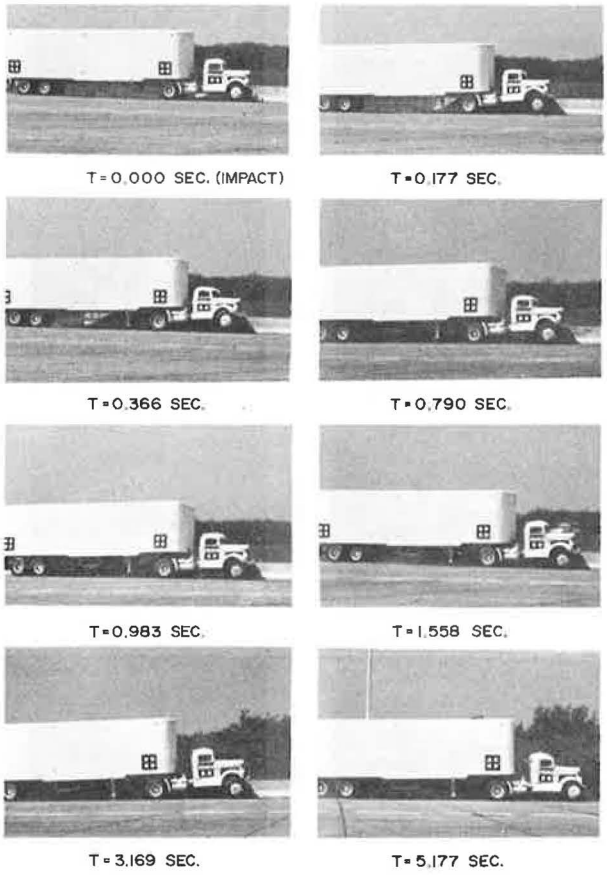

Figure 6. Sequence photographs of CMB-5 test (rear view).

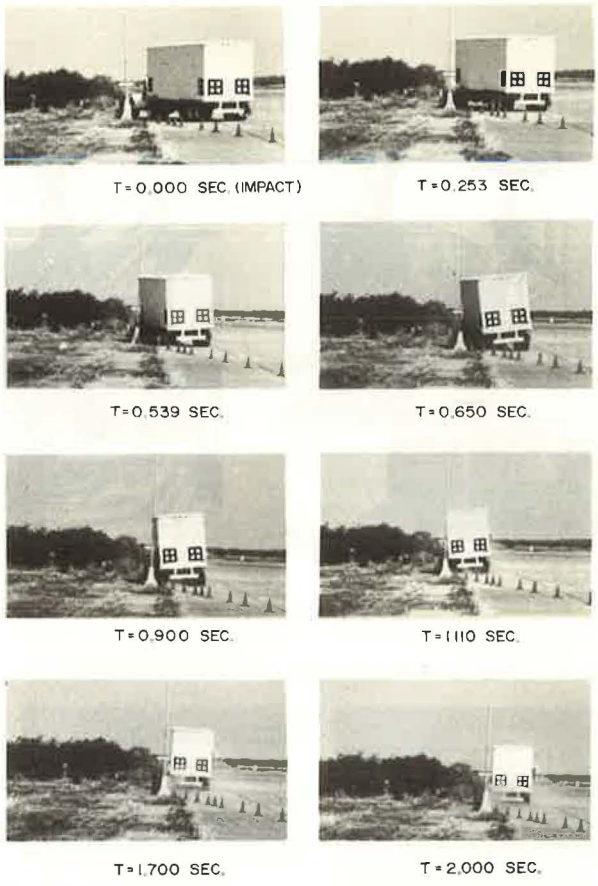

Figure 7. Sequence photographs of CMB-6 test.

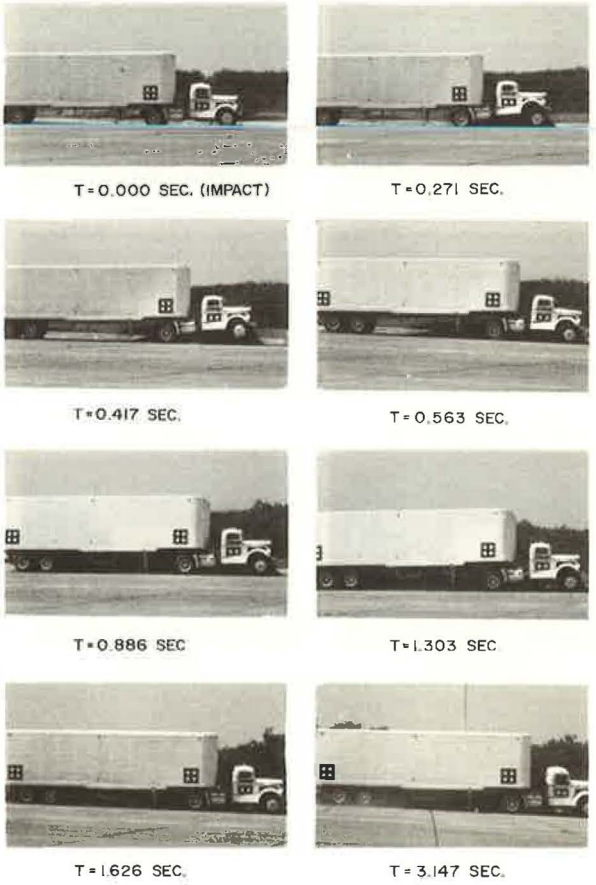

Figure 8. Sequence photographs of CMB-7 test.

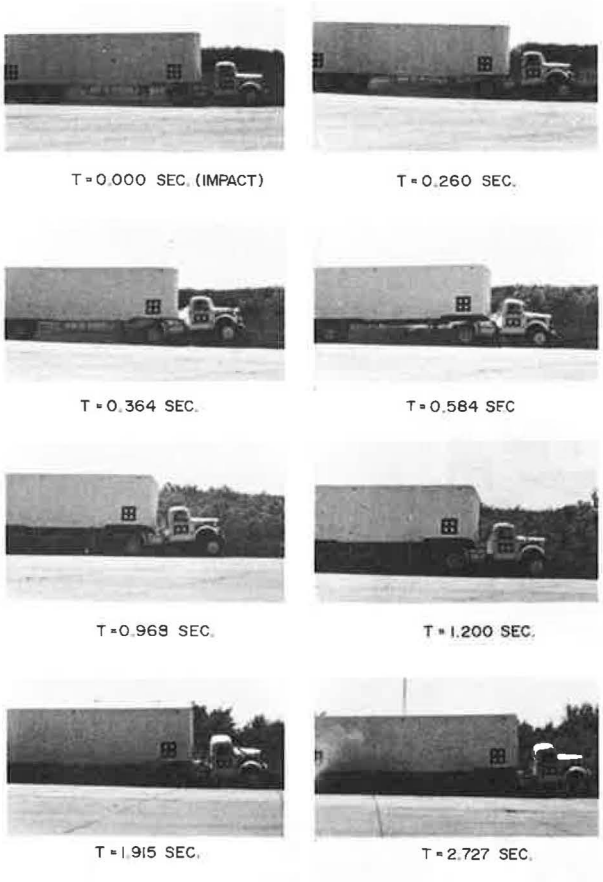

Figure 9. Motion of tractor relating to top of barrier.

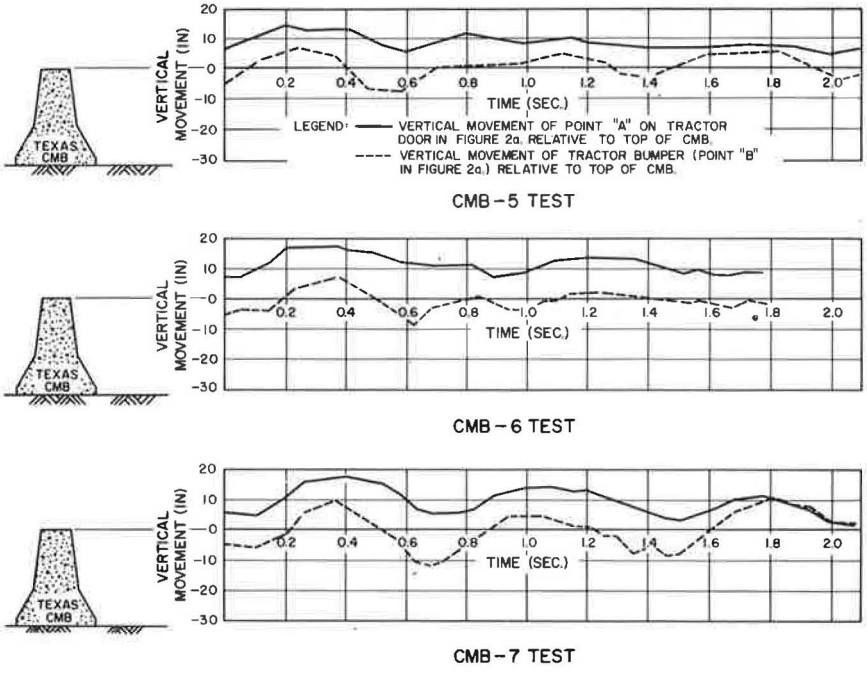

Figure 10. Rolling motion of truck trailer.

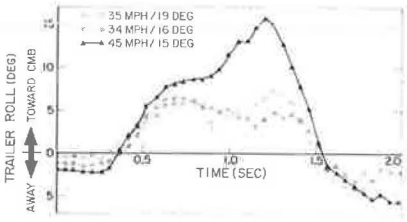

Figure 11. Tractor damage during CMB tests.

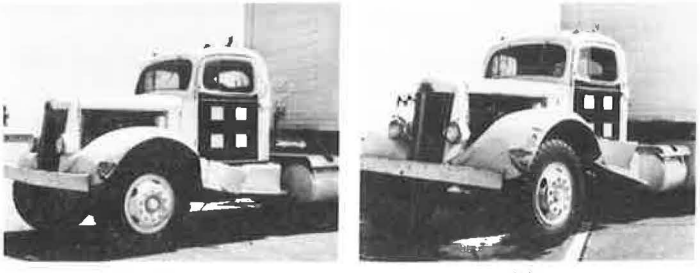

(a) (b)

Figure 12. CMB barrier damage.

OVERALL VIEW OF BARRIER AFTER CMB-5, CMB-6, & CMB-7 TESTS.

BARRIER AFTER CMB-5 TEST.

BARRIER AFTER CMB-6, AND CMB-7 TESTS.

age to the trailer consisted of several small indentations near the rear tandem wheels. The window on the side of the passenger was cracked prior to testing.

The estimated cost required to repair the fender, bumper, and running board of the truck tractor was less than $200.

Barrier Damage

Photographs of the CMB after testing are shown in Figure 12. Maintenance of the barrier would require, at most, a light sandblasting job to remove the unsightly tire scrub markings. The small amount of concrete spalling that occurred would require no maintenance. It can also be seen in the photographs that the fencing and light pole on top of the barrier were not damaged.

The tire scrub markings extend over the entire length of the barrier beyond the points of impact because, as mentioned earlier, the front wheels were locked in a straight ahead steering position subsequent to impact.

CONCLUSIONS

Although preliminary in scope, this series of truck tests demonstrated that the performance of the Texas concrete median barrier is promising from a consideration of (a) low maintenance and (b) having the capability to restrain a large-sized truck. In turn, these considerations will result in increased safety and economy.

No attempt was made in this study to determine the conditions under which the performance of the Texas concrete median barrier would have been unsatisfactory.

ACKNOWLEDGMENT

The contents of this paper reflect the views of the authors who are responsible for the facts and the accuracy of the data presented herein. The contents do not necessarily reflect the official views or policies of the Federal Highway Administration. This report does not constitute a standard, specification, or regulation.

REFERENCES

1. Olson, R. M., Ivey, D. L., Post, E. R., Gunderson, R. H., and Cetiner, A. Bridge Rail Service Requirements as a Basis for Design Criteria. Texas Transportation Institute, Texas A&M Univ., Feb. 1972.
2. Lundstrom, L. C., Skeels, P. C., Englund, B. R., and Rogers, R. A. A Bridge Parapet Designed for Safety. Highway Research Record 83, 1965, pp. 169-187.
3. Hirsch, T. J., Hayes, G. G., and Post, E. R. Vehicle Crash Test and Evaluation of Median Barriers for Texas Highways. Texas Transportation Institute, Texas A&M Univ., Res. Rept. 146-4, June 1972, 109 pp.
4. McHenry, R. R., and Deleys, N. J. Vehicle Dynamics in Single Vehicle Accidents: Validation and Extension of a Computer Simulation. Cornell Aeronautical Laboratory, Buffalo, N.Y., Rept. VJ-2251-V-3, Dec. 1968, 276 pp.
5. Young, R. D., Ross, H. E., Jr., and Holcomb, R. M. Simulation of Vehicle Impact With the Texas Concrete Median Barrier. In Test Comparisons and Parameter Study, Vol. I, Texas Transportation Institute, Texas A&M Univ., Res. Rept. 140-5, June 1972.

ENERGY-ABSORBING BARRIER BEAMS SUSPENDED FROM LINEAR SUPPORTS

W. V. Brewer, University of Tulsa

ABRIDGMENT

•THIS research explores the possibilities of improving total guardrail system performance by further exploitation of beam properties. Two performance aspects are of interest: a more gradual application of deceleration forces and efficient use of the beam to absorb a standard amount of energy (4,000-lb vehicle at 65 mph and 25-deg inclination). The first is accomplished by hypothesizing a standoff suspension separating beam from post. Substantial research effort has been directed toward devices that offer promise as energy-absorbing standoff suspensions for guardrail beams (1-6). (The desired linear load-deflection relation should be obtainable as a modification or combination of these or other available techniques but is beyond the scope of this research.) It will have an overall linear load-deflection relation (initially elastic but plastic in the limit) rather than the usual rigid-plastic one associated with posts having no suspension. An efficient beam will utilize elastic-plastic flexure to absorb energy and stiffness to spread the work out over the support system. The appropriate size beam for the most cost-effective configuration depends on performance requirements and component costs that are incorporated in a mathematical model.

SYSTEM MODEL

A synthetic model is used that satisfies the following performance requirements simultaneously and identically: Energy absorbed is the amount that is necessary to effect vehicle redirection, and maximum lateral deceleration level is 5 g. The model gives the beam size and suspension requirements. Beam deflections are minimally consistent with the preceding performance requirements.

The barrier system will be designed to use the beam in flexure and does not develop resultant tensile loads. Classical theory for a beam on an elastic foundation (7) and ideal beam theory of plastic-hinge structural analysis (8) are used in the description of beam behavior. A Winkler type of model (7, p. 197) is used for the vehicle.

Given the energy to be absorbed and permissible lateral g-level, we can generate a spectrum of barrier systems ranging from strong beam and weak post to strong post and weak beam all of which satisfy the given requirements identically. A parameter R relating the amount of plastic hinge present is convenient for classification of these results: $R < 1$, no hinge; $1 < R < 2.43$, 1 hinge; and $R > 2.43$, 3 hinges—hence large deflections. Small values of R produce systems with large beams and small-capacity (or more widely spaced) suspension-post assemblies; the opposite is true for large R-values.

COMPARISONS AND DISCUSSION

A spectrum of R-values is used to evaluate the cost-effective beam size from available component cost information. For a steel beam of box section, proportions have been adjusted to prevent section instability due to plastic flexure. Table 1 gives abbreviated results for the cost-effective system among those for systems having the extreme values of R. The following input data were used in deriving the results given in Table 1:

1. Impact conditions—velocity, 65 mph and 25 deg; lateral deceleration, 5 g; and vehicle weight, 4,000 lb;
2. Material or component capacities—yield strength, 60,000 psi; elastic modulus, 30,000 ksi; maximum load of post, 5,000 lb; and energy absorbed by vehicle, 5,625 ft-lb; and
3. Component costs—galvanized steel, 20 cents per pound; standoff suspension (estimate), $12 per unit; post and preparation of beam at point of attachment, $12 per post; installation, $18 per post; and total support cost, $42 per unit.

Though all 3 systems satisfy the same performance requirements, a poor balance between beam and supporting structure (as indicated by R) could be costly. In addition to higher first costs, systems having R-values greater than 2 become plastic when they are remote from the impact site, thus increasing beam replacement cost. A cost-effective system utilizes the support structure that is remote from the impact site to absorb energy and thus reduce total required capacity per unit length (note "effective length" in Table 1). This does not increase repair cost when the remote portions of both beam and standoff suspension are held within the initially elastic load range. Large values of R produce more severe slope discontinuities. The cost-effective beam is deeper, narrower, and lighter (10 in. by 4.6 in. by 0.19 in. and 18.8 lb/ft) than the beam (8 in. by 6 in. by ¼ in. and 22 lb/ft) in current service.

Large beam deflections (greater than 5 ft) are necessary to meet the required 5-g lateral deceleration limit under the stated conditions. Eight-ft deflections are the result of gradually applied deceleration forces in this initially linear system.

Greater post spacing results from improved performance and higher cost of the standoff suspension. Cost of the suspension is a matter of conjecture at this time. Higher cost would force the optimum to lower values of R.

CONCLUSIONS

Higher performance requirements for increased speed with reduced deceleration levels will necessitate barrier systems capable of large beam deflections. Automobiles are not capable of large enough deflections to absorb any significant portion of the total energy at required g-levels. Economics will force the use of systems that spread the work out over a large portion of the support structure (smaller R-values). A proper balance between beam and support structure is essential to cost-effective performance. Satisfaction of energy and deceleration requirements simultaneously and identically is a necessary but insufficient condition for the most cost-effective system.

Table 1. Model results.

	Output Data		
Factor	R = 1	R = 1.8	R = 2.4
Cost (dollar/ft)			
Beam	9.37	3.75	2.58
Support structure	1.24	3.70	5.37
Total	10.61	7.45	7.95
Weight of beam (lb/ft)	49.9	18.8	12.9
Slope at hinge (deg)	0.0	-8.68	-13.9
Box beam section dimensions (in.)			
Depth	16.1	10.1	8.42
Width	7.24	4.58	3.80
Thickness	0.296	0.187	0.155
Cross-sectional area	13.8	5.51	3.79
Performance dimensions (ft)			
Post spacing	36.2	11.4	7.91
Maximum deflection	9.52	8.13	8.27
Effective length[a]	342.0	127.0	91.4

[a]Distance between 2 points of zero beam deflection on either side of the maximum.

RECOMMENDATIONS

Beam interaction with other types of suspension-post models should be investigated where the beam dimensions are adjusted so that all variants satisfy the same performance requirements. Promising suspensions should be developed to the point where their costs can be included in optimization studies. Optimum beam section proportions (as opposed to size) are not the same for guardrails as for beams used in other applications and should be investigated further.

ACKNOWLEDGMENTS

This investigation was supported by a National Science Foundation Research Initiation Grant and by the University of Tulsa.

I would like to express my gratitude to the people who contributed valuable information to this effort: Keith Bushnell and Bob Briere, Michigan Department of State Highways; George Seiders, L. B. Foster Co.; Larry Karns, Armco Steel; Alan Brooks and Howard Bonebrake, Alcoa Aluminum; Thomas Carroll, U.S. Department of Transportation.

The opinions, findings, and conclusions expressed are those of the author and do not necessarily reflect the views of the sponsors or contributors.

REFERENCES

1. Stocker, A. J., Ivey, D. L., and Hirsch, T. J. Full-Scale Crash Tests of the Fragmenting-Tube-Type Energy-Absorbing Bridge Rail. Highway Research Record 302, 1970, pp. 28-37.
2. Materials Applications. Industrial Research, April 1970, pp. 73-74.
3. Tamanini, F. J., and Viner, J. G. New Systems Designed to Reduce Highway Hazards. Public Works, Dec. 1969, pp. 69-73.
4. Ford Buys Into Makers of Energy Absorbers. Wall Street Journal, March 9, 1970.
5. Shaw, M. C. Designs for Safety: The Mechanical Fuse. Mechanical Engineering, April 1972, pp. 23-29.
6. McHenry, R. R., et al. Development of Analytical Aids for Minimization of Single Vehicle Accidents. Cornell Aeronautical Laboratory, Buffalo, New York, July 1971, p. 62.
7. Hetenyi, M. Beams on Elastic Foundation. Univ. of Michigan Press, Ann Arbor, 1946.
8. Hodge, R. G. Plastic Analysis of Structures. McGraw-Hill, New York, 1959.

WARRANTS FOR GUARDRAILS ON EMBANKMENTS

Hayes E. Ross, Jr., and Edward R. Post, Texas Transportation Institute,
Texas A&M University;
John F. Nixon and David Hustace, Texas Highway Department; and
Edward V. Kristaponis, Federal Highway Administration

The highway-vehicle-object simulation model, a computer model that describes an automobile and is capable of predicting the dynamic response of the automobile traversing selected terrain, was used to study the behavior of a standard-sized automobile traversing embankment side slopes at various speeds and departure angles. The accelerations obtained were used to compute a severity index that was then compared with a similarly computed severity index (from actual crash data) of a vehicle impacting a W-beam guardrail with posts on 6¼-ft spacing. An equal-severity curve was then developed that can be used as a guardrail installation criterion.

•WHEN a vehicle, traveling at a high speed, leaves the roadway and strikes a guardrail, a hazardous situation obviously exists. It is also hazardous when there is no guardrail and the vehicle must traverse the ditch. Neither event is desirable. Nevertheless, for a given type of guardrail, given ditch or embankment configuration, and given vehicle encroachment conditions, one situation will be less severe than the other.

To determine the need for guardrails on embankments, many highway engineers are using criteria developed by Glennon and Tamburri (11). Their study was based on a statistical analysis of accident information from the California state highways during 1963 and 1964. The two basic types of guardrail in use during the time of the accidents were a spring-mounted curved metal plate on 10-ft post spacing and a blocked-out W-section corrugated beam on 12-ft, 6-in. post spacing.

The primary type of guardrail used by the Texas Highway Department (THD) is a W-section corrugated beam on posts spaced on 6-ft, 3-in. centers, with no block-out of the rail from the post. Because the THD guardrail system differs considerably from the one in use during the California study (primarily in the post spacing), it was decided that criteria relevant to the THD system should be developed. The objective of this study was, therefore, to determine where it is safer to traverse an embankment than to impact the THD guardrail.

The approach of this study parallels that of Glennon and Tamburri (11) in that an equal-severity curve is established for determining the less severe alternative, guardrail or unprotected embankment. For an errant vehicle, the curve represents the combination of embankment heights and slopes that are equal in severity to impacting a particular guardrail. The major difference of the two approaches is the basis for measuring accident (guardrail impacts and embankment traversals) severity. Weighted severity values (11) were assigned to different occupant injury levels as determined from the accident reports. In the study described here, a combination of mathematical models and full-scale test data was used to determine vehicle accelerations during guardrail impacts and embankment traversals. Vehicle accelerations served as the measure of severity. In establishing need criteria, we believe that mathematical models and test data provide more flexibility than do accident records. Much of the subjectivity of accident records is removed. Although the criteria developed in this study pertain to a particular guardrail system, the methods used in the development are general, and any type of guardrail or embankment configuration can be investigated.

ESTABLISHING GUARDRAIL NEED

Approach

A mathematical model of an automobile (1), denoted herein as highway-vehicle-object simulation model (HVOSM), was used to determine the orientation and accelerations of a simulated automobile traversing various embankment configurations. A mathematical model (9) and full-scale test data (8, 10) were used to determine the accelerations of an automobile impacting a guardrail system similar to the THD system. Accelerations at the center of gravity of the automobile were used as the measure of severity. A severity index (SI), discussed in a report by Ross and Post (2), served to quantify the relative severity of each event for an unrestrained occupant.

To compare the severity of a vehicle impacting a guardrail with the severity of a vehicle traversing an embankment, one should use the same vehicle under the same encroachment conditions. These requirements were maintained as closely as possible. In the mathematical model studies of embankment encroachments, a 1963 Ford Galaxie was used. In most of the cases analyzed, a vehicle of similar size was used in the full-scale guardrail tests. Also, in most of the reported full-scale guardrail crash tests, the vehicle impacted at 60 mph and a 25-deg angle. Hence, for vehicle encroachment conditions, a 25-deg angle of departure and a speed of 60 mph were selected. These encroachment conditions are the criteria recommended for the structural design of guardrails (14).

A parameter study was made to evaluate the effects of encroachment conditions on the severity of an embankment traversal and a guardrail collision. The embankment in each case was a 3:1 side slope, 20 ft in height, with a flat-bottom ditch.

Embankment

The basic geometry of each embankment investigated consisted of a 10-ft shoulder adjoining a side slope of b:a and height H, with a flat-bottom ditch (Fig. 1). Slopes (b:a) of 2:1, 3:1, and 6:1 in combination with heights (H) of 10, 20, 30, and 50 ft were studied. In addition, a 3.25:1 slope with a height of 20 ft and a 4:1 slope with a height of 20 ft were studied. The reason for studying the latter two cases is explained later in the paper.

In the 14 embankment combinations studied, the simulated automobile was placed on the roadway with an initial velocity and encroachment angle θ_1. Throughout the maneuvers, the automobile was assumed to be out of control; that is, no attempt was made to steer the automobile.

In most cases (Table 1), the encroachment angle and speed of the automobile increased as the vehicle traversed the embankment slope. In all but the 6:1 slope combinations, the automobile became completely airborne (all tires off ground) for a period of time after leaving the shoulder. In traversing a 2:1 slope with a height of 10 ft, the automobile landed on the ditch bottom and then pitched over about its front end. For all other height and slope combinations, the automobile landed on the embankment slope after being airborne with no tendency to roll or pitch over.

Table 1 also gives the maximum average decelerations for a 50-msec period. These values were obtained by studying the computer output for those times when the larger decelerations occurred and then, by trial and error, selecting the 50-msec period with the highest average deceleration. The SI was computed from data given in another report (2).

Guardrail

The types of guardrail that can be studied by the Texas Transportation Institute's version of HVOSM are limited to those whose lateral resistance to vehicle penetration is independent of the longitudinal position of the vehicle contact point. Because the W-section guardrail on 6-ft, 3-in. post spacing does not fall in this category, the model could not be applied.

Two methods were used to investigate the severity of a guardrail collision. The first method was based on data from full-scale crash tests by Michie (8) and Beaton (10).

The second method was based on results obtained by mathematical equations presented by Olson (9).

A review of the literature revealed that no full-scale tests have ever been performed on the guardrail system now used in Texas for embankment protection. However, the tests conducted by Michie (8) and Beaton (10) were conducted on a guardrail system similar to the THD guardrail. The one difference between the two systems was that the "as-tested" rail was, in all but one case, blocked out from the post, whereas the THD rail butts against the post. The difference in the collision performance of the two systems is subject to conjecture. The possibility for snagging in the non-blocked-out system appears greater, and, if so, the severity of colliding with the THD system may be higher. If snagging does not occur, it seems reasonable to assume that the severity of impact would be similar for the two systems. This assumption is based on the fact that the lateral resistance of the two systems is essentially the same. In any case, it was hypothesized that the severity of impacting the THD system would be equal to or greater than that of the as-tested systems. As such, the criteria may be conservative as to the need for the THD guardrail system; i.e., more guardrail protection may be required by these criteria than is needed. On the other hand, the criteria are directly applicable to the as-tested system (8, 10).

The SI's of guardrail collisions conducted by Michie (8) were computed and are given in Table 2. These tests were selected on the basis of being conducted at an impact speed and angle of approximately 60 mph and 25 deg. Also, the vehicles used in these tests were similar in size and weight to the one used in the simulation studies. The SI was computed for longitudinal and lateral decelerations occurring over two time intervals; 50 msec and 325 to 450 msec. The longer time interval was measured from the instant of impact to the time when the automobile becomes parallel to the centerline of the guardrail. The SI was computed over the longer interval so that it could be compared with the work of Olson (9), which is presented later. As discussed in the report by Ross and Post (2), the tolerable deceleration limits for the two time intervals were based on an interpretation of the findings of Hyde (4).

An analysis of three full-scale crash tests conducted by Beaton (10) at impact conditions of approximately 60 mph and 25 deg is given in Table 3. Because no acceleration-time data were reported by Beaton, the automobile decelerations perpendicular ($G^{\#}_{lat}$) and parallel ($G^{\#}_{long}$) to the guardrail were computed from the following equations developed by Olson (9):

$$G^{\#}_{lat} = \frac{V_I^2 \sin^2(\theta)}{2g\{AL \sin(\theta) - B[1 - \cos(\theta)] + D\}} \quad (1)$$

$$G^{\#}_{long} = \mu G^{\#}_{lat} \quad (2)$$

where

V_I = impact velocity,
θ = impact angle,
AL = distance from front bumper to center of gravity,
2B = width of vehicle (B = one-half of vehicle width),
D = lateral dynamic displacement of barrier, and
μ = coefficient of friction between vehicle and barrier [a value of 0.3 was used (Table A1, 9)].

The primary assumption in developing these equations was that the deceleration was constant from impact to the time in which the automobile becomes parallel to the guardrail. Olson (9) demonstrated that these equations were accurate within ±20 percent.

To compute an SI we must transform the decelerations computed by Eqs. 1 and 2 to the decelerations along the automobile coordinate system axes. This was accomplished with the following two transformation equations:

$$G_{lat} = G^{\#}_{lat}[\cos(\theta) - \mu \sin(\theta)] \quad (3)$$

Figure 1. Embankment geometry and center-of-gravity path of automobile.

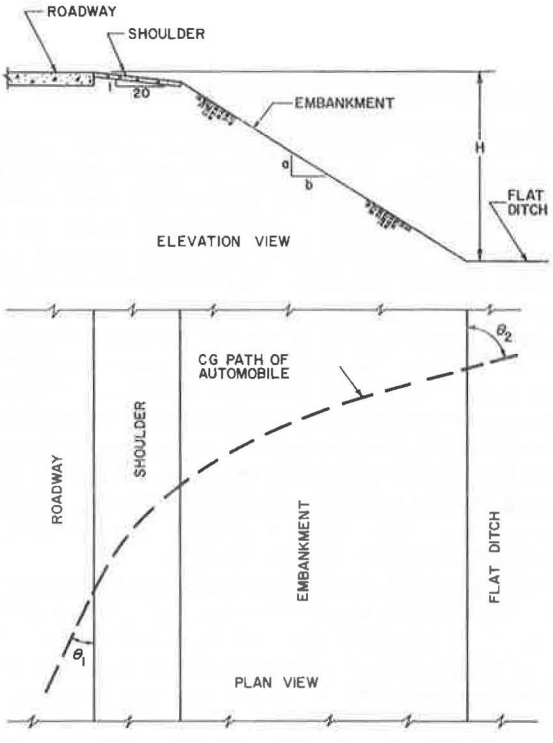

Table 1. Simulation results on embankments of various heights and slopes.

Run No.	Terrain		Automobile							
	Embankment Height (ft)	Embankment Slope (b:a)	Maximum Roll Angle (deg)	Maximum Pitch Angle (deg)	Angle Automobile Contacts Flat Ditch (deg)	Speed Automobile Contacts Flat Ditch (deg)	Average Deceleration >50 msec			
							G_{long}	G_{lat}	G_{vert}	SI
1	10	2:1	33	RO[a]	24	60	2.6	3.4	4.7	1.1[b]
2	10	3:1	29	10	25	61	0.2	0.6	5.3	0.9
3	10	6:1	11	5	29	62	0.1	0.3	2.2	0.4
4	20	2:1	48	15	24	62	2.6	4.9	6.3	1.5
5	20	3:1	30	12	40	62	1.3	0.8	7.6	1.3
6	20	6:1	11	5	34	65	0.1	0.4	2.8	0.5
7	20	3.25:1	27	10	37	64	1.3	0.7	4.5	0.8
8	20	4:1	20	9	30	64	—	0.5	3.7	0.6
9	30	2:1	47	23	32	58	0.3	1.3	6.8	1.2
10	30	3:1	29	13	36	66	0.4	0.9	4.9	0.8
11	30	6:1	11	5	33	67	0.0	0.6	3.5	0.6
12	50	2:1	47	26	66	55	7.6	3.4	9.7	2.1
13	50	3:1	29	13	43	68	1.2	1.3	6.4	1.1
14	50	6:1	11	6	43	70	0.2	0.5	3.7	0.6

Note: Encroachment speed = 60 mph, shoulder width = 10 ft, encroachment angle (θ_1) = 25 deg, and shoulder slope = 20:1.

[a]Automobile rolled over about its front end as it contacted flat ditch after being airborne.
[b]Severity index when contact with flat ditch occurs (just prior to roll-over).

Table 2. Guardrail full-scale crash tests (8).

Test No.	Guardrail				Automobile								
								Decelerations (G)					
								50 msec			325 to 450 msec		
	Post	Blockout	Post Embedment (in.)	Dynamic Displacement (ft)	Weight (lb)	Impact Speed (mph)	Impact Angle (deg)	G_{long}	G_{lat}	SI[a]	G_{long}	G_{lat}	SI[b]
101	8- by 8-in. wood	8-in. wood	36	4.25	4,042	55	31	4.6	4.5	1.1	2.9	3.1	0.9
103	8- by 8-in. wood	8-in. wood	36	2.64	4,123	60	22	3.1	6.1	1.3	2.2	3.3	0.9
119	6B8.5	None	42	2.74	4,169	53	30	4.5	4.4	1.1	2.3	2.7	0.8
120	6B8.5	1-6B8.5	42	4.05	3,813	57	28	3.9	6.6	1.4	2.9	3.5	1.0
121	6B8.5	2-6B8.5	42	3.10	4,478	56	27	3.6	6.7	1.5	1.9	3.3	0.9
122	6B8.5	2-6B8.5	42	4.95	4,570	63	25	3.9	7.6	1.6	2.3	3.9	1.0

Note: Rail height = 27 in. and post spacing = 6 ft, 3 in. All rail members tested were steel W-beam.

[a]G_{XL} = 7 and G_{YL} = 5 (Appendix B, 2). [b]G_{XL} = 6 and G_{YL} = 4 (Appendix B, 2).

$$G_{long} = G^{*}_{lat} [\sin(\theta) - \mu \cos(\theta)] \quad (4)$$

Observations of high-speed photography show that, for the time interval between impact and maximum guardrail displacement (dynamic displacement), the heading angle of the automobile changes only slightly. It is during this interval that the maximum deceleration usually occurs. Therefore, in applying the preceding transformation equations, the initial impact angle was used.

A comparison of the SI's computed for the California tests in Table 3 with those in Table 2 further demonstrates that the mathematical equations presented by Olson (9) provide reasonable results. Equations 1 through 4 were used to predict the severity of guardrail collisions for various impact speeds and angles, as described later in this paper.

Comparison of Relative Severities

The SI's of embankment traversals (Table 1) are shown in Figure 2. Superimposed on the figure is the range of SI's for impacts with the guardrail from Tables 2 and 3. The range of SI's shown in Figure 2 for the guardrail was based on accelerations averaged over the longer time duration.

It was anticipated that the SI would increase as the embankment height increased for a given slope. However, this was not always the case, as shown in Figure 2. Two good examples of this anomaly were the SI's for a 2:1 slope with a 20-ft fill height and for a 3:1 slope with a 20-ft fill height (runs 4 and 5, Table 1). Both values were considerably higher than anticipated. Examination of the output from runs 4 and 5 showed that, when the vehicle reached the flat-bottom ditch, both the front and rear bumpers of the automobile simultaneously contacted and penetrated the terrain, causing large resistive forces. In other runs, front and rear bumper contact did not occur simultaneously; hence, the effect of bumper contact on the SI was not as pronounced.

Additional runs (runs 7 and 8, Table 1) were made on a 20-ft fill height to determine the variation of the SI between a 3:1 and 6:1 slope because of the large difference in the index between these slopes. As seen in Figure 2, flattening the slope from a 3:1 to a 3.25:1 and to a 4:1 resulted in a considerable reduction in the SI. A sharp transition was therefore found to exist in the SI at a slope of about 3:1 for the 20-ft embankment height. As discussed, both front and rear bumper contact occurred simultaneously for the 2:1 and 3:1 slopes on a 20-ft fill height, and, as a consequence, the forces and accelerations were greatly increased. Front and rear bumper contact did not occur simultaneously for the 3.25:1 and 4:1 slopes. Vehicle attitude during initial contact with the ditch is therefore a significant factor influencing the relative severity of an embankment traversal.

Table 4 gives those combinations of embankment slope (measured as a ratio and in degrees) and height that are equal in severity to the upper bound, average, and lower bound guardrail severities. Each combination represents the intersection point of a given embankment height curve with a given guardrail severity line shown in Figure 2. For example, traversal of an embankment with a 3.14:1 (or 18-deg) slope, 20 ft in height, is equal in severity to an automobile impacting the guardrail, based on the average guardrail severity.

Equal-severity curves based on the upper and lower bound of guardrail severities are shown in Figure 3. The coordinates of the four points from which each curve was drawn were taken from Table 4. As shown in Figure 3, a line through a slope equal to 3:1 (dotted line) appears to be an average equal-severity curve. By the average curve, an embankment with a slope steeper than 3:1 should be protected, and, conversely, slopes flatter than 3:1 would not need guardrail protection.

Embankment heights of less than 10 ft were not investigated. Nevertheless, it seems reasonable to assume that a line through a 3:1 slope can also be used as the equal-severity curve for heights of 10 ft or less. Implementation of the criteria would be simplified in so doing.

For comparison with this study, other equal-severity curves are shown in Figure 4. The relation established by Glennon and Tamburri (11) was based on a statistical anal-

Table 3. Guardrail full-scale crash tests (10).

Test No.	Guardrail: Wood Post Blockout (in.)	Guardrail: Post Spacing (in.)	Guardrail: Post Embedment (in.)	Guardrail: Rail Height (in.)	Guardrail: Dynamic Displacement[a] (ft)	Automobile: Weight (lb)	Automobile: Impact Speed (mph)	Automobile: Impact Angle (deg)	Average Decelerations of 275 to 300 msec: G^*_{at} (Eq. 1)	G^*_{ms} (Eq. 2)	G_{lat} (Eq. 3)	G_{long} (Eq. 4)	SI
106	8	6-3	41	30	2.45	4,570	60	25	3.9	1.2	3.1	2.7	0.9
107	8	6-3	35	27	2.10	4,570	60	25	4.2	1.3	3.3	2.9	1.0
108	8	6-3	35	24	2.10	4,570	59	25	4.1	1.2	3.2	2.8	0.9

Note: AL = 7.95 ft and 2B = 6.5 ft. All rail members tested were steel W-beam, and posts (with 6[8.2 rubbing rail) were 8- by 8-in. wood.
[a]Dynamic displacement taken as 1.4 times permanent set (8).

Figure 2. Severity comparison of automobile traversing embankment and colliding with guardrail.

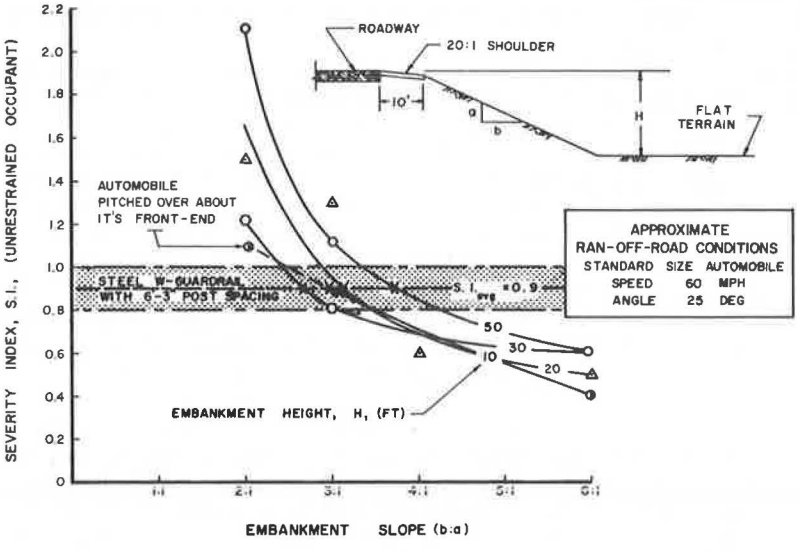

Table 4. Equal severity combinations.

Embankment Height (ft)	Embankment Slope at Intersection of Guardrail and Embankment SI Curves[a]: Upper Bound b:a	Upper Bound Deg	Average b:a	Average Deg	Lower Bound b:a	Lower Bound Deg
10	2.42:1	22	2.92:1	19	3.50:1	16
20	2.88:1	19	3.14:1	18	3.44:1	16
30	2.42:1	22	2.65:1	21	3.02:1	18
50	3.34:1	17	3.75:1	15	4.26:1	13

Note: For upper bound SI = 1.0, for average SI = 0.9, and for lower bound SI = 0.8.
[a]Values obtained from Figure 2.

Figure 3. Warrant for guardrails on embankments.

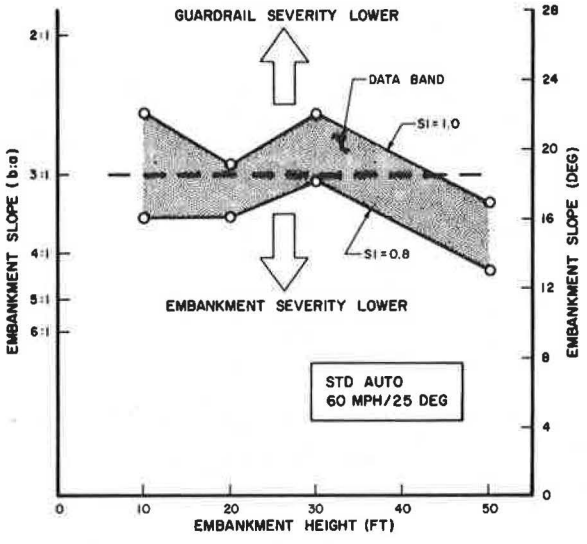

Figure 4. Comparison of warrants for guardrails on embankments.

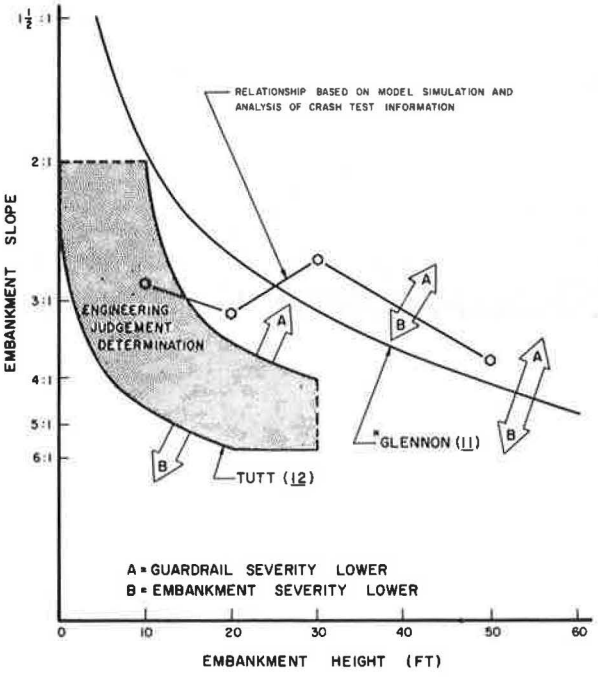

ysis of accident information compiled on the California highways during the years of 1963 and 1964. Their work is currently used by many highway engineers.

As evident in Figure 4, the relation established by Glennon and Tamburri generally agrees with the relation established in this study. The differences existing between these two independently established curves are attributed to the following: The conditions of encroachment of 60 mph and 25 deg investigated in this study are probably more severe than those conditions occurring in the majority of the accidents statistically analyzed, and the Texas guardrail system is stiffer than that used at the time of the accidents because of a smaller post spacing.

A guide to determine if a guardrail is needed on roadway embankments was also presented by Tutt (12) and is shown in Figure 4. As in the criteria presented by Tutt, engineering judgment must be used in applying the results of this study. Where a hazardous condition exists along or at the bottom of the embankment, a guardrail may be warranted in the immediate vicinity of the hazard. It is also noted that the safer option (guardrail versus no guardrail) determined by use of this criterion will not necessarily ensure a safe situation; i.e., severe injuries may still occur. This approach will, however, provide an objective means of selecting the safer of two hazardous situations.

PARAMETER STUDY OF ENCROACHMENT CONDITIONS

In previous sections, severity values for automobiles traversing different embankment heights and slopes and automobiles colliding with guardrails were presented. The encroachment conditions were a speed of 60 mph and an angle of 25 deg. The effects of the encroachment conditions on the vehicle's behavior and the severity of the event were determined by making a series of runs where the speed and encroachment angle were varied. An embankment having a 3:1 slope and a 20-ft height was selected for the study.

The majority of full-scale crash tests on a guardrail have been conducted at an impact speed of 60 mph and an angle of 25 deg. Prediction of the severity of guardrail damage for different conditions of impact was made by using the mathematical equations developed by Olson (9). It was shown earlier that these equations, Eqs. 1 and 2, compare favorably with measured accelerometer information.

Before Eq. 1 could be used, a method was needed to estimate the dynamic displacements D of a guardrail for various conditions of impact. This was done by assuming that the displacement of a guardrail is proportional to the loss in kinetic energy of an automobile as it is being redirected. The kinetic energy KE expended by a guardrail from the instant of impact to the time when the automobile is parallel to the guardrail was approximated as follows:

$$KE = C\left[\tfrac{1}{2}\frac{W}{g} V_i^2 \sin^2(\theta)\right] \tag{5}$$

Note that $V_i \sin \theta$ is the component of vehicle velocity normal to the guardrail.

Equation 5 does not account for the kinetic energy expended by changes in the vertical and longitudinal velocity components. The C-coefficient is the portion of the kinetic energy of the vehicle expended by the guardrail. The remainder of the energy of impact is expended primarily in sheet metal crushing of the automobile.

Using information from full-scale crash tests, we approximated the dynamic displacement of a guardrail as follows:

$$\left(\frac{D}{KE}\right)_{test} = \left(\frac{D}{KE}\right)_{\substack{selected \\ conditions}}$$

$$\left\{\frac{D}{C\left[\tfrac{1}{2}\frac{W}{g} V_i^2 \sin^2(\theta)\right]}\right\}_{test} = \left\{\frac{D}{C\left[\tfrac{1}{2}\frac{W}{g} V_i^2 \sin^2(\theta)\right]}\right\}_{\substack{selected \\ conditions}}$$

Therefore, assuming $C_{test} = C_{selected\ conditions}$

$$(D)_{\substack{selected\\conditions}} = \left[\frac{D}{WV_i^2 \sin^2(\theta)}\right]_{test} \left[WV_i^2 \sin^2(\theta)\right]_{\substack{selected\\conditions}} \tag{6}$$

The values used for the test parameters in Eq. 6 were selected from the tests on the California guardrail system (8- by 8-in. wood posts), as given in Table 3. The test values used were W = 4,570 lb, D = 2.37 ft (average of 4 tests), V_i = 60 mph = 88 ft/sec, θ = 25 deg, and (sin 25 deg) = 0.423. Thus

$$\left[\frac{D}{WV_i^2 \sin^2(\theta)}\right]_{test} = \left[\frac{2.37}{(4,570)(88)^2(0.423)^2}\right] = 3.74 \times 10^{-7} \frac{sec^2}{lb - ft}$$

Equation 6 was thus reduced to

$$(D)_{\substack{selected\\conditions}} = (3.74 \times 10^{-7})(W\ V_i^2 \sin^2\theta)_{\substack{selected\\conditions}} \tag{7}$$

The properties of the automobile simulated in HVOSM (1963 Ford Galaxie), which are needed in Eqs. 1 through 4 and Eq. 7, were as follows: W = 4,750 lb, AL = 81.52 in., B = 39.50 in., and μ = 0.3. Substitution of the preceding value of W into Eq. 7 gives

$$(D)_{\substack{selected\\conditions}} = (1.78 \times 10^{-3})(V_i^2 \sin^2\theta)_{\substack{selected\\conditions}} \tag{8}$$

In Table 5, values for V_i and θ were inserted in Eq. 8 to compute the guardrail dynamic displacements.

The duration ΔT of the guardrail impact was estimated by using Eq. 9.

$$\Delta T = \frac{V_i \sin\theta}{g\ G_{lat}^{*}} \tag{9}$$

The numerator and denominator of the right-hand side of Eq. 9 are respectively the component of vehicle velocity normal to the guardrail and vehicle acceleration normal to the guardrail.

The computed decelerations and SI's for an automobile redirected by a guardrail for various encroachment conditions are given in Table 5. The tolerable accelerations used to compute the SI's were for the 225- to 450-msec duration (Table B1, 2).

Table 6 gives the results of the parameter study on the selected embankment (3:1 side slope, 20 ft in height). The dynamic behavior of an automobile at speeds of 50, 60, and 70 mph and encroachment angles of 10, 17.5, and 25 deg were investigated by using HVOSM.

SI curves for guardrail and the typical embankment as a function of encroachment conditions are shown in Figure 5. The severity curve for the 25-deg encroachment angle shows a sharp decrease as the speed of the automobile increases from 60 to 70 mph. Intuitively, this phenomenon appears incorrect. However, as discussed in a previous section, at 60 mph the front and rear bumpers of the automobile contacted the ditch bottom simultaneously, causing high resistive forces and accelerations. At 70 mph, front and rear bumper contact did not occur simultaneously, and the resistive forces were lower. For comparative purposes, the SI for a 3.25:1 slope and encroachment conditions of 60 mph and 25 deg (run 7, Table 1) is shown in Figure 5.

It can be seen in Figure 5 that, for a 17.5-deg angle of encroachment or less, embankment severity is less than guardrail severity at all speeds. This suggests that the criteria shown in Figure 3 may require more guardrail than needed for most accident situations because the encroachment angle of most errant vehicles is less than 25 deg.

Table 5. Computed guardrail severity indexes.

Impact Speed (mph)	Impact Angle (deg)	Guardrail Dynamic Displacement (ft)	G^*_{lat} (Eq. 1)	G^*_{long}, Eq. 2 (μ = 0.3)	Time Duration, Eq. 9 (msec)	G_{long} (Eq. 3)	G_{lat} (Eq. 4)	SI
50	10.0	0.29	1.8	0.5	224	0.8	1.7	0.4
50	17.5	0.86	2.8	0.8	249	1.6	2.4	0.7
50	25.0	1.71	3.5	1.1	276	2.1	2.7	0.8
60	10.0	0.41	2.4	0.7	202	1.1	2.2	0.6
60	17.5	1.25	3.5	1.0	237	2.0	3.0	0.8
60	25.0	2.47	4.3	1.3	271	3.0	3.3	1.0
70	10.0	0.57	2.9	0.9	191	1.4	2.7	0.7
70	17.5	1.70	4.1	1.2	233	2.4	3.6	1.0
70	25.0	3.35	4.9	1.5	273	3.4	3.9	1.1

Figure 5. Guardrail and embankment severity as function of encroachment speed and angle.

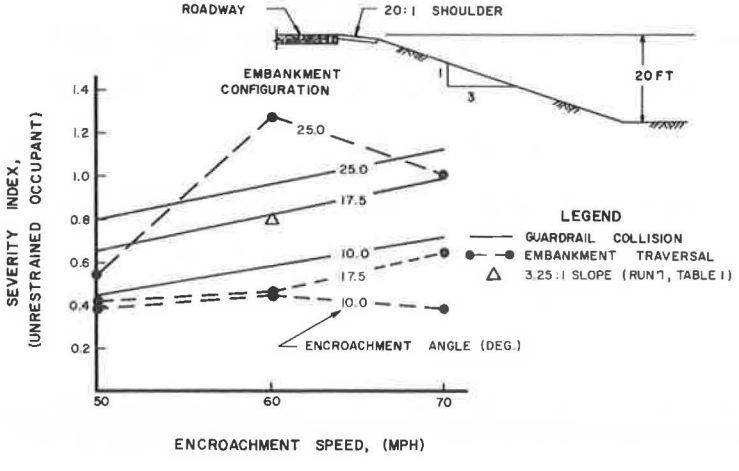

Table 6. Simulation results on 20-ft and 3:1 slope embankment.

Terrain			Automobile									
Run No.	Embankment Height (ft)	Embankment Slope (b:a)	Encroachment Speed (mph)	Encroachment Angle (deg)	Maximum Roll Angle (deg)	Maximum Pitch Angle (deg)	Angle Automobile Contacts Flat Ditch (deg)	Speed Automobile Contacts Flat Ditch (mph)	Average Decelerations >50 msec G_{long}	G_{lat}	G_{vert}	SI
15	20	3:1	50	10.0	22	8	26	55	0.6	0.5	2.2	0.4
16	20	3:1	50	17.5	25	10	29	55	0.8	0.8	2.2	0.4
17	20	3:1	50	25.0	27	12	35	54	1.3	0.8	2.9	0.5
18	20	3:1	60	10.0	23	7	23	64	0.6	0.5	2.6	0.5
19	20	3:1	60	17.5	27	9	26	64	0.9	1.0	2.4	0.5
5	20	3:1	60	25.0	30	12	40	62	1.3	0.8	7.6	1.3
20	20	3:1	70	10.0	25	6	19	74	0.5	0.6	2.2	0.4
21	20	3:1	70	17.5	31	9	26	73	1.2	1.1	3.5	0.7
22	20	3:1	70	25.0	32	16	37	69	0.1	1.5	6.1	1.1

Note: Shoulder width = 10 ft and shoulder slope = 20:1.

CONCLUSIONS

The paper supports the following conclusions:

1. Criteria are presented for making objective decisions on the need for guardrail protection for embankments. The guardrail system for which these criteria are applicable is the steel W-beam supported on a post spaced at 6-ft, 3-in. centers. The criteria show that, for side slopes flatter than 3:1 and fill heights 40 ft or less, guardrail protection is not warranted.
2. The criteria referred to in conclusion 1 were based on an automobile encroachment condition of 25-deg departure angle and 60-mph speed. The effects of vehicle encroachment speed and angle on the severity of both guardrail impacts and embankment traversals were studied. It was concluded that, for speeds of 50, 60, and 70 mph and for shallow encroachment angles (less than 17.5 deg), a collision with the guardrail (as described in conclusion 1) is higher in severity than traversing a 3:1 embankment with a 20-ft fill height. However, as the speed and angle of departure increase, the severity of traversing the embankment approaches that of striking the guardrail.
3. The analysis techniques used in this study, consisting of both mathematical models and full-scale tests, could be used to develop need criteria for various types of guardrail and for various encroachment conditions.

ACKNOWLEDGMENT

This research was sponsored by the Texas Highway Department in cooperation with the U.S. Department of Transportation, Federal Highway Administration. The contents of this paper reflect the views of the authors who are responsible for the facts and the accuracy of the data presented herein. The contents do not necessarily reflect the official views or policies of the Federal Highway Administration. This paper does not constitute a standard, specification, or regulation.

REFERENCES

1. McHenry, R. R., and Segal, D. J. Determination of Physical Criteria for Roadside Energy Conversion Systems. Cornell Aeronautical Laboratory, Rept. VJ-2251-V-1, July 1967.
2. Ross, H. E., Jr., and Post, E. R. Criteria for Guardrail Need and Location on Embankments—Volume I, Development of Criteria. Texas Transportation Institute, Texas A&M Univ., Res. Rept. 140-4, April 1972.
3. Young, R. D., Edwards, T. C., Bridwell, R. J., and Ross, H. E. Documentation of Input for Single Vehicle Accident Computer Program. Texas Transportation Institute, Texas A&M Univ., Res. Rept. 140-1, July 1969.
4. Hyde, A. S. Biodynamics and the Crashworthiness of Vehicle Structures. Wyle Laboratories, Huntsville, Rept. WR 68-3, March 1968.
5. Weaver, G. D. The Relation of Side Slope Design to Highway Safety. Texas Transportation Institute, Texas A&M Univ., Rept. 626-1, Feb. 1970, p. 29.
6. Tamanini, F. J., and Viner, M. Energy Absorbing Roadside Crash Barriers. ASCE New York, Jan. 1970.
7. Nordlin, E. F., Woodstrom, J. H., and Hackett, R. P. Dynamic Tests of the California Type 20 Bridge Barrier Rail Series XXIII. Materials and Research Laboratory, California Division of Highways, M&R Rept. 636459, Sept. 1970, pp. A6-7.
8. Michie, J. D., Calcote, L. R., and Bronstad, M. E. Guardrail Performance and Design. NCHRP Rept. 129, Jan. 1970.
9. Olson, R. M., Post, E. R., and McFarland, W. F. Tentative Service Requirements for Bridge Rail Systems. NCHRP Rept. 86, 1970, pp. 11-12.
10. Beaton, J. L., Nordlin, E. F., and Field, R. N. Dynamic Tests of Corrugated Metal Beam Guardrail. Highway Research Record 174, 1967, pp. 42-87.
11. Glennon, J. C., and Tamburri, T. N. Objective Criteria for Guardrail Installation. Highway Research Record 174, 1967, pp. 184-206.
12. Tutt, P. R., and Nixon, J. F. Roadside Design Guidelines. HRB Spec. Rept. 107, 1970, p. 124.

13. Young, R. D. A Three-Dimensional Mathematical Model of an Automobile Passenger. Texas Transportation Institute, Texas A&M Univ., Res. Rept. 140-2, Aug. 1970.
14. Highway Research Board Circular 482, Sept. 1962.

VEHICLE CRASH TEST AND EVALUATION OF MEDIAN BARRIERS FOR TEXAS HIGHWAYS

Edward R. Post, Teddy J. Hirsch, and Gordon G. Hayes, Texas Transportation Institute, Texas A&M University; and
John F. Nixon, Texas Highway Department

Full-scale tests were conducted to evaluate and compare the performance of three median barriers of different configuration and lateral stiffness: the semirigid metal beam guard fence, which consists of two back-to-back steel W-beam guardrails on breakaway steel posts; the relatively rigid E-3, which consists of two different sizes of strong elliptical steel rail members mounted on strong fabricated steel posts; and the rigid concrete median barrier with inclined faces. All three barriers satisfactorily restrained and redirected a standard-sized 4,000-lb passenger vehicle under the severe impact conditions of about 60 mph and 25 deg. However, severe snagging occurred on a post of the E-3 barrier as a result of the vehicle mounting the lower rail member. The semirigid fence barrier is the most economical with regard to initial construction costs and the safest concerning probability of injury to unrestrained occupants during test impact conditions. However, the barrier will cost the most to repair, and its use in narrow medians is not desirable because of the possibility of the vehicle displacing the barrier and knocking the light pole onto the roadway. The barrier would be satisfactory for use on rural roadways with wide shoulders and wide medians. The rigid medium barrier is the most economical when both initial construction costs and estimated repair costs are considered.

•ENGINEERS in Texas became concerned about the performance of certain median barriers being used or being considered for use on Texas highways. Consequently, three different types of median barriers were selected by the Texas Highway Department (THD) for full-scale vehicle crash testing in order to determine their performance under controlled impact conditions.

The three barriers selected by THD were the metal beam guard fence, which consists of two back-to-back steel W-beam guardrails on breakaway steel posts; the E-3, which consists of two different sizes of strong elliptical steel rail members mounted on strong fabricated steel posts; and the concrete median barrier with inclined faces.

Median barriers are effective in preventing head-on vehicle accidents. The three selected median barriers were subjected to severe impact conditions (1): a standard-sized passenger vehicle weighing about 4,000 lb impacting at a speed of 60 mph and an angle of 25 deg. Conducting the tests under similar impact conditions also provides a means of comparing the performance of the three barriers.

Most concrete median barriers are located in narrow medians in large urban areas, and many collisions occur at relatively shallow angles. Therefore, two additional tests were conducted on the concrete median barrier at impact angles of 7 and 15 deg.

One other objective of this study was to determine if a passenger vehicle would snag or dislodge a light pole mounted on the top of the concrete median barrier. One test was conducted under the impact conditions of 60 mph and 25 deg to investigate this problem.

DESCRIPTION OF MEDIAN BARRIERS

Metal Beam Guard Fence

The metal beam guard fence (MBGF) consists of two standard 12-gauge steel W-shaped rail members mounted back-to-back on each side of a 6 WF 8.5 support post (Fig. 1). The posts are spaced on 6-ft, 3-in. centers, and the height above the roadway to the top of the rail member is 27 in.

The $^3/_8$-in. fillet welds connecting the outer faces of the two post flanges and the base plate are designed to fracture in restraining and redirecting a standard-sized passenger vehicle under high impact speeds and moderate to large angles. Failure of the welded connections allows the two back-to-back rail members to displace several feet laterally, thereby reducing the vehicle decelerations and incidents of injury. Also, failure of the welds allows the posts to displace laterally with the rail member without pulling the rail member down, thereby preventing vehicle ramping.

E-3 Median Barrier

The E-3 median barrier consists of two strong elliptical-shaped steel rail members mounted on strong fabricated steel posts (Fig. 2). The height from the roadway to the top of the lower rail member is 14 in., and the height to the top of the upper rail member is 30 in. The posts are spaced on 10-ft centers.

The rail members are rolled from a round to an elliptical shape to increase the moment-carrying capacity under lateral loading. Also, the lower rail member is larger than the upper rail member because the larger portion of the lateral load is developed in the area of the wheel hub and structural frame of a passenger vehicle, whereas the upper rail member is subjected to primarily sheet metal crushing.

A post consists of two high-strength steel rectangular shapes that extend through the lower rail member. Fillet welds are used to connect the post to the two rail members and the high-strength steel base plate. The base plate is anchored by two $^3/_4$-in. A325 U-shaped bolts embedded in an 18-in. diameter concrete shaft.

The E-3 median barrier is considered to be a rigid barrier capable of undergoing only small displacements in redirecting a standard-sized passenger vehicle because of the relatively strong posts and rail members.

Concrete Median Barrier

The Texas concrete median barrier (CMB-70) is a massive concrete barrier with inclined plane surfaces (Fig. 3). The prototype CMB has a weight of about 507 lb/lin ft, a height of 32 in. above the roadway, a lower 10-in. high inclined surface of about 55 deg, an upper 18-in. high inclined surface of about 84 deg, a base width of 27 in., and a top width of 8 in.

As shown in Figure 3, the CMB was constructed in two longitudinally reinforced continuous length sections of 150 and 50 ft. The construction joint between the two sections offers no lateral restraint.

The light pole was mounted on top of the shorter 50-ft section. Three 18-in. diameter drilled concrete shafts were used to support the shorter CMB section. The Texas plans and specifications require that a drilled concrete shaft be used directly under each light pole to support a CMB section against possible overturning resulting from wind and vibratory forces on high light poles. The other two exterior drilled concrete shafts were used to prevent movement of the barrier during the full-scale test.

The longer 150-ft CMB section, on which three tests were conducted, contains no mechanical anchors to the roadway. The 1-in. layer of hot-mix asphalt at the base of the CMB provided some restraint to sliding during a vehicle collision.

VEHICLE TEST SETUP

Vehicle Control Apparatus

The test vehicles were guided along collision paths by a cable guidance system. In this system, a breakaway flange attached to the left front wheel hub follows a cable

Figure 1. Metal beam guard fence.

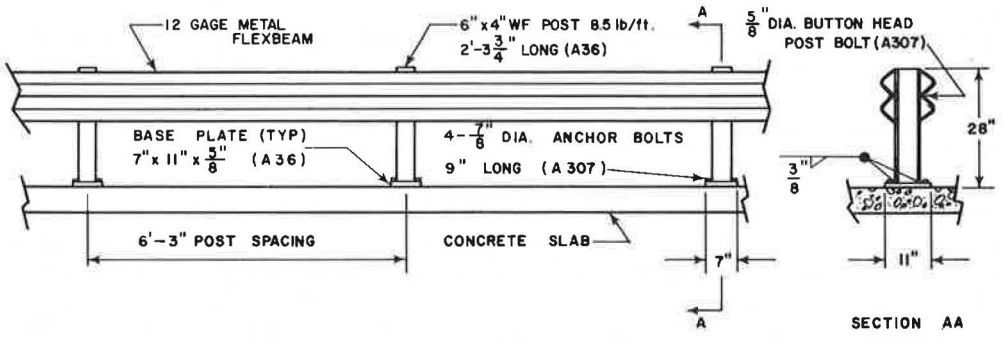

Figure 2. Texas E-3 barrier.

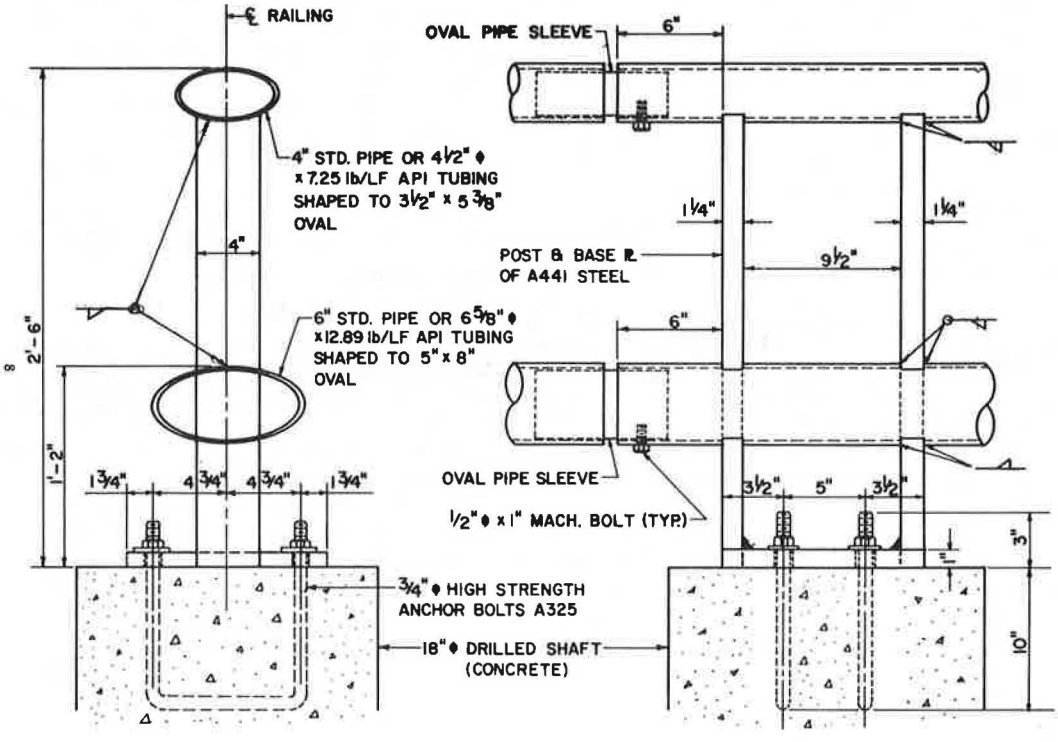

stretched along the path. Before impact, this device shears off and leaves the vehicle unguided.

The vehicles were brought to test speed by a cable attached through a pulley system to a reverse tow vehicle. The cable has an eye in the end that is looped around a pin welded to the front bumper of the test vehicle. As the test vehicle approaches the impact area, the pulley system exerts a downward force on the cable and causes it to disengage from the towing pin on the bumper.

Instrumentation

The barrier tests were recorded photographically using high-speed and documentary motion-picture cameras. The high-speed film (usually 500 frames per second) had accurate timing marks placed on the edge from which elapsed times were computed. Vehicle displacements were measured from the film using stadia boards on the vehicle and range poles on other targets. The position of the vehicle in the horizontal plane was determined by using two cameras and a triangulation technique.

The test vehicles had accelerometers mounted on the longitudinal frame members behind the front seat. One accelerometer was mounted transversely and one longitudinally on each frame member. During the tests on the E-3 and MBGF, the signals from the accelerometers were transmitted by a shielded cable to a nearby instrumentation mobile trailer. The data were recorded on magnetic tape.

The later tests on the CMB were conducted using a telemetry data acquisition system that transmitted the accelerometer data by radio signals to a ground station. The data were recorded on magnetic tape. The telemetry system eliminates the need for a physical connection to the test vehicle.

A 160-lb anthropometric dummy simulated a driver secured by a lap belt. A load cell attached to the belt measured the lap belt force. The accelerometer and lap belt data were passed through an 80-Hz low-pass active filter.

Data Reduction Techniques

The impact speed of the vehicle was determined from film obtained with a camera located perpendicular to the vehicle approach path, and the position of the vehicle was determined at the end of successive small time intervals throughout redirection.

The average lateral and longitudinal decelerations from the film data were calculated from impact to the time when the vehicle was parallel to the barrier. It is to be noted that these decelerations are perpendicular and parallel to the barrier, whereas the decelerations from the vehicle accelerometers are perpendicular and parallel to the longitudinal axis of the vehicle. The longitudinal and lateral decelerations from the film were calculated as given in Tables 1 and 2, which contain a summary of the E-3 and MBGF and CMB test results respectively.

Peak decelerations were read directly from the accelerometer traces, whereas the average decelerations from the traces were computed over the interval from impact to the point where significant accelerations had ceased.

DISCUSSION AND EVALUATION OF TESTS

A discussion and evaluation of the six full-scale tests conducted on the three median barriers follow.

MBGF Test

The MBGF test was conducted at an impact speed of 57.3 mph and an impact angle of 25 deg using a 1963 Plymouth weighing 3,460 lb with instrumentation and dummy. The point of impact was near a support post.

Sequential photographs of the vehicle collision and its redirection are shown in Figure 4. A summary of the test results from an analysis of the film data and accelerometer traces are given in Table 1.

A peak longitudinal deceleration of 12.8 g indicated that snagging on the posts was not severe. The change in heading speed of the vehicle during redirection was 25 mph, the

Figure 3. Texas CMB-70.

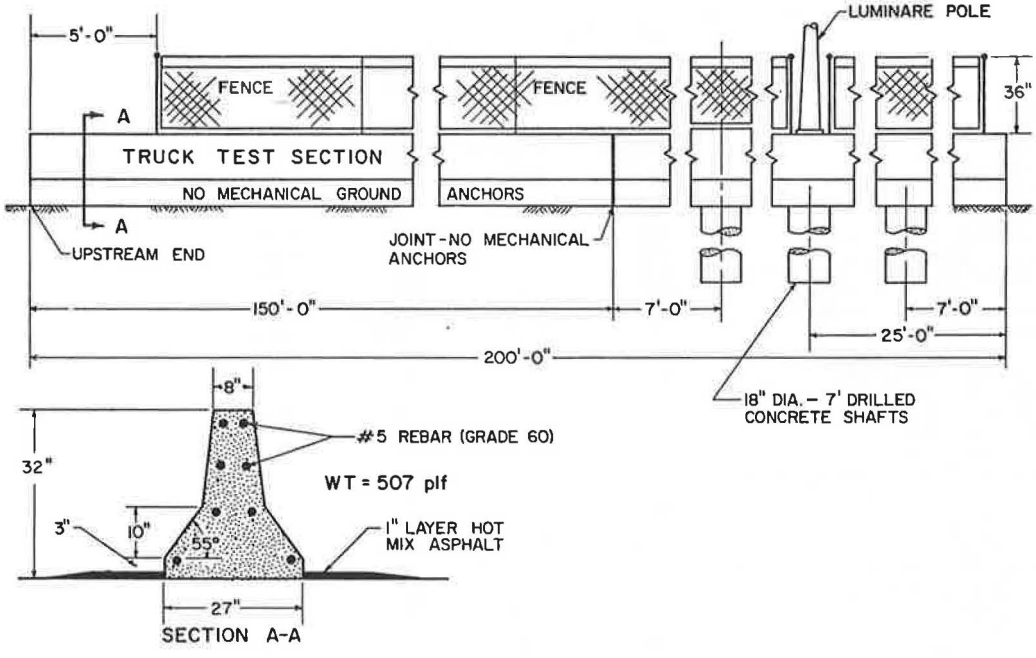

Table 1. Test data summary for E-3 and MBGF tests.

Item	Barrier Test	
	E3	MBGF
Vehicle		
Year	1963	1963
Make	Plymouth	Plymouth
Weight (lb)	3,610	3,640
Impact angle (deg)	25	25
Film data		
Initial impact speed (mph)	59.3	57.3
Speed at parallel (mph)	28.9	32.7
Longitudinal distance to parallel (ft)	20.7	17.5
Dynamic barrier displacement (ft)	0.7	1.5
Lateral distance to parallel (ft)	3.4	4.28
Time to parallel (sec)	0.394	0.270
Average longitudinal deceleration[a], parallel to barrier (g)	3.3	3.0
Average lateral deceleration[b], normal to barrier (g)	6.2	4.6
Departure angle (deg)	8.7	19.7
Accelerometer data		
Longitudinal deceleration, parallel to longitudinal axis of vehicle (g)		
Maximum	21.3	12.8
Average	4.1	3.0
Time (sec)	0.533	0.560
Transverse deceleration, normal to longitudinal axis of vehicle (g)		
Maximum	6.1	—
Average	0.4	—
Time (sec)	0.537	—

[a] $G_{long} = \frac{(V_i \cos\theta)^2 - V_p^2}{2g\, S_{long}}$.

[b] $G_{lat} = \frac{V_i^2 \sin^2\theta}{2g\, S_{lat}}$ where $S_{lat} = AL \sin\theta - B(1 - \cos\theta) + D$.

Table 2. Test data summary for CMB tests.

Item	Barrier Test			
	CMB-1	CMB-2	CMB-3	CMB-4
Vehicle				
Year	1963	1964	1963	1963
Make	Plymouth	Chevrolet	Chevrolet	Chevrolet
Weight (lb)	4,000	4,230	4,210	4,210
Impact angle (deg)	25	25	7	15
Film data				
Initial impact speed (mph)	62.4	55.7	60.9	60.7
Speed at parallel (mph)	47.2	—	58.8	50.5
Longitudinal distance to parallel (ft)	15.3	—	17.6	23.0
Dynamic barrier deceleration (ft)	0.0	0.0	0.0	0.0
Lateral distance to parallel (ft)	2.9	2.9	0.85	1.74
Time to parallel (sec)	0.223	0.320	0.206	0.298
Average longitudinal deceleration[a], parallel to barrier (g)	2.0	—	0.4	1.3
Average lateral deceleration[b], normal to barrier (g)	8.0	6.4	2.2	4.7
Departure angle (deg)	7.3	6.0	6.5	11.5
Accelerometer data				
Longitudinal deceleration, parallel to longitudinal axis of vehicle (g)				
Maximum	8.7	10.3	8.4	7.8
Average	3.2	1.8	0.5	1.4
Time (sec)	0.184	0.271	0.325	0.244
Transverse deceleration, normal to longitudinal axis of vehicle (g)				
Maximum	16.1	13.3	29.2	14.0
Average	4.4	2.8	1.8	3.0
Time (sec)	0.254	0.280	0.282	0.264

[a]See Table 1 footnote. [b]See Table 1 footnote.

Figure 4. MBGF test.

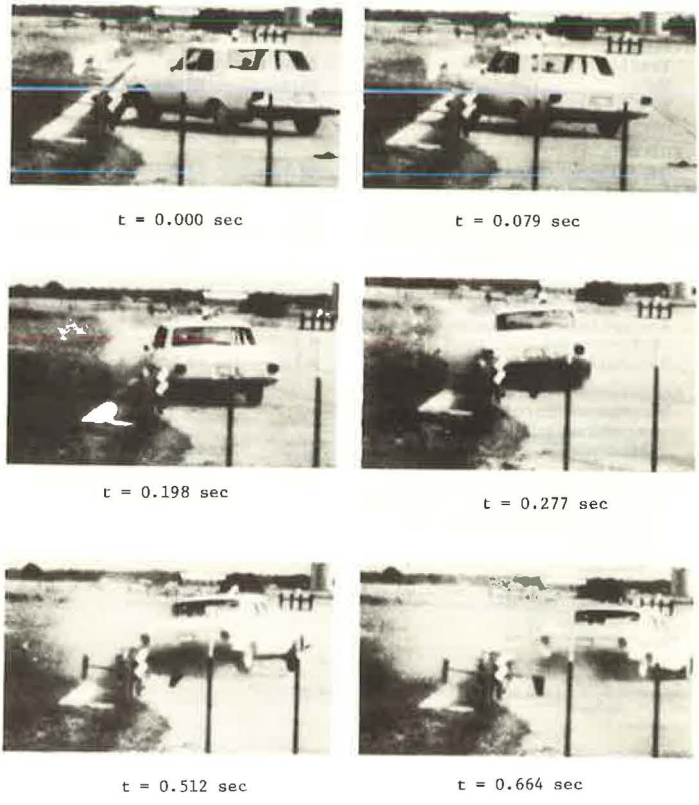

departure angle from the barrier was 20 deg, and the maximum dynamic lateral displacement of the barrier was 1.5 ft.

The large departure angle was due to the side ramping effect resulting from the large displacements of the rail member. In any event, the large departure angle would probably not create a hazardous condition to other nearby traffic because the severely damaged wheel pulled the vehicle toward the barrier after redirection (Fig. 5).

The effectiveness of the breakaway fillet welded post connection in allowing the posts to displace laterally without pulling the rail member down, and thereby preventing any tendency of the vehicle to ramp, is evident in the photographs of the damaged barrier.

It can be seen in Figure 5 that the MBGF remained intact under the severe test conditions. Maintenance would essentially require the replacement of three posts and one 25-ft length section of the two back-to-back W-beam guardrails. It appears that the damaged barrier would, prior to repair, be functional under a possible second low-angle collision.

The damaged test vehicle is shown in Figure 6. The left front quarter was damaged, but the windshield remained intact and the passenger compartment area was not warped.

E-3 Test

The E-3 test was conducted at an impact speed of 59.3 mph and an impact angle of 25 deg using a standard-sized 1963 Plymouth weighing 3,610 lb with instrumentation and dummy. The point of impact was slightly upstream from the splice connections in the rail members and support post (Fig. 7).

Sequential photographs of the vehicle collision and its redirection are shown in Figures 8 and 9. Summary data are given in Table 1.

The longitudinal accelerometer traces on the right and left frame members of the vehicle indicated that a large amount of snagging occurred on a support post during the time interval of 100 to 160 msec after impact. The peak acceleration was 21.3 g. The tire marks and the motion of the vehicle (Fig. 9) show that the vehicle had climbed on the lower rail member. It appears that the snagging on a post could be greatly reduced by placing the lower rail member higher.

As indicated in Table 1, the change in heading speed of the vehicle during redirection was 30 mph, the departure angle from the barrier was 9 deg, and the maximum dynamic lateral displacement of the top rail member was 0.7 ft.

It can be seen in Figure 7 that the barrier remained intact and was not extensively damaged under the test conditions. Maintenance would require the replacement of one 10-ft long upper rail member and straightening of one support post. It appears that the damaged barrier would, prior to repair, be functional under a possible second collision.

The damaged test vehicle is shown in Figure 10. It can be seen that the left front quarter and wheel were severely damaged, the windshield was knocked out, and the passenger compartment area was warped.

CMB-1 Test

The first rigid concrete median barrier test, designated CMB-1, was conducted to determine if a standard-sized 4,000-lb vehicle would snag and knock down a light pole mounted on top of the barrier under the impact conditions of about 60 mph and 25 deg.

Sequential photographs of the vehicle collision and its redirection are shown in Figures 11 and 12. The contact point of the left front fender was approximately 9 ft upstream from the light pole. As the vehicle was redirected, it climbed to the top of the barrier and lightly scraped the light pole and fence.

The change in heading speed during redirection was 15 mph, the average lateral vehicle deceleration was 8.0 g, and the departure angle from the barrier was 7 deg (Table 2).

The damaged vehicle is shown in Figure 13. As can be seen, the front quarter and wheel were severely damaged, the door on the side of the driver was sprung open, and the windshield was cracked.

Figure 5. Damage to MBGF.

Figure 6. Vehicle damage after MBGF test.

Figure 7. Damage to E-3 barrier.

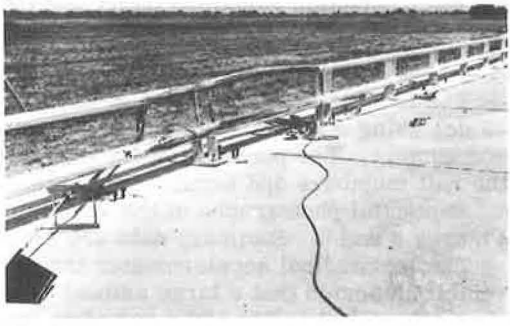

Figure 8. E-3 barrier test (rear view).

t = 0.000 sec

t = 0.063 sec

t = 0.116 sec

t = 0.213 sec

t = 0.309 sec

t = 0.382 sec

t = 0.441 sec

t = 0.567 sec

Figure 9. E-3 barrier test (side view).

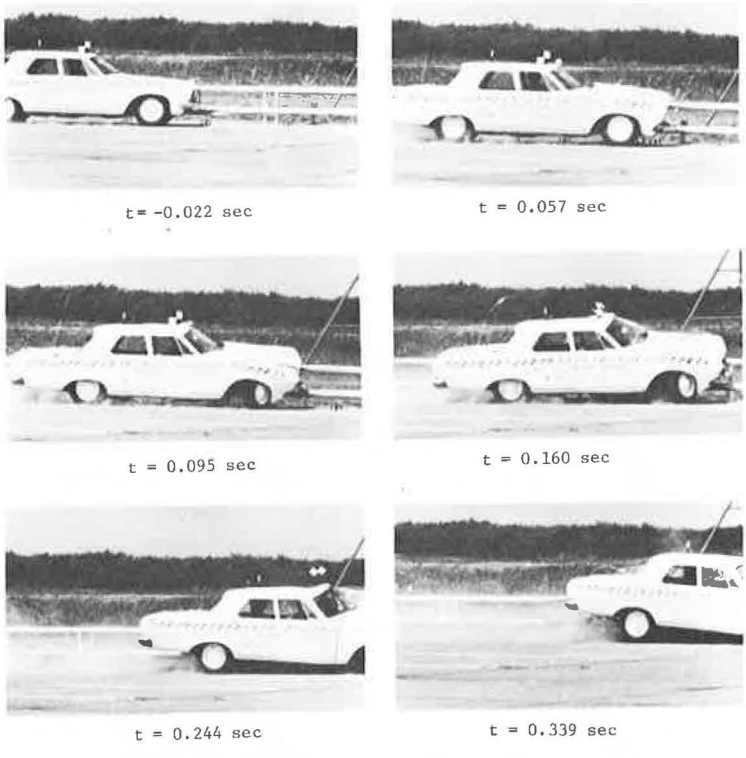

Figure 10. Vehicle damage after E-3 test.

Figure 11. CMB-1 test (rear view).

t=0.000 sec.

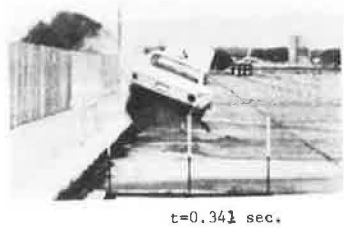

t=0.341 sec.

t=0.094 sec.

t=0.587 sec.

t=0.169 sec.

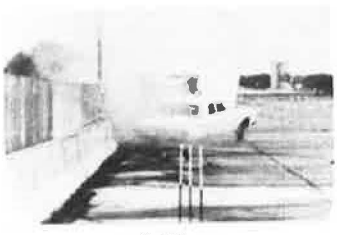

t=0.954 sec.

t=0.223 sec.

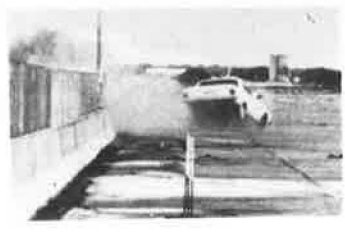

t=1.396 sec.

Figure 12. CMB-1 test (side view).

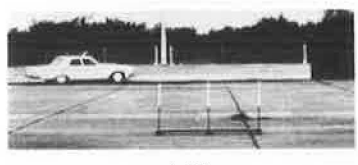

t = 0.000 sec

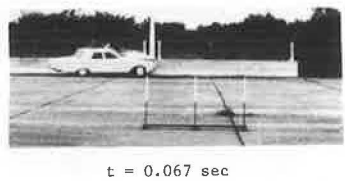

t = 0.067 sec

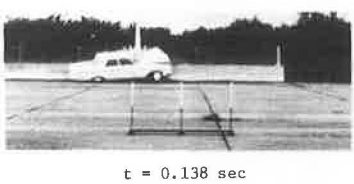

t = 0.138 sec

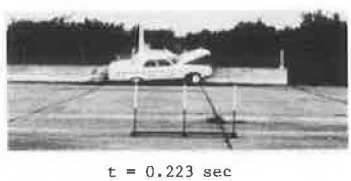

t = 0.223 sec

t = 0.302 sec

t = 0.456 sec

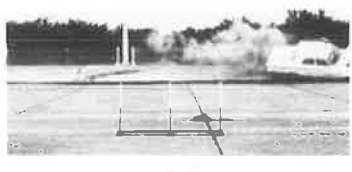

t = 0.631 sec

t = 0.742 sec

CMB-2 Test

The CMB-2 test was conducted to determine if the 150-ft unanchored section of the CMB, with continuous steel reinforcement, would slide or rotate or both in restraining and redirecting a standard-sized 4,000-lb passenger vehicle under the impact conditions of about 60 mph and 25 deg.

The vehicle-barrier interaction in the CMB-2 test was similar to that of the CMB-1 test. While the vehicle was being redirected, the left front fender was crushed, and the tire rode up to the top of the barrier. Sequential photographs of the vehicle collision and redirection are shown in Figure 14, and photographs of the minor barrier damage are shown in Figure 15.

Linear displacement voltage transducers (LDVT) placed on the barrier showed that the lateral and rotational displacements of the barrier were negligible. The LDVT placed 2 in. above the asphalt showed a maximum displacement of 0.03 in., whereas the LDVT placed near the top of the barrier showed a maximum displacement of 0.09 in.

The average lateral vehicle deceleration in this test of 6.4 g was smaller than that in the previous test because the impact speed was about 6 mph less. For all practical purposes, the departure angle of 6 deg in this test was the same as in the previous test (Table 2).

The damaged vehicle is shown in Figure 16. It can be seen that the 6-mph lower impact speed in this test also resulted in slightly less vehicle damage than that encountered in the CMB-1 test. For instance, the door was not sprung open in this test.

CMB-3 Test

Concrete median barriers with inclined faces are currently being used mostly on urban roadways having narrow medians and carrying high traffic volumes. The majority of the accidents under these conditions usually occur at shallow angles of 15 deg and less. This test, designated CMB-3, was therefore conducted to evaluate the performance of the barrier in redirecting a 4,000-lb passenger vehicle under representative in-service impact conditions of about 60 mph and 7 deg.

This test was again run on the 150-ft length section of the CMB that was not anchored to the roadway. Sequential photographs of the vehicle collision and redirection are shown in Figure 17. The vehicle quickly climbed up the lower face of the barrier and was redirected when the tire contacted the steeper upper face of the barrier. The maximum height of climb was approximately 18 in.

The departure angle was, for all practical purposes, the same as in the two previous 25-deg angle collisions. The change in the vehicle heading speed of 2 mph was much lower than in the 25-deg angle collision because the redirection of the vehicle occurred primarily as the result of an interaction between the vehicle tire and the barrier. Also, the average lateral vehicle decelerations of 2.2 g were very low in comparison to the previous tests (Table 2).

The damaged test vehicle is shown in Figure 18. The relatively minor damage consisted of bumper and sheet-metal crushing.

CMB-4 Test

The CMB-4 test was conducted to determine the performance of the barrier in redirecting a 4,000-lb passenger vehicle under somewhat of an upper bound on in-service collisions of 60 mph and 15 deg.

The 150-ft unanchored section of the CMB was again used. Sequential photographs of the vehicle collision and redirection are shown in Figure 19. The vehicle motion was similar to that in the two previous 25-deg tests in that the vehicle climbed all the way to the top of the barrier and caused minor damage to the barrier and fence.

For some unknown reason, the change in the vehicle heading speed of 11 mph was roughly double the speed of the CMB-1 test, which was run at a much larger impact angle and, hence, probably developed greater sheet-metal frictional forces. However, the greater change in heading speed could be the reason for the departure angle of 12 deg being roughly double the departure angles in previous test runs. In any event, it appears

Figure 13. Vehicle damage after CMB-1 test.

Figure 14. CMB-2 test.

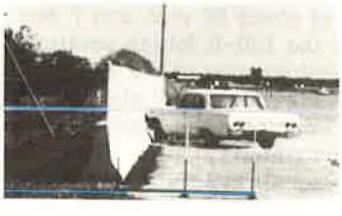
t = 0.000 sec

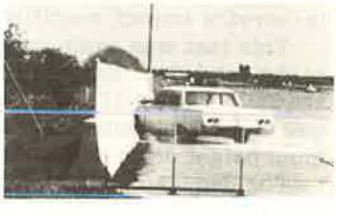
t = 0.033 sec


t = 0.099 sec


t = 0.144 sec

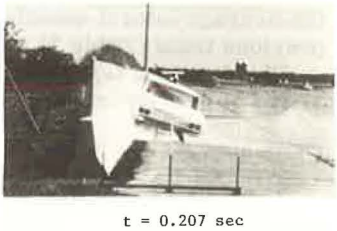
t = 0.207 sec

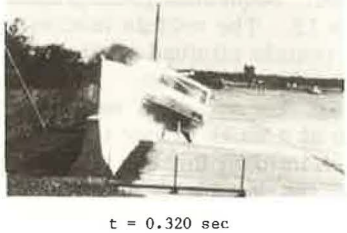
t = 0.320 sec

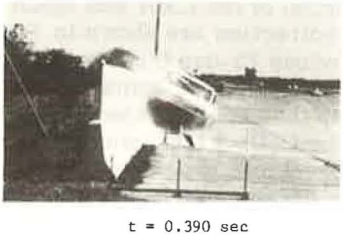
t = 0.390 sec

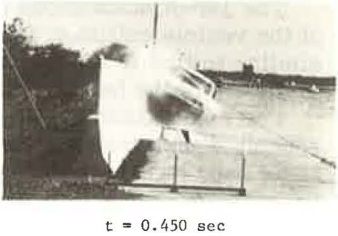
t = 0.450 sec

Figure 15. Damage to CMB-2.

Figure 16. Vehicle damage after CMB-2 test.

Figure 17. CMB-3 test.

t = -0.033 sec

t = 0.019 sec

t = 0.057 sec

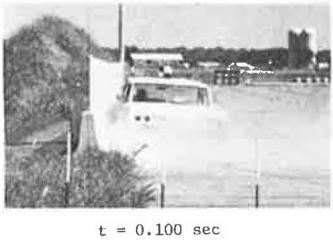

t = 0.100 sec

t = 0.112 sec

t = 0.150 sec

t = 0.211 sec

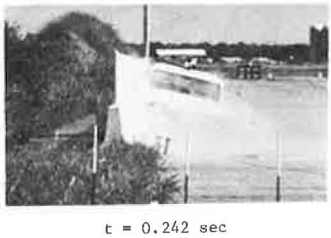

t = 0.242 sec

Figure 18. Vehicle damage after CMB-3 test.

Figure 19. CMB-4 test.

t = -0.010 sec

t = 0.023 sec

t = 0.077 sec

t = 0.128 sec

t = 0.176 sec

t = 0.199 sec

t = 0.273 sec

t = 0.327 sec

that this larger departure angle would most likely not create any hazardous situation to other nearby vehicles because the drag forces of the damaged front wheel pulled the vehicle back toward the barrier.

The damaged vehicle is shown in Figure 20. The damage to the vehicle in this test was slightly less than the damaged vehicles in the CMB-1 and CMB-2 tests that were run at larger impact angles.

INJURY PROBABILITY

Vehicle damage appears to be, at the present time, a good indicator of the probability of occupant injury. Michalski (2) recently established from a statistical analysis of accident information a relation among type of collision, vehicle damage, and percentage of vehicles in which injuries occurred to unrestrained occupants.

Predictions on the probability of injury for the three median barriers of different configuration and lateral stiffness are given in Table 3. These predictions were based on the average damage rating values of nine research engineers using the seven-point photographic scales developed by the National Safety Council (3).

The comparison of the three barriers during a 25-deg collision clearly illustrates the desirable effect of barrier displacements in enhancing safety; that is, the semirigid MBGF undergoing the largest displacement of 1.5 ft resulted in the lowest probability of injury. Also, the effects of snagging are reflected in the results given in Table 3 because the relatively rigid E-3 barrier undergoing a displacement of 0.7 ft resulted in the highest probability of injury.

A comparison of the safety aspects of the three median barriers cannot be reached in this study for the more representative in-service impact conditions of 15 deg and less because no tests were conducted on the E-3 and MBGF.

ESTIMATED CONSTRUCTION COSTS AND REPAIR COST

In order to properly evaluate the three selected barriers, it is important that one take into consideration initial construction costs and maintenance costs.

Initial construction costs for the three selected barriers are given in Table 4. The unit cost breakdowns were adjusted to agree with the total cost per linear foot figures obtained from the Texas Highway Department (5). As evident, the construction cost of $19.20/lin ft for the E-3 barrier is relatively high in comparison to the more efficient CMB with a cost of $13.40/lin ft and the MBGF with a cost of $11.75/lin ft.

The estimated maintenance repair costs for the three barriers after the comparable 4,000-lb automobile tests of 60 mph and 25 deg are given in Table 5. The initial construction costs for the E-3 and MBGF were increased by a factor of 1.5 for purposes of repair to a small section.

CONCLUSIONS

A summary of the comparative results made on the three Texas median barriers is given in Table 6. One could conclude from the results that the MBGF is the most economical barrier with regard to initial construction costs and that it is the safest with regard to probability of injury to unrestrained occupants during a crash under test conditions. However, the MBGF would cost the most to maintain, and its use in narrow medians is not desirable because of the possibility of the vehicle displacing the barrier a sufficient distance and knocking the light pole onto the roadway. It appears that the MBGF would probably be satisfactory for use on rural roadways with wide shoulders and wide medians.

One could further conclude that the CMB is the most economical when both initial construction costs and estimated maintenance costs are considered. The CMB with light poles would be very desirable for use on urban roadways with narrow medians and carrying high-speed and high-volume traffic. In addition, low maintenance reduces the amount of exposure time and, hence, increases safety to maintenance personnel.

It is important that one keep in mind that all three median barriers investigated in this study have performed adequately while in service. Also, other factors in addition

Figure 20. Vehicle damage after CMB-4 test.

Table 3. Injury probability.

Angle (deg)	Rigid CMB (percent)	Rigid E-3 (percent)	Semirigid MBGF (percent)
7	10	No test	No test
15	60	No test	No test
25	70	80 (snagging)	50

Table 4. Initial construction costs.

Barrier	Structural Component	Unit Cost Including Labor	Dollar Cost per Linear Foot
CMB-70	Steel forms (rental and labor)		4.00
	8-pcs No. 5 reinforcing steel	$0.30/ft	2.40
	Concrete (ready-mix)	$45/yd^3	5.50
	Site preparation, stabilize soil, 1 in. asphalt at base, contingencies		1.50
	Total		13.40
E-3	Top rail member (7.25 lb/ft)	$0.60/lb	4.35
	Bottom rail member (12.89 lb/ft)	$0.60/lb	7.75
	Fabricated posts (10 ft on centers)		4.25
	Drilled concrete shafts (18-in. diameter)		1.00
	Base plates and anchor bolts		1.00
	Contingencies		0.85
	Total		19.20
MBGF	2 to 12 gauge steel W-beams	$0.45/lb	6.00
	6 B 8.5 posts (6 ft, 3 in. on centers)	$0.45/lb	1.50
	Drilled concrete shafts (18-in. diameter)		1.80
	Base plates and anchor bolts		1.60
	Contingencies		0.85
	Total		11.75

Note: These costs do not include the costs of the fence and light poles because in roadway medians they would be common to all three barriers.

Table 5. Estimated maintenance costs.

Barrier	Required Maintenance	Dollar Cost per Linear Foot[a]	Total Cost[b] (dollars)
CMB-70	Occasional sandblasting to remove tire scrub marks		0
E-3	Replace one 10-ft long section upper rail Straighten one support post Paint touchup (galvanized)	19.20 (1.5)	290
MBGF	Replace one 25-ft long section of two back-to-back W-beam guardrails Replace three breakaway support posts	11.75 (1.5)	440

[a]The initial construction costs for the E-3 and MBGF barriers were increased by a factor of 1.5 for purposes of repair to a small section.
[b]Values rounded off to the nearest $10.

Table 6. Comparative summary of three barriers.

Basis for Comparison	CMB-70 (longitudinally reinforced concrete)	E-3 (tubular rails)	MBGF (back-to-back W-beams)
Initial construction cost[a] (dollar/ft)	13.40	19.20	11.75
Estimated maintenance after impact (dollars)	0	290	440
Predicted probability of injury (percent)	70	80	50
National Safety Council vehicle damage rating	5.8	6.1 (snagging)	5.2
Should barrier be used on narrow medians with light poles under test impact conditions	Yes (negligible barrier displacements)	Probably (small barrier displacements of 0.7 ft, lower rail raised to prevent snagging)	Probably not (barrier displacements of 1.5 ft may allow automobile to knock down light pole)
Appearance	Simple and smooth lines	Smooth and thin tubular rails	Adequate

Note: Data based on 4,000-lb automobile impacting at 65 mph and 25 deg.
[a]Cost does not include chain link fence (glare screen) or light poles.

to those presented here should be considered when selecting a barrier. For example, Hutchinson and Kennedy (6) present data that indicate that approximately 75 percent of vehicle collisions are at angles of 15 deg or less. At lower impact angles, the safety and maintenance aspects of all three median barriers would improve.

ACKNOWLEDGMENT

The contents of this paper reflect the views of the authors who are responsible for the facts and the accuracy of the data presented herein. The contents do not necessarily reflect the official views or policies of the Federal Highway Administration. This report does not constitute a standard, specification, or regulation.

REFERENCES

1. Highway Research Board Circular 482, Sept. 1962.
2. Michalski, C. S. Model Vehicle Damage Scale: A Performance Test. Traffic Safety, Vol. 12, No. 2, June 1968, pp. 34-39.
3. Vehicle Damage Scale for Traffic Accident Investigation. Traffic Accident Data Project, National Safety Council, TAD Bull. 1, 1968, 18 pp.
4. McFarland, W. F., and Walton, N. E. Economic and Accident Potential Analysis of Roadway Lighting Alternatives. Highway Research Record 377, 1971, pp. 92-102.
5. Texas Highway Department D-8 Interoffice Memorandum to Mr. John Nixon from R. S. Williamson, April 10, 1972.
6. Hutchinson, J. W., and Kennedy, T. W. Medians of Divided Highways—Frequency and Nature of Vehicle Encroachments. Eng. Exp. Sta., Univ. of Illinois, Bull. 487, 1966.

DESIGN OF SLIP BASES FOR BREAKAWAY SIGNS

Bruce F. McCollom, State Highway Commission of Kansas

The object of the study was the design of economical slip bases for breakaway sign supports. The style of baseplate previously used in Kansas, although most economical to fabricate, was too heavy because the baseplate thickness had been based on a theoretical analysis that contained several conservative assumptions. Therefore, full-scale tests were run using experimental stress analysis techniques to determine a more accurate analysis method. A design method was developed based on these results. Application of the method allows the use of flat baseplates that meet the maximum weight recommendations set forth by the Texas Transportation Institute. This is estimated to result in an annual savings of $20,000 in Kansas.

•THIS paper discusses the design of the slip base portion of breakaway sign supports, specifically the baseplates. Recommendations for design of sign supports of this type were developed at the Texas Transportation Institute (TTI) as part of a cooperative highway research project sponsored by several states and the Federal Highway Administration (1-6). The Federal Highway Administration recommended that certain criteria (6) be followed in the design of breakaway supports.

One of the elements specified in the TTI criteria is baseplate weight. The TTI researchers checked the effect of baseplate weight on collision performance using a computer simulation that they developed from actual crash test data. They found that the weight of the baseplate had very little effect on system response within certain practical limitations. The maximum baseplate weights recommended in the criteria are assumed to be these practical limits.

Kansas began using breakaway supports on an experimental basis in 1966. The bases used on the heavier post sections in Kansas differed from those used in Texas and tested at TTI (Fig. 1). The Kansas base is more economical because it requires less labor to fabricate. As part of a project to update all sign supports to match revised AASHO specifications, the Kansas designs were reviewed in 1970. Some baseplates on these designs were found to be significantly heavier than those recommended (6). It was desired to continue use of this type of base in Kansas but to reduce its weight.

In the early Kansas designs the thickness of the baseplates had been based on a theoretical analysis containing several conservative assumptions: that the plates bent in a single curvature about the post flange when the base was subjected to a moment, that the load causing this bending was equal to the bolt load (due to base moment and calculated by statics) applied at the centerline of the bolts, and that the baseplate bending stress should be limited to the same allowable value as the post flange (assuming that the plate and flange are of the same material). This method overestimates thickness requirements because plasticity effects and the reinforcement provided by the weld are not considered. Also, the bolts and washers provide some bending restraint and provide a load application point that is closer to the post flange than the bolt centerline.

Because thicknesses determined by the old design method generally result in baseplate weights that are greater than those recommended (6), full-scale tests were run to determine a more accurate method. Most of the test results for one of the four test designs are given in this paper. The full test data are given elsewhere (3). A design method based on these tests is developed, and application of the new design method to bases to be used in Kansas is discussed.

STATIC STRENGTH TESTING

It appears that the static strength of slip bases subjected to a moment as shown in Figure 2 would be dependent on the following geometric variables: S, T1, T2, C, A, E, d, flange width, flange thickness, web thickness, and bolt diameter. In addition, the strength parameters of the materials would be important, but these relations are known. A complete testing program would require a large number of tests. This was not considered necessary because most of the variables have a small range of values for practical designs. It was decided to test specimens of actual proposed designs in which the thickness of the top baseplate was such that its weight would approximately be equal to that recommended (6). This would prove or disprove the adequacy of the designs tested and allow development of a design method for bases of similar proportions.

Test Procedure and Equipment

Tests were run on the four bases with dimensions as given in Table 1. In all tests the loading setup was arranged to produce moment at the slip base as shown in Figure 2. The load was applied at a slow rate. Work was stopped at incremental stages to observe the strain measuring devices. Loading was done with a 450,000-lb universal testing machine and a special mounting frame (Fig. 3). The W 12×19 test was run first to determine if further tests were necessary and to try out the testing procedure. Calculations indicated that, if the W 12×19 base tested could develop the full moment resistance of the post, a $\frac{5}{8}$-in. thick plate could be used for smaller post sections, and further testing would not be required. This was found not to be the case, so tests on three more bases were performed. It was assumed that the worst loading condition for bases with the same top and bottom plates would be with the load close to the base because for a given moment the shear would be higher. For this reason, the first tests were run with the load at the point nearest the base for which slipping of the baseplates would not occur. The location of this point was determined by the value of the coefficient of friction. In the W 12×19 test, the coefficient-of-friction value was taken as 0.35 in calculating the load position. Problems with slippage occurred, so the value used was lowered to 0.20 for the final set of tests. Problems with slippage still occurred, so the load was moved out to a point 60 in. from the base; this provided for a coefficient of friction of about 0.10.

Data from which to develop the design method were obtained by using strain measuring devices in the tests. These included brittle coatings, photoelastic coatings, and electric resistance strain gauges. Figure 4 shows the location of these devices on the bases tested. In the W 12×19 test, the only strain gauge used was rosette A, which was a paperbacked wire rosette with 0.28-in. gauge lengths. A six-channel bridge balancing unit was used in a half bridge circuit with temperature compensation provided by a matching gauge mounted on a block of steel.

For tests on the other three bases, phenolic glass-backed foil-stacked rosettes, with 0.12-in. gauge lengths, were used. The shorter gauge lengths and stacked arrangement provide better results because sharp strain gradients were present. Gauges E and F were phenoloc glass-backed foil gauges with 0.06- and 0.12-in. gauge lengths, and gauge G was purchased preassembled in the bolt. A 20-channel bridge balancing unit was used in half bridge circuit with a dummy precision resistor in the inactive bridge arm. The gauges were temperature-compensated.

Contact cement was used for installation of gauges in all tests, and a null balance strain indicator was used to read out data in all tests.

Aerosol application-type brittle lacquers were used in all tests along with a special calibration device.

Photoelastic coatings were used on all but the W 12×19 base. The coating used had a strain optical coefficient of 0.15, a thickness of 0.125 in., and a fringe constant of 605 μ strain/fringe. A reflection polariscope was used to obtain orthochromatic fringe patterns and isoclinal lines. These were recorded on color slides using a 35-mm camera.

Figure 1. Comparison of Texas breakaway base and Kansas breakaway base.

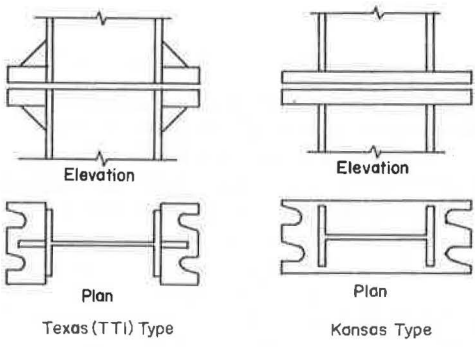

Figure 2. Kansas base.

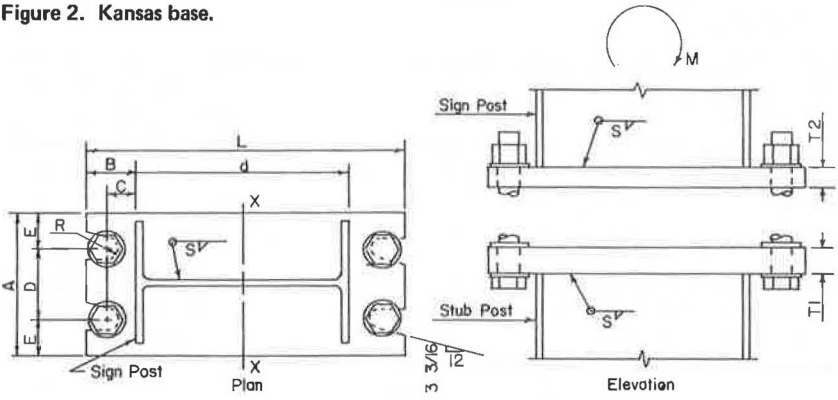

Table 1. Dimensions of bases tested.

Type of Post	Dimension (in.) S	T1	T2	A	B	C	D	E	L	R	Bolt Size (in.)
W 12×19	1/4	5/8	5/8	4 5/8	2	1 1/8	2 1/2	1 1/16	14 1/8	13/32	3/4 by 2 3/4
W 6×8.5	1/4	7/8	5/8	4 5/8	1 7/8	1 1/8	2 1/2	1 1/16	9 5/8	11/32	5/8 by 3
W 10×11.5	1/4	1	3/4	4 5/8	1 7/8	1 1/8	2 1/2	1 1/16	13 5/8	11/32	5/8 by 3 1/2
W 10×21	1/4	1 1/4	7/8	6 3/8	2 1/4	1 1/4	3	1 11/16	14 3/8	15/32	7/8 by 4

Note: Structural shapes and plate according to ASTM A-36 and bolts according to ASTM A-325.

Figure 3. Test setup.

Test Results

Raw strain readings from rosettes were reduced to maximum and minimum principal strains using a calculator. The principal strain at these rosettes was very nearly perpendicular to the post flange. The maximum or minimum principal strain at each rosette location was plotted against base moment. Strain at gauge E was plotted against base moment. Gauges F and G were at locations where the stress could be reliably determined by theory and served mainly as a check. Stress at gauge F and bolt load at gauge G were plotted against moment at gauge F and base moment respectively.

The extent of stress-coat cracking was marked at each increment where it was observed, and photographs showing the marks were taken.

Orthochromatics were recorded at each load increment where the strain gauges were read. Isoclinal line patterns were recorded at only one load increment for 15-deg rotations of the polarizer-analyzer. These were then displayed one at a time and traced on the same sheet of paper.

In the W 12×19 test, bending of the base bottom baseplate was observed at a base moment of 387 kip-in. The test was continued to a moment of 454 kip-in. at which the gap between the baseplates, on the side where the bolts are in tension, had grown to about $\frac{1}{4}$ in. In the W 6×8.5 test, first bending of the top baseplate on the tension bolt side was observed at 220 kip-in., and the largest test moment was 252 kip-in. Bending of the tensile bolts was observed at about the same time and rate as the bending of the baseplate. The largest test moment in the W 10×11.5 was 420 kip-in. and in the W 10×21 was 726 kip-in. No significant bending of baseplates was noted in either of these tests. The moment in the W 10×11.5 test was limited to the proof load of the strain-gauge bolt to avoid damaging it. In the W 10×21 test, the moment was limited by the deflection of the testing frame.

After testing of the bases was completed, tensile strength specimens were cut from the baseplates and were tested. The results of these tests are given in Table 2.

Analysis of Results

In some cases the test results indicated the adequacy of the design tested. Because the W 12×19 bottom baseplate began bending at a moment of 387 kip-in. and because it would take a moment of 840 kip-in. to produce the yield point stress (39.3 ksi) in the post flanges, it was concluded that this design was unsatisfactory. A moment of 200 kip-in. would produce yield point stress (38.9 ksi) in the post flange of the W 6×8.5, but this base was subjected to a moment of 220 kip-in. before baseplate bending was noted: It was concluded that this design was satisfactory because the post would fail before the baseplate. In the other two tests the largest moments reached (420 and 726 kip-in.) were less than the post yield moments of 474 kip-in. (at 45.2 ksi) and 970 kip-in. (at 42.2 ksi) respectively.

The results obtained from the strain indicating devices clarify the stress behavior of the Kansas type of breakaway base. The stress-coat crack patterns all indicate concentrations of stress near the bolts. This verifies that the strain rosettes were located in the proper places to detect maximum strains. It also indicates the importance of dimensions C and A (Fig. 2). The measured strains were primarily dependent on base moment and almost independent of base shear. This is shown by the closeness of results from test series done with the load applied at different points on the same specimen.

Maximum principal strain results always occurred at rosette A (Fig. 4) except in the W 12×19. This is contrary to what theory predicts because base moment causes compression at rosette A, whereas base shear causes tension at rosette A (both in the direction of principal strain). At rosette B, on the other hand, theory says that the strains caused by base shear and moment are additive. The author believes this phenomenon is due to the difference in restraint caused by the bolts and washers. The bolts on the tension side (where rosette A is located) were observed to bend in one of the tests. This is logical because they are not as stiff as the baseplate. The orthochromatics do not clearly indicate whether there is any restraint causing double

curvature or not. The isoclinics do appear to indicate double curvature of the tension side baseplates. On the compression side (where rosette B is located), the middle washer is in compression. Because this washer cannot deform sufficiently to provide for much rotation, between baseplates, it must offer some restraint. Perhaps the most important results are that maximum measured principal strains ranged from only 59 to 73 percent of those predicted by the old design assumptions and that about 50 percent additional load can be taken, after the yield strain level is reached, before significant bending of the baseplates takes place. This latter fact can be explained by plasticity theory when it is remembered that the shape factor for a rectangular section is 1.5.

Figure 5 shows close agreement between the measured flange stress at gauge F and the calculated flange stress (x - x moment at gauge F divided by post section modulus). Figure 6 shows close agreement between the measured bolt load and the calculated bolt load (x - x base moment divided by 2d).

Based on the results obtained in these tests and general knowledge of structural behavior, a theory was developed to explain the behavior of the bases. First, it was shown by the tests that the top baseplates fail by bending about the tension flange of the post. It was also shown that the critical principal strain was mainly dependent on base moment. Therefore, it was assumed that the principal strain of the baseplate is linearly proportional to the moment in the plate divided by the section modulus of the plate. Second, the bending load is applied to the baseplate by the bolts; therefore, the baseplate bending moment is linearly proportional to the bolt load times the distance from bolt to flange. Third, the bolt load can be calculated by static strength from base moment; this was verified by the measured bolts. All of the preceding assumptions were used in previous theoretical analyses. The lower principal strain values observed in the tests can be accounted for by introducing other parameters. These parameters must account for the following factors: restraint caused by the bolts and washers, load being applied through the washers rather than through the centerline of bolts, reinforcing effect of the weld, and uneven bending stress distribution in the plate. Based on only three tests, it was impossible to account for all of these factors. (The W 12×19 test was not considered at this point because its design was such that the bottom plate failed rather than the top.) The first three factors had about the same effect in the other three tests and would have about the same effect for all practical designs. Observation of stress-coat crack patterns demonstrated that the last factor was dependent on the ratio C/A (Fig. 2). It was decided that, to arrive at one dimensionless parameter (K) to represent all four parameters, this parameter would be dependent on C/A. A solution was desired in the form ϵ-plate = f(M, T2, K), and it was known that $\epsilon\text{-plate} = \frac{6}{29 \times 10^3 \text{ ksi}} \frac{M\,C}{A(T2)^2\,(2C + d)}$ for K = 1, based on the first three assumptions given earlier. Terms used in equations are shown in Figure 2. A plot of C-plate (measured) divided by C-plate (calculated with K = 1) versus C/A was constructed (Fig. 7). It showed good correlation between the two tests with the same C/A ratio and indicated that the stress concentration factor decreases with increasing C/A as was expected. The ϵ-plate (measured) and ϵ-plate (calculated K = 1) were determined for M such that ϵ-plate measured equaled ϵ-yield. From this plot, the equation K = 0.78 - 0.80 (C/A) was determined. Thus, the equation for baseplate stress becomes

$$f = \frac{6MC\,[0.78 - 0.80\,(C/A)]}{A(T2)^2\,[2C + d]} \qquad (1)$$

It is felt that this equation can be used with reasonable confidence for bases similar to the ones tested.

DEVELOPMENT OF DESIGN METHOD

Equation 1 serves as the basis for a new design method. An additional consideration required for design is the correct value of allowable stress (Fb). Most elastic design specifications provide for an increase in allowable stress based on plasticity theory

Figure 4. Location of strain measuring devices.

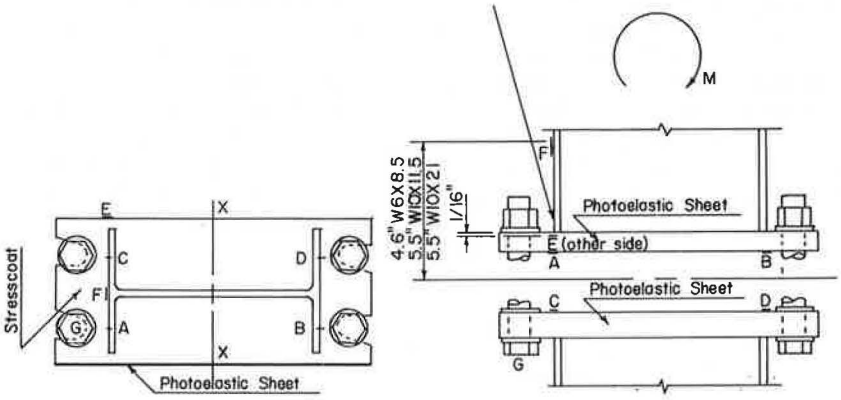

Table 2. Results of tensile tests.

Specification No.	Plate Thickness (in.)	Yield Point (psi)	Ultimate Stress (psi)	Elongation of 2-in. Gauge (percent)	Type of Post
1	5/8	38,895	65,888	36.5	W 6×8.5
2	3/4	45,231	72,820	26	W 10×11.5
3	7/8	42,154	73,846	33	W 10×21
4	5/8	39,289	65,990	33	W 12×19

Figure 5. Stress at gauge F as function of moment for W 6x8.5.

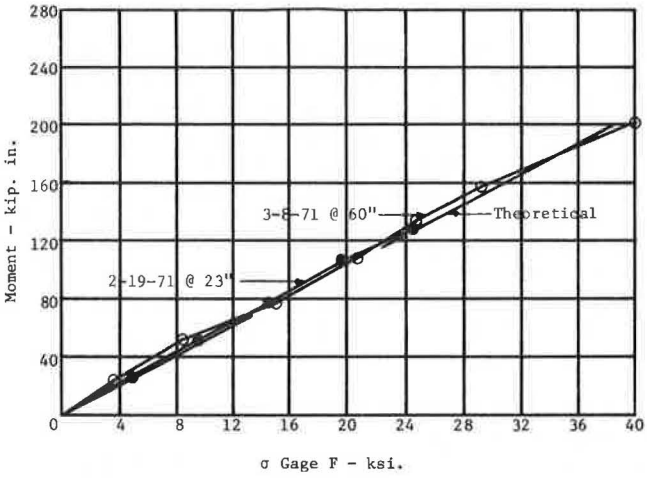

when the full or partial plastic moment can be developed by the member. For example, AASHO specifications allow a 9 percent increase for compact W-sections and 20 percent for round or oval tubes. A similar increase should be allowed for the rectangular baseplate. The shape factor for W-sections varies from 1.10 to 1.18, and a 9 percent increase is used with them. Because the shape factor for rectangular sections is 1.5, a 45 percent increase should be allowed for baseplates. For design, it is desirable to solve Eq. 1 for T2 in order to find plate thickness required for a given design moment and for M in order to find the allowable moment for a given design. This was done for an AASHO group II loading that allows an additional 45 percent increase in allowable stress, resulting in the following equations:

$$T2 = \frac{2.86\ MC[0.78 - 0.80(C/A)]}{Fb\ A\ [2C + d]} \tag{2}$$

$$M = \frac{FbA(T2)^2[2C + d]}{2.86\ C\ [0.78 - 0.80(C/A)]} \tag{3}$$

The design moment should be based on AASHO group II loading.

For purposes of comparison with test results, ultimate moments were computed for the bases tested using Eq. 3 with Fb = Fy/1.45. The moments obtained were 210 kip-in. for the W 6×8.5, 522 kip-in. for the W 10×11.5, 790 kip-in. for the W 10×21, and 374 kip-in. for the W 12×19. These compare with test moments where bending was noted of 220 kip-in. for the W 6×8.5 and 387 kip-in. for the W 12×19. Note that the design method is on the conservative side. Moments of 420 kip-in. for the W 10×11.5 and 726 kip-in. for the W 10×21 were the highest obtained in those tests with no bending noted.

Some concern has been voiced regarding the rigidity of the Kansas design baseplates. The concern apparently centers around the following statement (part II, p. 4:123, 6): "It must be pointed out that rigidity of the base plates is very important to the operation of the base and the theory developed to explain it. If significant changes are made in the design of the base, the force-slip characteristics should be re-evaluated by laboratory test."

Regarding this, the author wishes to make the following points. Texas and other states are using the Kansas design for small post sections, and there are many documented cases of their satisfactory performance (2). The removal of the stiffener tends to make the Kansas design base less rigid than the Texas design; however, the continuation of the plate between post flanges tends to make the Kansas design base more rigid than the Texas design. A coefficient of friction of 0.2 was found at small slips for two of the bases tested. The 0.2 figure was calculated by the same method as used by TTI and is within the range of values reported (part II, p. 3:45, Fig. 3.3.1, 6). In comparing coefficients of friction, it should be remembered that the surface condition of the baseplates is important. In this project, the tests were run on ungalvanized bases that had been cleaned of mill scale. Ungalvanized steel surfaces generally have a higher coefficient of friction than galvanized surfaces, but mill scale removal lowers the value somewhat.

It is the author's opinion that the Kansas design does not constitute a significant change that would affect the force-slip characteristics.

The design method herein developed is recommended only for use in design of bases similar to those tested. Use of the method results in allowable moments about $2\frac{1}{2}$ times as large or baseplate weights about two-thirds as much as those designed by previous theoretical methods. Based on discussion with fabricators, who make both types of bases, it is believed that fabrication labor for the Kansas base is about half that for the Texas base. Material, shipping, and installation costs for both bases are believed to be small. Because contract bid prices for breakaway bases in Kansas have averaged about $25, it appears that fabrication labor must average about $20. Because Kansas installs about 1,000 bases per year, it is estimated that a $20,000 annual savings will be realized by the use of bases designed by this method.

Figure 6. Bolt load as function of moment for W 6x8.5.

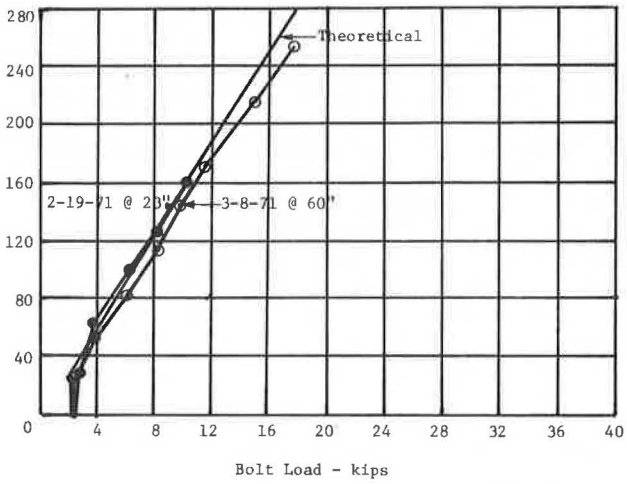

Figure 7. Relative strain as function of C/A.

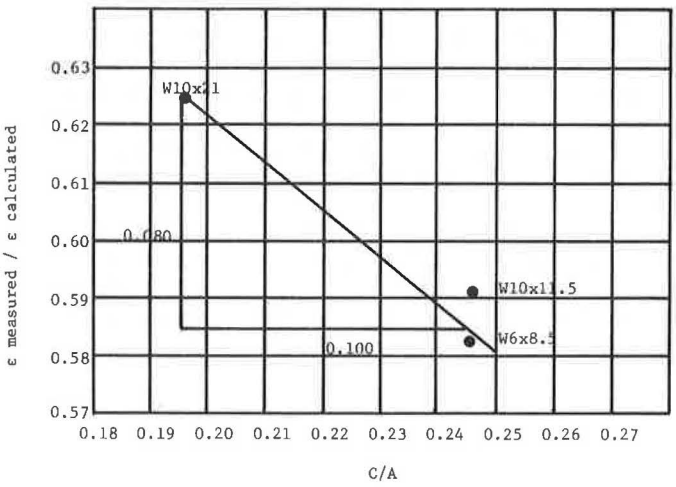

Table 3. Dimensions of Kansas breakaway bases.

Type of Post	Dimension (in.) S	T1	T2	A	B	C	D	E	L	R	Bolt Size (in.)
W 6x8.5	1/4	7/8	5/8	4 5/8	1 7/8	1 1/8	2 1/2	1 1/16	9 5/8	11/32	5/8 by 3
W 10x11.5	1/4	1	3/4	4 5/8	1 7/8	1 1/8	2 1/2	1 1/16	13 5/8	11/32	5/8 by 3 1/4
W 10x21	3/8	1 3/8	1	6 5/8	2 3/8	1 3/8	3	1 11/16	14 5/8	15/32	7/8 by 3 3/4

Note: Structural shapes and plate according to ASTM A 441 and bolts according to ASTM A 325.

IMPLEMENTATION: DESIGN OF BASES FOR USE IN KANSAS

The new design method has been used to design three slip bases for standard break-away supports. The W 6×8.5 and W 10×11.5 are the same as those tested, but the W 10×21 has a larger fillet weld and thicker baseplate. The baseplates are fabricated from ASTM A 441 steel as are the posts. The design moments used in designing the bases were equal to the maximum allowable moment on each post. Size of bolts and welds was determined by AASHO specifications. The dimensions of Kansas standard designs are given in Table 3; they correspond to those shown in Figure 2. The plan dimensions are the minimum ones that will allow sufficient clearance and edge distances for bolts and welds. When the dimensions and design moment were known, Eq. 2 was used to determine the required thickness. In the case of the W 10×21, the required thickness turned out to be such that the plate would weigh slightly more than the maximum value recommended (6). The weight was reduced by taking clips out of the plate between flanges. Although this probably reduces the strength slightly, the thickness provided in going to standard plate thickness is more than the minimum required, and the design is felt to be satisfactory.

REFERENCES

1. Darnes, L. W. Progress Report on the Design Concept and Field Performance of Break-Away Sign Supports in Texas. Region Six, Bureau of Public Roads, Fort Worth, June 1966.
2. McCollom, B. F. Design of Slip Bases for Break-Away Signs. State Highway Commission of Kansas, Topeka, 1972.
3. Olson, R. M. Instrumentation and Photographic Techniques for Determining Displacement, Velocity Change, and Deceleration of Vehicles With Break-Away Sign Structures. Texas Transportation Institute, Texas A&M Univ., Res. Rept. 68-3, Sept. 1966.
4. Rowan, N. J., Olson, R. M., Edwards, T. C., Gaddis, A. M., and Williams, T. G. Impact Behavior of Sign Supports—II. Texas Transportation Institute, Texas A&M Univ., Staff Progress Rept. 68-2, Sept. 1965.
5. Samson, C. H., Rowan, N. J., Olson, R. M., and Tidwell, D. R. Impact Behavior of Sign Supports. Texas Transportation Institute, Texas A&M Univ., Res. Rept. 68-1, March 1965.
6. Highway Sign Support Structures, Vol. 1: Break-Away Roadside Sign Support Structures. Texas Transportation Institute, Texas A&M Univ., 1967.

EVALUATION OF BREAKAWAY LIGHT POLES FOR USE IN HIGHWAY MEDIANS

N. E. Walton, T. J. Hirsch, and N. J. Rowan, Texas Transportation Institute, Texas A&M University

Crash tests were conducted to determine the impact behavior of median-mounted light poles and secondary collisions of vehicles striking downed poles on a traffic lane. A relative hazard index was developed to describe the relative hazard created by the proximity and frequency of light poles. It was concluded that a 20-deg impact by a 2,900-lb vehicle at 45 mph would not cause a pole to encroach on the opposing traffic lane if the median is 40 ft wide. A 4,000-lb vehicle impacting at 25 deg and 60 mph would cause a pole to encroach approximately 11 ft into the opposing lane. Under both conditions, the impacting vehicle would cross into the opposing lanes and might be more of a hazard than the poles themselves. A medium-sized vehicle impacting a downed pole within the traffic lane presents no more hazard than the original impact. From a relative hazard standpoint, median-mounted luminaire systems produce less hazard than house-side systems for median widths of 30 ft or greater.

•AS substantial mileage of the Interstate Highway System was being completed, there arose a need for safer and more efficient methods of lighting those facilities. Previous methods had consisted of relatively low luminaire mounting heights and frequent spacings with the supports located close to the roadway edge on rigid bases. These practices were acceptable for the low-operating speeds and volumes found on city streets but were unacceptable for the high-speed, high-volume characteristics of the freeway. The low mounting heights and frequent spacings produced uncomfortable environments for drivers as they passed through "hot spots" and "dark spots" on the roadway (1). The frequent spacings and location of the supports close to the roadway edge on rigid bases produced even more unacceptable environments. Frequent collisions with the supports by out-of-control vehicles resulted in severe vehicle damage and injury or death to the occupants (2).

The advent of higher output light sources provided partial solutions to the unacceptable conditions. Higher mounting heights with corresponding longer spacings and setbacks from the roadway were possible with the higher output light sources (3). This provided for a reduction in the "ladder" effect created by the "hot and dark spots." There remained, however, the potential for vehicle-support impact.

A similar problem had already been encountered with roadside signs mounted close to the roadway edge. This problem was successfully solved through the development and use of sign supports that would shear or break away when struck by an errant vehicle (4). Success with the breakaway sign supports led to the development of similar techniques for light poles.

Slip joints, cast aluminum transformer bases, cast aluminum inserts, notched bolt inserts, progressive-shear bases, and cast aluminum flanged bases have all been used with a high rate of success (2). These devices have provided for great flexibility in the location of light poles.

As a result of the safer supports, median-mounted luminaires have become very popular for the illumination of freeway facilities. Quality of illumination provided by this location and economy have contributed to the popularity. Objection has been voiced, however, to the use of median mountings where the height of support exceeds the median width. This objection has been based on the premise that secondary collisions may

occur with a downed pole occupying a traffic lane. This report is in response to this objection.

STUDY OBJECTIVES

The objectives of this research are to investigate the impact behavior of median-mounted light poles and the behavior of secondary vehicle-support impact and to develop a hazard index to describe the relative hazard created by the proximity and frequency of light poles.

DETAILS OF TESTS

Three vehicle crash tests were conducted on 50-ft double-mast arm light poles with frangible transformer bases. The first two tests simulated accidents in which vehicles ran off the road and struck the breakaway supports. The third test simulated an accident in which an oncoming vehicle ran over a light pole that had been knocked into the traffic lane by a second vehicle that had left the opposing roadway.

In the first two tests, the vehicles were equipped with accelerometers attached to each longitudinal frame member. The tests were recorded on documentary and high-speed films for time-displacement analysis. The third test was recorded photographically, but no electronic accelerometers were used. Instead, a mechanical device called an Impact-O-Graph was used to measure triaxial accelerations.

In the first two tests, the poles and mast arms were oriented at angles to the direction of vehicle travel. The orientations were such that a vehicle would be veering to the right of its normal traffic lane in these tests. The supports were oriented in this manner because of space and hardware restrictions. However, the double-mast arm supports are designed for median installations and would normally be exposed to impacts by vehicles running off the road to the left of the normal traffic flow. Because the supports and the front ends of the vehicles are symmetrical, the response of the poles in such impacts is a mirror image of that in an impact at the same angle from the other side. Therefore, the final positions of the supports are shown in the drawings as they would have been if struck in the same manner by a vheicle encroaching the median. For purposes of these simulations, a 40-ft wide median (including shoulders) has been assumed.

Test LS-1

Test LS-1 simulated a relatively lightweight vehicle striking the support at a 45-mph speed and a 20-deg angle to the direction of the roadway. The octagonal galvanized pole was mounted on a frangible aluminum transformer base (Fig. 1).

The vehicle contacted the pole 18 in. to the right of the vehicle's centerline, but the base shattered, allowing the support to rotate up and clear the vehicle as intended. Sequential photographs of the test are shown in Figure 2. Figure 3 shows the fragmented base after the test. The front of the vehicle before and after the impact is shown in Figure 4. The vehicle sustained a residual deformation to the right front of 0.6 ft.

Table 1 gives the pertinent vehicle data. The speeds from the films are average speeds over about 3-ft intervals preceding contact and following the interval of accelerometer activity. The accelerometer data given in Table 1 are the average of the right- and left-frame accelerometers.

The final position of the light pole in relation to its original position and a hypothetical 40-ft median strip is shown in Figure 5. In this case, the support would have remained within the median. However, the errant vehicle entered the oncoming traffic lanes without significantly altering its course. The only conclusion that can be drawn from this is that, if the vehicle was traveling straight at an angle to the road upon impact with no driver control and the median was flat and level, then such an impact would cause encroachment of the oncoming traffic lanes by the errant vehicle.

Test LS-2

Test LS-2 was similar to LS-1 except that the vehicle was heavier, the impact angle was increased to 25 deg, and the impact speed was 60 mph instead of 45 mph.

Figure 1. Light pole base before test LS-1.

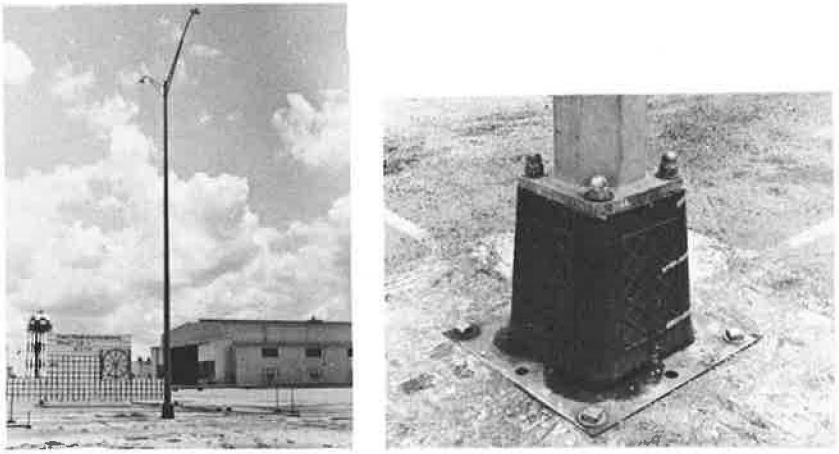

Figure 2. Test LS-1.

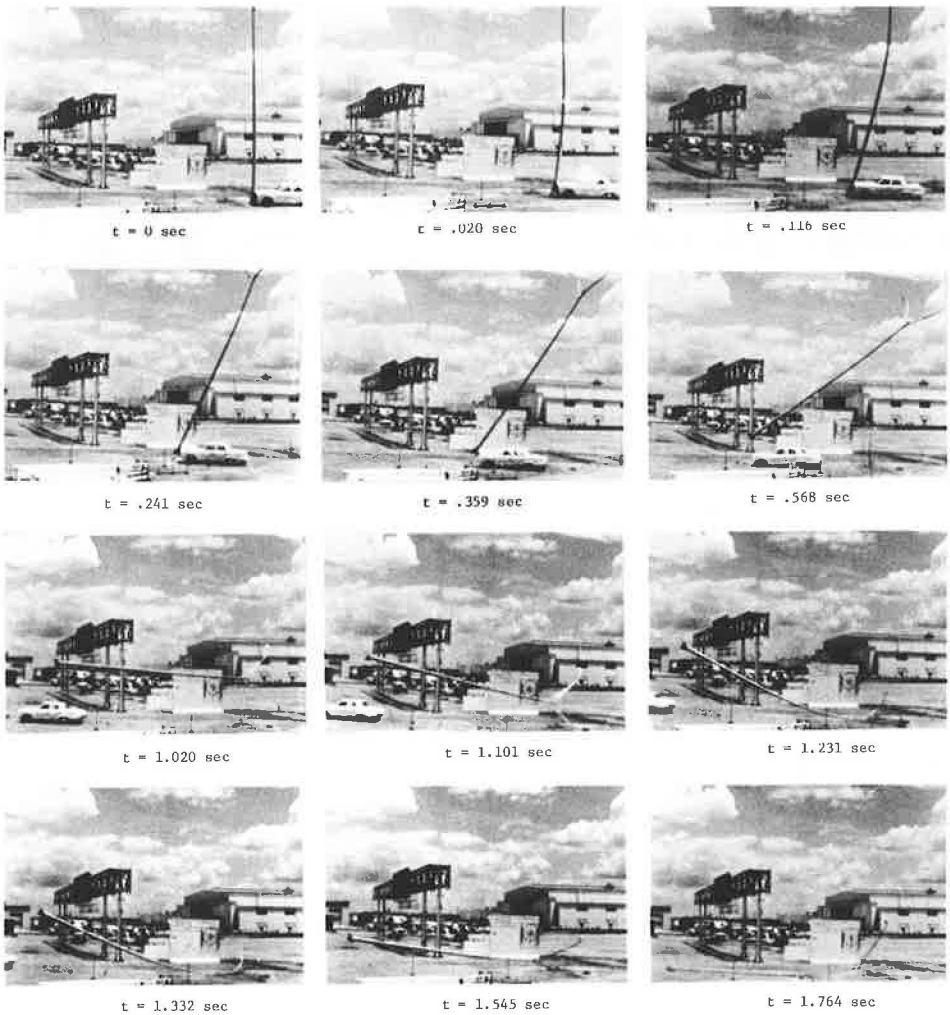

Figure 3. Frangible transformer base after test LS-1.

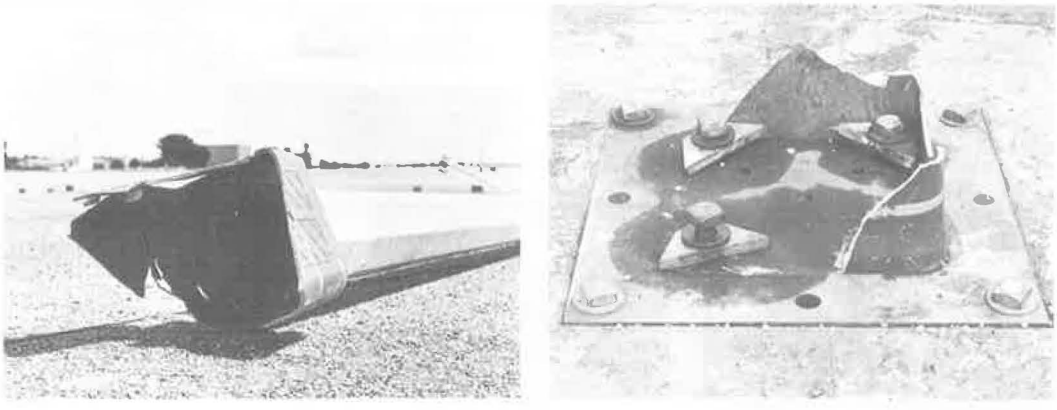

Figure 4. Front of vehicle before and after test LS-1.

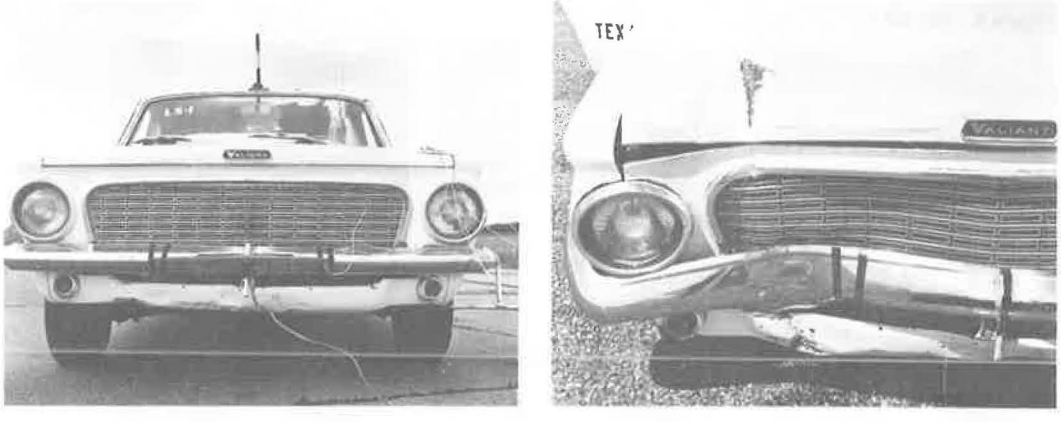

Table 1. Tests LS-1 and LS-2 data.

Factor	LS-1	LS-2
Vehicle		
Year	1963	1961
Make	Plymouth	Chevrolet
Weight, lb	2,900	4,040
Angle of approach, deg	20	25
Residual deformation, ft	0.6	1.5
Film data		
Initial speed, ft/sec	67.2	87.6
Initial speed, mph	45.8	59.7
Final speed, ft/sec	60.7	78.4
Final speed, mph	41.4	53.3
Average longitudinal deceleration[a], g	2.0	4.1
Change in momentum[b], lb-sec	585	1,155
Accelerometer data		
Maximum longitudinal deceleration, g	14.4	8.2
Average longitudinal deceleration, g	2.5 over 0.110 sec	3.6 over 0.072 sec

[a] $(V_i^2 - V_f^2)/2gS$. [b] $\Delta P = (W/g)(\Delta V)$.

The cast aluminum transformer base (Fig. 6) shattered as expected, and the pole rotated up and cleared the vehicle as the vehicle continued on its course. Sequential photographs of the test are shown in Figure 7; the shattered base is shown in Figure 8.

The front end of the vehicle had a residual deformation of 1.5 ft (Fig. 9). The increased damage is primarily due to the higher impact speed.

The vehicle data given in Table 1 show that the significant deceleration period was about two-thirds as long as that in test LS-1, which was conducted at a lower speed.

Figure 10 shows the final position of the light pole. If the pole had been mounted in the center of a 40-ft median, the base after the test would have projected 11 ft horizontally into the oncoming "inside" traffic lane at an angle of 33 deg to the roadway. Under these simulated conditions, the vehicle would have crossed the oncoming lanes.

Test LS-3

Test LS-3 was designed to determine the behavior of an automobile striking a "downed" light pole under conditions that would have resulted from a crash such as that of test LS-2. The support from test LS-2 was placed in such a way that the 12.5-ft wide concrete slabs that make up the test apron would simulate the oncoming inside traffic lane. That is, the base extended 11 ft into the simulated lane at an angle of 33 deg and pointed toward the approaching test vehicle as shown in Figures 11 and 12. The test vehicle, which was traveling in the center of the simulated traffic lane, struck the support at 61 mph, passed over it, and continued virtually straight ahead as shown in Figure 13. Figures 14 and 15 show the support after the test; Figure 16 shows the path of the vehicle.

Table 2 gives the film and Impact-O-Graph data on the vehicle. The Impact-O-Graph, being primarily mechanical, is not as accurate as electronic devices for measuring accelerations of this nature, but it has been found to give representative data. Note that the average decelerations (or accelerations) are low, but the peak accelerations are substantial in the vertical and transverse directions. However, these peaks are of short duration, and the vehicle exhibited no tendency to spin out or otherwise deviate significantly from its original path except for a gradual curvature to the left. Both the left-front and right-rear tires were deflated by the impact.

The light pole was pushed around to an angle of 85 deg to the roadway and extended 25 ft into the traffic lanes after the test. Note in Figure 13 that the vehicle did not contact the fragmented base but ran over the shaft only.

DISCUSSION OF TESTS RESULTS

The breakaway behavior of 50-ft double-mast arm light poles with frangible transformer bases is satisfactory under the conditions of the first two tests. The vehicles passed under the supports, after shearing them from their bases, and continued on essentially their original paths.

If the poles were installed in the center of a 40-ft median (including shoulders), a 20-deg impact by a 2,900-lb vehicle at 45 mph would probably not cause the pole to encroach on the opposing traffic lanes. However, in the single test under these conditions, the final position was marginal, the base of the support being 1 ft from the roadway. A 4,000-lb vehicle impacting at 25 deg and 60 mph causes the pole to encroach 11 ft into the opposing inside traffic lane. Both conditions allowed the vehicles to cross into the hypothetical traffic lanes, and this may be more of a hazard than the poles themselves.

If a medium-sized vehicle encounters a support in its traffic lane and strikes it with all wheels on the pole shaft (not straddling the base nor attempting to maneuver) at 60 mph, it may be able to continue straight ahead until control is regained. However, no firm conclusions can be drawn from one test. The support struck in such a manner would possibly be shifted into the adjacent traffic lane and thereby furnish a further hazard to other traffic.

Figure 5. Final position of light pole in test LS-1.

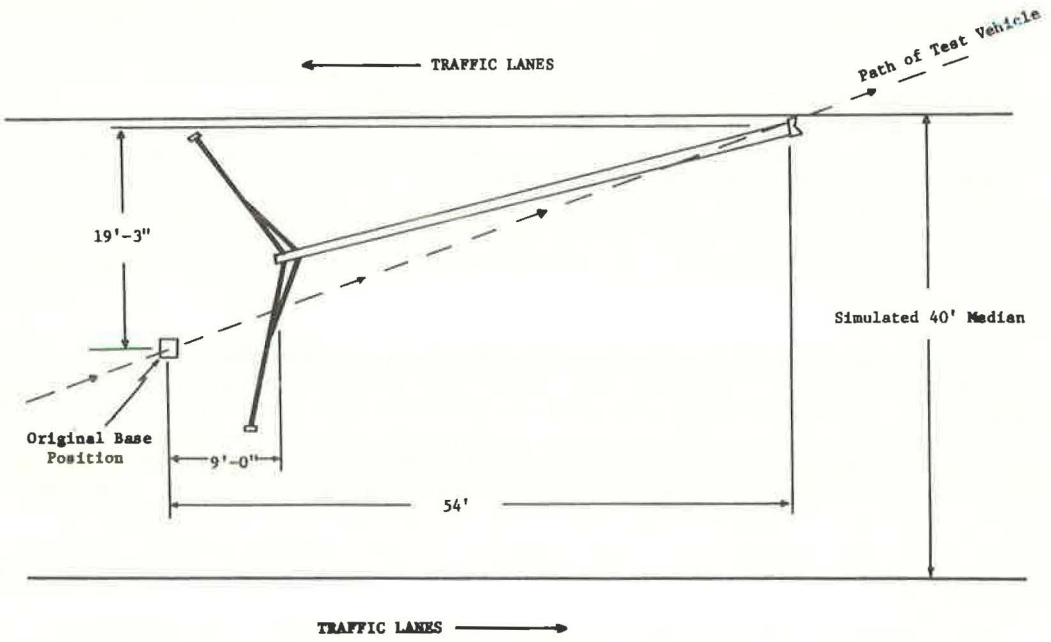

Figure 6. Light pole base before test LS-2.

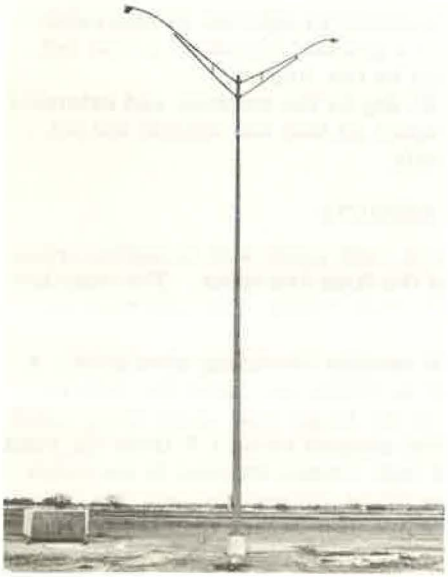

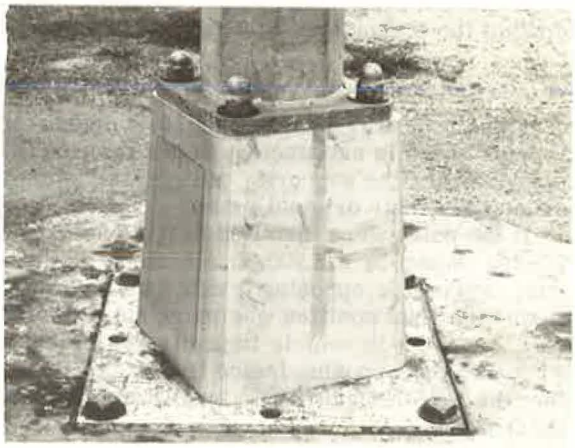

Figure 7. Test LS-2.

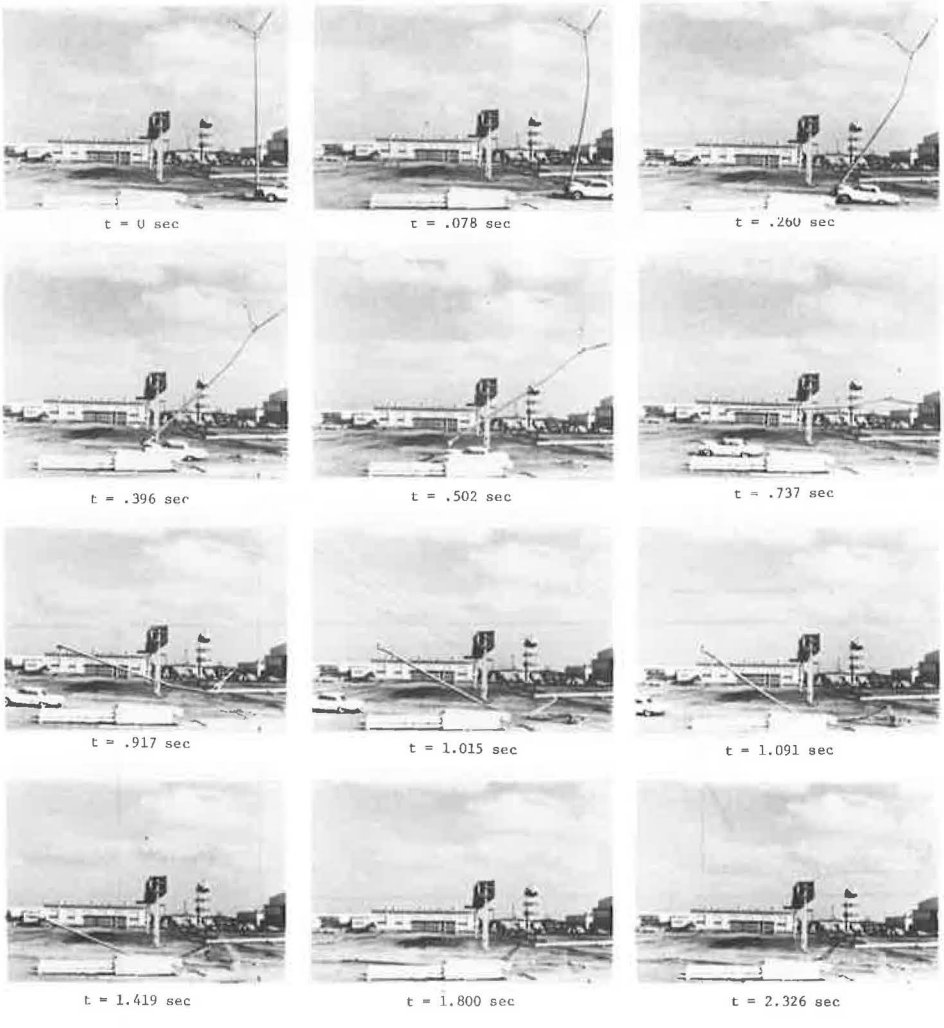

Figure 8. Frangible transformer base after test LS-2.

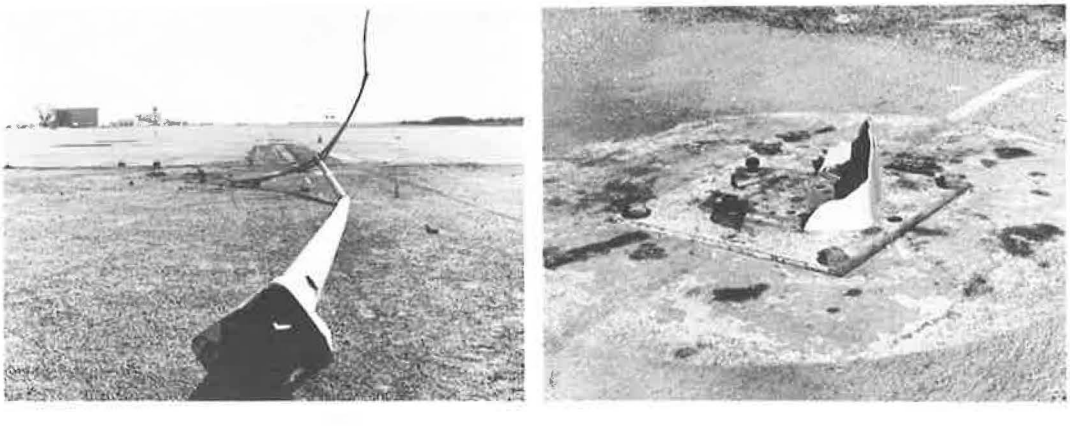

Figure 9. Front of vehicle before and after test LS-2.

Figure 10. Final position of light pole in test LS-2.

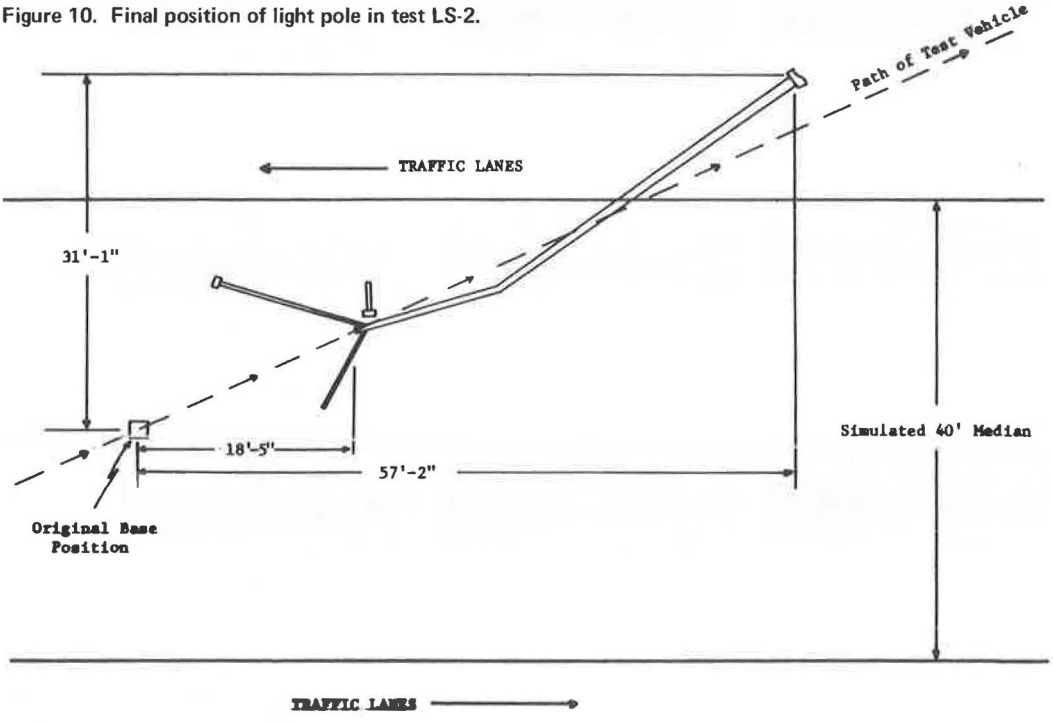

Figure 11. Light pole before test LS-3.

Figure 12. Position of light pole before test LS-3.

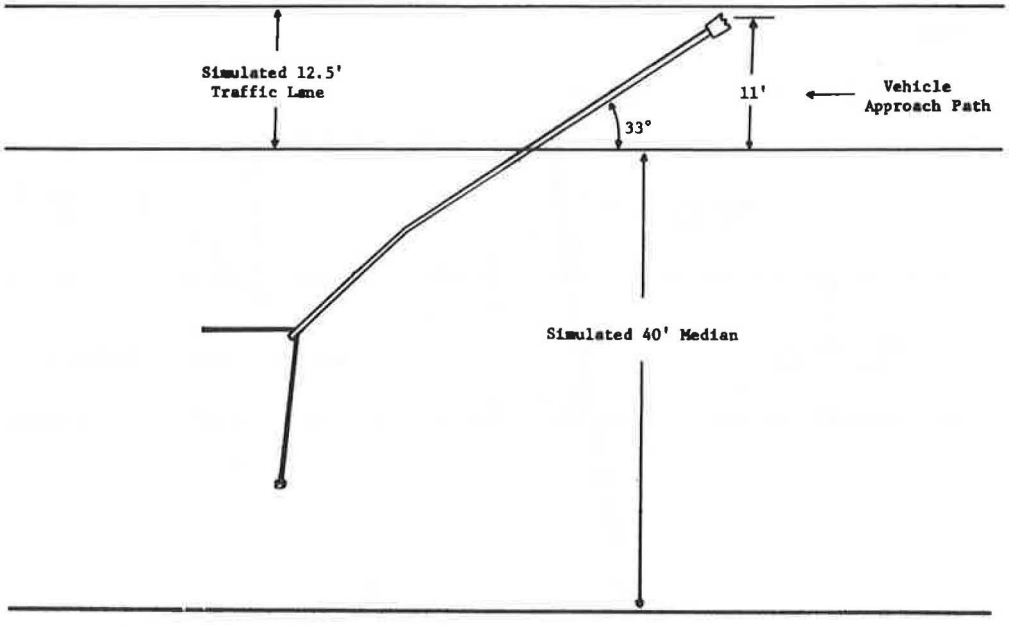

Figure 13. Test LS-3.

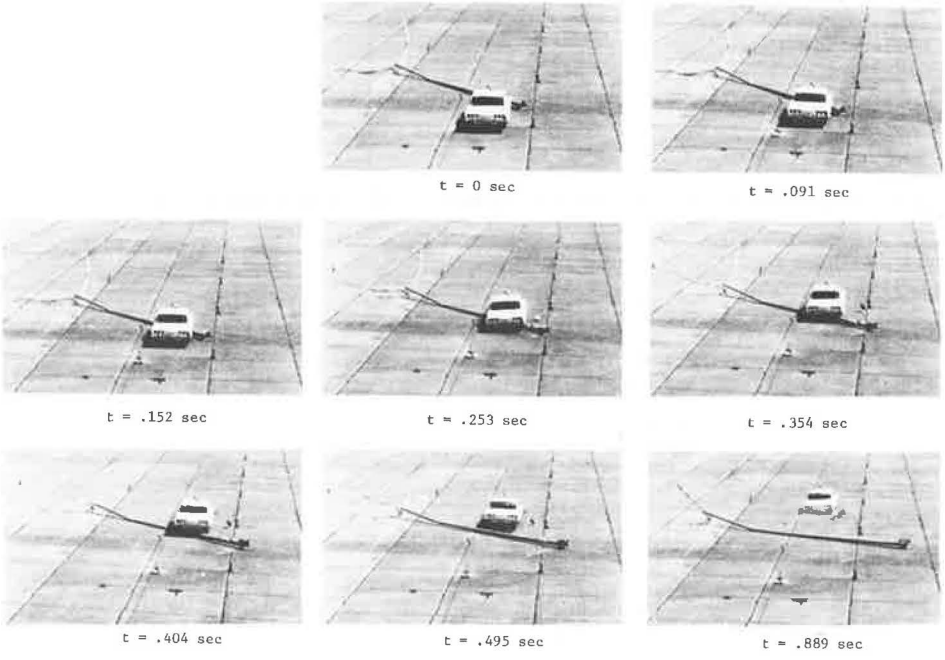

Figure 14. Light pole after test LS-3.

Figure 15. Position of light pole after test LS-3.

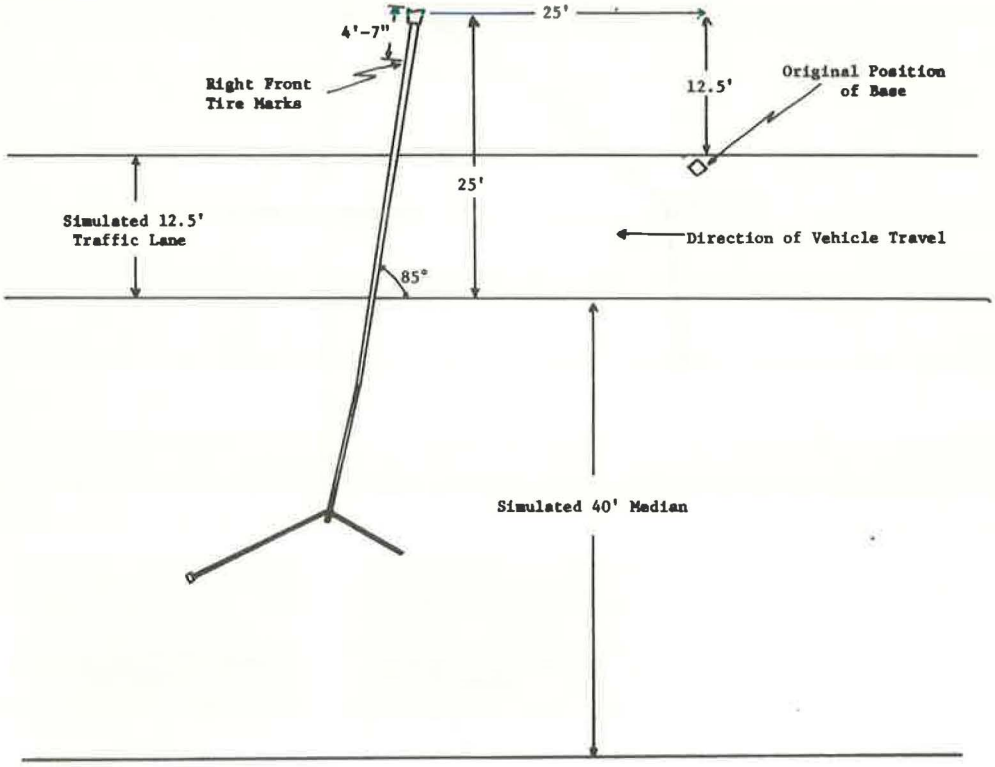

Table 2. Test LS-2 data.

Factor	LS-3
Vehicle	
Year	1963
Make	Chevrolet
Weight, lb	3,630
Film data	
Initial speed, ft/sec	89.6
Initial speed, mph	61.1
Final speed, ft/sec	84.1
Final speed, mph	57.3
Time in contact, sec	0.355
Average longitudinal deceleration[a], g	0.5
Impact-O-Graph data	
Longitudinal deceleration	
Maximum, g	3.4
Average, g	0.1
Time, sec	0.502
Vertical acceleration	
Maximum, g	13.5
Average, g	0.2
Time, sec	0.502
Transverse acceleration	
Maximum, g	13.5
Average, g	0.05
Time, sec	0.502

[a] $\Delta V/g\Delta T$.

DEVELOPMENT OF A RELATIVE HAZARD INDEX FOR LIGHT POLES

The purpose of this section is to formulate the procedure for determining a relative hazard index for alternative lighting systems on a typical freeway facility. Specifically, the relative hazard index describes the relative hazard created by the proximity and frequency of light poles.

The alternative lighting systems presented are basically median-mounted and house-side lighting systems at mounting heights of 30, 40, 45, and 50 ft at a 5:1 spacing-to-mounting height ratio. Each of the systems is shown in Figure 17.

Table 3 summarizes the data for each of the alternative lighting systems and presents the relative hazard index for a 44-ft median, a design of special current interest. A similar comparison can be made for any median width. This relative hazard index is computed as the product of the relative index of a vehicle impacting a light pole based on lateral distance from the traveled way, the relative number of hazards per unit length of roadway, and the relative number of traffic streams (directions) to which the light poles are exposed. To explain the source of each of these factors, reference is made again to Table 3. Column 5 gives the lateral distance of the support from the edge of the traveled way for each of the alternative designs. The two distances given for alternative designs 5 and 6 represent two supports in alternative design 5 and an offset situation in alternative design 6. Column 6 of Table 3 gives the percentage of probability that an errant vehicle will travel a sufficient lateral distance from the traveled way to become involved in a collision with a support. These values are based on frequently referenced data reproduced in Figure 18a from Hutchinson reported by Stonex (5).

Column 7 of Table 3 gives the estimated percentage of probability of secondary collisions caused by the light pole falling in an opposing traffic lane and being struck by an oncoming vehicle. The percentage of probability is determined on the basis that only supports struck at angles greater than 20 deg will fall in the opposing traffic lanes. Further, this effect is considered only for 45- and 50-ft supports. Shorter support lengths are assumed to always fall within the median. The percentage of probabilities was obtained from Figure 18b.

In test LS-3, in which a vehicle ran over a downed 50-ft steel light pole, there was strong evidence that the secondary collision was of no greater severity than the initial impact with the upright support. Therefore, the relative probability index of collisions (column 8) was determined by increasing the percentage of probabilities (column 6) by the estimated percentage of impact greater than 20 deg (column 7). The percentage of probability (column 6) actually used was a computed average.

In column 9, the relative frequency of exposure of a vehicle to light poles is computed using the 250-ft spacing of the 50-ft median-mounted system as unity.

Column 10 lists the exposure indexes based on the exposure of the traffic streams to light poles. The median-mounted systems can be struck from either direction, whereas the house-side systems can only be struck from one direction.

Column 11 represents the combined total hazard index (of a vehicular collision with a light pole) based on lateral distance from the roadway to the light role, the relative number of hazards per mile, and the exposure to traffic flows. It is obtained by computing the product of columns 8, 9, and 10.

For ease of interpretation, the total hazard index values of column 11 are converted to a base of unity by dividing all values by the smallest value in the column. These values, called the relative hazard index, are given in column 12.

RELATIVE HAZARD INDEX AND MEDIAN WIDTH

The relative hazard for various median widths was composed by making a similar analysis for a 50-ft median-mounted system in median widths ranging from 10 to 60 ft. The details of the analysis are given in Table 4.

It should be noted that column 5 of Table 4 contains the relative probability of a secondary collision occurring because of opposing traffic striking the downed support in the opposing traffic lane. This is based on test LS-2, a 4,000-lb vehicle striking a 50-ft support at 25 deg and 60 mph, in which the lateral translation of the pole base

Figure 16. Path of vehicle in test LS-3.

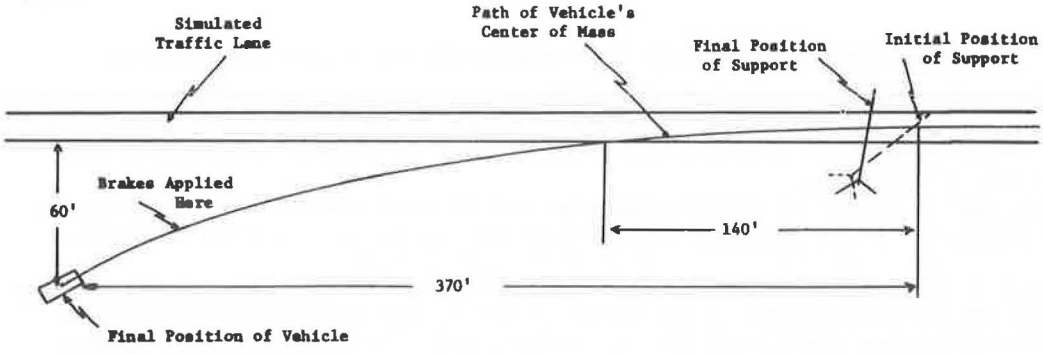

Figure 17. Light pole design systems.

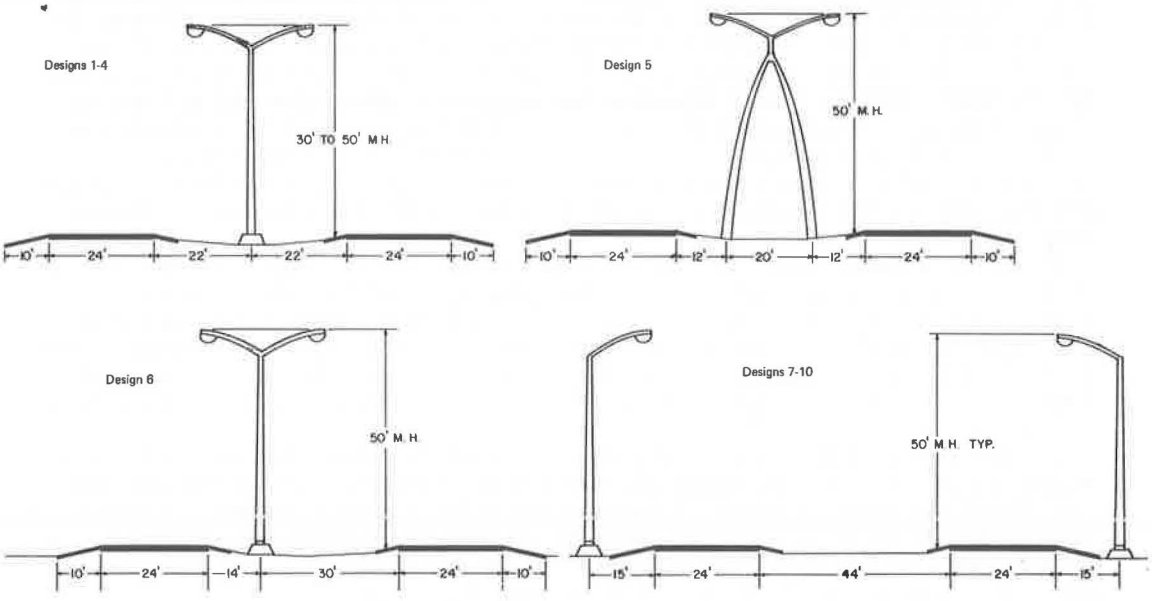

Table 3. Relative hazard index.

Alternative Design (1)	Mounting Height of Luminaires (ft) (2)	Longitudinal Spacing of Light Pole[a] (ft) (3)	Location of Light Pole (4)	Distance From Roadway to Light Pole (ft) (5)	Percentage of Probability[b] (6)	Estimated Percentage of 20-deg Impact (7)	Relative Probability Index of Vehicle Collision With Light Pole (8)	Relative No. of Light Poles per 250 Ft (9)	No. of Traffic Streams Exposed to Light Poles (10)	Total Hazard Index (11)	Relative Hazard Index (12)
1	30	150	Median	22	22		0.22	1.66	2.00	0.730	1.58
2	40	200	Median	22	22		0.22	1.25	2.00	0.55	1.19
3	45	225	Median	22	22	5	0.231	1.11	2.00	0.513	1.11
4	50	250	Median	22	22	5	0.231	1.00	2.00	0.462	1.00
5	50	250	Median	12	55						
				32	9		0.32	2.00	2.00	1.280	2.77
6	50	250	Median	30	11						
				14	46	10	0.308	1.00	2.00	0.616	1.33
7	50	250	House-side	15	45		0.45	2.00	1.00	0.900	1.95
8	45	225	House-side	15	45		0.45	2.22	1.00	1.000	2.16
9	40	200	House-side	15	45		0.45	2.50	1.00	1.124	2.43
10	30	150	House-side	15	45		0.45	3.32	1.00	1.492	3.23

[a]5:1 spacing-to-mounting height ratio. [b]Based on Hutchinson's findings (5). [c]Assumes support may fall across two lanes.

Figure 18. Relation of cross section design and highway safety.

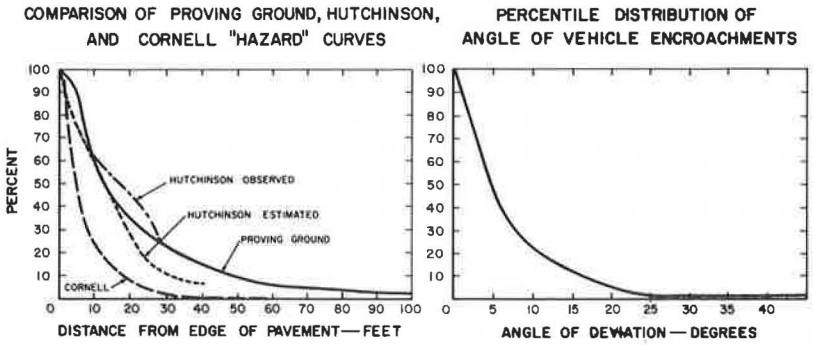

Table 4. Median width and relative probability index.

Location (1)	Median Width (ft) (2)	Distance From Roadway to Light Pole (ft) (3)	Percentage of Probability[a] (4)	Estimated Percentage of 20-deg Impact (5)	Relative Probability Index of Vehicle Collision With Light Pole (6)	No. of Traffic Streams Exposed to Light Poles (7)	Relative No. of Supports per 250 Ft (8)	Total Hazard Index (9)	Relative Hazard Index (10)
Median	60	30	11	—	0.110	2.00	1.00	0.220	1.00
Median	55	27.5	13	—	0.130	2.00	1.00	0.260	1.18
Median	48	24.0	18	5	0.189	2.00	1.00	0.378	1.72
Median	46	23.0	20	5	0.210	2.00	1.00	0.420	1.91
Median	44	22.0	22	5	0.231	2.00	1.00	0.462	2.10
Median	42	21.0	25	5	0.263	2.00	1.00	0.526	2.39
Median	40	20.0	28	5	0.294	2.00	1.00	0.588	2.67
Median	35	17.5	37	5	0.388	2.00	1.00	0.776	3.53
Median	30	15.0	45	10	0.495	2.00	1.00	0.990	4.50
Median	25	12.5	52	10	0.572	2.00	1.00	1.144	5.22
Median	20	10.0	59	10	0.650	2.00	1.00	1.300	5.91
Median	15	7.5	67	10	0.738	2.00	1.00	1.476	6.71
Median	10	5.0	75	10	0.825	2.00	1.00	1.650	7.50
House-side		15	45	—	0.45	1.00	2.22[b]	1.00	4.55

[a]Based on Hutchinson's findings (5). [b]Recommended spacing of 225 ft for house-side installations.

Figure 19. Relation of relative hazard index and median width.

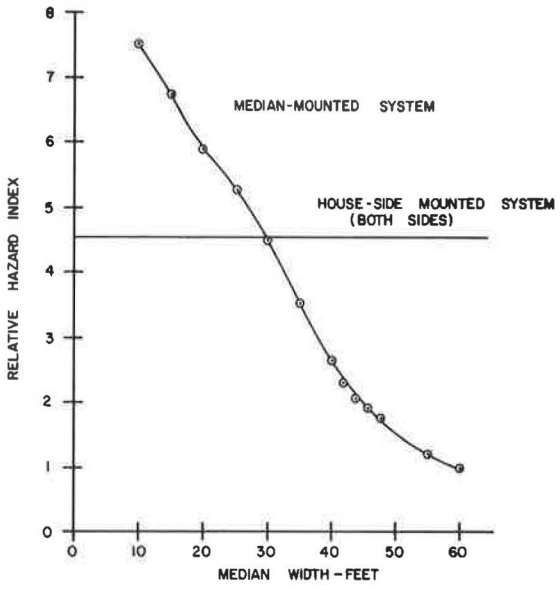

was 31 ft. Given that an encroachment of more than 4 ft into a traffic lane may result in a collision, the estimated percentage of impacts greater than 20 deg was determined from Figure 18b.

Figure 19 shows a plot of the values for relative hazard index and median width for a median-mounted system and for a 50-ft house-side system with supports located 15 ft from the edge of the roadway on both sides. This comparison indicates that median-mounted lighting systems produce less hazard than house-side systems for median widths 30 ft or greater.

CONCLUSIONS

Based on the results of the three crash tests and development of the relative hazard index, the following conclusions are drawn:

1. The breakaway behavior of 50-ft double-mast arm light poles with frangible bases is satisfactory under the conditions of tests LS-1 and LS-2.
2. A 20-deg impact by a 2,900-lb vehicle at 45 mph would probably not cause a pole to encroach on the opposing traffic lane if the median is 40 ft wide (including shoulders).
3. A 4,000-lb vehicle impacting at 25 deg and 60 mph would cause a pole to encroach approximately 11 ft into the opposing inside traffic lane if the median is 40 ft wide (including shoulders).
4. Both conditions 2 and 3 would allow the impacting vehicle to cross into the opposing traffic lanes, and this may be more of a hazard than the poles themselves.
5. A medium-sized vehicle that encounters a support in its traffic lane and strikes it with all wheels on the pole shaft (not straddling the base nor attempting to maneuver) at 60 mph would probably be able to continue straight ahead until control is regained.
6. From a relative hazard standpoint, 50-ft high median-mounted light poles produce less hazard than house-side systems for median widths of 30 ft or greater.

ACKNOWLEDGMENTS

This study was conducted under a cooperative program between the Texas Transportation Institute and the Texas Highway Department. It was sponsored by the Texas Highway Department and the Federal Highway Administration.

The contents of this report reflect the views of the authors who are responsible for the facts and the accuracy of the data presented herein. The contents do not necessarily reflect the official views or policies of the Federal Highway Administration. This report does not constitute a standard, specification, or regulation.

REFERENCES

1. Rowan, N. J., and McCoy, P. T. An Interim Report on a Study of Roadway Lighting Systems. Texas Transportation Institute, Texas A&M Univ., Res. Rept. 75-1, April 1966.
2. Edwards, T. C., Martinez, J. E., McFarland, W. F., and Ross, H. E., Jr. Development of Design Criteria for Safer Luminaire Supports. NCHRP Rept. 77, 1969, 82 pp.
3. Walton, N. E., and Rowan, N. J. Supplementary Studies in Highway Illumination. Texas Transportation Institute, Texas A&M Univ., Res. Rept. 75-13F, Aug. 1969.
4. Break-Away Roadside Sign Support Structures. Texas Transportation Institute, Texas A&M Univ., July 1967.
5. Stonex, K. A. Relation of Cross-Section Design and Highway Safety. Paper presented at the 35th Annual Highway Conf., Univ. of Colorado, Denver, Feb. 23, 1962 (supplemented Jan. 1963).

BASE-BENDING SINGLE SIGNPOSTS

Edward C. Zobel, Wayne State University

ABRIDGMENT

•EXPERIMENTAL work on the evaluation of base-bending single signposts was conducted by researchers at Wayne State University in 1970. Study of base-bending single signposts was the initial effort of a multiphase program (11). Primary data reduction was based on photogrammetric information obtained from three high-speed cameras. Backup information was obtained from a fifth wheel attached to the tow vehicle and speed traps. Photogrammetric techniques were evolved to be used in conjunction with the development at Wayne State University of a new, simplified methodology for the analysis of high-speed motion picture data, planned ultimately to provide three-dimensional kinematic information. The signpost study contributed to the initial steps in this direction.

STUDY APPROACH

Signposts may be categorized as either base-shearing or base-bending, depending on mode of failure on vehicular impact. Generally speaking, single metal signposts supporting small or medium sign markers are base-bending structures and will be passed over by an impacting vehicle. When heavier single metal posts are required to support large signs, base-shearing features are ordinarily designed into the post near ground level, permitting the signposts, upon impact, to fly up and allowing the vehicle to pass beneath.

Base-bending signposts have been investigated at the University of Cincinnati (1, 2, 5), the General Motors Corporation (3), and the Unistrut Corporation (4). With the exception of two 50-mph tests in the series performed at the University of Cincinnati, all others were conducted at lower impact speeds.

The single metal signpost experimental program at Wayne State University was designed to answer specific research questions by evaluating kinematic and phenomenological response of the post configurations under consideration over the full operational range of all significant impact parameters. The large number and wide ranges of these parameters made a full factorial test program impractical, and, accordingly, a structural fractional factorial experimental design was employed (7).

DISCUSSION OF TESTS

The physical testing period for the signpost tests began in August 1970 and extended through December of that year. Full-scale crash tests were conducted on a runway at Willow Run Airport near Ypsilanti, Michigan.

Three single signposts were tested: 2-in. (nominal) diameter steel pipe, 2½-in. (nominal) diameter steel pipe, and 8-lb/ft steel flanged-channel signposts.

Except in two cases (tests 13 and 17), in which the signposts were embedded in concrete (12 in. in diameter) to a depth of 3½ ft, all signposts were driven into the sandy loam soil to specified depths of 3½, 4, and 4½ ft.

The 2-in. steel-pipe signposts were 13½ ft long and carried 1½-ft by 2-ft by 0.081-in. aluminum sign markers; the 2½-in. steel-pipe signposts were 14 ft long and displayed 2-ft by 2½-ft by 0.081-in. aluminum sign markers; the 8-lb/ft flanged-channel signposts were 15½ ft long and carried 4-ft by 5-ft by ¾-in. plywood sign markers. The size of the sign marker for each post was determined according to design specifications of the Michigan Department of State Highways (6).

Vehicle damage was observed as slight, moderate, or severe. Because all vehicles after the first two tests were equipped with a modified bumper, all damage assessments are relative.

Table 1 gives a summary of the results of the 16 single signpost tests conducted during the testing period.

Typically, the phenomenological response of the single steel-pipe signposts to impact showed nearly instantaneous formation of a plastic hinge at the point of initial contact, followed by plastic hinge formations approximately 6 to 12 in. below ground level. During the formation of these hinges, the upper portion of the signpost tended to remain inertially fixed, resulting in the angular inclination of the post toward the vehicle as it traveled along its path following impact. This angle of inclination, referred to as the post deflection angle, is the maximum angle as measured from a vertical reference line. As the signpost wrapped around the front of the vehicle, it was often pulled from the ground. A third area of plastic hinge formation sometimes occurred when the signpost contacted the hood of the vehicle.

Initial response of the 8-lb/ft flanged-channel signposts was similar to that described previously. As the post bent, however, the $\frac{3}{8}$-in. steel bolts, tying the 4-lb/ft channels together on 16-in. centers, sheared, permitting the channels to bend independently, flare open, and be torn from the ground. In the final test of the year, in which the signpost was embedded in frozen soil, the channel on the impact side was sheared at the bumper impact point, and the adjacent channel was bent at ground level and was ruptured in tension at the bumper point. The remainder of the post remained intact. The sign marker, as was the case for each test involving a plywood sign, became detached from the signpost and fell closely within the signpost area after the vehicle passed beneath. In this test the marker struck the top of the vehicle above the windshield and contacted the car a second time on the trunk lid.

INTERPRETATION OF RESULTS

The data from which kinematic responses of the vehicle were measured were taken from the high-speed movies by observing a convenient target attached to the side of the crash vehicle. For purposes of comparison, the average values of deceleration during the time required for the vehicle to move 2 ft following impact has been defined as the maximum deceleration. This corresponds to the maximum deceleration as defined by Cook and Bodocsi (5) in the lower speed signpost tests conducted by them at the University of Cincinnati and permits comparison of full-scale crash tests on similar signposts.

Table 1. Signpost test data.

Test No.	Soil Embedment (ft)	Signpost	Vehicle Weight (lb)	Impact Velocity (mph)	ΔV (mph)	a_{max} (g) (2 ft) (ft/sec²)	a_{avg} (g) (4 ft) (ft/sec²)	Post Deflection (deg)	Damage		
									Passenger	Driver	Vehicle
1	4	2 in.	3,720	44.3	-2.8	—	-1.8	24.5	N[a]	N	Slight
2	3½	2 in.	3,720	45	—	—	—	30	—	—	Slight
3	4½	2 in.	3,720	57.6	-5.9	—	-2.6	44.2	N	N	Slight
4	3½	2½ in.	3,720	37.5	-3.4	-1.3	-1.8	30.4	N	N	Slight
5	4½	2½ in.	3,720	58.2	-3.2	-4.5	-4.3	52.8	N	N	Slight
6	3½	2 in.	3,720	48.2	-2.6	-2.1	-2.1	50.8	N	N	Moderate
7	4½	2 in.	3,720	36.7	-4.0	-1.2	-1.5	28.1	N	N	Moderate
8	3½	2 in.	2,455	65.4	-1.2	-2.1	-2.1	69.4	N	N	Moderate
9	3½	2 in.	3,400	59.2	-1.0	-0.7	-1.2	66.6	N	N	Moderate
10	3½	2 in.	3,265	63.4	-1.8	-2.7	-2.8	70.1	N	N	Moderate
11	3½	2½ in.	3,345	48.7	-4.2	-0.6	-1.6	56.2	N	N	Moderate
13	3½ C[b]	2½ in.	3,265	48.9	-5.7	-4.1	-4.7	45.1	M[c]	M	Severe
15	3½	2½ in.	2,826	71.3	-7.6	-5.9	-6.6	62.6	M	M	Severe
16	3½	8 lb/ft	4,500	54.8	-3.6	-3.5	-3.8	45.8	N	N	Slight
17	3½ C	8 lb/ft	4,500	57.7	—	—	—	44.6	—	—	Slight
18	3½	8 lb/ft	2,514	30.3	-8.4	-4.5	-4.4[d]	84.3[e]	M	M	Moderate

[a]N = no probable injury.
[b]C = concrete.
[c]M = marginal (secondary impact probable).
[d]Calculation based on 3 ft.
[e]Not equivalent to other deflections because of base-shearing action of signpost.

The average value of deceleration of the vehicle is that that occurs during the time period required for the vehicle to move 4 ft following impact. The 4-ft distance was chosen because, for all practical purposes, the significant part of the impact event was complete during the corresponding time frame. Additionally, this tended to provide a standard with which kinematic and phenomenological results could be compared.

The significance of the post deflection angle is that it provides an estimate of probable vehicle passenger compartment penetration. As might be anticipated, physical tests indicate that increases in post deflection angles are related somewhat proportionately to increases in impact velocities. It appears that specification of minimum signpost heights can minimize the possibility of passenger compartment penetration by the signpost at high speeds.

In addition to making phenomenological observations of both signpost and crash vehicle and obtaining the associated kinematic data, we wished to provide some degree of probable occupant injury assessment. As indicated in other reports (2, 9, 10), a definitive relation associating occupant injury with vehicle decelerations does not currently exist. Researchers have used the Stapp curve and the Cornell Aeronautical Laboratory (CAL) suggested limits of tolerable deceleration as a gross means of possible evaluation for occupant injury. Results of the Wayne State University signpost impact tests indicate no probable injury for any properly restrained occupant under either the Stapp or CAL criteria. However, in an effort to provide unrestrained occupant injury assessment criteria, a simple engineering model was devised on the basis of certain reasonable assumptions. In Figure 1, it is presumed that, below the vehicle acceleration-time curve, no secondary contact of the occupants will occur within the vehicle and, consequently, no injury will occur. Above the vehicle deceleration-time curve, secondary impact within the vehicle is probable with occurrence of injury likely.

The curves shown in Figure 1 are based on the assumption that the driver of the vehicle has approximately 12 in. to move inside the vehicle before contacting the vehicle. It is presumed that the unrestrained driver, upon impact, can apply sufficient force to his body to cause an absolute deceleration of 1 g to his body. The 1-g value is presumed from the fact that most people when lying face down can produce a sufficient force on their body with their hands and arms to sustain a 1-g acceleration in a push-up maneuver. Similarly, for the passenger a distance of 24 in. and a force of 0.5 g have been assumed. The 0.5 g would result as a minimum from frictional forces applied to

Figure 1. Unrestrained occupant injury assessment curve.

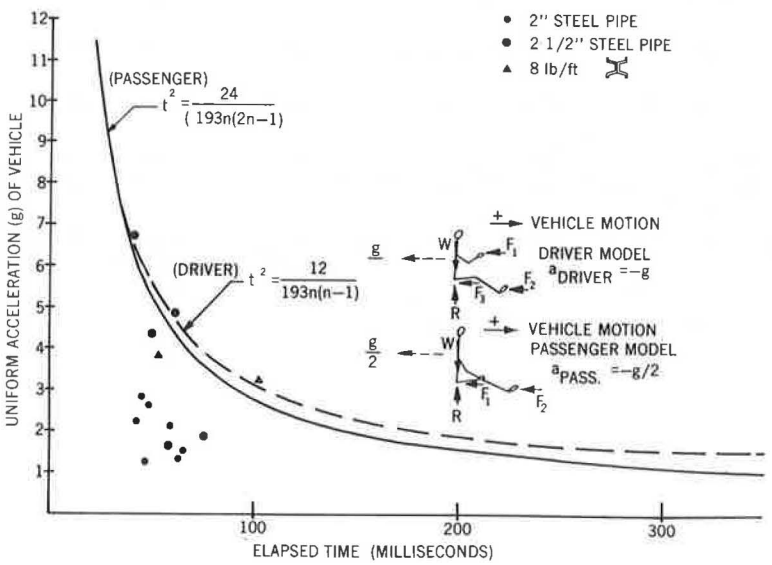

the passenger by the seat cushion. In Figure 1, n is the number of g's of deceleration of the vehicle during the duration of impact t.

For the curves shown in Figure 1, some of the average values of deceleration during the impact period (as previously defined) fall within the marginal area. Calculations indicate that, in test 13, the driver would impact the wheel at 2.4 ft/sec and the passenger would impact the interior of the vehicle at 3.9 ft/sec. In test 15, comparable values would be 0 and 7.7 ft/sec respectively.

CONCLUSIONS

On the basis of the 16 full-scale crash tests performed on single signposts, including unrestrained occupant injury assessments, the following single signpost recommendations are made:

1. Two-in. steel pipe signposts driven to an embedment depth of 3½ ft in soil should be used,
2. A minimum signpost height above ground of 9 ft is desirable, and
3. Single 2½-in. steel pipe signposts and single 8 lb/ft flanged channel signposts are adequate where the single 2-in. signposts cannot be used; however, they should be driven in soil to an embedment depth of 3½ ft (placement in concrete is not recommended).

ACKNOWLEDGMENT

The opinions, findings, and conclusions expressed in this paper are those of the author and not necessarily those of the Michigan Department of State Highways or the Federal Highway Administration.

REFERENCES

1. Cook, J. P., and Bodocsi, A. An Interim Report on Impact Yielding Sign Supports. Cincinnati Univ., 1969.
2. Cook, J. P., and Bodocsi, A. Final Report—Criteria for Yielding Highway Sign Supports. Cincinnati Univ., May 1970.
3. Dynamic Testing of 8# Piggy-Back Steel Post Sign Installation. Tests conducted by GM Proving Ground for state of Michigan.
4. Telspar Perforated and Solid Telescoping Tubing. Unistrut Corp., Wayne, Michigan, 1967.
5. Cook, J. P., and Bodocsi, A. Impact-Yielding Sign Supports. Highway Research Record 346, 1971, pp. 58-66.
6. Typical Locations, Roadside Signs and Supports. Michigan Department of State Highways.
7. Hicks, C. R. Fundamental Concepts in the Design of Experiments. Holt, Reinhart and Winston, 1964.
8. Symonds, P. S. Survey of Methods of Analysis for Plastic Deformation of Structure Under Dynamic Loading. Brown Univ., 1967.
9. Graham, M. D., Burnett, W. C., Gibson, J. L., and Freer, R. H. New Highway Barriers: The Practical Application of Theoretical Design. Highway Research Record 174, 1967, pp. 88-184.
10. Test and Evaluation of Vehicle Arresting, Energy Absorbing, and Impact Attenuation Systems. Texas Transportation Institute, Texas A&M Univ., Nov. 30, 1971.
11. Zobel, E. C., et al. Investigation of the Dynamic Impact on Roadside Obstacles—Interim Rept., Wayne State Univ., Nov. 15, 1971.

SPONSORSHIP OF THIS RECORD

GROUP 2—DESIGN AND CONSTRUCTION OF TRANSPORTATION FACILITIES
John L. Beaton, California Division of Highways, chairman

GENERAL DESIGN SECTION
F. W. Thorstenson, Minnesota Department of Highways, chairman

Committee on Traffic Safety Barriers and Sign, Signal and Lighting Supports (as of December 31, 1972)
E. F. Nordlin, California Division of Highways, chairman
Verdi Adam, Gordon A. Alison, W. C. Anderson, William C. Burnett, Edward M. Conover, James J. Crowley, Malcolm D. Graham, Alf H. Hansen, Wayne Henneberger, Robert N. Hunter, Jack E. Leisch, Edwin C. Lokken, Jarvis D. Michie, Gilbert E. Morris, Jr., Robert M. Olson, John M. Quigg, Edmund R. Ricker, Neilon J. Rowan, F. G. Schlosser, Richard A. Strizki, Flory J. Tamanini, James A. Thompson, Charles Y. Warner, M. A. Warnes, Earl C. Williams, Jr.

Lawrence F. Spaine, Highway Research Board staff